KFA

KERNFORSCHUNGSANLAGE JÜLICH GmbH

Projektleitung Energieforschung
International Energy Agency IEA

Implementing Agreement for Co-Operation in the Development of Large Scale Wind Energy Conversion Systems

Fourth Meeting of Experts -
Rotor Blade Technology with Special Respect to Fatigue Design Problems

Organised by
Project Management for Energy Research (PLE)
of the Nuclear Research Establishment Jülich (KFA)
on behalf ot the
Federal Minister of Research and Technology
and The National Swedish Board for Energy
Source Development

Jül - Spez - 82
Juli 1980
ISSN 0343-7639

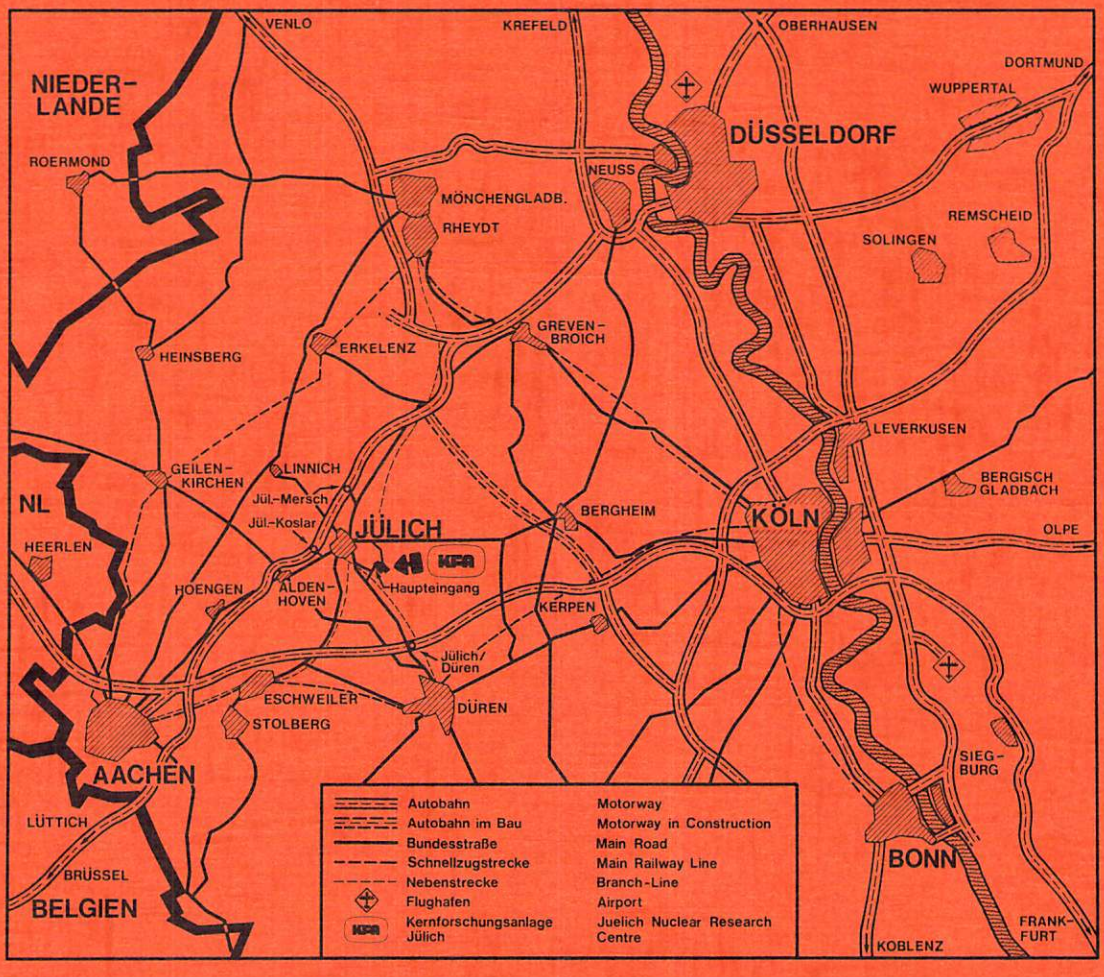

Als Manuskript gedruckt

Spezielle Berichte der Kernforschungsanlage Jülich - Nr. 82

Projektleitung Energieforschung Jül - Spez - 82

Zu beziehen durch: ZENTRALBIBLIOTHEK der Kernforschungsanlage Jülich GmbH

Postfach 1913 · D-5170 Jülich (Bundesrepublik Deutschland)

Telefon: 02461/611 · Telex: 833556 kfa d

Implementing Agreement for Co-Operation in the Development of Large Scale Wind Energy Conversion Systems

Fourth Meeting of Experts -
Rotor Blade Technology with Special Respect to Fatigue Design Problems
Stockholm, April 21-22 1980

Organised by
Project Management for Energy Research (PLE)
of the Nuclear Research Establishment Jülich (KFA)
on behalf ot the
Federal Minister of Research and Technology
and The National Swedish Board for Energy
Source Development

Scientific Coordination:
E. Hau (MAN München), S. Hugosson (NE Stockholm)
and R. Windheim (PLE KFA Jülich)

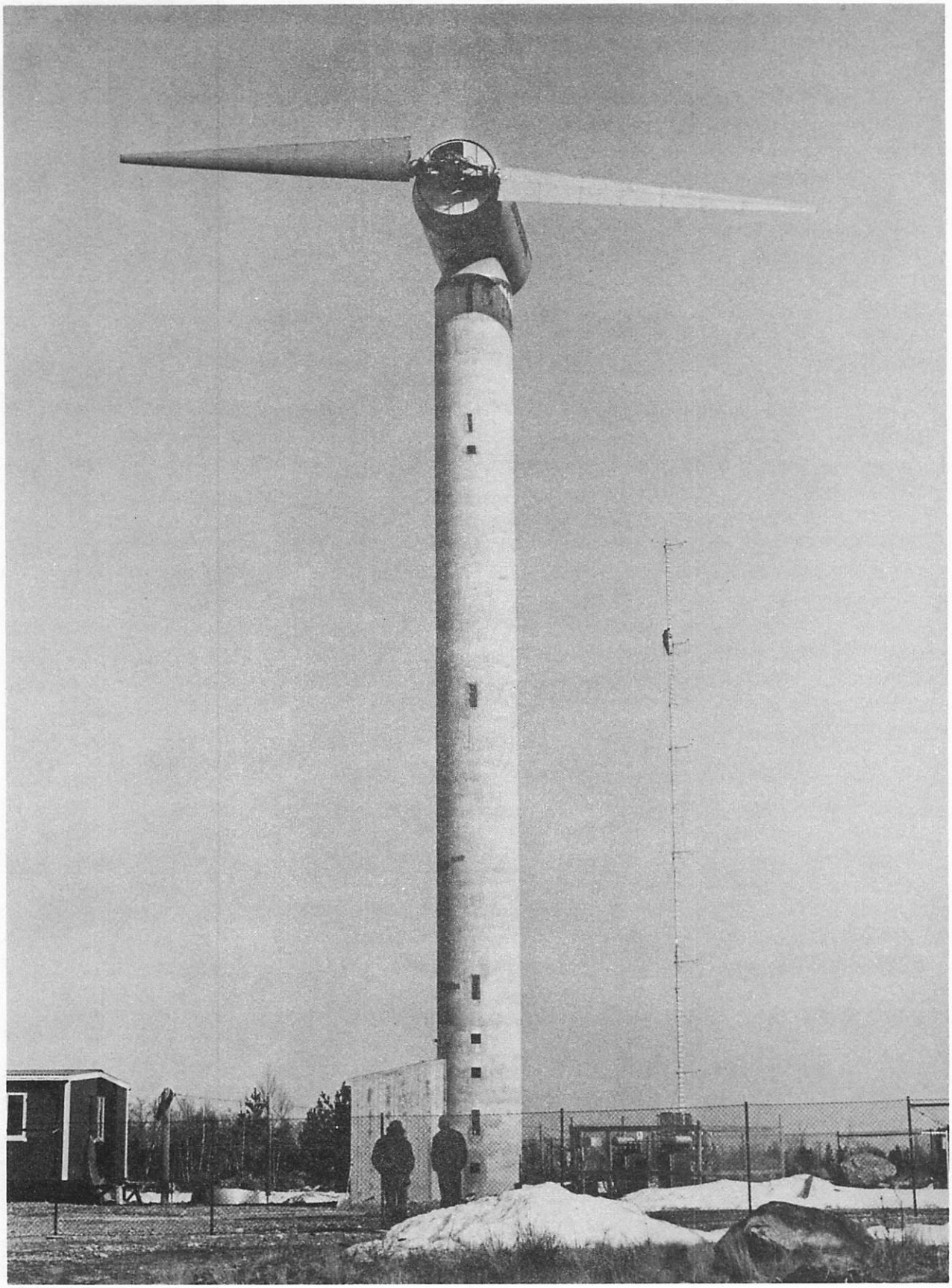

The Swedish 60 kW research unit
at Kalkugnen

CONTENTS

Paper presented at 4th Expert Meeting "Rotor Blade Technology with special respect to Fatigue Design Problems" in Stockholm April 21th and 22th, 1980.

Preliminary Results from Blade Load Measurements for the Nibe "A" Wind Turbine

by
Per Lundsager and Helge Petersen
Risø National Laboratory, Denmark

The Nibe "A" wind turbine is one of the two wind turbines erected by the

Wind Power Program of the Ministry of Commerce
and the Electric Utilities of Denmark

near the town Nibe in Jutland, Denmark.

The wind turbine has a diameter of 40 metres, a height of 45 m and is equipped with an asynchronous generator rated at 630 kW.

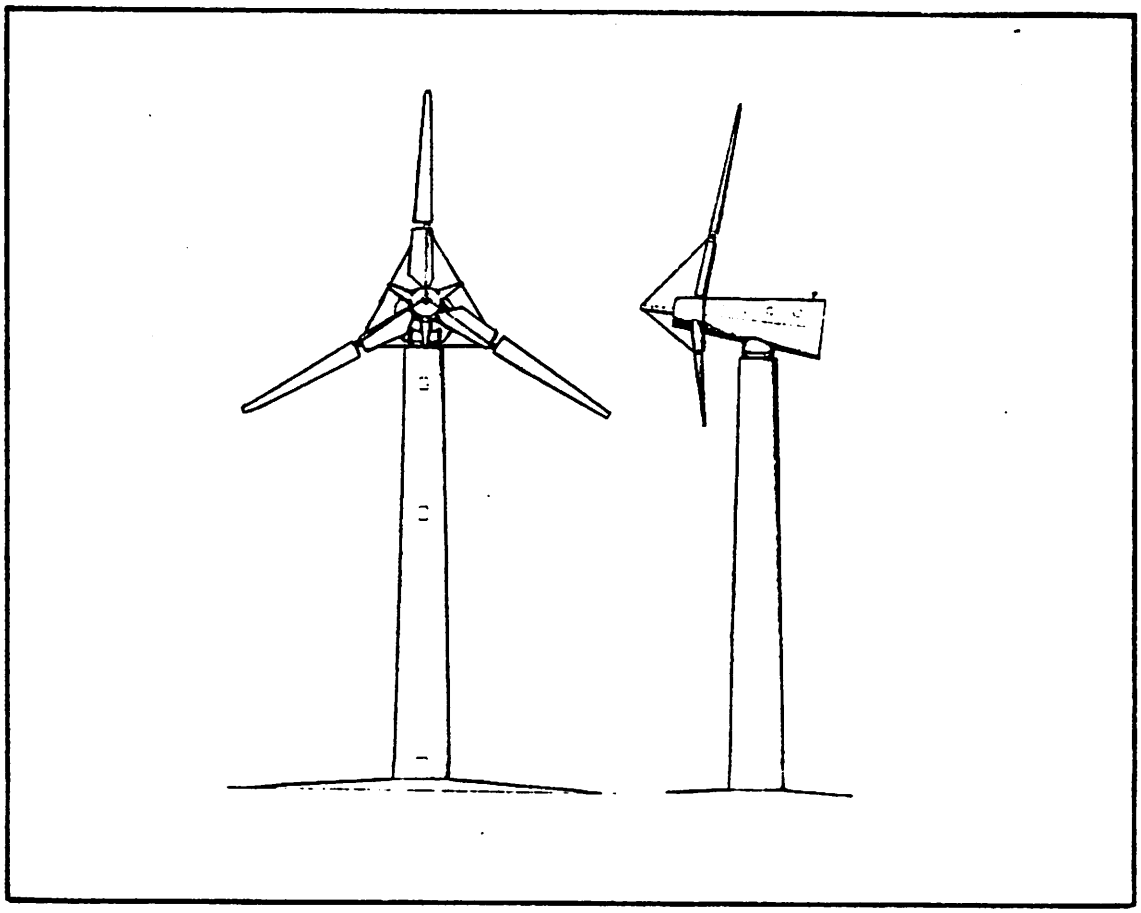

1. THE PRELIMINARY MEASUREMENT SYSTEM

The preliminary measurement system was established by connecting a number of operational parameter sensors to a six channel brush writer and an xy-plotter. A total of twelve operational parameters are available (cf. Table 1.1), the channels being connected to the brush writer six at a time through a patch panel located adjacent to the writer in the bottom of the tower of the turbine. In addition all strain gauge rotor channels are available at the patch panel three at a time through slip rings on the rotor shaft. Changes of rotor channel combinations are made by changing cable connections in the rotor hub. A diagram of the total system is shown in Fig. 1.1. Drop resistances on current signals are indicated.

Channel	Sensor	Range volt	Range Phys.	Conversion
3	Wind Speed at 58 m	0-3.0		9.3v+0 m/s
4	Rel. Wind Direction	0-2.5	-180/+180 deg	144v-180 deg
5	Blade pitch angle	0-2.2	-20/+15 deg	16v-20 deg
6	Rotor shaft torque	0-4.5	0/180 kNm	40v+0 kNm
7	RPM Generator	0-8.5	0/2250 vpm	180v+0 vpm
9	Force a. Pitch regulation	0-4.4	0/91 bar	36.4v+0 bar
10	Force b. Pitch regulation	0-4.4	0/91 bar	36.4v+0 bar
11	Nacelle position	0-4.4	-180/180 deg	162v-180 deg
12	Active power	0-2.0	-120/1200 kW	660v-120 kW
13	Reactive power	0-5.0	0/500 kVar	100v+0 kVar
14	Current	0-2.0	0/40 Amp	20v+0 Amp
15	Voltage	0-5.0	0/25 kV	5v+o kV
1	Rotor channel 1	-	-	-
16	Rotor channel 2	-	-	-
2	Rotor channel 3	-	-	-
NS	Acc NS tower top	0-1.0	0/2.45 m/s^2	2.45v+0 m/s^2
WE	Acc WE tower top	0-1.0	0/2.45 m/s^2	2.45v+0 m/s^2

Table 1.1 List of sensors

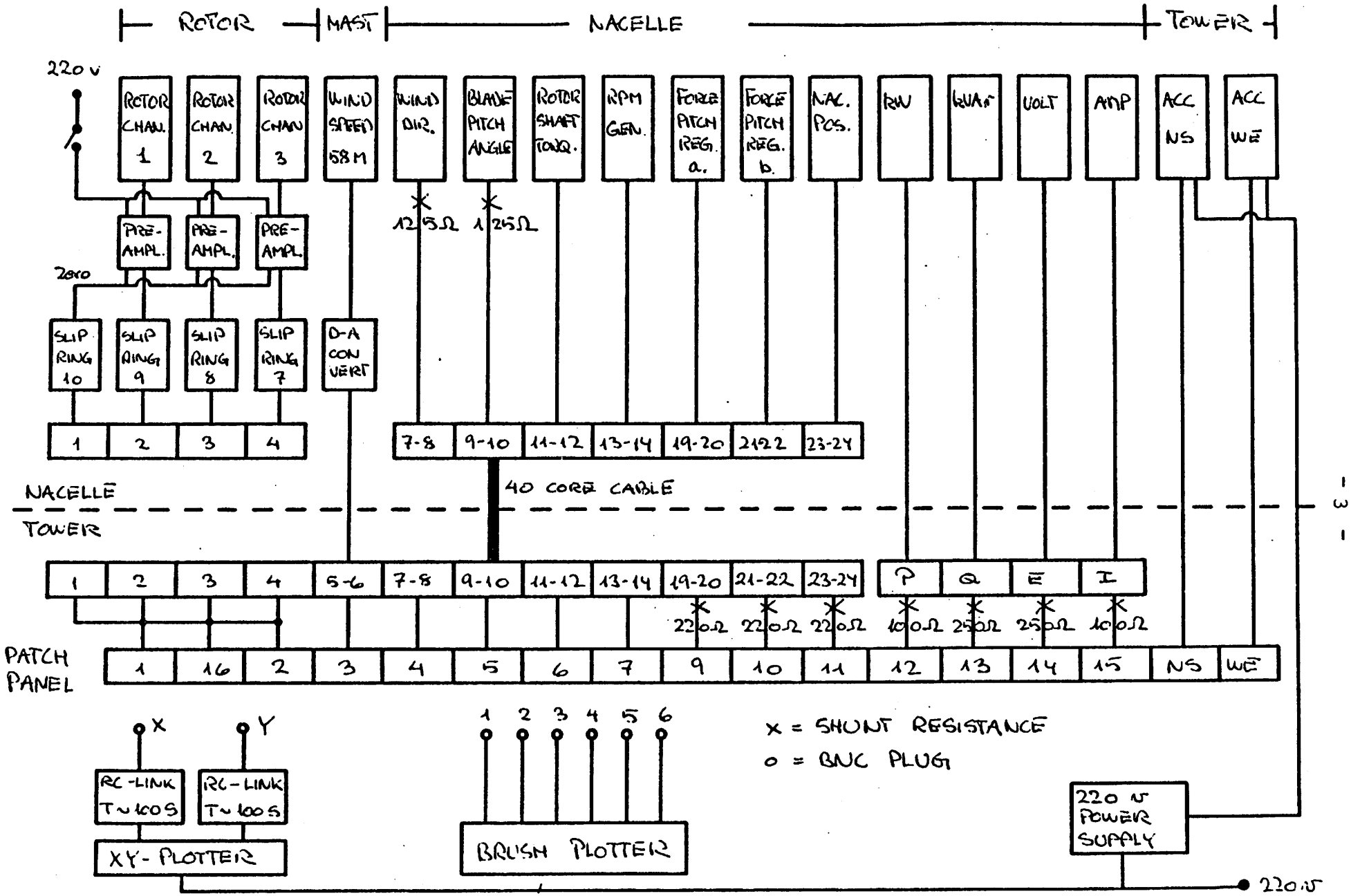
ROTOR
MAST
NACELLE
TOWER
220 V
ROTOR CHAN. 1
ROTOR CHAN. 2
ROTOR CHAN 3
WIND SPEED 58 M
WIND DIR.
BLADE PITCH ANGLE
ROTOR SHAFT TORQ.
RPM GEN.
FORCE PITCH REG. a.
FORCE PITCH REG. b.
NAC. POS.
KW
KVAr
VOLT
AMP
ACC NS
ACC WE
PRE-AMPL.
PRE-AMPL.
PRE-AMPL.
Zero
SLIP RING 10
SLIP RING 9
SLIP RING 8
SLIP RING 7
D-A CONVERT
12.5Ω
1.25Ω
1 2 3 4
7-8 9-10 11-12 13-14 19-20 21-22 23-24
40 CORE CABLE
NACELLE
TOWER
1 2 3 4 5-6 7-8 9-10 11-12 13-14 19-20 21-22 23-24 P Q E I
22Ω 22Ω 22Ω 10Ω 25Ω 25Ω 10Ω
PATCH PANEL
1 16 2 3 4 5 6 7 9 10 11 12 13 14 15 NS WE
X
Y
RC-LINK T~100S
RC-LINK T~100S
XY-PLOTTER
1 2 3 4 5 6
BRUSH PLOTTER
X = SHUNT RESISTANCE
o = BNC PLUG
220 V POWER SUPPLY
220 V

Figure 1.1

Fig. 1.2 shows the rotor channels available. Sections numbered A1 to A4 are sections on mod A blades instrumented for measuring bending moments (indicated by S) or strains (indicated by T).

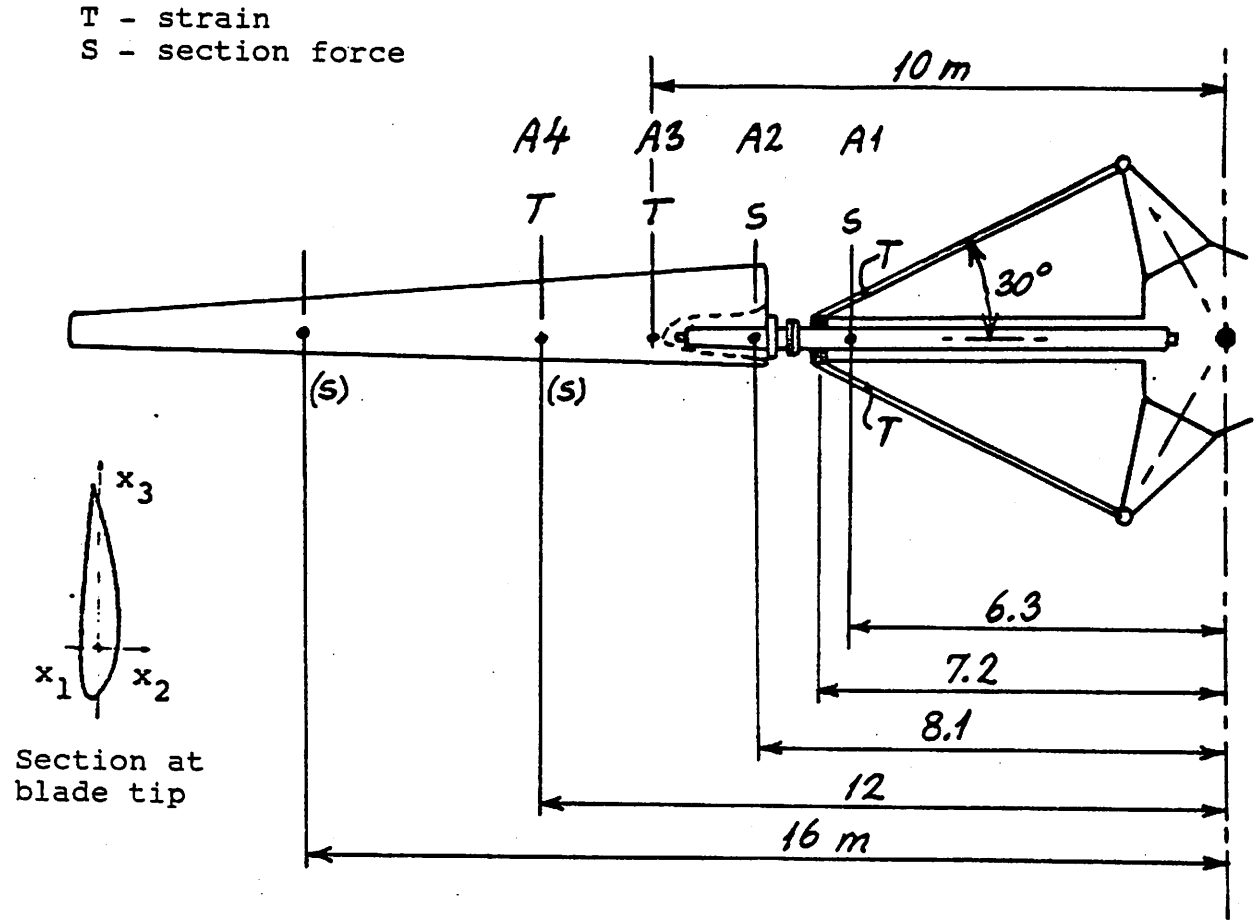

Figure 1.2

The xy-plotter is intended to give a preliminary power curve and is therefore usually permanently coupled to the wind speed and electric power channels in a mode where it plots a point every half minute. In order to simulate time-averaging in a simple manner the channels are connected to the plotter through RC-links having a time constant of approx. 100 s. Thus, excessive scatter of the points is avoided. Due to the voltage divider effects of the RC-links the plotter had to be calibrated by known voltages.

The Brush writer sentivities have been calibrated by applying known voltages. Otherwise the operational parameter signals have not been calibrated in this context; instead the calibration constants given by the operators of the turbine have been adopted in the determination of conversion factors for the preliminary measurement system. Conversion factors for the rotor channels are based on laboratory tests (ref. 1.1) conducted as part of the measurement program described in ref. 1.2. The accuracy of the results based on strip chart readings is estimated to be 5-15%. The Brush writer is able to resolve frequencies correctly up to at least 10-20 Hz.

The measurement procedures are very simple: Reconnecting channels to the brush writer using the patch panel including resetting of zero and sensitivities on the writer is accomplished in a few minutes. Reconnecting the rotor channels in the hub takes less than 30 minutes including readjustment of zero settings of the strain gauge preamplifiers. Coordination of the measurements with the operation of the turbine is performed by telephone contact with the people operating the turbine from the nacelle.

For the operational parameter signals zero voltage corresponds to a known absolute value, so that interpreting the resulting curves poses no problems. This is not the case for the rotor channels, as described in detail in refs. 1.3 and 1.4. In this presentation the rotor channel signals are referred to a zero that is obtained as the average of the max and min values of the signal during a slow revolution at the start of the turbine.

2. SURVEY OF MEASUREMENTS

Following the installation and running-in of the system four campaigns have been made as per primo April 1980. The measurement system has been used by Risø National Laboratory and by the Deparment of Fluid Mechanics of the Technical University Denmark, ref. 2.1. Some results from ref. 2.1 are included in this presentation.

In Table 2.1 the campaigns are listed and their primary aims are indicated. The rotor channel combinations available are also indicated. During each campaign a variety of operational parameters were recorded partly as aids in the commissioning of the turbine and partly as preliminary checks on the calculations of the response of the turbine. Table 2.2 shows the rotor channel combinations.

The results and conclusions in this presentation are based on records made during these four campaigns.

Campaign No	Date	Rotor Channel combination	Purpose
1	30.1.80	1	First indication of out-of-plane blade loads
2	13.2.80	1	Check of blade pitch regulation - - tower resonance
3	27-28.2.80	1	Investigation of blade pitch angle influence on blade loads and power production (ref.2.1)
5	5-6.3.80	2-4	Investigation of blade loads.

Table 2.1 List of campaigns Jan.-Mar. 1980.

Rotor channel combination	Rotor channels available
1	Out-of-plane bending moments at station A2 for all 3 blades
2	Out-of plane bending moments at station A1 for 2 blades. Force in one in-plane stay.
3	In-plane bending moments at station A1 for all 3 blades
4	In-plane bending moment for 1 blade. Forces in adjacent in-plane stays

Table 2.2 Rotor channels available

3. RESULTS

The results given in this section are recorded by the instrumentiation shown in Fig. 1.1. In Section 3.2 some results are shown, that have been obtained by means of an FFT analyzer plugged in on the patch panel. The analyzer is a Hewlett Packard 3721A that performs an actual analysis in a chosen period of time, extracting all frequencies simultaneously.

3.1. Location of sensors on the rotor.

Figure 3.1 shows the root of the outer blade and the trunnion on which it is mounted. The trunnion is shown in Fig. 3.2 together with the blade shaft. The shaft is supported by a bearing, mounted in a bearing house at the end of a tube and supported by two struts in the rotor plane and one strut out-of-plane. The figure shows the instrumented sections for which results are shown in the following sections. The strain gauges in Section A of Fig. 3.2 give flapwise bending moments used in Sections 3.3 and 3.4 of this paper. The strain gauges in Section B give flapwise bending moments used in Section 3.4 as well as chordwise bending moments shown in Section 3.5 of this paper. The struts are also equipped with strain gauges giving the tensile forces used in Section 3.5.

3.2 Determination of the tower eigenfrequency

The tower eigenfrequency has been determined by recording accelerations of the wind-induced vibrations of the tower top as well as by recording the accelerations during the upstart of the mill and identifying the resonance point.

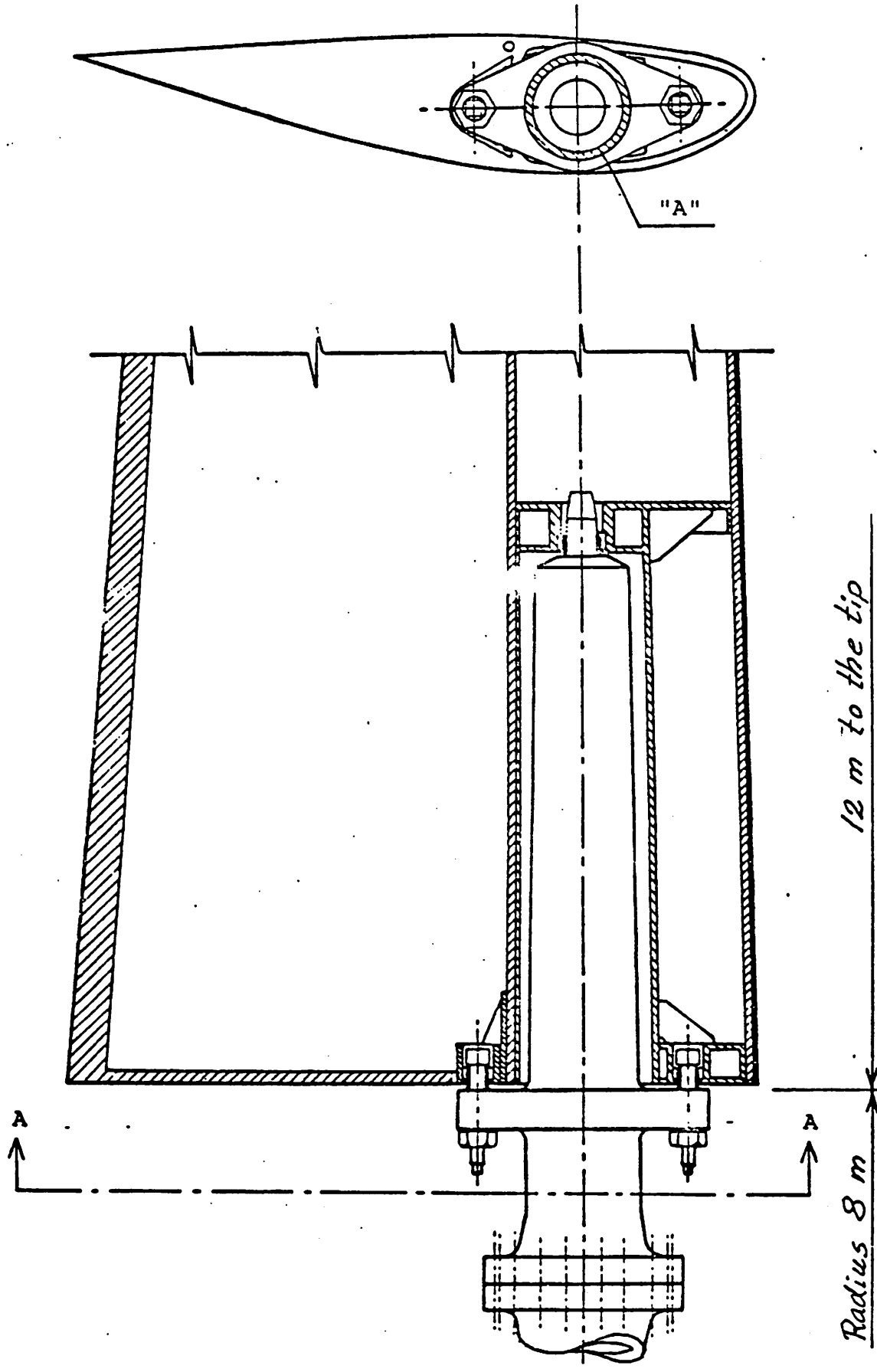

The glass-fibre wing mounted on the trunnion

Figure 3.1

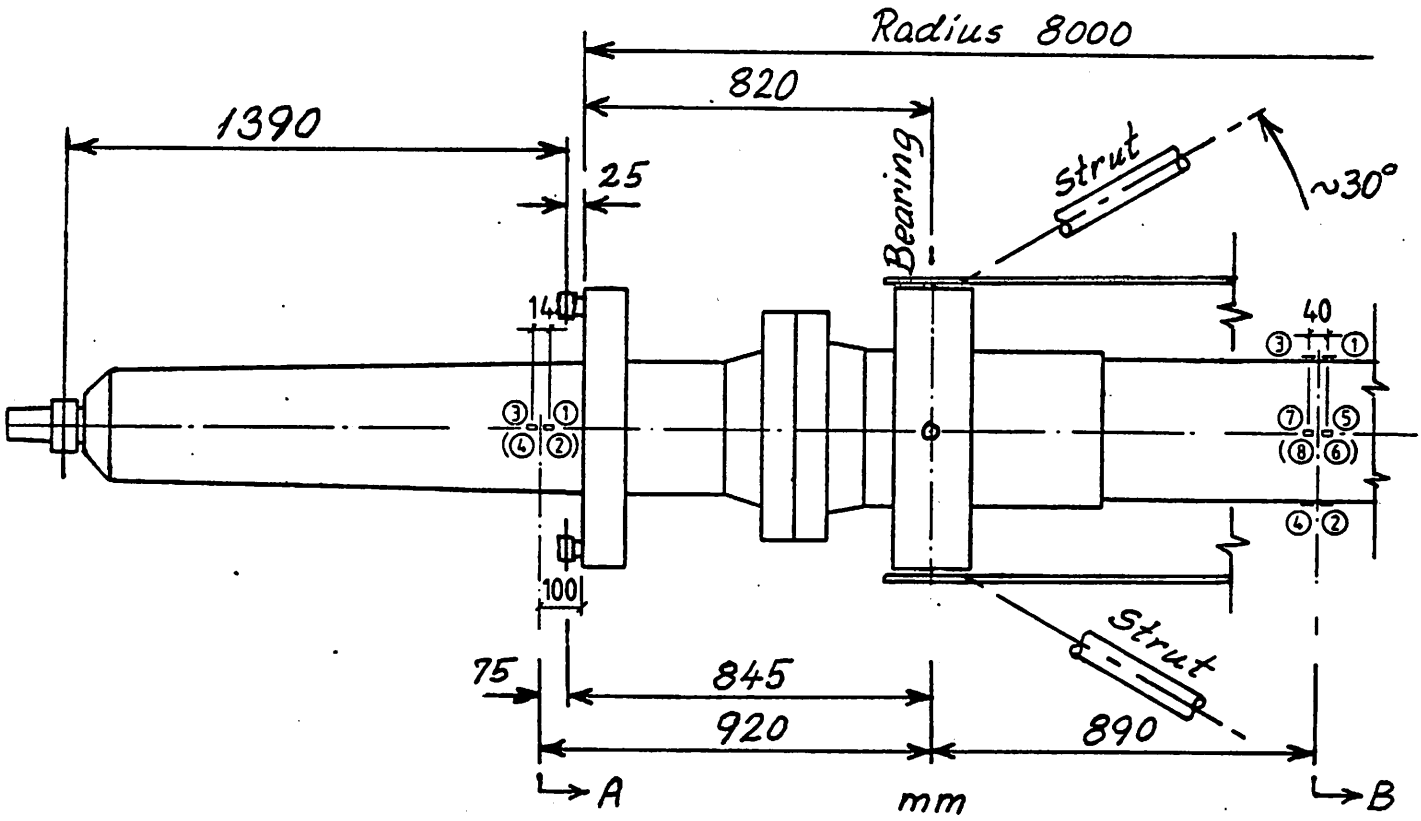

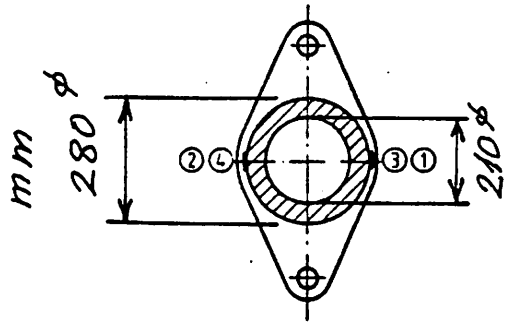

Section A
Trunnion

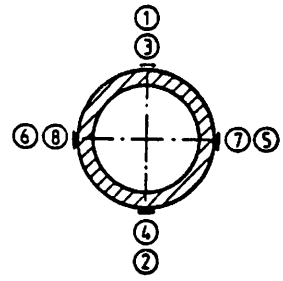

Section B
Shaft

Figure 3.2

Figure 3.3 shows time tracks of both north-south (NS) and west-east (WE) acceleration components recorded with the stopped rotor. Thus the vibrations are wind induced, and by measuring the time between tops as indicated in the figure, frequencies of 1.29 Hz and 1.34 Hz are found for the NS and WE directions, respectively.

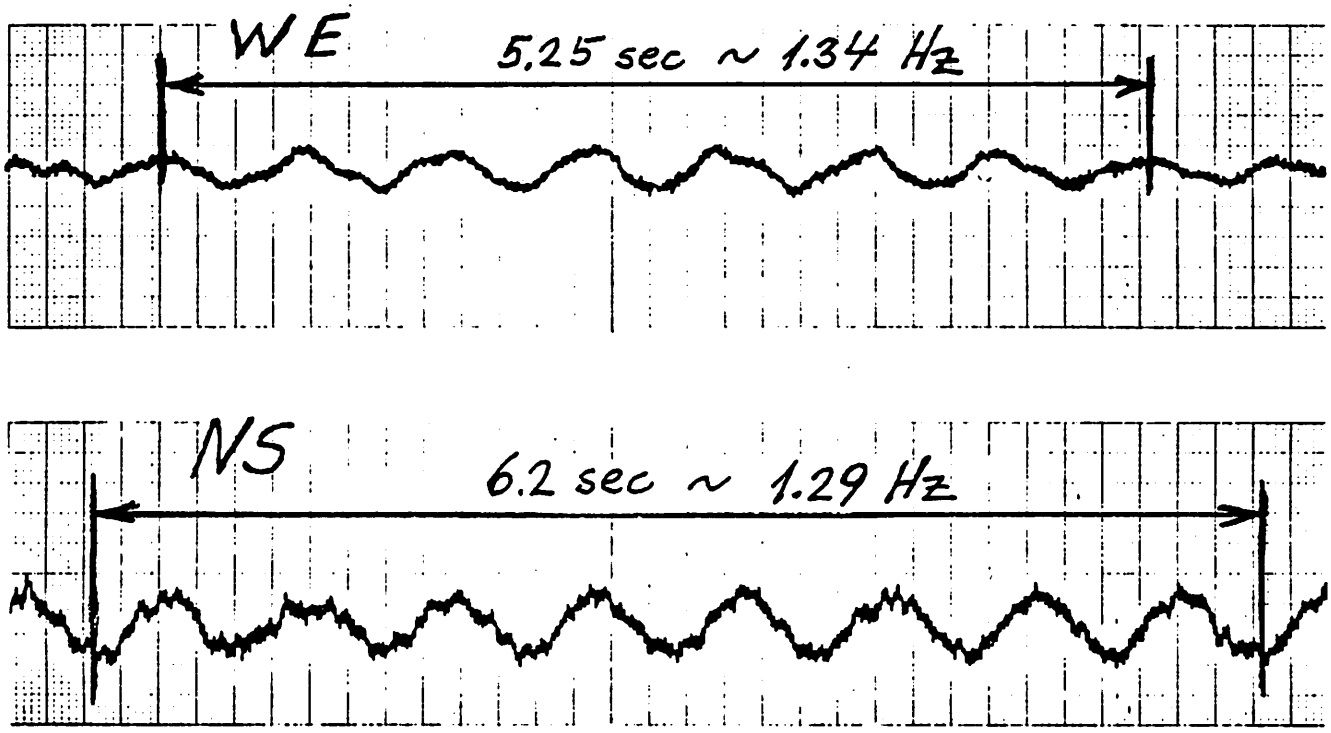

Figure 3.3

Figure 3.4 shows corresponding time tracks during a start-stop sequence. As indicated in the figure a resonance occurs at 1215 RPM on the generator shaft, corresponding to 27 RPM on the rotor shaft or 0.45 Hz. At this speed the blade passage frequency is $3 \cdot 0.45 = 1.35$ Hz.

Figure 3.5 shows the calculated values as given by the tower designer in October 1978. The calculated value 1.28 Hz is confirmed by the measurements, considering the accuracy level of this preliminary instrumentation. The signal level of the accelerometers ($\sim \pm 0.1$ V) was too small for the FFT analyzer, and therefore the eigenfrequency could not be determined by the frequency analyzer which was available.

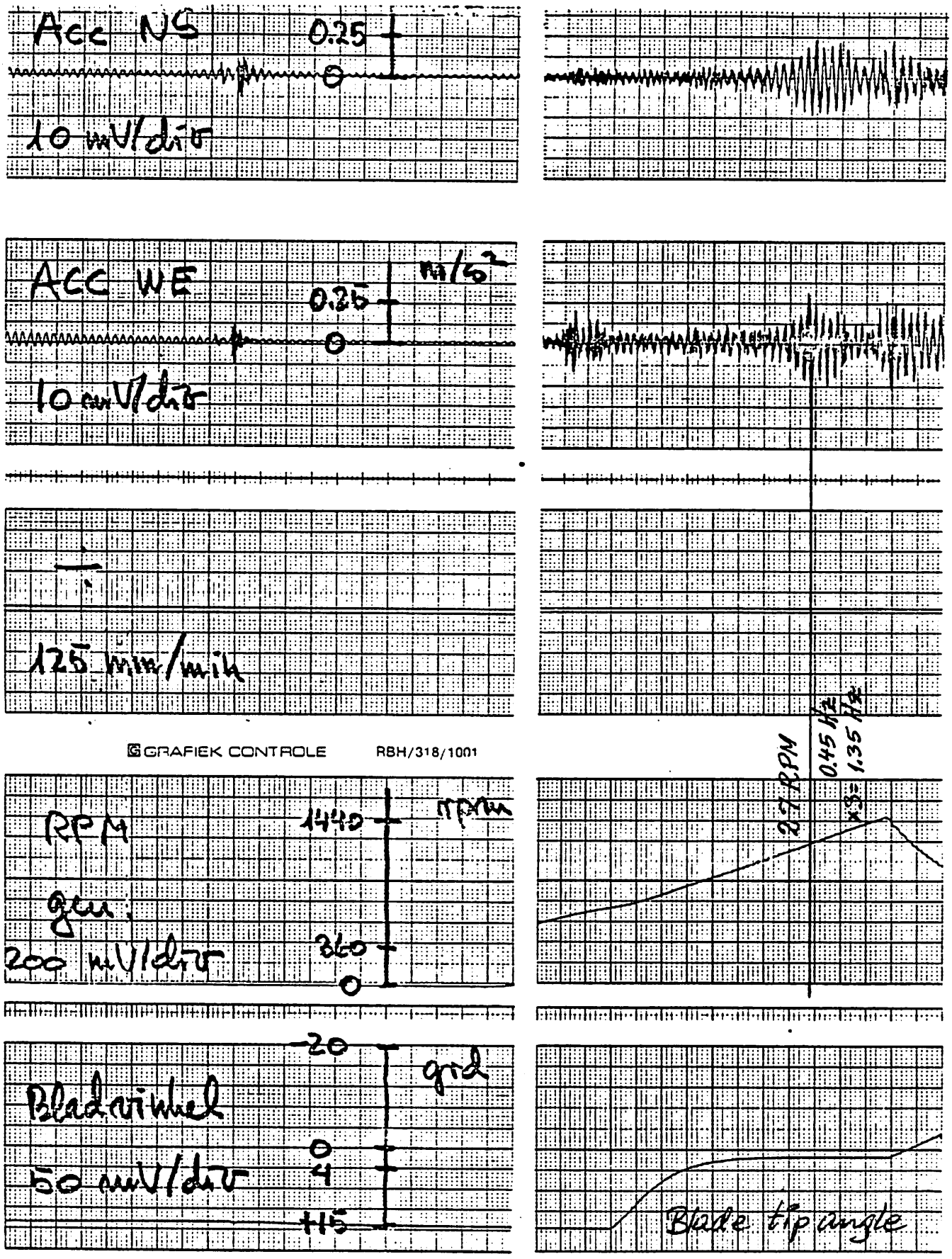
Acc NS
0.25
0
10 mV/div
Acc WE
m/s²
0.25
0
10 mV/div
125 mm/min
GRAFIEK CONTROLE
RBH/318/1001
RPM
1440
rpm
gen.
200 mV/div
360
0
27 RPM
0.45 Hz
x3= 1.35 Hz
-20
grd
Bladwinkel
50 mV/div
0
4
+15
Blade tip angle

Figure 3.4

B. Højlund Rasmussen, rådgivende civilingeniører | Sag nr. 1496 | Udarb. S-Y | Kontr. | Dato 19/10-78

mode shapes (max amplitude = 1000)

mode no	1	2	3	4	5
mode no.	u_x	u_x	Θ_z	u_z	u_x
1	1000	-684	1000	1000	-395
2	884	-221	968	926	850
3	702	266	835	894	811
4	627	645	712	863	1000
5	508	892	599	824	831
6	398	1000	494	780	413
7	299	978	397	733	-95
8	212	856	307	681	-535
9	139	662	224	627	-788
10	80	438	148	570	-800
11	36	222	79	510	-580
12	4	28	5	438	-106
13	0	0	0	335	0
Frequencies	1,28	7,00	9,93	13,3	16,4
	bending		torsion		bending

Figure 3.5

3.3. Determination of frequencies of the stationary rotor

The frequencies were determined by a series of tests in which one of the blades was bent by pulling the tip towards the tower and releasing it. The signals from the strain gauges on the trunnion (section A in Figure 3.2) was used, and the first 10 to 15 secs were recorded and analyzed. A typical record is shown in Fig. 3.6. All three blades were successively exited, and FFT analysis was made of signals from the exited blade as well as from the other blades.

Figure 3.7 shows a typical output from the FFT analyzer. In the range 1.9- 2.3 Hz, three peaks are appearent, and a fourth one may be identifyed above 3 Hz.

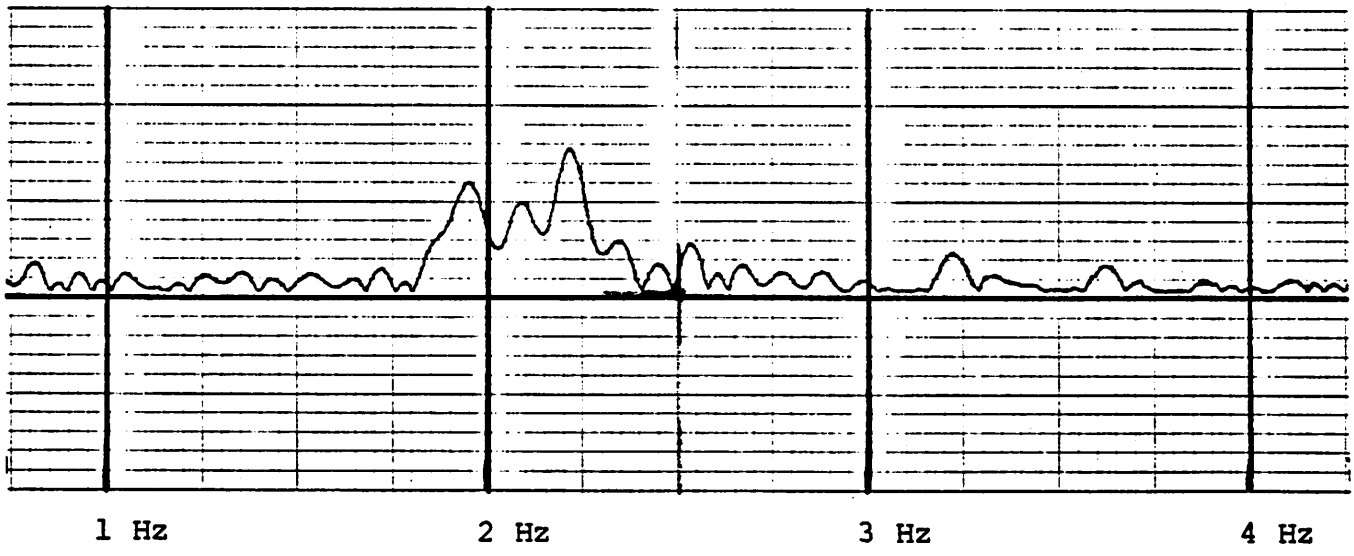

Figure 3.7

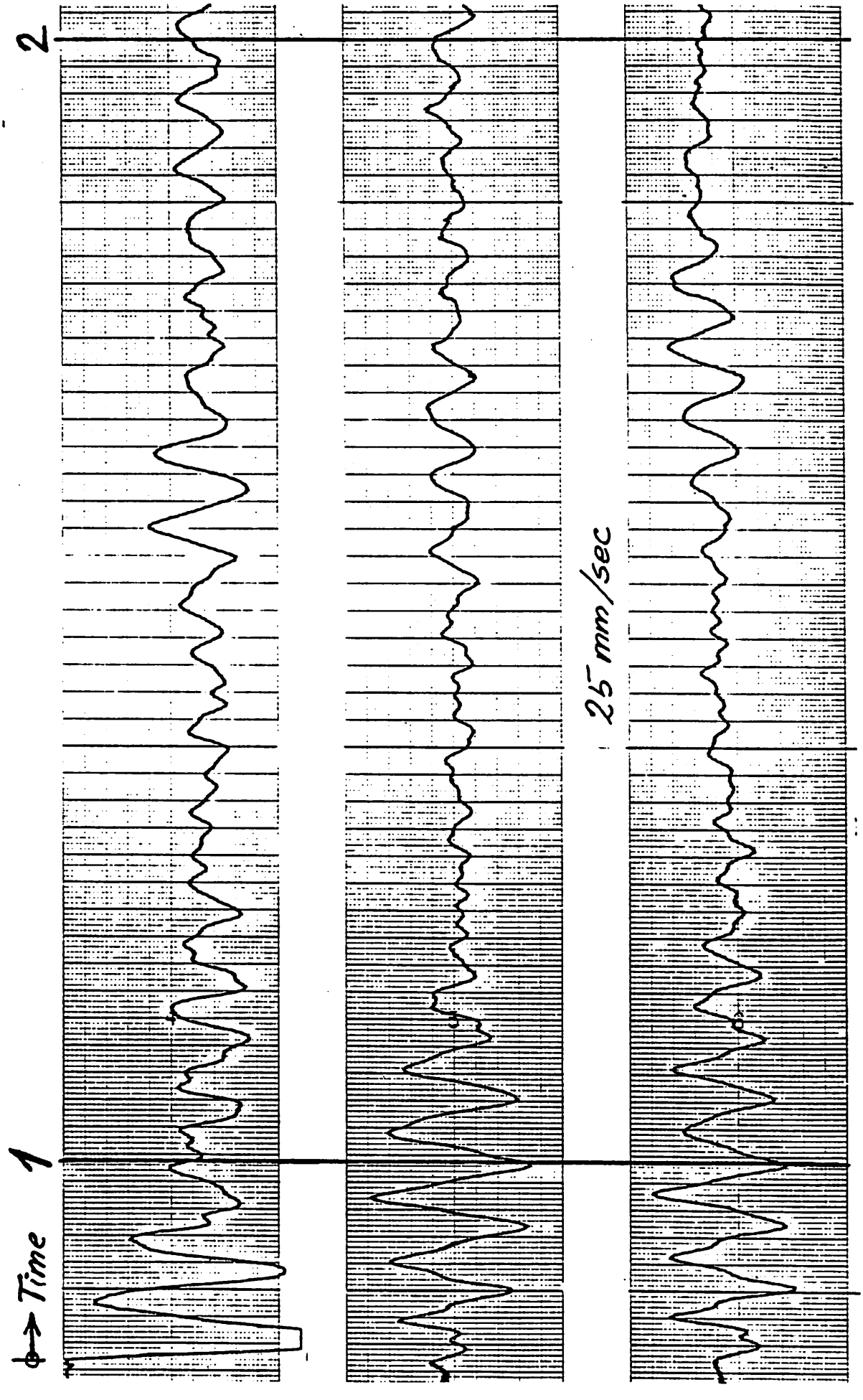

Figure 3.6

Figures 3.8a - 3.8c shows plots of calculated eigenmodes for the stationary rotor, ref. 3.1, Table 3.1 indicates the corresponding eigenfrequencies according to the latest calculations together with the eigenfrequencies determined on the basis of a series of 18 runs with the FFT analyzer.

Mode	Calculated Hz	Measured Hz	
1	1.99	1.95 ± 0.04	RMS
2	1.99	2.12 ± 0.04	-
3	2.12	2.24 ± 0.03	-
4	3.33	3.44 ± 0.03	-

Table 3.1 Rotor eigenfrequencies

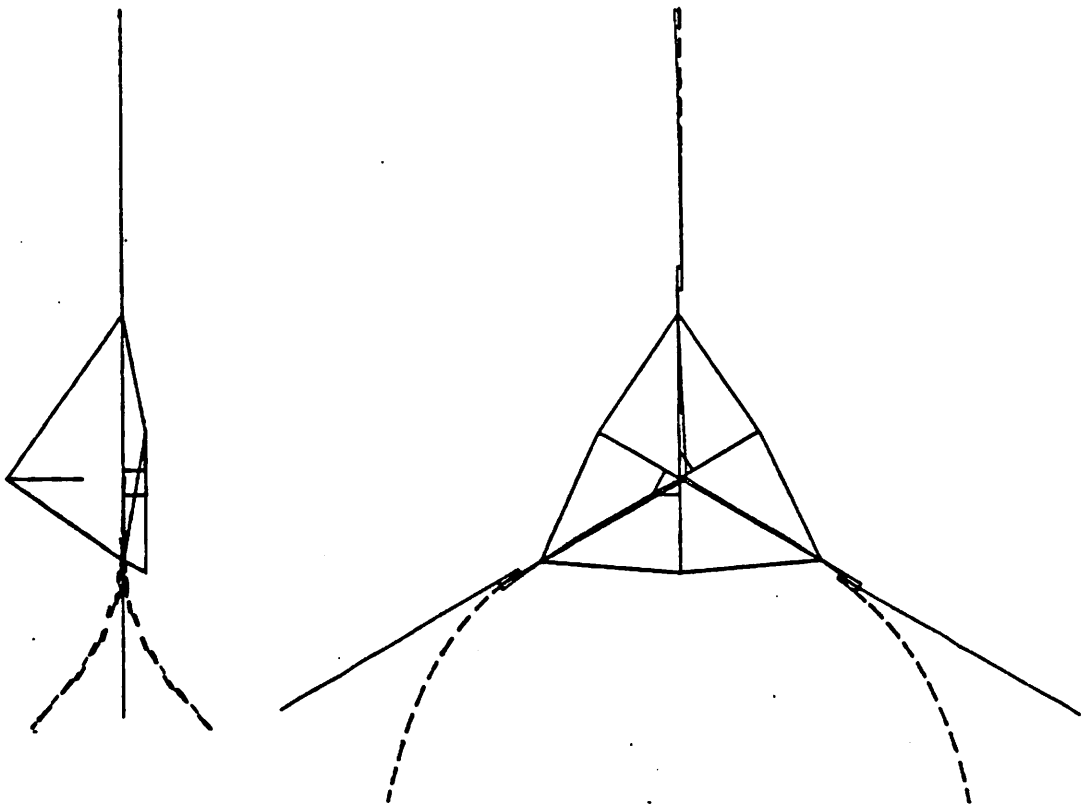

Mode 1

Figure 3.8a

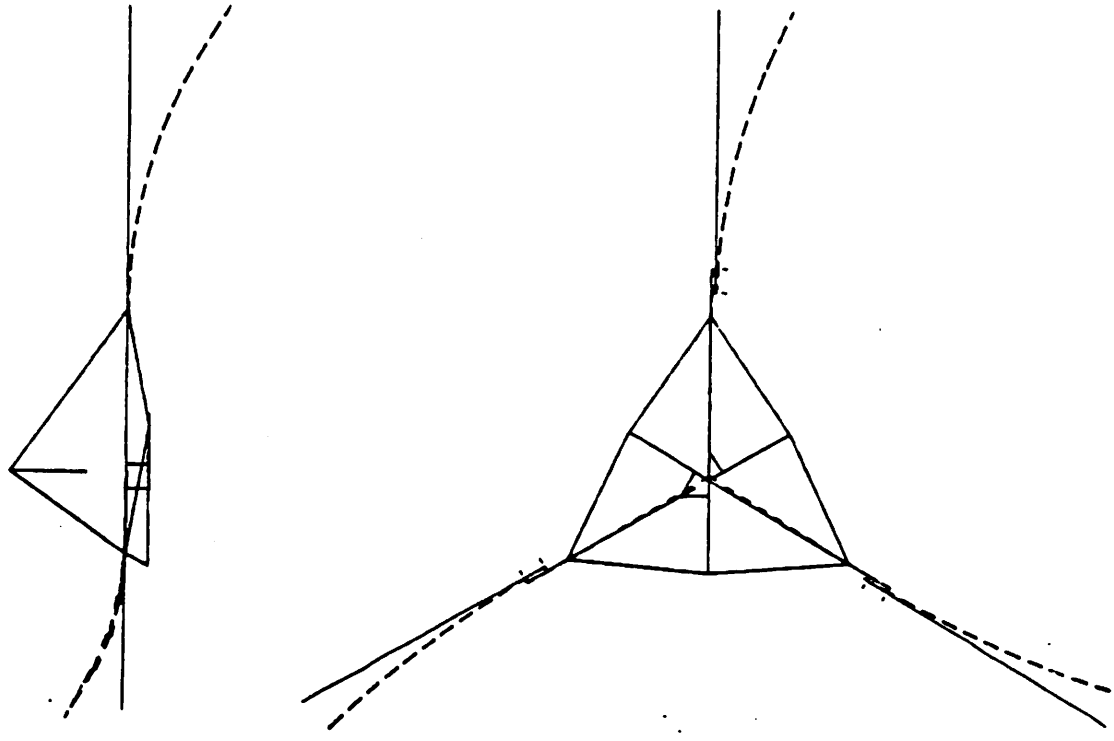

Mode 2

Figure 3.8b

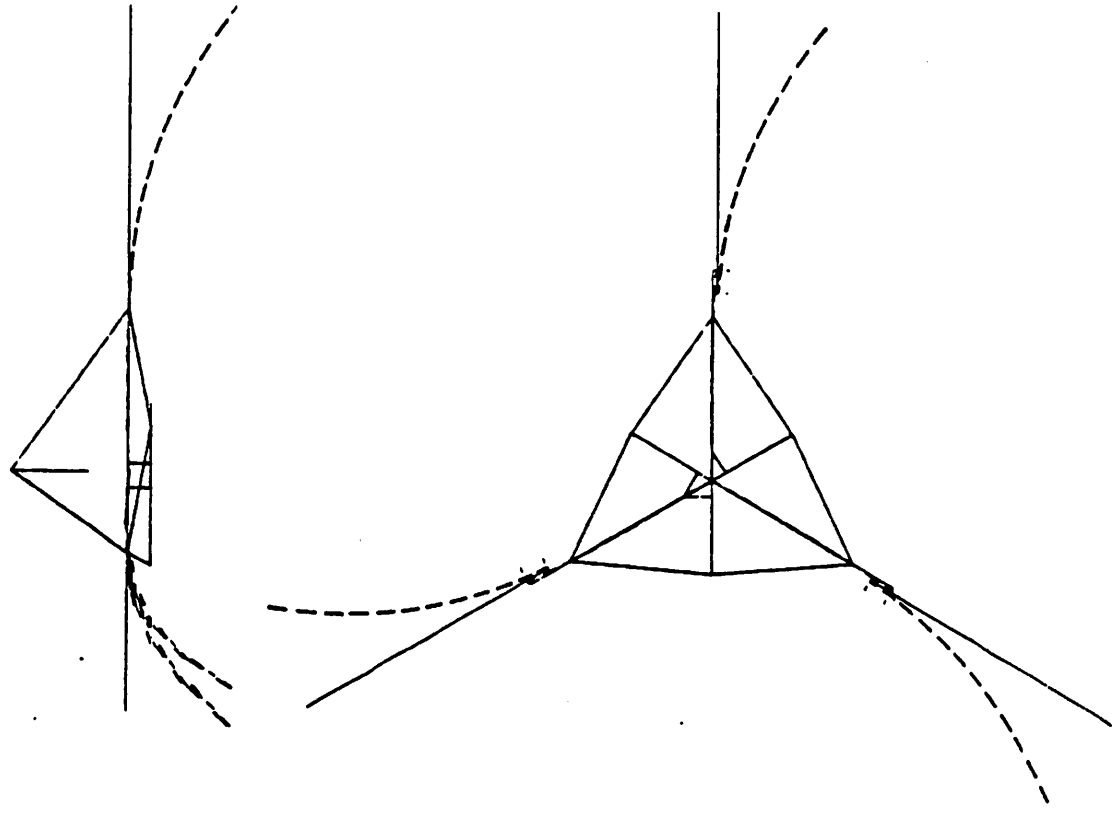

Mode 3

Figure 3.8c

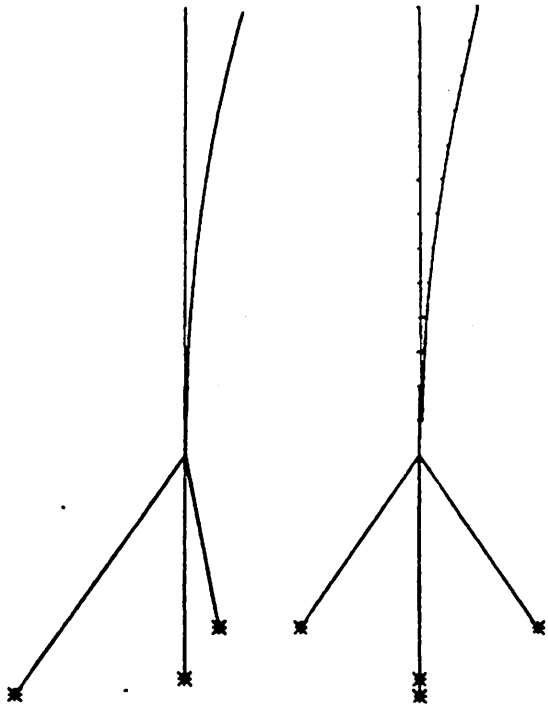

2.12 Hz

Figure 3.9a

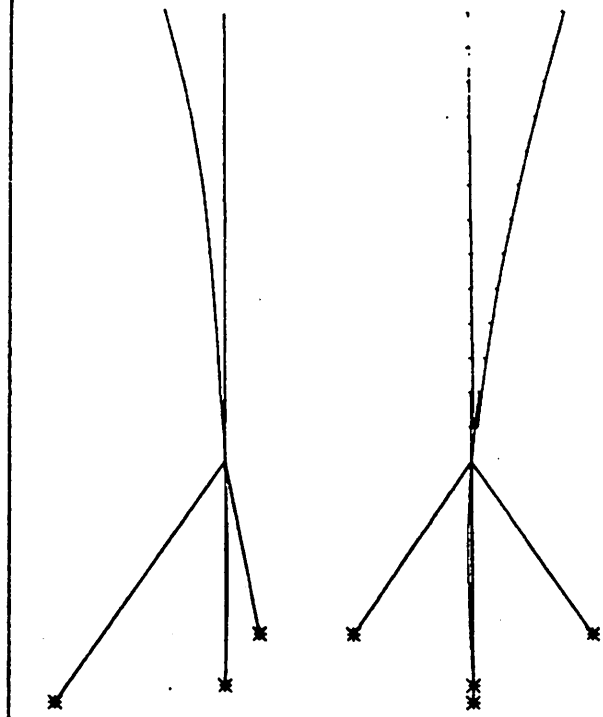

3.33 Hz

Figure 3.9b

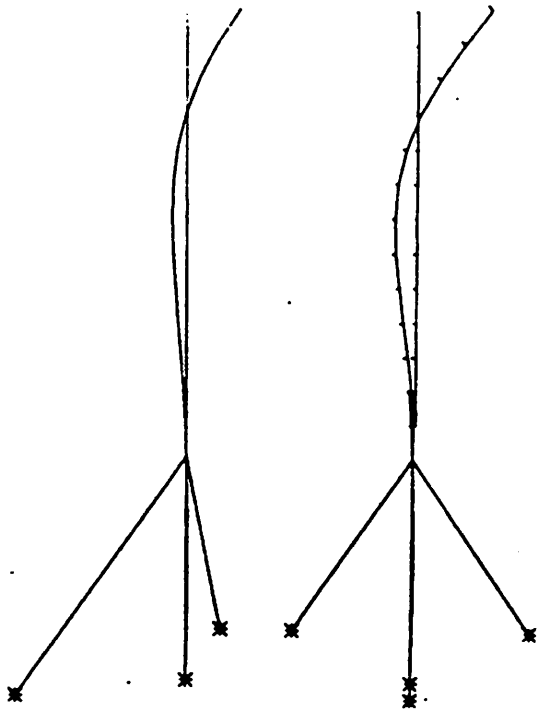

Flapwise Chordwise

6.37 Hz

Figure 3.9c

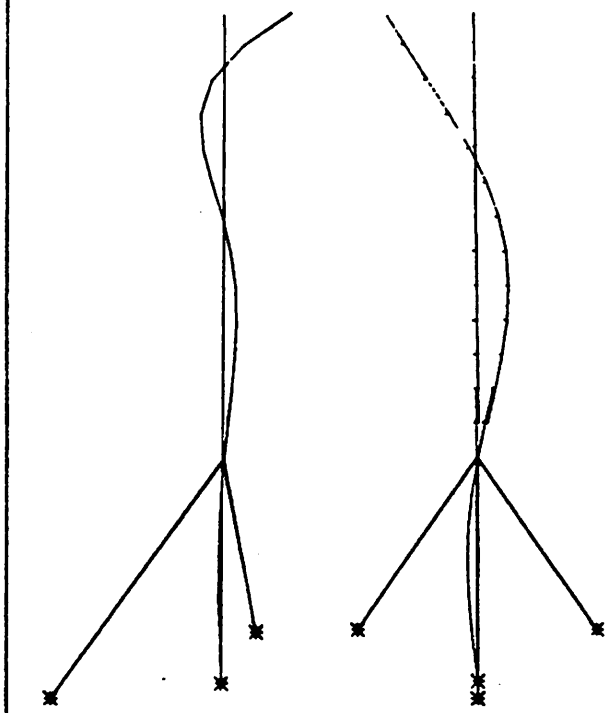

Flapwise Chordwise

12.8 Hz

Figure 3.9d

The fourth calculated eigenfrequency corresponds to the eigenmode shown in Fig. 3.9b, calculated for a single blade. The calculated frequencies are within 10% of the measured values.

The uppermost time track of Fig. 3.6 is the signal from the excited blade. At the time indicated by 1 the excited blade has a phase lag of 180 deg to the two other blades, indicating that mode 2 is predominant. After approx. 10 secs at the time indicated by 2 one blade is almost stationary while the two others are in phase, indicating that mode 1 now is predominant.

3.4. Flapwise bending moments during operation

Figure 3.10 shows records of the flapwise moments at section A, Fig. 3.2, during a normal stop at low wind speed. The dominant feature is the pronounced peak occurring when the stop sequence is initiated. From an average of approx. 44 kNm and an amplitude of approx. 23 kNm the level rises to about 95 kNm with a peak to about 140 kNm. This is due to the pitching of the blades during a normal stop gradually through maximum C_L-values to the stalled condition over a period of approx. 5 secs. This load cycle is experienced once during each stop. This occurs each time the turbine attempts to start in low wind and fails to connect to the grid.

It appears from Fig. 3.11, where a stop from approx. 13 m/s is shown that the peak of Fig. 3.10 does not occur. However, the average level of ∿ 95 kNm corresponds to the average level during the stop (Fig. 3.10) as the blade is already partly stalled at this condition. Therefore the peak of 130 kNm may be caused by dynamic amplification. It causes a stop from low winds to be more severe for flapwise bending than a stop from high winds.

Figure 3.12 shows records similar to those in Fig. 3.10, but taken from the flapwise sensors at section B, Fig. 3.2. Again the pronounced rise in level during the stop sequence from low speed is seen, but the peak is not so pronounced. From a level of ∿ 30 kNm and an amplitude of ∿ 24 kNm the level rises to ∿ 88 kNm with a maximum of ∿ 110 kNm.

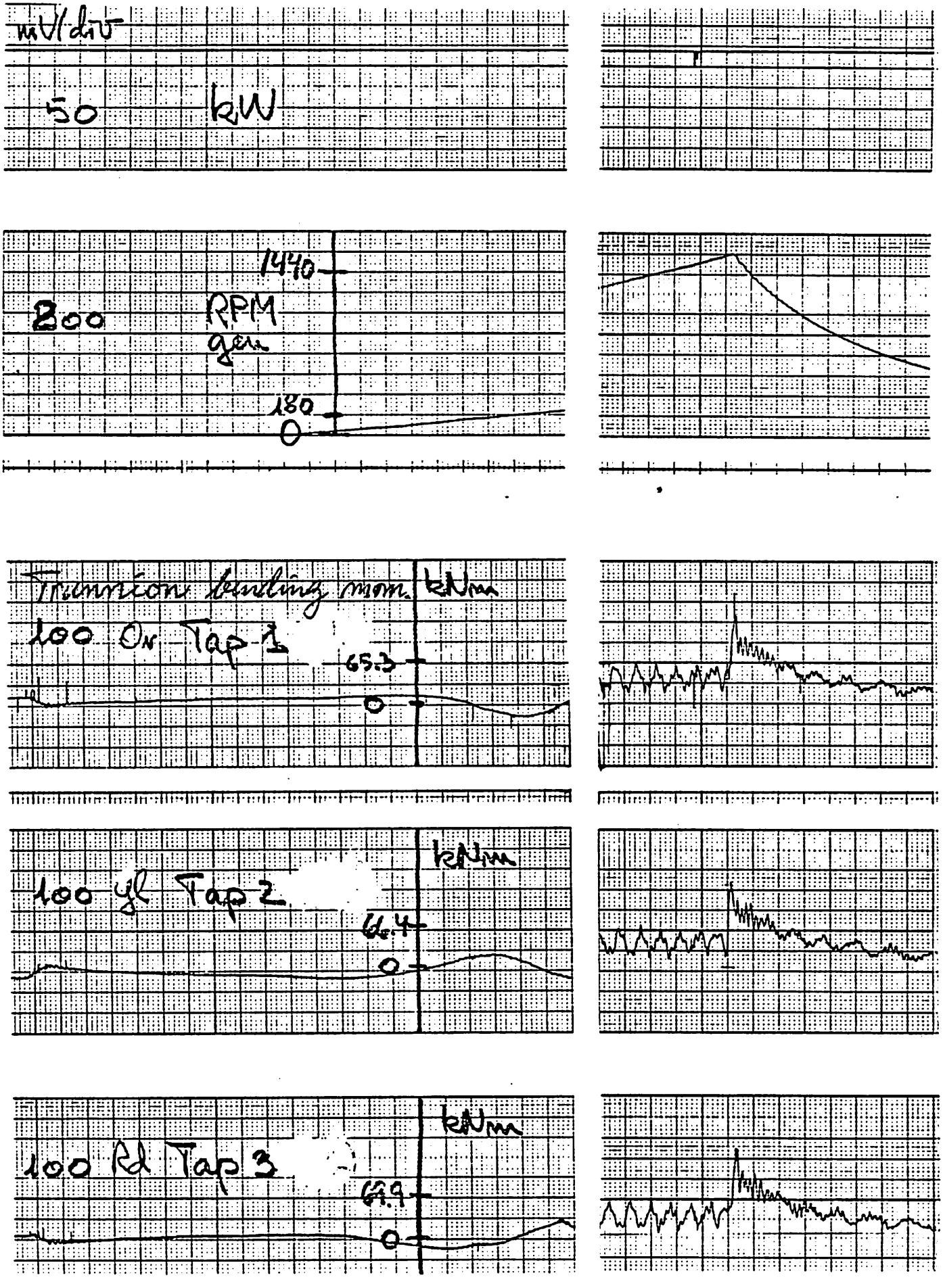
mV/div
50
kW
1440
800
RPM
gen
180
0
Trunnion bending mom.
kNm
100 Or Tap 1
65.3
0
kNm
100 yl Tap 2
64
0
kNm
100 Rd Tap 3
64.9
0

Figure 3.10

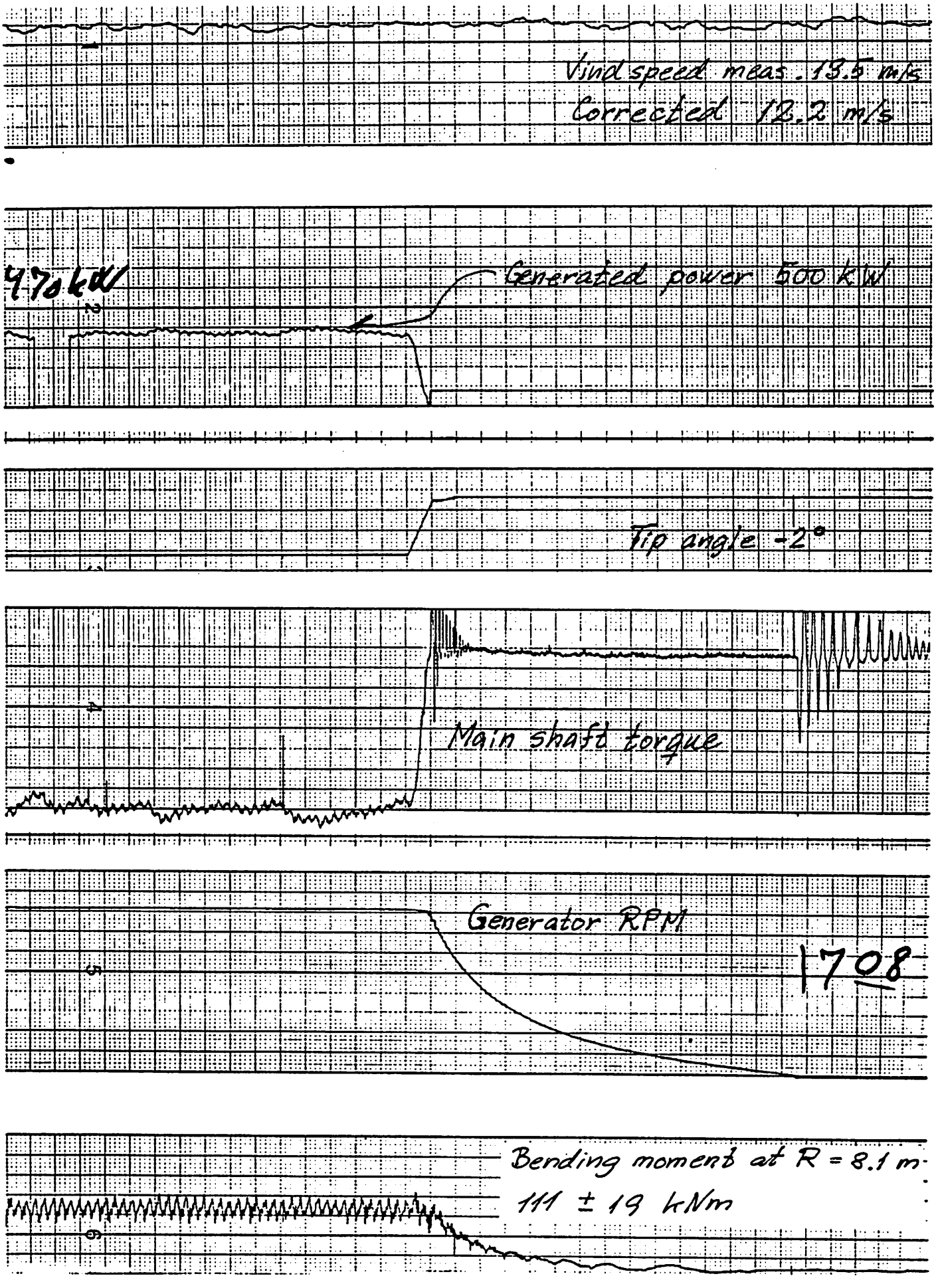
Vind speed meas. 13.5 m/s
Corrected 12.2 m/s
970 kW
Generated power 500 kW
Tip angle -2°
Main shaft torque
Generator RPM
1708
Bending moment at R = 8.1 m
111 ± 19 kNm

Figure 3.11

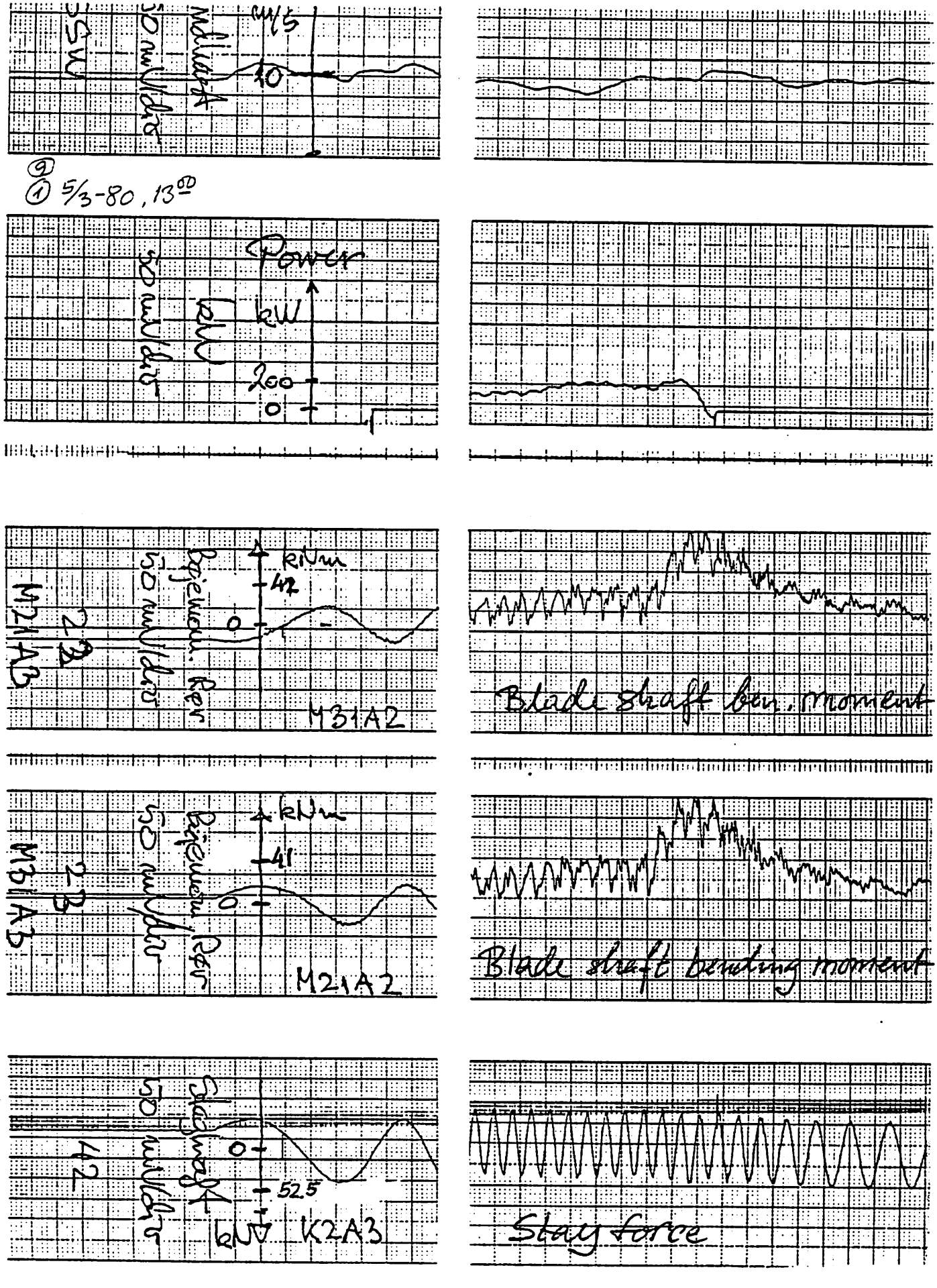
m/s
10
Power
kW
200
0
M31A2
M21A2
K2A3
Blade shaft ben. moment
Blade shaft bending moment
Stay force

Figure 3.12

Figure 3.13 shows the calculated flapwise bending moment distributions due to a triangular aerodynamic load (above) and the corresponding moments due to the centrifugal forces acting through the coning angle of the blade (below). By adding the centrifugal force moments at stations A and B to the levels of 95 kNm and 88 kNm, respectively, measured during stop, the moments 147 kNm and 141 kNm due to aerodynamic forces in station A and B, respectively, are obtained. This corresponds to the ratio 1.04 between the values indicated on the uppermost Fig. 3.13. Thus the computational predictions on which the design has been based are confirmed by the measurements.

Figure 3.14 shows the design spectrum calculated from wind speed statistics by the Department of Fluid Mechanics for the flapwise bending moments due to aerodynamic loads referred to zero radius. By referring the values of Figures 3.10 to 3.12 to zero radius one obtains an average of 364 kNm and an amplitude of 42 kNm. These values are within the values shown in Fig. 3.14 for $1 \cdot 10^8$ - $3 \cdot 10^8$ cycles corresponding to 42% of the operational life. The peaks of Figs. 3.10 and 3.12 referred to zero radius are $\sim$ 400 kNm, which are within the values given for cycles up to $6 \cdot 10^5$, corresponding to $< 1\%$ of operational life. Thus these measurements so far do not contradict the design assumptions.

3.5. Stresses in the trunnion and the shaft

The dimensions of the steel trunnion at station A Fig. 3.13, and of the shaft in the bearing, station C, are given in Fig. 3.15. The observed peak of the bending moment during stop, Fig. 3.10, is approx. 140 kNm, and the corresponding stresses are shown in Table 3.2.

Station	Moment of inertia 10^{-4} m^4	Eccentricity m	Stress MN/m^2
A, R = 8 m	2.15	0.14	91
C, R = 7.2 m	3.10	0.16	72

Table 3.2.

At station C the stress is superposed by a tensile stress due to the centrifugal force. This tension is ~ 6 MN/m^2. The material is St. 52-3 for which the yield stress is 350-400 MN/m^2.

3.6 Driving bending moments during operation

Figure 3.16 shows the driving moment at station B, Fig. 3.2, for one blade and the forces in the two adjacent in-plane struts during a normal stop sequence. The figure shows that gravity forces are entirely dominant and that a normal stop is undramatic, although the first in-plane mode (mode 4 of Table 3.1) of $\sim$ 3.4 Hz is excited when the generator is disconnected from the grid. The peaks on the trace for the main shaft torque are due to slack in the power train (cf. ref. 2.1).

Figure 3.17 shows in more detail the traces of the driving moments in all blades at station B, the moment M31A2 being shown 2½ times enlarged compared to the two others. The traces are basically sinusoidal, but clearly superposed by the fourth mode of Table 3.1 ($\sim$ 3.4 Hz in-plane). In addition to these oscillations the trace of M31A2 shows regular cusps at the bottom of each period. One month later this cusp has developed into the abnormal trace shown in Fig. 3.18, which indicates some mechanical problem, most probably in the bearing of that particular blade (cf. Fig. 3.2).

Figure 3.19 shows the predicted in-plane moment distribution due to gravity forces when the blade is horizontal. From Fig. 3.17 the amplitude 40 kNm is read, which corresponds well to the value shown in Fig. 3.19 for the gauge on the shaft.

From Fig. 3.16 the tensile forces 10 kN and 16 kN are found in the struts pointing forward and backwards, respectively, during a short period just before stop. This corresponds to a driving force of 3 kN at radius 8 m, which again corresponds to a rotor shaft torque of 72 kNm. This agrees well with the torque 76 kNm recorded for the torque in the shaft. By comparison with the recorded electric power of 190 kW the efficiency of the power train and generator at this power is 0.75.

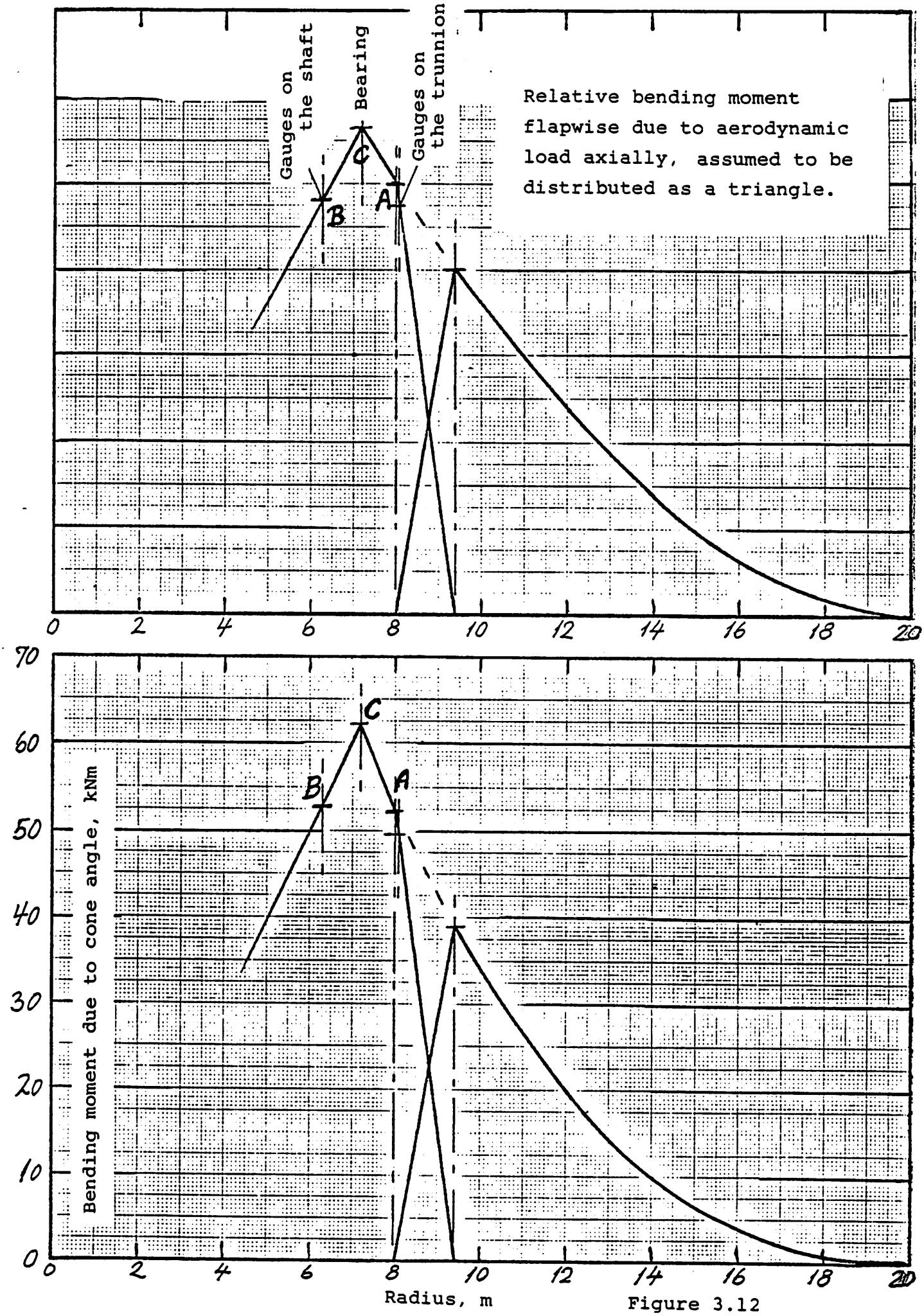
Gauges on the shaft
Bearing
Gauges on the trunnion
A
B
C
Relative bending moment flapwise due to aerodynamic load axially, assumed to be distributed as a triangle.
0
2
4
6
8
10
12
14
16
18
20
Bending moment due to cone angle, kNm
0
10
20
30
40
50
60
70
Radius, m

Figure 3.12

LASTSPEKTRUM, BLAD
DG-LIN-12
NACA4412-28 RU
V_T = 170 m/s
M_{x_2}
$M_{x_{2\phi}}$, $M_{x_{2n}}$, kNm
$M_{x_{2\phi}}$
$M_{x_{2n}}$
100
200
300
400
500
N

Figure 3.14

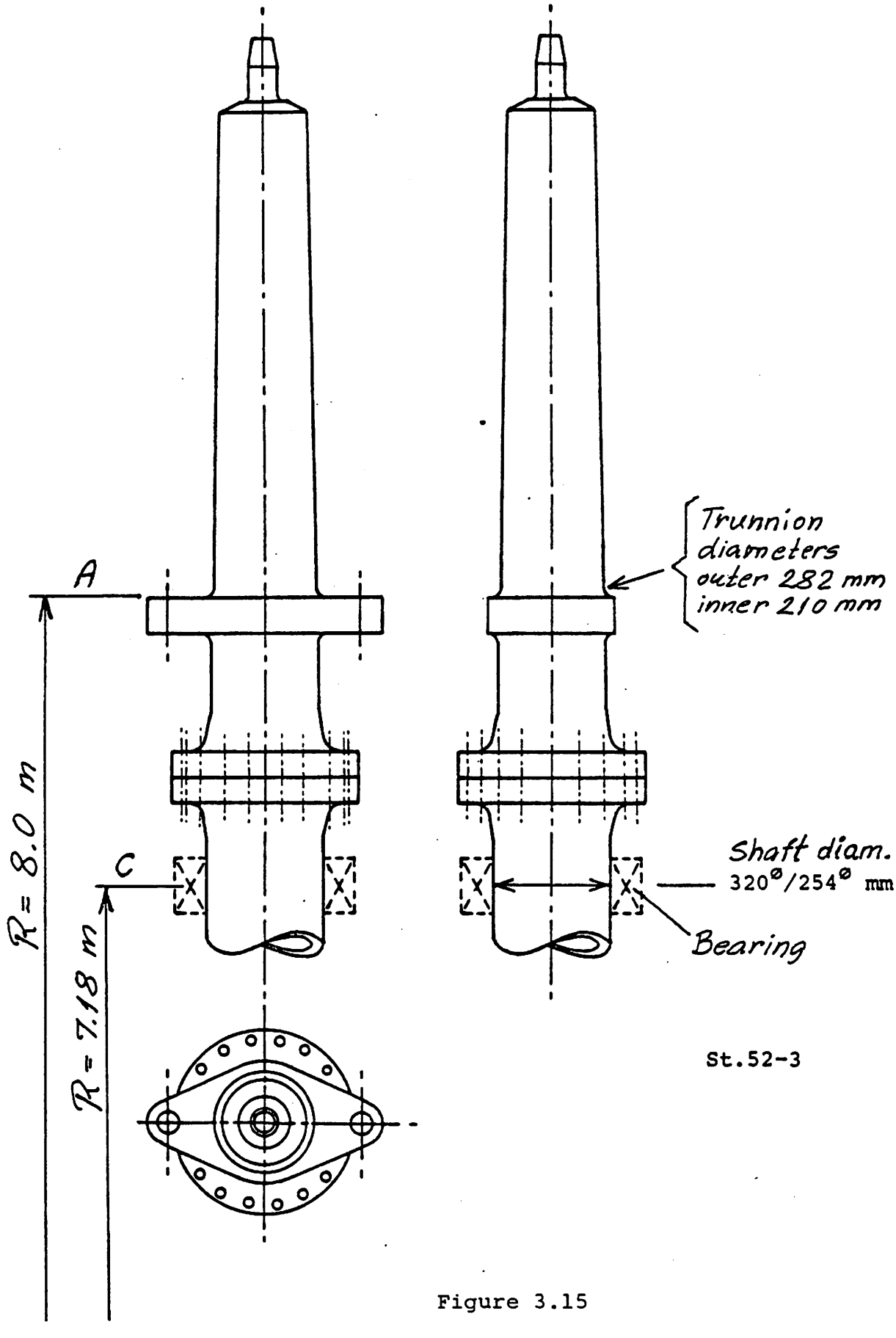
A
C
R = 8.0 m
R = 7.18 m
Trunnion
diameters
outer 282 mm
inner 210 mm
Shaft diam.
320°/254° mm
Bearing
St.52-3

Figure 3.15

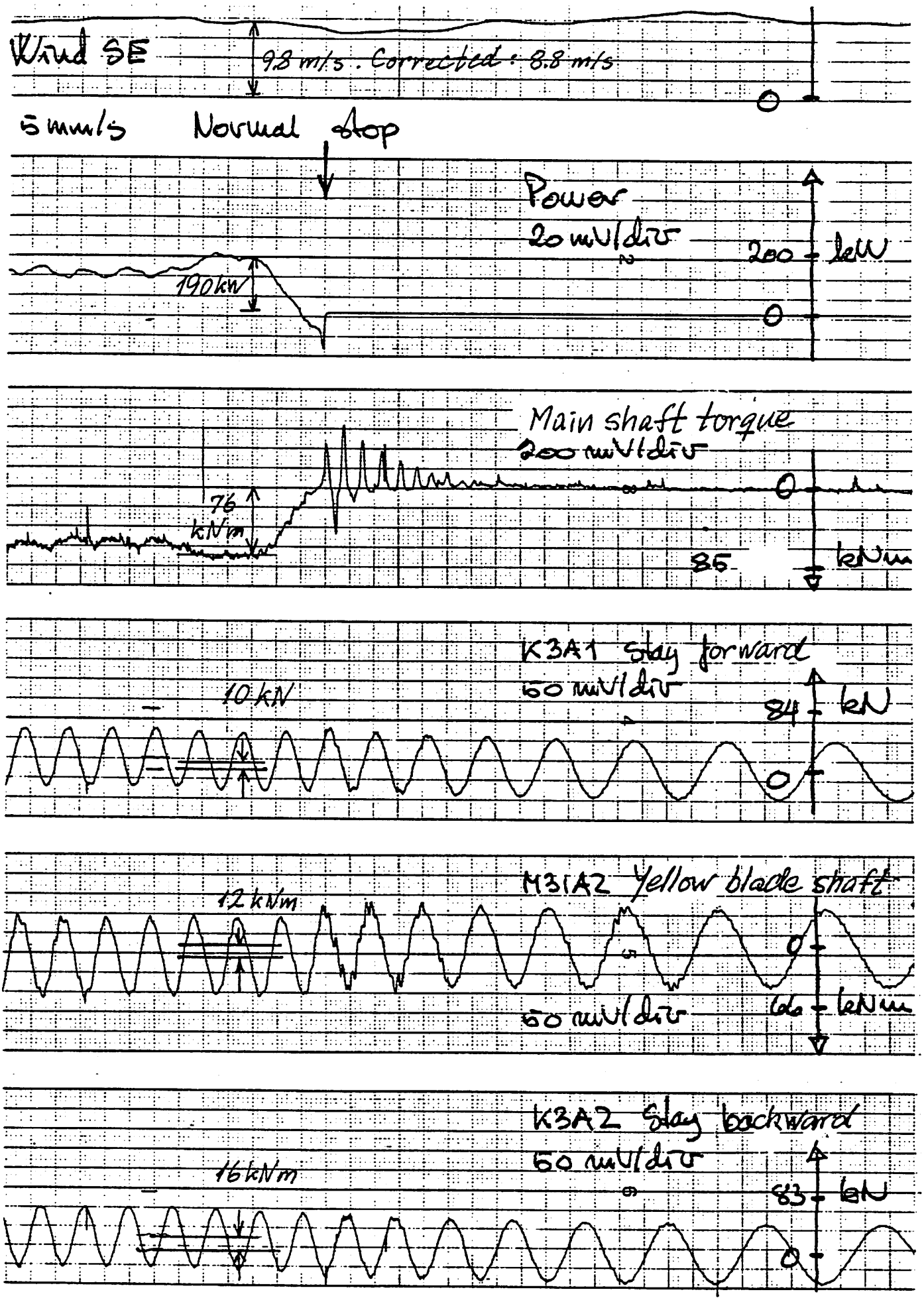
Wind SE
9.8 m/s . Corrected : 8.8 m/s
0
5 mm/s
Normal stop
Power
20 mV/div
200
kW
190kW
0
Main shaft torque
200 mV/div
0
76
kNm
85
kNm
K3A1 Stay forward
50 mV/div
84
kN
10 kN
0
M31A2 Yellow blade shaft
12 kNm
0
50 mV/div
66
kNm
K3A2 Stay backward
50 mV/div
83
kN
16kNm
0

Figure 3.16

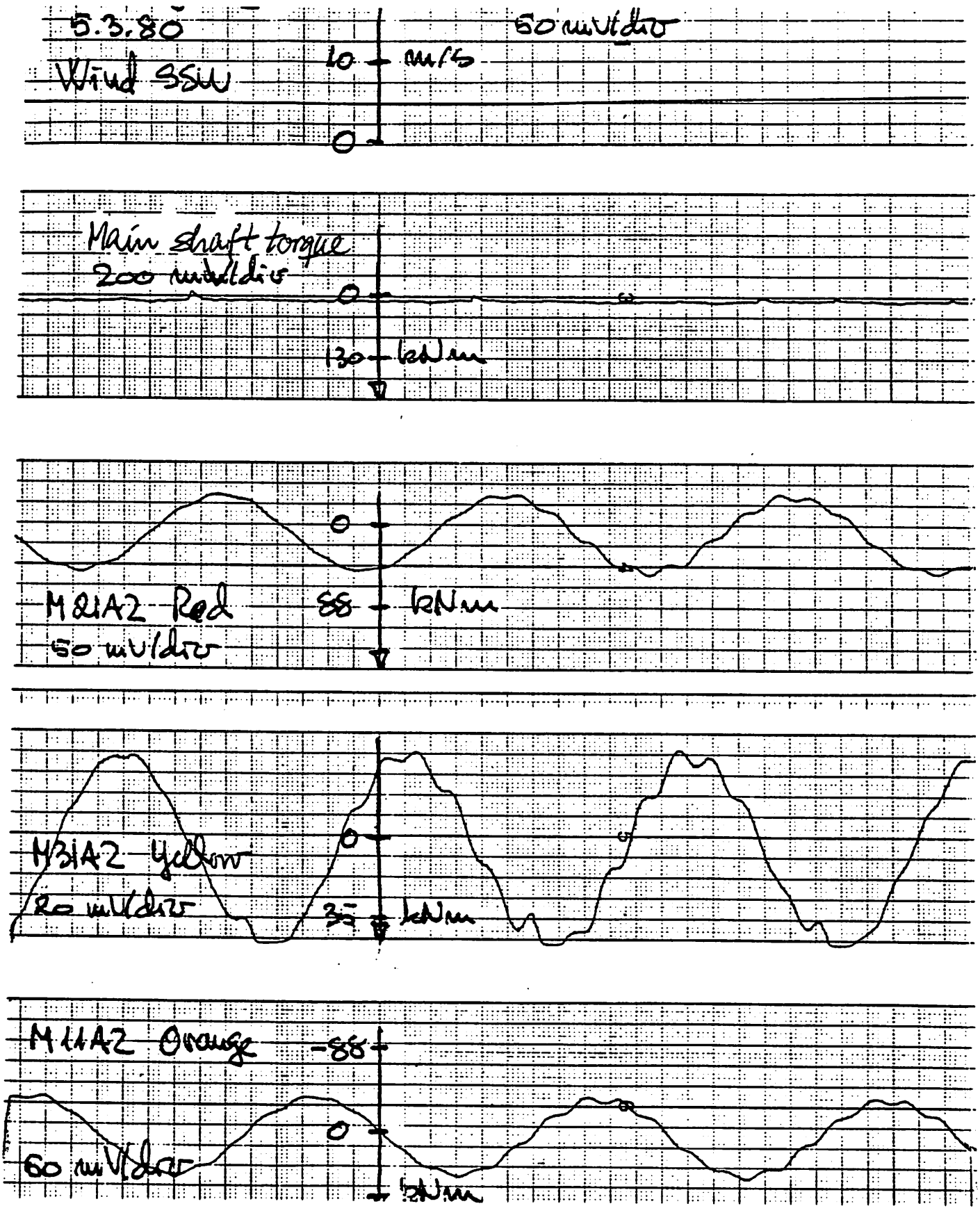
5.3.80
50 mV/div
Wind SSW
10
m/s
0
Main shaft torque
200 mV/div
0
130
kNm
0
M2A2 Red
50 mV/div
88
kNm
0
M3A2 Yellow
80 mV/div
35
kNm
M1A2 Orange
-88
0
60 mV/div
kNm

Figure 3.17

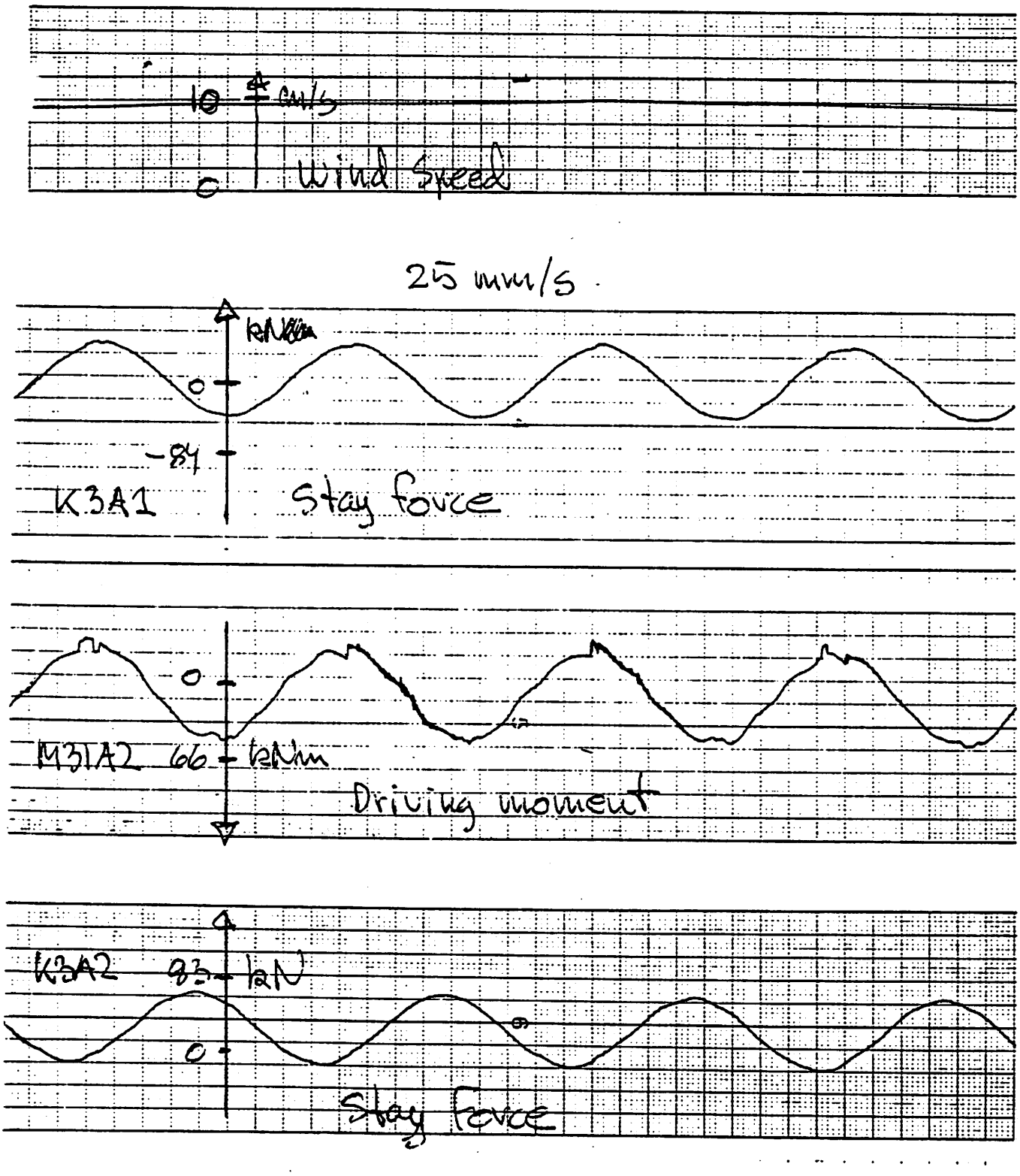
10 ± cm/s
0
Wind speed
25 mm/s
0
-84
K3A1
Stay force
0
M31A2 66
Driving moment
K3A2 93
0
Stay force

Figure 3.18

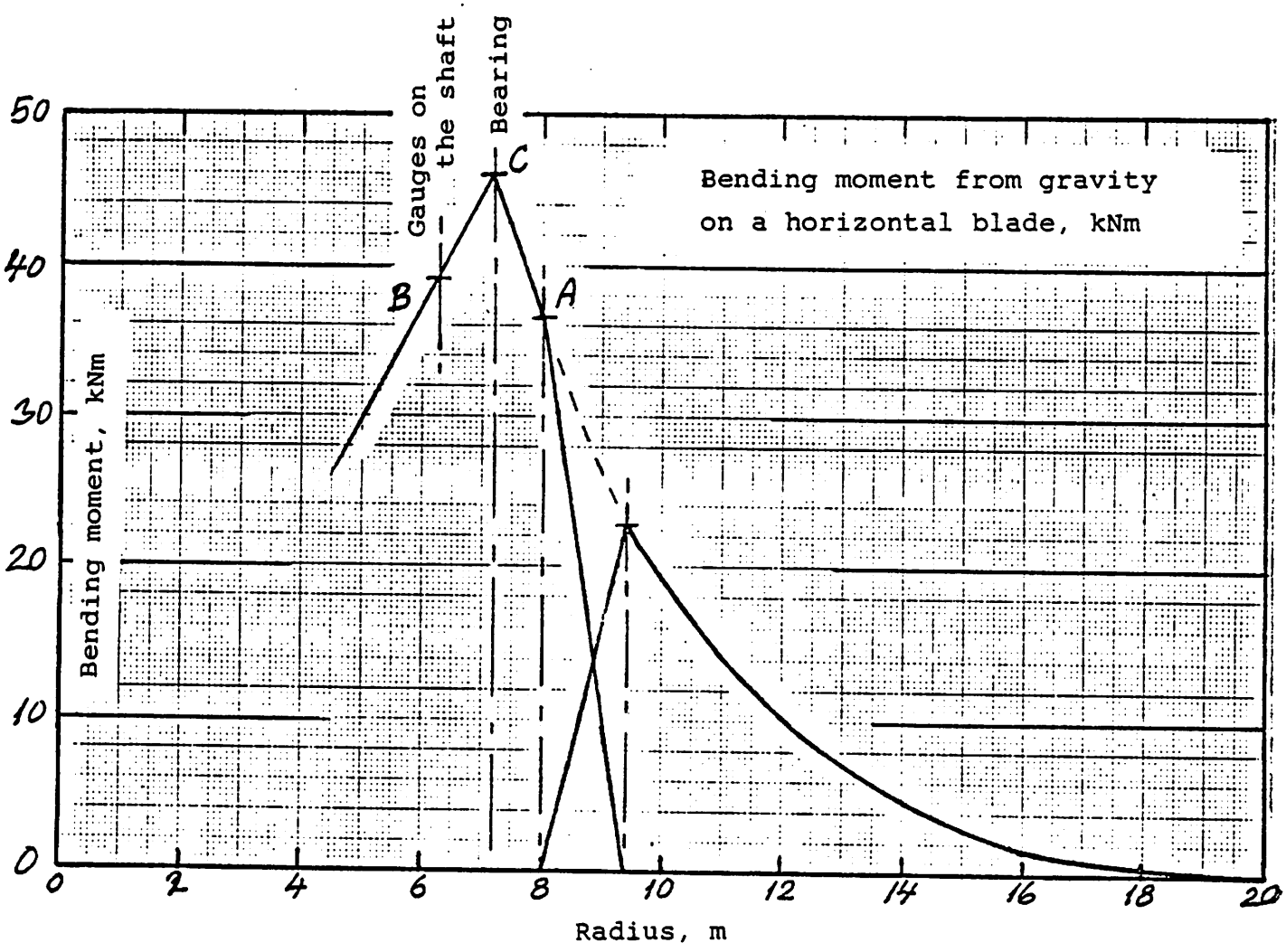

Figure 3.19

It should be noted that in both stays of Fig. 3.16 there are positive tensile forces. This means that the bearing seems to be sticking in the house and therefore carries a radial load which was unintentional. This could be the reason for the abnormal trace of the driving moment in Fig. 3.18.

3.7. Stresses due to gravity forces

The bending moment in the trunnion due to gravity is 37 kNm according to Fig. 3.19. The stress is correspondingly $\pm$ 24 MN/m^2. The superposed stress from the driving moment is of the order of 14 MN/m^2 at maximum power.

3.8. Deflections of the blade

Figure 3.20 shows a calculation of the blade deflection carried out by the Department of Engineering, Ole Gunneskov, Risø, ref. 3.2. The load case is calculated for a duty condition for which the power at the rotor shaft is 609 kW, the maximum power calculated at blade tip angle -4°. The deflected shapes are shown for a pure radial blade in curve 1 and for a blade with cone angle 6° in curve 2. The coning effect reduces the tip deflection by 25 % and the maximum axial bending moment in the steel shaft is correspondingly reduced by 40 % as shown in fig. 3.21.

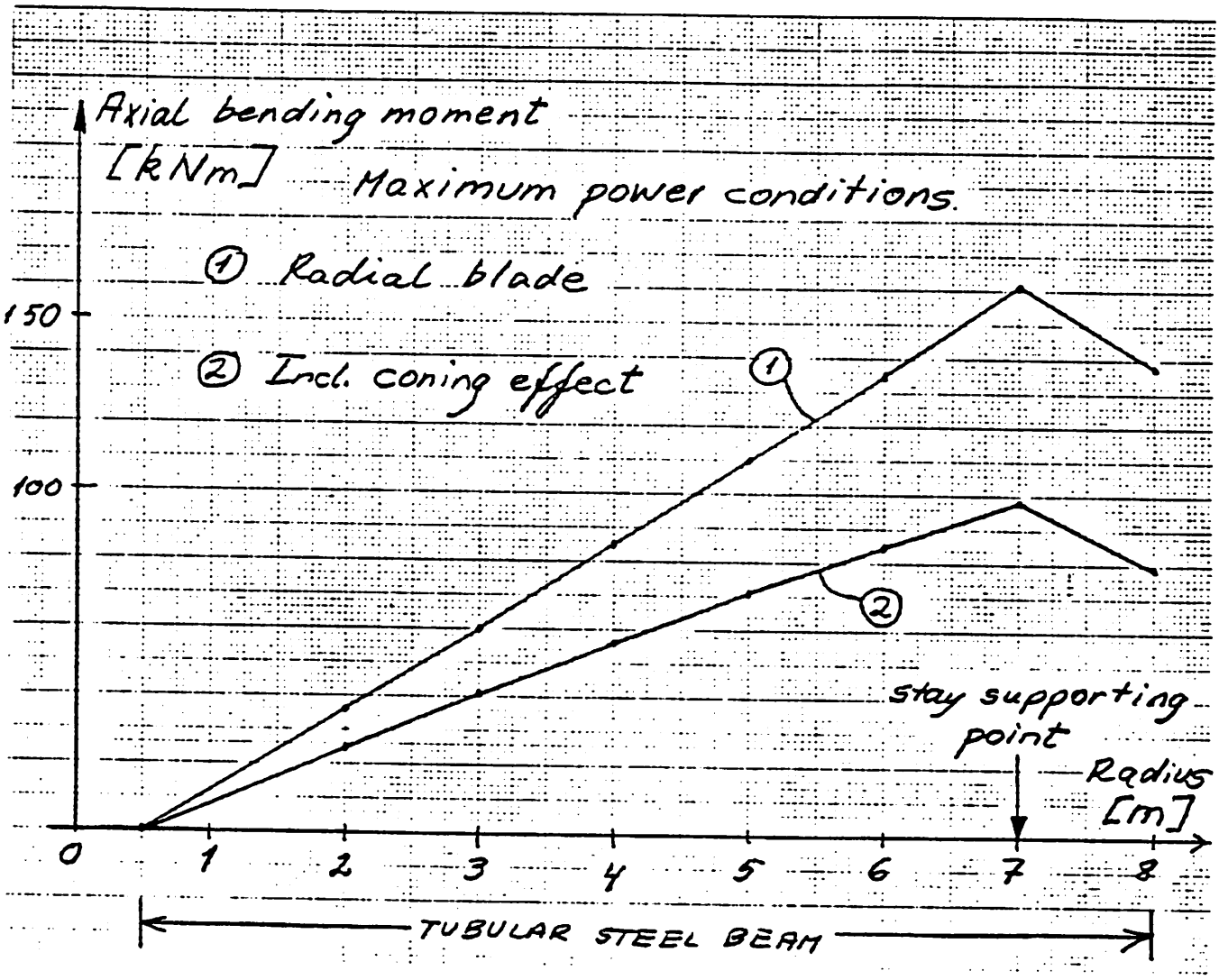

Figure 3.21

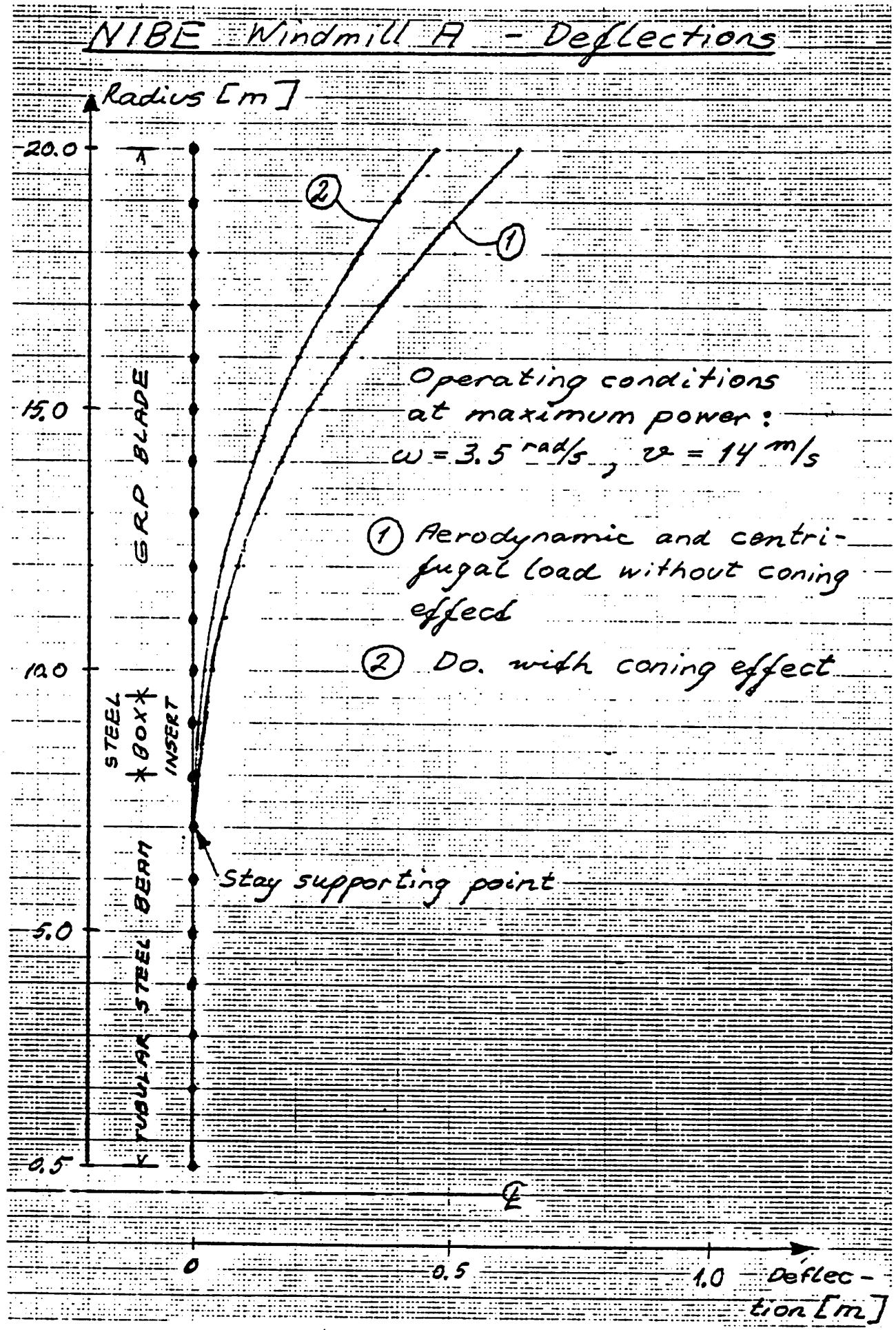
NIBE Windmill A - Deflections
Radius [m]
20.0
15.0
10.0
5.0
0.5
GRP BLADE
STEEL BOX INSERT
TUBULAR STEEL BEAM
Operating conditions at maximum power:
ω = 3.5 rad/s, v = 14 m/s
① Aerodynamic and centrifugal load without coning effect
② Do. with coning effect
Stay supporting point
0
0.5
1.0
Deflection [m]

Figure 3.20

4. DISCUSSION

4.1. The preliminary measurement system.

This ad hoc measurement system was relatively easily established; the main problem was the influence of the measurement system on some of the channels shared with the turbine's microcomputer. After separating the system from the computer by amplifiers there have been no problems in the recording of operational parameters. The recording of the rotor channels has been hampered by noise caused by the long cables absorbing radio signals. This occasionally caused the strain gauge preamplifiers to oscillate, but modifications on the preamplifier installation have removed these oscillations.

The system has served - and still serves - as a means of obtaining preliminary data in a versatile way. This means that it may be used by interested persons with a minimum of instructions, thus permitting early assessments of turbine behavior and of the validity of the design calculations. Therefore a similar system will be established on the mod B turbine. The penalty is an accuracy of not better than 5-15%. The Brush plotter is not ideally suited because it is able to resolve frequencies far beyond the frequency range of interest in the wind turbines, while the amplitudes of the records are limited to about 5 cm. However, the plotter has proved reasonably reliable while standing unattended for several months in an unheated room in the turbine tower, and its ability to record up to 6 channels simultaneously has proved valuable.

4.2. The results

The measurement results are in good agreement with the predicted values. However, they also show some anomalies that should be investigated further.

The most pronounced characteristics of the stayed, stall-regulated mod A wind turbine as they appear from the measurements are:

- Gravity forces are clearly the most dominant in-plane forces. As indicated in Fig. 3.19 the in-plane struts play a very important role in keeping the resulting blade moment low.

- For the out-of-plane loads it is characteristic for a turbine which is regulated as the mod A turbine that during a normal stop sequence the blade passes through high lift coefficients to a stalled condition. This means that the blade is exposed to loads of the same magnitude as those at high wind speeds.

References

1.1: V. Askegaard, C. Dyrbye, S. Gravesen:
"Laboratory Tests on Gedser Wind Turbine's Blades".
Structural Research Laboratory, Technical University of Denmark. Report S 28/77 Nov. 1977.

1.2: P. Nielsen:
"Measuring Program for Two Windmills at Nibe, Denmark".
Proc. IEA Expert Meeting on LS-WEC's.
September 26-27, 1979, Boone, North Carolina, USA.

1.3: P. Lundsager, C.J. Christensen, S. Frandsen:
"The Measurements on the Gedser Wind Turbine 1977-1979".
The Wind Power Program of the Ministry of Commerce and the Electric Utilities of Denmark, November 1979.

1.4: P. Lundsager, C.J. Christensen, S. Frandsen, S.A. Jensen:
"Analysis of Data from the Gedser Wind Turbine Measurements 1977-1979".
The Wind Power Program of the Ministry of Commerce and the Electric Utilities in Denmark, May 1980.

2.1: B. Maribo Pedersen:
"Målinger på Nibemølle A, den 27. og 28. februar 1980" (Measurements on Nibe Wind Turbine mod. A, February 27th and 28th, 1980. In Danish). AFM Notat VK-62-800325.
Department of Fluid Mechanics, the Technical University of Denmark.

3.1: P. Lundsager, O. Gunneskov:
"Static deflection and eigenfrequency analysis of the Nibe wind turbine rotors. Theoretical Background".
Risø-M-2199, Nov. 1979.

3.2: O. Gunneskov, P. Lundsager:
"Static Deflection and Eigenfrequency Analysis of the Nibe Wind Turbine Rotors. Analysis and Results.
Risø-M-2200,(to appear).

Appendix A.

A Note about Wind Turbine Rotor Lay-Out Minimizing the Material Fatigue Problem
by Helge Petersen

An obvious feature of a blade which produces design problems is the division of the blade in order to pitch it. The two Nibe wind turbines shown in Fig. A1., are conventional in this respect.

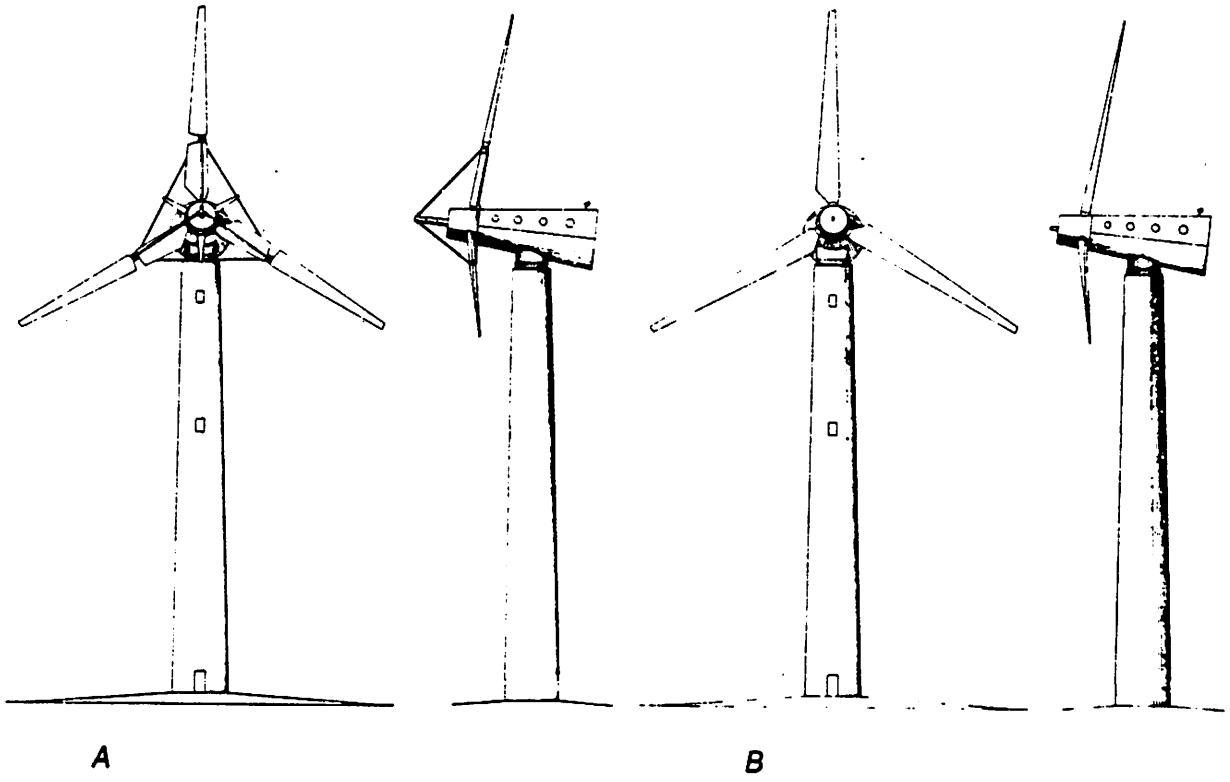

Figure A.1.

For the mod A the blade is divided in an outer and an inner blade part, the outer blade part is structually "shrunk" to be able to pass through the bearing at the end of the fixed inner blade part.

For mod B the whole blade is carried by a large bearing at the blade root and this limits the structural diameter.

Two other solutions are shown in Fig. A.2 and A.3, named Concept "28" and Concept "50", respectivily.

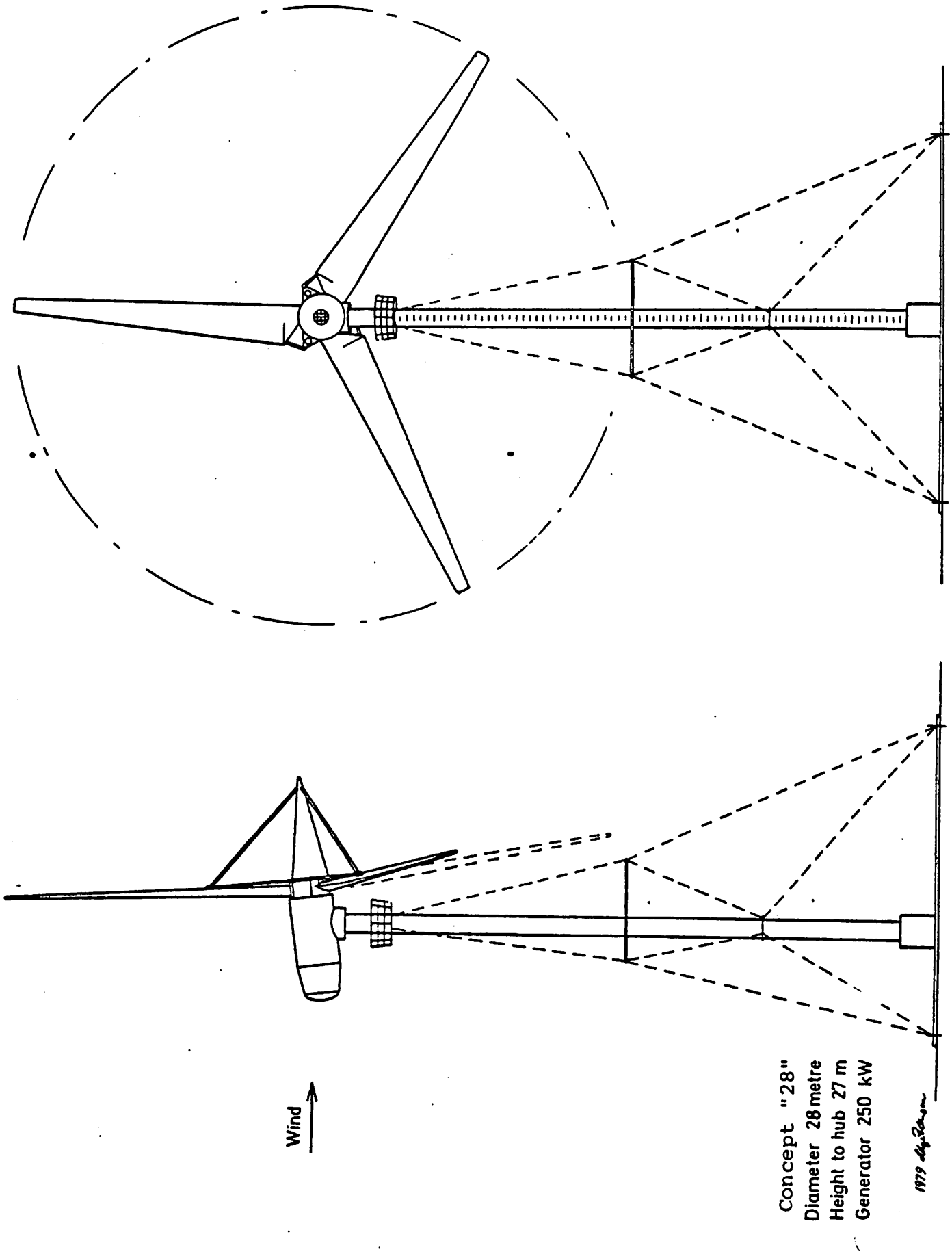
Wind
Concept "28"
Diameter 28 metre
Height to hub 27 m
Generator 250 kW
1979

Figure A.2

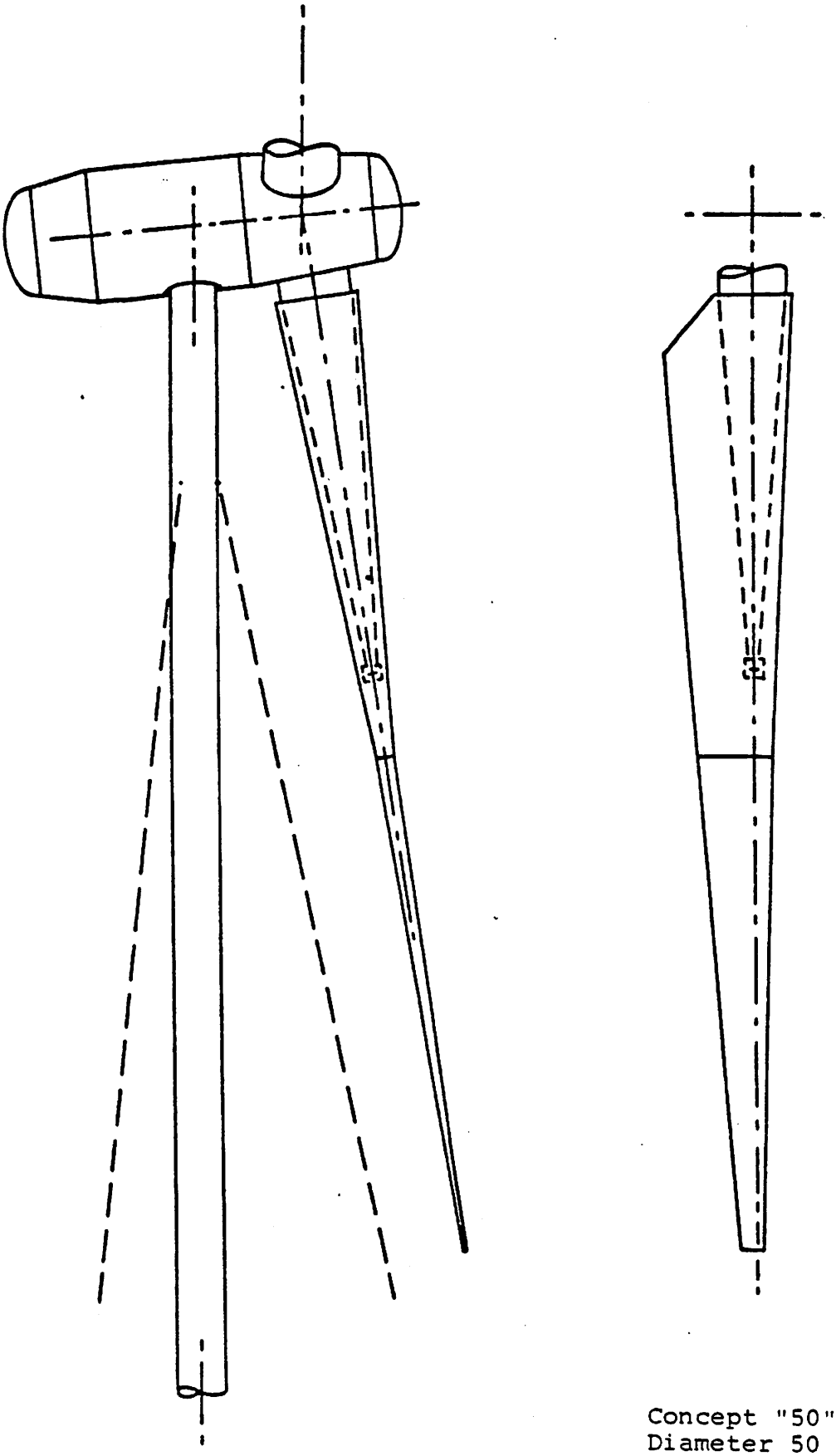

Concept "50"
Diameter 50 m
Power 1000 kW

Figure A.3.

The wind turbine in Fig. A.2, Concept "28", has strutted blades. However, the struts are hinged to the blade, the hinge being placed outside of the blade structure, and the root of the blade is hinged to the hub. Still the blade can pitch 90^{o}. In this way the blade structure is not interrupted by a shaft and bearing.

The wind turbine shown in Fig. A.3, Concept "50", has a cantilever structure fixed to the hub and surrounded by the hollow blade. This allows the blade to pitch around the carrying member. As for Concept "28" the bending moment decreases from the position of the outer bearing at the end of the carrying member towards the hub. In the carrying member of "50" the bending moment is zero at the outer bearing and increases towards the hub. However, it is less difficult to design a fixed structure strong enough to withstand the fatigue loads.

Wind Turbine

Vølund

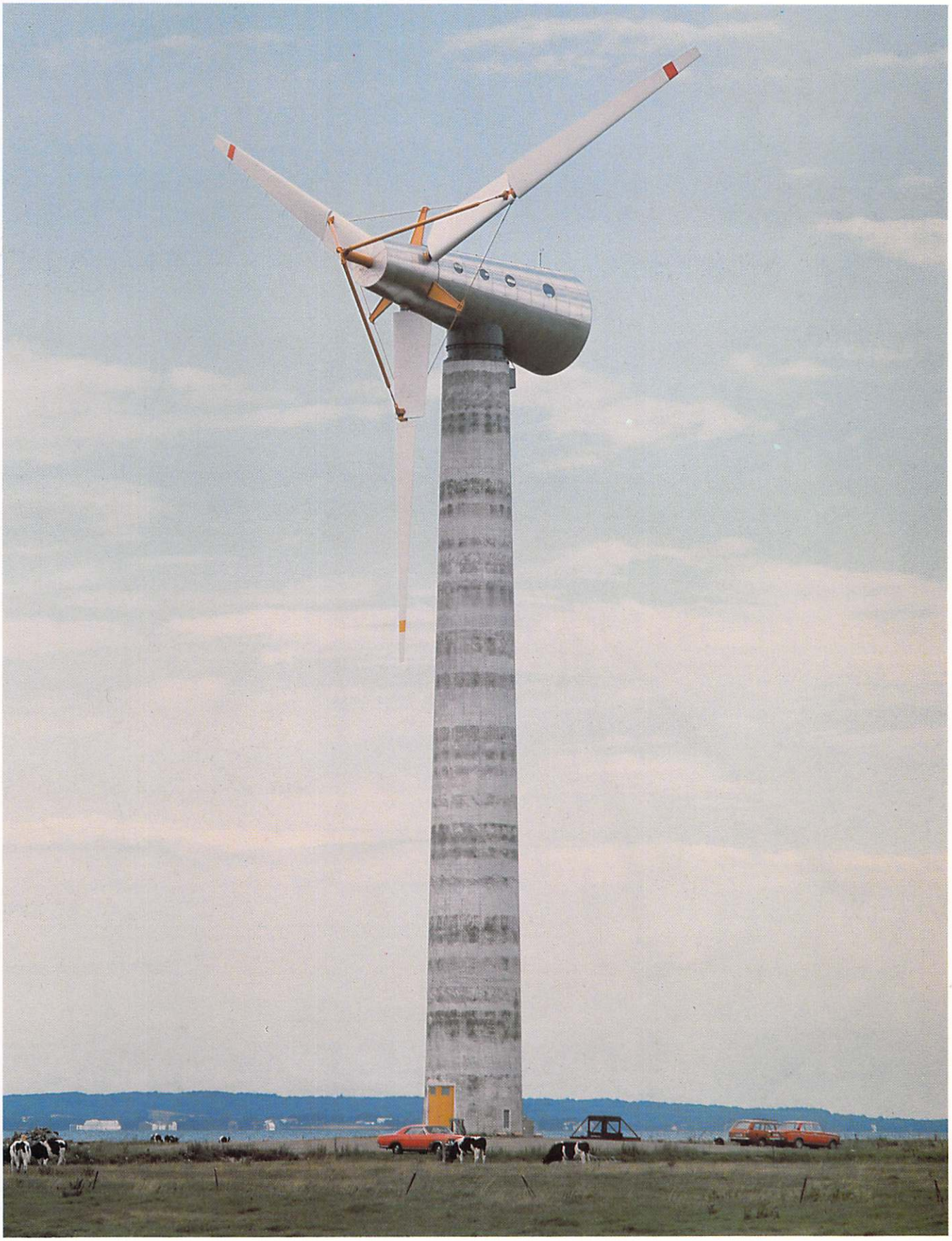

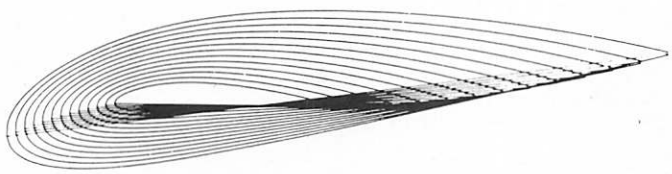

AFM 1978

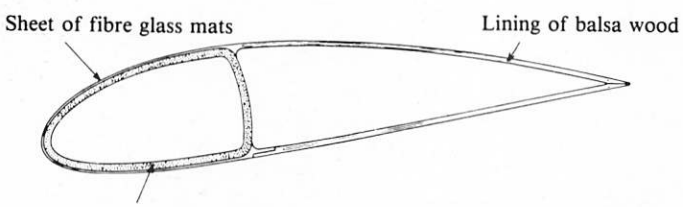

Cross section of the 12 m endsection of the blade

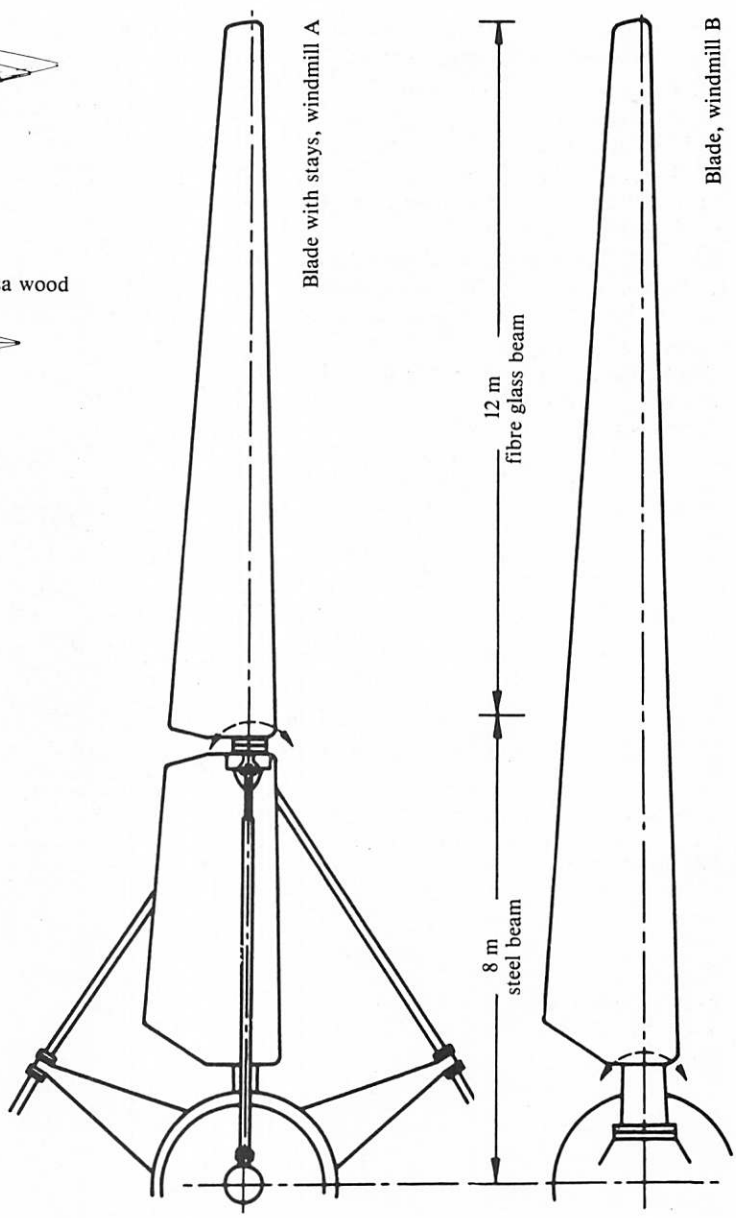

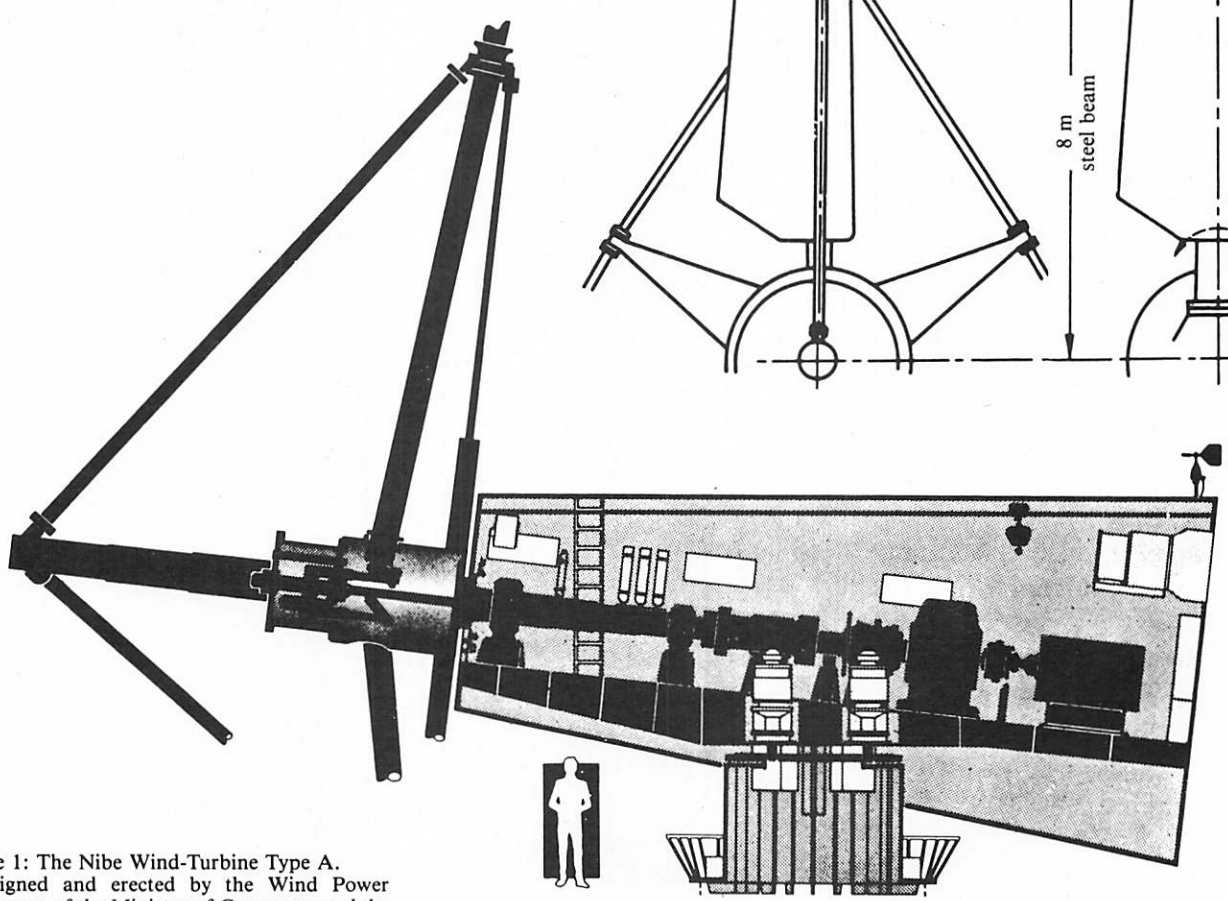

Side 1: The Nibe Wind-Turbine Type A. Designed and erected by the Wind Power Program of the Ministry of Commerce and the Electricity Utilities in Denmark.

Nacelle with rotor hub (windmill A) and tower top section

A wind power programme is aimed at the development of larger electricity producing wind power plants.
The programme involves research and development work on large-scale wind power pilot plants, with special emphasis on positive solutions which are feasible in practise.
Based on this research and the operation experience of the wind power plants the background will be procured for steps into new and advanced investigations concerning the technology, economy and environmental sides of wind power.

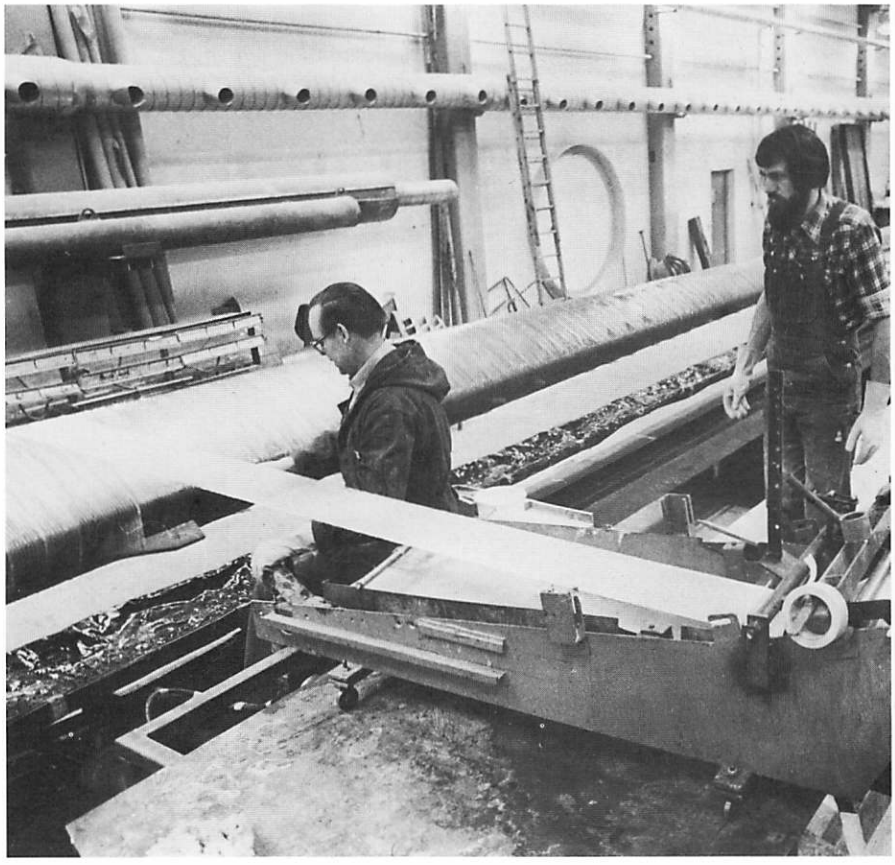

Manufacture of D-spar of glass-fibre plastic with the rovings all laid longitudinally on a rotating mandrel.

Front and side views
of the two Nibe windmills.

Windmill A

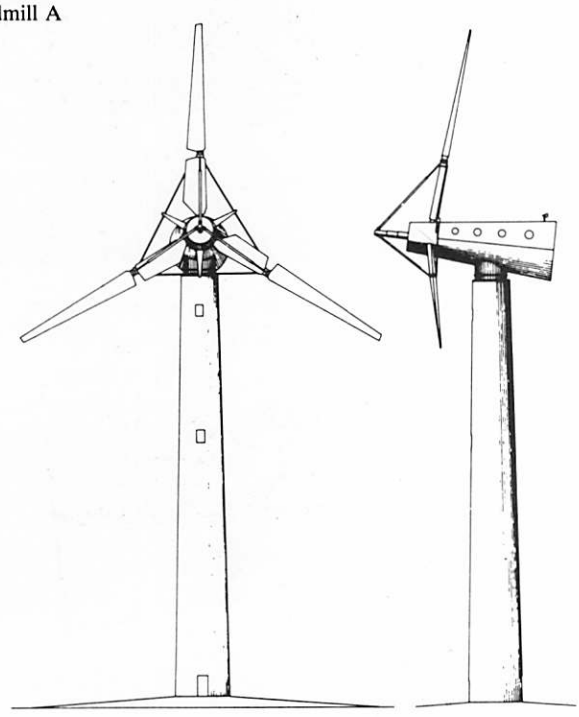

Windmill B

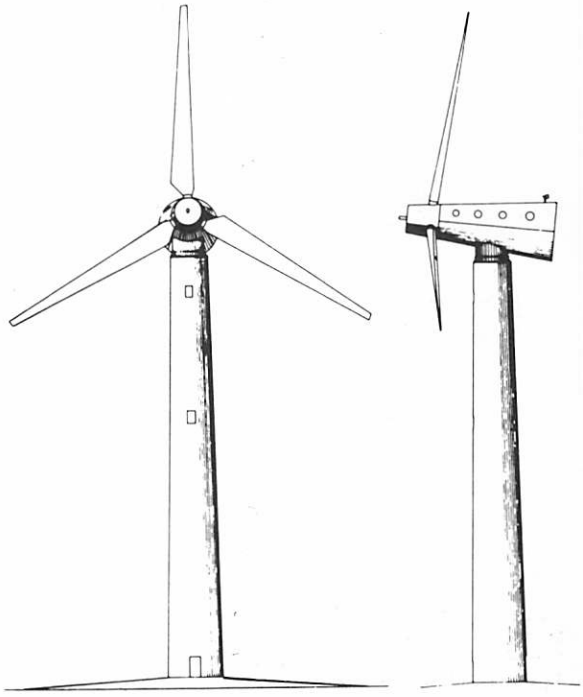

The Vølund program for the Energy Technology Plants All over the World

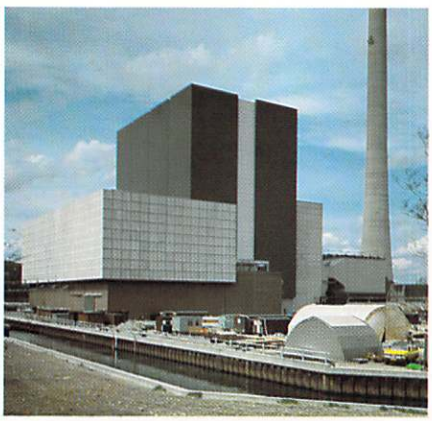

630 MW Power Station "The Ensted Power Station", Denmark.

Design and manufacture of water-tube boilers for production of steam pressurized hot water for power stations and industries, as well as all types of smoke-tube boilers for hot water from 10 KW. Storage tanks, load bearing steel constructions of all types, heat exchangers and air coolers. Marketing of turn-key heating plants for industry, district heating and apartment blocks.

10,000 tonsmetre Tower Crane, delivered to G.P.U. Service Corp., New Jersey, U.S.A.

Development, production and marketing of industrial building cranes and special cranes for shipyards, power plants and harbours. Has delivered the world's largest rotary tower crane with a lifting capacity of 10,000 tonmetre and constantly develops new types of "heavy rigging equipment". 90% of the production are exported all over the world.

The two Nibe Turbines, each 630 KW, Denmark.

Design and manufacture of wind turbine blade or turn-key windmills. Production of fibreglass-reinforced polyester products for various industries (chemical, galvanizing, food, textile) as well as for agriculture, construction industry and institutions.

Vølund

Fibreglass Technology Division
Marsk Stigs Vej 4
DK-8800 Viborg · Denmark
Phone +4 56 62 34 99
Telex 66225 volund dk

Abildager 11
DK-2600 Glostrup · Denmark
Phone +4 52 45 22 00
Telex 33150 volund dk

ITABASHI Incinerator Plant, Tokyo, Japan. Capacity 1200 TPD (Metric)

Equipment for the protection of the environment, thermic treatment of solid, sludgy and liquid waste with heat recovery and re-use of clinkers. Plants are designed and installed as turn-key projects, or equipment is delivered and commissioned. Agents and licensees all over the world.

Helideck to the "Danfield platform E", The North See.

Production of steel chimney stacks, machinery for fish meal production, electro-hydraulic crane buckets, construction, repair and service work for the on- and off-shore industry. Agents all over Western Europe.

Glass-polyester materials for a 20 m rotorblade

H. Lilholt

Metallurgy Department
Risø National Laboratory
Roskilde, Denmark

Abstract

The materials specification, fabrication, materials testing and fatigue behaviour of glass-polyester for a rotorblade is described.

Introduction

A windturbine of nominal power 630 kW has been designed and built by the Danish electricity utilities. The design of the rotor and of the wingblades was carried out with little previous experience in this field. The rotor of diameter 40 m consists of three wingblades, which are composed of an inner wing of length 8 m and an outer wing of length 12 m. The conceptual design of the wingblade is a (load-bearing) tubular spar with aerodynamically shaped shells. The inner wing has a spar of steel while the outer wing has a D-shaped spar of glassfibre reinforced polyester. The shells are made of polyester with glassmats in a sandwich construction with a balsa core. A preliminary design was used to evaluate

static and dynamic stresses, deflections, and resonance frequencies of the wingblade, in particular the outer wing. This paper discusses only the design and materials of the outer wing, in particular the spar material, fig. 1.

The dynamic stresses (in the spar material) vary and are estimated to be ca. 35 ± 7 MN/m^2 for ca. 20% of the operational time, ca. 21 ± 11 MN/m^2 for ca. 40% of the time, and 6 ± 6 MN/m^2 for ca. 40% of the time. These stresses are compressive, the corresponding tensile stresses are slightly less.

The resonance frequency for a single outer wing (12m) is ca. 2.2 Hz, and for the rotor 1.93 Hz. The imposed frequency due to rotation is three times the rotational frequency, i.e. 3 x 0.557 = 1.67 Hz.

The materials specifications for the spar and the shells of the outer wing were based on these performance data.

Materials

The performance requirements lead to a spar material of high (bending) modulus, high static and dynamic strength and of low weight; the torsion modulus is not considered to be a critical material parameter. Glass fibre reinforced polyester was chosen, rather than e.g. carbon fibre reinforced epoxy, because it is a known material to the (Danish) manufacturing industry. The requirements to the materials properties and the geometrical parameters of the spar suggest a glass-polyester material of high volume fraction ($> 40\%$) of glass fibres, and of highly oriented fibres, ideally parallel to the longitudinal axis of the spar.

An available and convenient technique for spar fabrication is (filament) winding of glass fibres onto a mandrel. A winding technique with the use of a woven glass tape was developed. The glass tape has about 90% of the fibres (rovings) transverse to the length of the tape, with the remaining 10% of glass forming lengthwise supporting rovings. Winding of this tape onto a mandrel produces a laminate with the 90% fibres nearly parallel to the axis of the spar and the 10% fibres nearly at 90° to the axis. For further details

see Johansen et al. (1980).

Mechanical tests in tension were made on samples cut from the spars. The specimens had a gauge section of 200 mm x 25 mm x ca. 23 mm (E-modulus) and a gauge section (machined on the same specimens) tapered from 25 mm at the ends to 15 mm at mid-length (ultimate tensile strength and strain).

The elastic tensile modulus, the limit of proportionality in terms of stress and strain, and the ultimate tensile strength as well as an estimate of the ultimate tensile strain are listed in table 1 as average values from 12 tests on specimens from 6 spars.

Table 1

Density		1.75	g/cm^3
Fibre volume		45.2	%
Porosity		~ 5	%
E-modulus		32.4	GN/m^2
Limit of proportional.	stress	~ 75	MN/m^2
	strain	~ 0.23	%
Ultimate tensile	stress	544	MN/m^2
	strain	~ 1.9	%

The values of the E-modulus are plotted versus the volume fractions, fig. 2. The simple straight line from the law of mixtures for unidirectional composites is drawn as a reference, and we see that the laminates are rather close to this maximum line.

The strain at the limit of proportionality is 0.2-0.3%, this is close to values found in other glass fibre reinforced polyester composites (Norwood et al. 1980), and also close to values for the first detectable acoustic emission.

The ultimate tensile strength is acceptable for the present application, but is probably affected by porosity. The ultimate tensile strain is difficult to define, because internal damage starts at lower loads and causes a jerky stress-strain curve, see fig. 3.

Fatigue behaviour

The outer wings were not specifically designed for fatigue loads, the materials have not been tested for fatigue, and no component tests in fatigue were made.

Qualitatively, the material behaviour is considered to be acceptable under fatigue loadings, the high volume fraction of glassfibres ($\sim$45%) and the well aligned fibres ($\Theta \sim 5\text{-}10^{o}$) should ensure good fatigue behaviour. The expected loads on the wingblades during (normal) operation are mainly tensile and/or compressive in the most heavily loaded parts of the spar; rather low loads in shear are expected. It is known that shear loads and (longitudinal) compressive loads reduce the fatigue properties of fibre reinforced materials, mainly because the matrix cracks and the interface debonds, (Composites 1977, Dew-Hughes et al. 1973).

Internal damage (matrix cracks and debonding at the interface) is likely to occur in fibre composites during fatigue conditions, and at rather low loads. Thus, except at very low fatigue loads, internal damage is likely to occur early in the life time of the material. It will often be inefficient to use very low design loads, and therefore a fibre composite material is likely to have some internal damage during most of its life time; perhaps even from the start due to incomplete fabrication of the fibre composite.

The effects of internal damage are a reduction in the elastic constants (among these the E-modulus) and a larger risk of water uptake. The effect of water is partly an increase in the weight of the component and partly a softening of the matrix, e.g. polyester. These effects must be addressed during the design of components.

Large "single" loads can also cause internal damage which is irreversible, and thus has the same effects as damage produced from fatigue loads.

Fatigue loadings can be uniform cycling or random cycling or combinations of these. Predictions of fatigue life times require a rule for the accumulation of part lives at various types of loading. The linear rule based on fractional lives is not likely to work, and other rules have been proposed (Owen 1972).

Part of the explanation is that the irreversible damage has effects on the mechanical behaviour of the material and thus its (fatigue) performance later in its life time.

Large "single" loads early in a planned life period can consume a (large) fraction of the accumulated life time. During loadings, which are not predictable in detail and sequence, such as wind loads, it may not be possible to predict a total life time, but only a statistical (total) life time.

Estimates of fatigue behaviour

The fatigue life times of the Danish windturbines are based on the angular velocity of 3.5 s^{-1} and a nominal design life time of 30 years. With an efficiency factor of 0.85 the number of cycles are:

1 month	$N = 1.24 \times 10^6$
1 year	$N = 1.5 \times 10^7$
30 years	$N = 4.5 \times 10^8$

A simple estimate of the fatigue performance, which can only be of approximate value during complex loadings, can be obtained from British Standard no. 4994. The design factor, which is composed of several parts, is estimated for 10^6 cycles and for 10^9 cycles. The allowable fatigue stress is

$$\sigma_f = \sigma_{UTS} / K$$

where $\sigma_{UTS} = 544$ MN/m^2 for the spar material.

The calculated, accumulated loadings (Petersen 1979) are evaluated in terms of strains, and the corresponding stresses are calculated for the spar material, see table 2.

Table 2

N	K	σ_f MN/m^2	ε_{max} %	ε_{min} %	σ_{max} MN/m^2	σ_{min} MN/m^2
10^6	7.9	69	0.12	0.06	37	18
5×10^8			-0.014	-0.023	- 4	- 7
10^9	11.5	47				

The operative loadings appear to be well within the allowable stresses.

A more detailed description of the material behaviour is obtained with diagrams which include the number of cycles, the mean stress (or strain) and the stress (or strain) amplitude. Such diagram are e.g. the Smith-diagrams which use mean stress and maximum/minimum stress for fixed number of cycles.

Data from the literature do not contain information on the specific glass-polyester laminate used for the spars. Based on relevant information from the literature on glass-resin composites with aligned or cross-plied (woven) fibres we have estimated the likely fatigue curves for the spar material. The various data are more conveniently compared in terms of strains, rather than stresses, and therefore we have plotted the Smith-diagrams in terms of strains. The relevant information is contained in the references Malmo et al. (1975), Dharan (1975) and Owen (1977).

We have estimated fatigue curves for "early damage" and for "failure" to illustrate the influence of these situations on the allowable fatigue strains.

Most fatigue studies do not contain data for cycles up to 10^9 cycles, and some extrapolation has been done to estimate the behaviour at these high cycles. The qualitative conclusions are (schematically):

"early damage"	$\varepsilon(10^6) \lesssim \varepsilon(10^9)$
"failure"	$\varepsilon(10^6) > \varepsilon(10^9)$
$N = 10^6$	ε(failure) $>$ ε(early dam.)
$N = 10^9$	ε(failure) $\simeq$ ε(early dam.)

The fatigue strain diagrams for the glass-polyester are estimated from this information and the characteristics of the spar material (table 1), see fig. 4 and 5.

The operative strains are estimated from the accumulated loadings and are (at wing radius 9.5m):

$N = 10^6$	$\bar{\varepsilon} = 0.09$ %	$\Delta\varepsilon = 0.03$ %
$N = 5\times10^8$	$\bar{\varepsilon} = -0.02$ %	$\Delta\varepsilon = 0.01$ %

Early measurements of the loadings during operation of the windturbine, mill A,have given bending moments at wing radius ca. 8m of $M = 110$ kNm $\pm$ 20 kNm, which corresponds to strains of

$\bar{\varepsilon} \sim 0.12$ % $\Delta\varepsilon = 0.02$ %

calculated at wing radius 9.5 m.

These operative strains are plotted in the diagrams and are reasonably within the allowable strains at 10^6 cycles, and closer to the allowable strains at 10^9cycles. It will be necessary to investigate the material behaviour and the operative loadings in more detail before more precise predictions can be made.

"Single" loadings

Loadings, which "overload" the material and cause internal damage, can be of importance for the fatigue performance.

Strains (static, tensile) of 0.2-0.3 % in glass-resin composites appear (Norwood et al. 1980) to correspond to a limit of proportionality for the stress-strain curve, this limit is often close to strains at which the first acoustic emission is detected. These observations indicate internal damage of the glass-resin material and the damage is probably irreversible. Thus it has effects similar to those mentioned for fatigue loadings.

The limit of proportionality of the spar material is ca. 0.23 % (table 1), and is thus in agreement with the above values.

Cases of large "single" loadings are given by Petersen (1979) and include for mill A gale and oblique wind direction, and for mill B gale, aerodynamic braking and mechanical braking. The strains are calculated (Lilholt 1980) at wing radius 10 m and are the compressive strains of the curved wing surface, and are presented in table 3.

Table 3

	Bending moment	Wing	
		stress	strain
	kNm	MN/m^2	%
Mill A			
Gale	170	27	0.2
Oblique wind	110	18	0.13
Mill B			
Gale	130	21	0.15
Aerodyn. braking	129	21	0.15
Mech. braking	40	6.4	0.05

These loadings could be important for the fatigue performance, depending on the number of occurrences.

Conclusions

The material (glass-polyester) and the wings show the expected mechanical behaviour for static loads. The material behaviour and loadings in fatigue have been discussed qualitatively and mainly in relation to simple unidirectional tensile loading; the fatigue behaviour appear qualitatively acceptable, but substantiation is necessary.

References

BS 4994, 1973, British Standards Institution.

Composites: special issue: fatigue of frp, 1977, vol 8, no.4.

D. Dew-Hughes, J.L.Way, 1973, Composites,4,167-173.

C.K.H.Dharan, 1975, Proc. Int. Conf. Composite Materials, ICCM, vol 1, 830-839.

B.S.Johansen, H.Lilholt, Aa.Lystrup, 1980, 3. Int. Conf. Composite Materials, ICCM-3 (to be held in Paris, 26-29 Aug. 1980), 13pp.

H.Lilholt, 1980, Report VK-Metal-7, 25.March, 9pp.

J. Malmo, S.Torp, 1975, Report no. 88 5400/1, Det Norske Veritas, 40pp.

L.S.Norwood, A.F.Millman, 1980, Composites,11,39-45.

M.J.Owen, --Howe, 1972, J.Appl. Phys.,5,1637-1649.

M.J.Owen, 1977, "Designing with fibre reinforced materials", I. Mech. Eng. Conf. Publ. 1977-9, paper C223/77, 5pp.

H. Petersen, 1979, Report Risø-M-2195, 67pp.

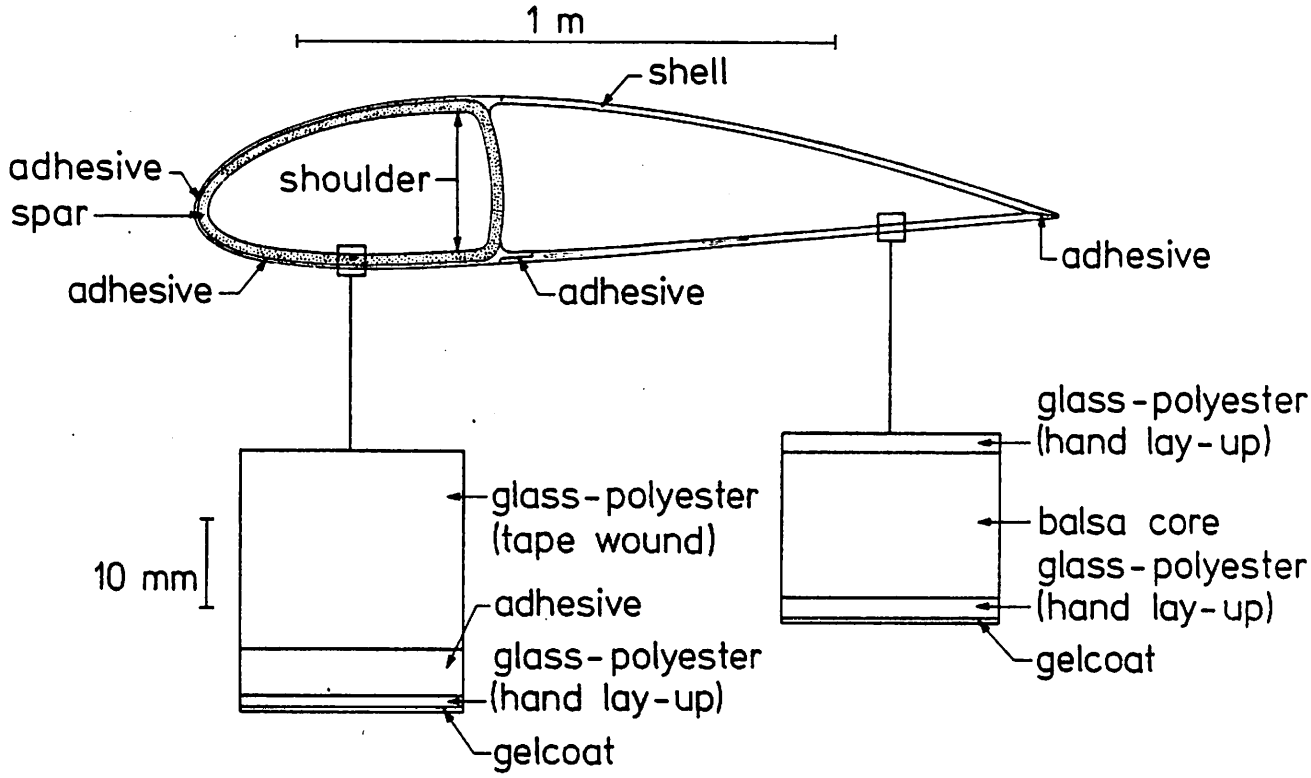
1 m
shell
adhesive
spar
shoulder
adhesive
adhesive
adhesive
glass-polyester
(hand lay-up)
balsa core
glass-polyester
(hand lay-up)
gelcoat
10 mm
glass-polyester
(tape wound)
adhesive
glass-polyester
(hand lay-up)
gelcoat

Fig. 1.

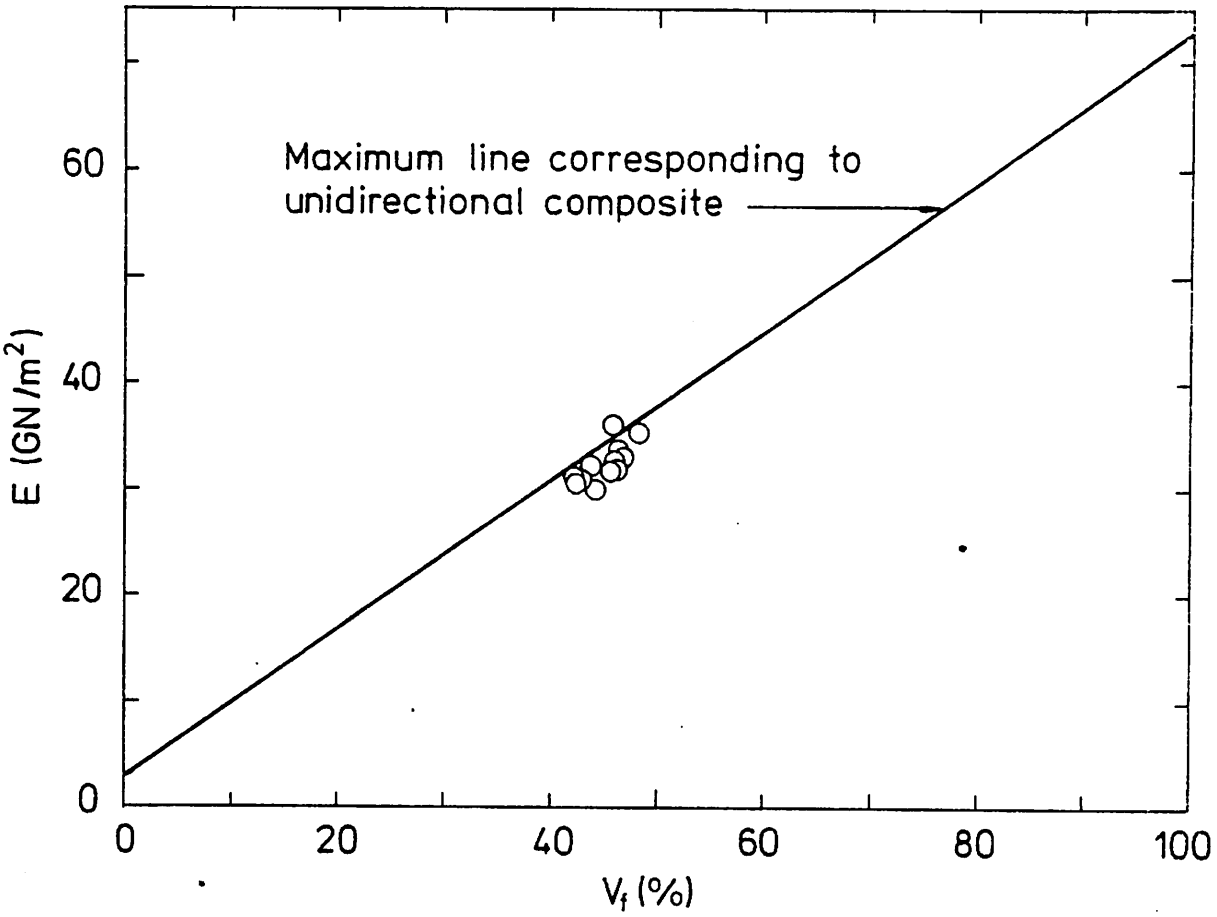
Maximum line corresponding to
unidirectional composite
E (GN/m²)
0
20
40
60
0
20
40
60
80
100
Vf (%)

Fig. 2.

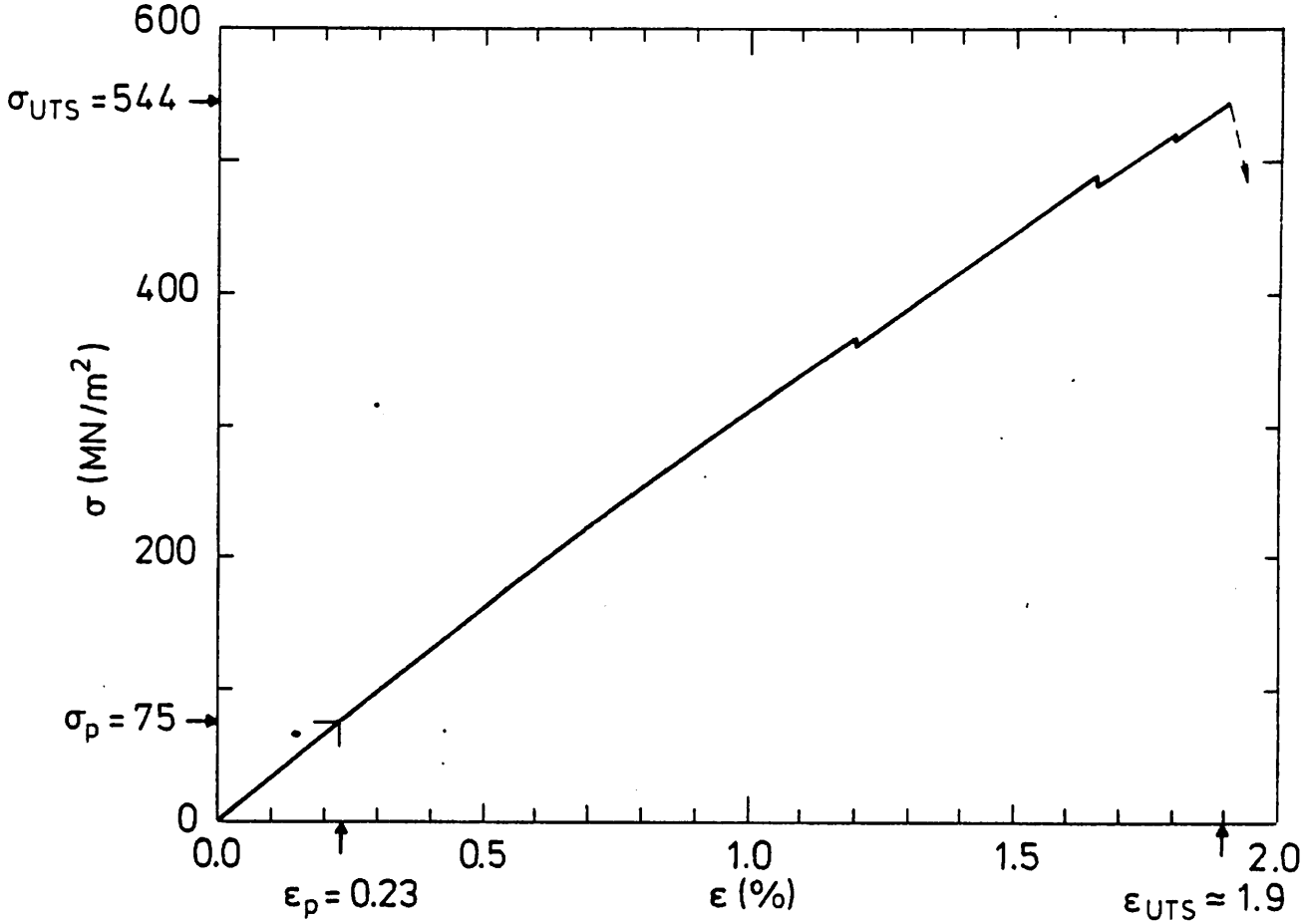
600
400
200
0
$\sigma_{UTS} = 544$
$\sigma_p = 75$
σ (MN/m^2)
0.0
0.5
1.0
1.5
2.0
$\varepsilon_p = 0.23$
ε (%)
$\varepsilon_{UTS} \approx 1.9$

Fig. 3.

Glass- Polyester

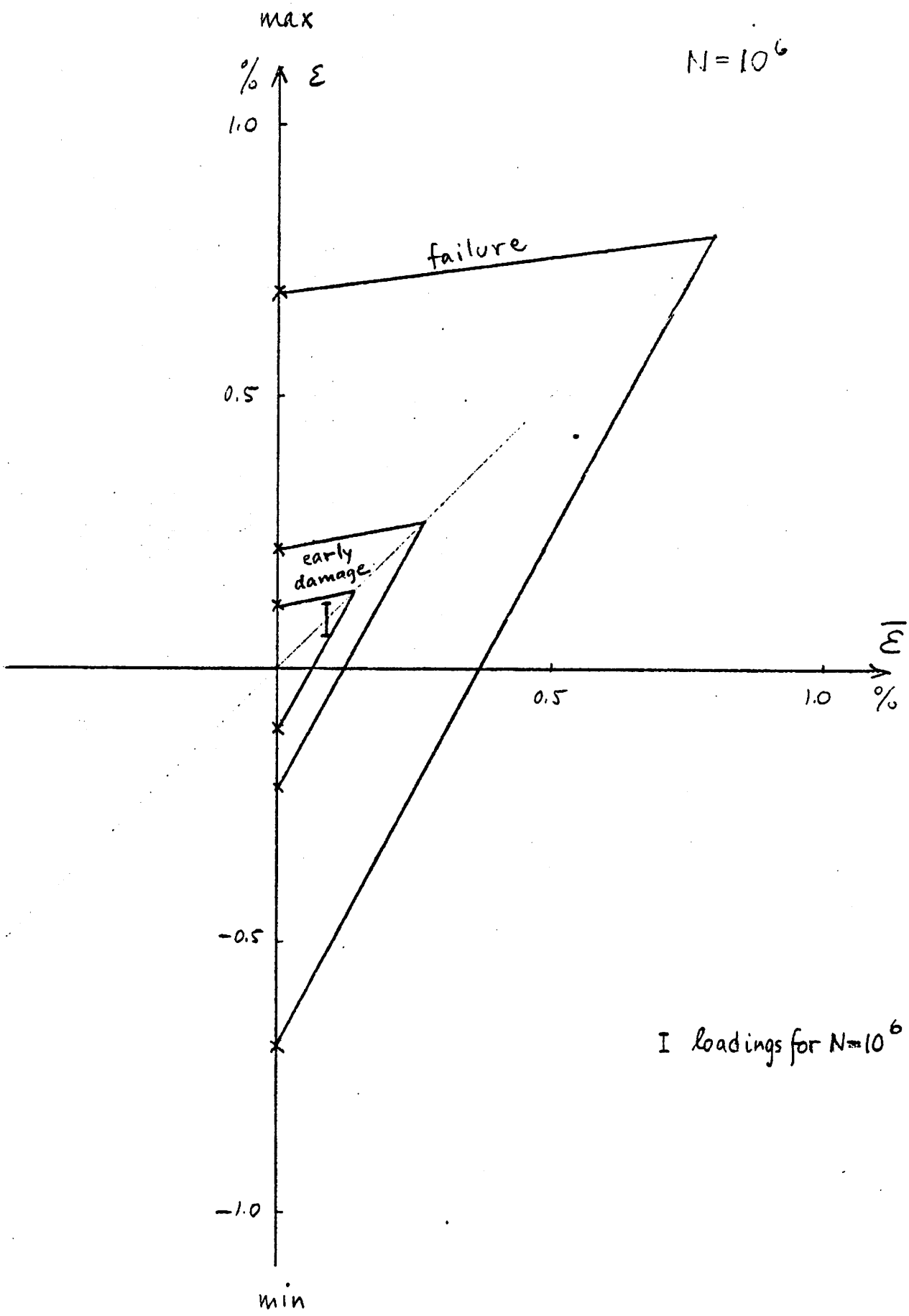

I loadings for N=10^6

Fig 4

Glass – Polyester

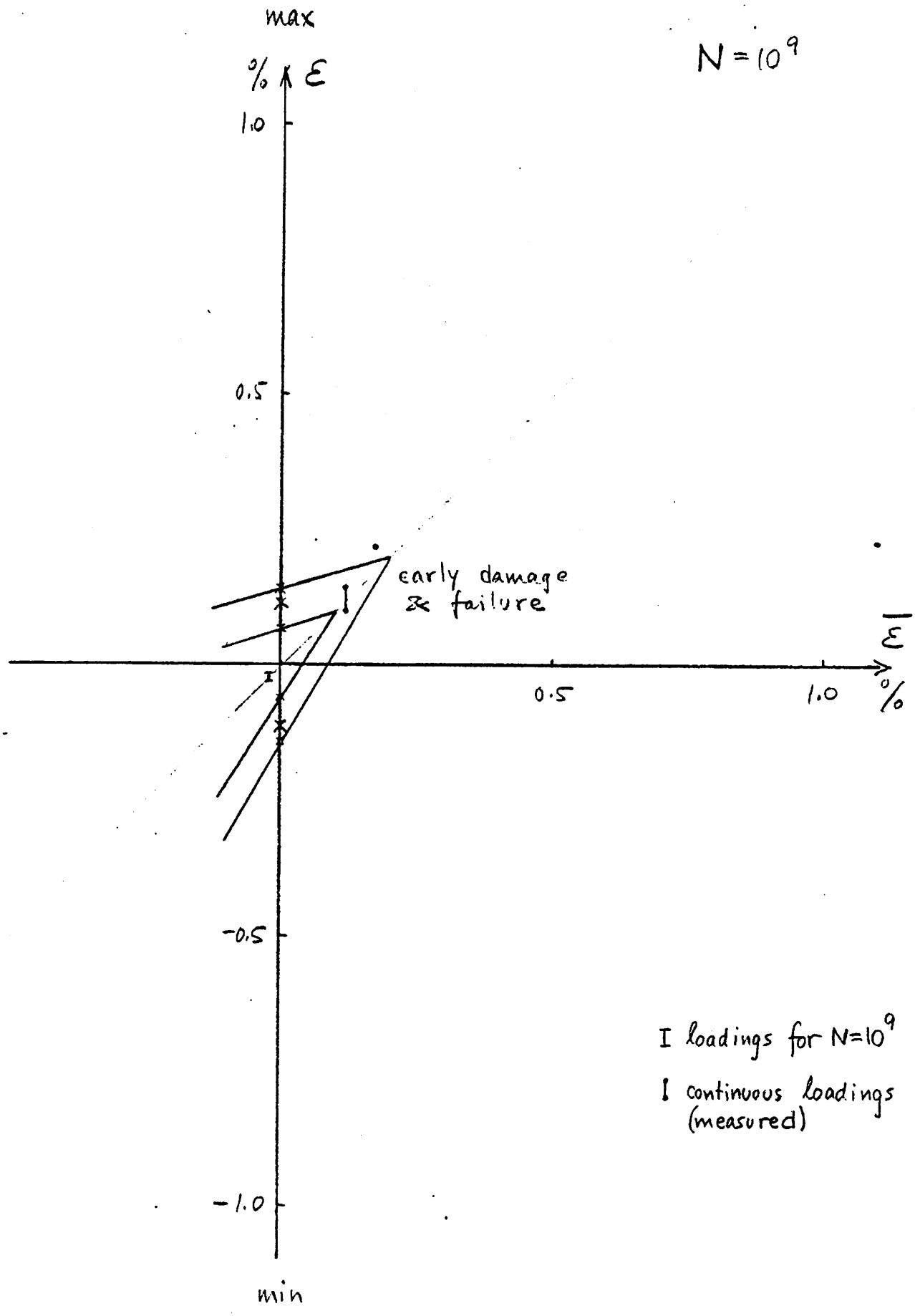

I loadings for $N=10^9$

I continuous loadings (measured)

Fig 5

Production Development, Manufacturing and Test of the G R O W I A N - Rotor Blade

IEA - 4th Expert Meeting
16.4. - 17.4.80 in Stockholm
Sweden

by H.M. Thiele

Munich: March 1980

MAN-Maschinenfabrik-Augsburg-Nürnberg
Aktiengesellschaft

N E U E T E C H N O L O G I E

8 München 50 West Germany

Introduction

During the definition phase of the GROWIAN I-project, two different blade-construction concepts have been examined:

a) layout as a carbon-fibre-composite-structure between station R = 15 m and R = 50 m with a lateral-load connection to the hub.

b) layout as a carbon-fibre-composite-structure between station R = 50 - R 30 m. From station 30 m to the hub a design with a steel-spar as load carrying element and an airfoil of glassfibre-composite was chosen.

Static and dynamic tests with components of original size have shown, that rotor blades constructed in carbon-fibre composites were not being qualified enough to be installed in the first GROWIAN experimental unit. Problems are seen especially in the connection of the composite to the steel-structure and in the fabrication-technology to reach a constant material quality.

For the installation of the first experimental unit of GROWIAN I rotor blades with a steel spar and a glassfibre composite airfoil are used. The development, construction and test of this blade configuration is being performed by MAN by order of the KFA for the Federal Minister of Research and Technology.

1. Blade Geometry

The GROWIAN-rotorblade has a double trapezoidal shape (Fig. 1). The nominal length is 50 m about 40 m are aerodynamically effective. The chord is 1,3 m at the tip and 4,9 m at the root. The relative thickness varies from 15,1% to 50%. From the hub the blade-bearing reaches to the station R = 10 m which splits into two bearings, one at station R = 4,3 m and one at station R = 10 m. The important blade data are summarized in Fig. 2. For the aerodynamical layout three laminar Wortman airfoils series FX-77-W are used (Fig.3).

2. Design Concept

Load carrying structure of the blade is a hexagonal untwisted steel spar. The aerodynamic airfoil-shape is given by a glasfibre-composite sandwich-construction, which is connected via fittings with the spar. The use of this GFRP-construction results from the high requirements of the laminar airfoil to the surface waveness and roughness. This type of construction has been adapted from the sail-plane fabrication.

The GFRP-shell is build up in order to optain only a very low percentage of the chord- and flapwise stiffness of the spar. On the other hand the shell is worked out in circumferential direction in a manner that the angle of attack is hardly changed. Differences in the strains between the two materials under temperature are compensated by the build up of the laminate (Fig. 4).

3. Steel Spar

The spar is untwisted and has a hexagonal cross-section, which is lead to a truncated cone at station R = 10 m. To reach the hexagonal shape and reduce the welding to a minimum, the sheets are bent. From station R = 15 m to R = 35 m the spar consists of two semi-shells. From R = 35 to the tip it is build up by quarter-shells. To keep its shape under load it is stiffened by ribbs. By reasons in handling and fabrication the spar is divided into 6 sections which are welded together. The fittings to mount the airfoil-shells are situated at the chord-wise front and rear end of the spar.

The spar is positioned in the blade geometry in order to get a balanced stress-distrubution in the girders (Fig.5). As material steel QST 52-3-Z3 is chosen. The wall-thickness of the spar varies from 20 mm to 6 mm. Fig.6 shows the stress-distribution over the length of the spar for nominal and peak load. In Fig. 7 the assembly jig of the spar is pictured.

4. Aerodynamic airfoil-covering

The blade shape is given by the aerodynamic-airfoil covering (Fig.8). It is build up as a GFRP-sandwich-construction and has to carry aerodynamic forces, which are lead via fittings into the spar. Due to handling and fabrication, the shelltype airfoil-covering is produced in segments. From station R = 50 m to R = 27,5 m it is build up in semi-shells which are separated in the chord line. From station R = 27,5 m to R = 10 m these semi-shells are divided chord wise behind the spar. The shells are fabricated in negative moulds, a standard method used in the composite fabrication.

This method guarantees a high accuracy of the airfoil shape and the required surface quality. Fig. 9 shows the manufacturing of the moulds. Fig. 10 the model of station R = 50 m to R = 37,5 m to construct the moulds.

5. Testing

The prototype of the blade will be tested in static tests. Fatigue-tests with 10^8 cycles are being not performed due to the large amplitudes by time reason.

The tests will be performed in order to simulate the nominal loads in certain blade areas approximately. Fig. 11 shows the test stand. Test rigg and sample form a closed system in order that no outer reaction loads will arise. The test-loads will be applied by hydraulic jacks and induced via a load carrying structure to the sample. Five tests will be performed: a dynamic vibration test, two static tests and a test to measure the friction moment of the blade bearings. The final test will be a rupture test.

Fig. 12 shows the GROWIAN-blade in a size comparison with American windturbine-blades of MOD 1 and MOD 2 as well as a wing of the air-transporter GALAXY.

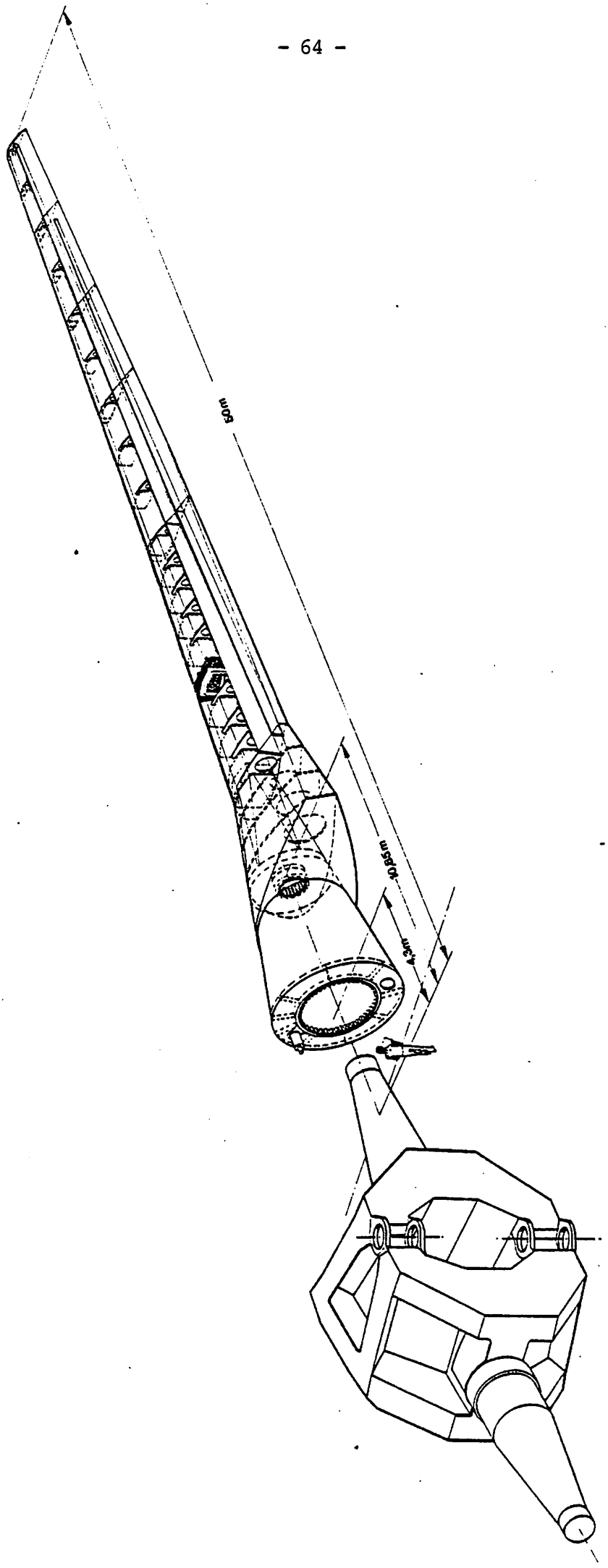

Fig. 1 **GROWIAN Rotorblade**
Full steel spar version

BLADE DATA

Length	(nominal)	l_n	=	50,2 m
Chord	at tip	t_1	=	1,3 m
	at root	t_2	=	4,9 m
Thickness	relativ	δ	=	15,1 - 50%
	absolut	d	=	0,3 - 2,4 m
Twist	/non linear)	ϑ	=	18^0
		A	=	105 m^2
Tapering		T	=	0,26
Aspect ratio		Λ	=	15,4
Airfoil		FX-79-W 151 A FX-77-W 253 FX-77-W 343		
Weight		m	=	23000 kg
Eigenfrequences	1^{st} flap	f_1	=	1,07 H_z
	1^{st} chord	f_2	=	1,34 H_z
	1^{st} torsion	f_3	=	9,34 H_z
Rotorspeed		n	=	18,5 rpm
Design life		20 year		

Fig.: 2

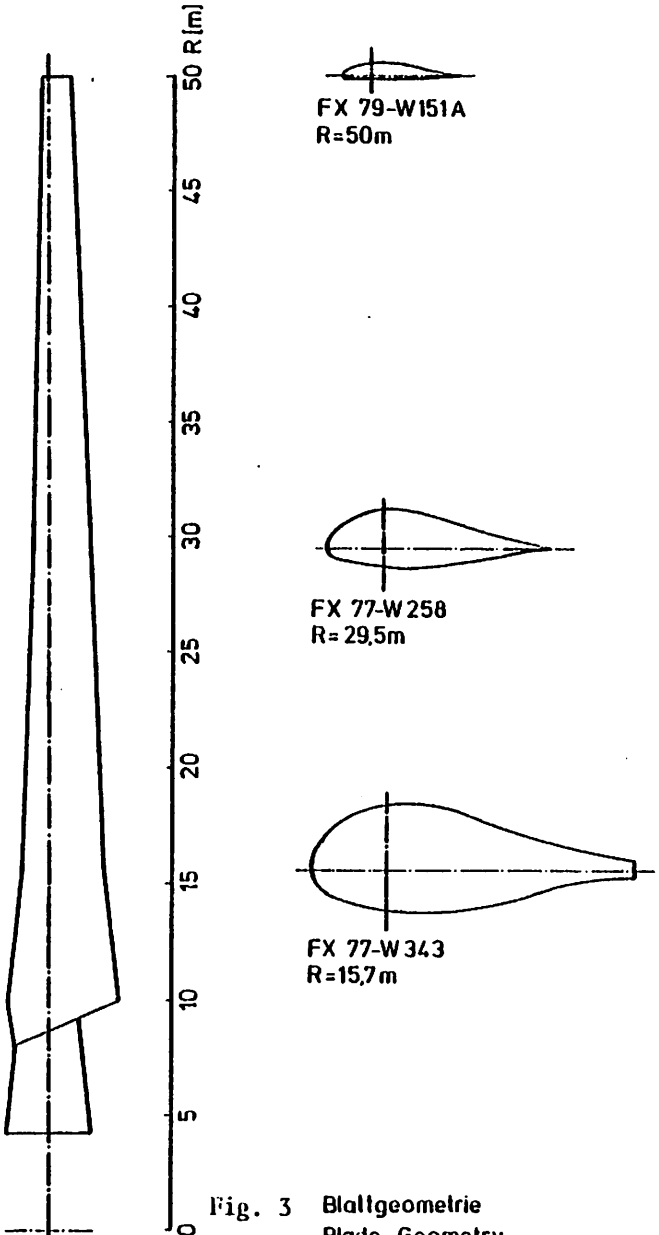

Fig. 3 Blattgeometrie
Blade Geometry

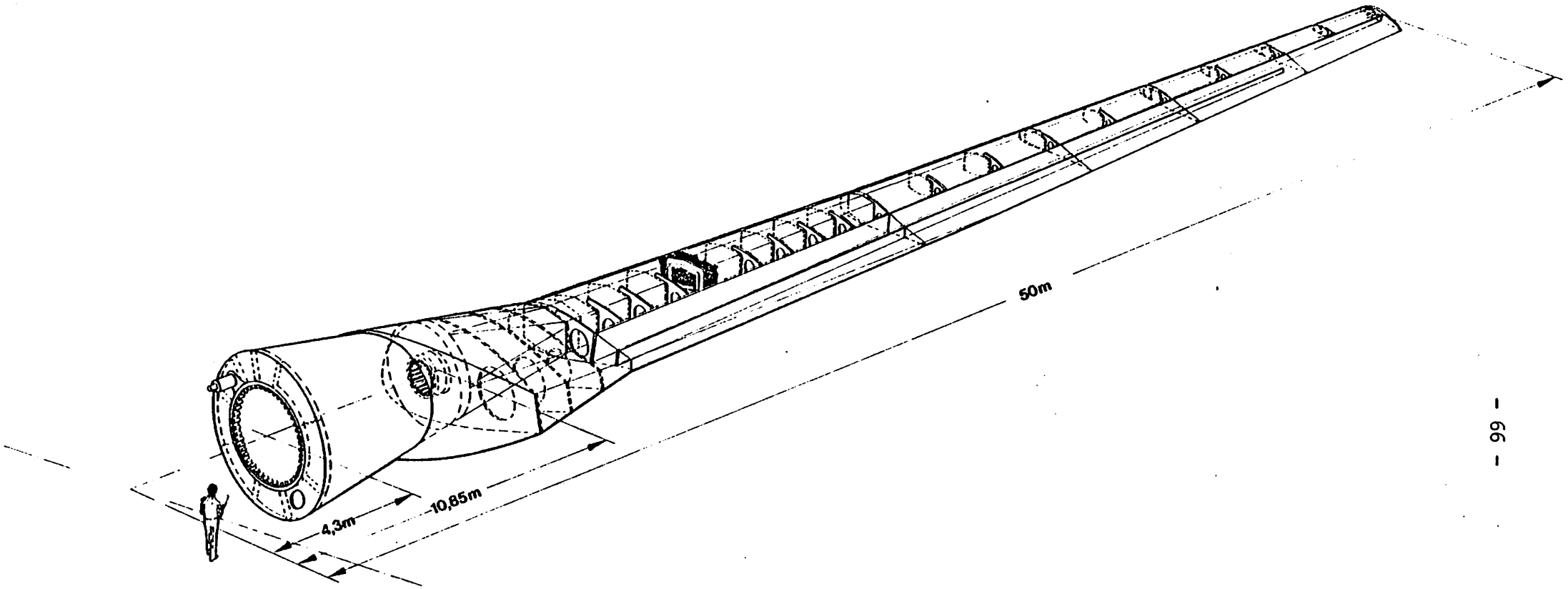

Fig. 4 **GROWIAN Rotorblade**
Full steel spar version

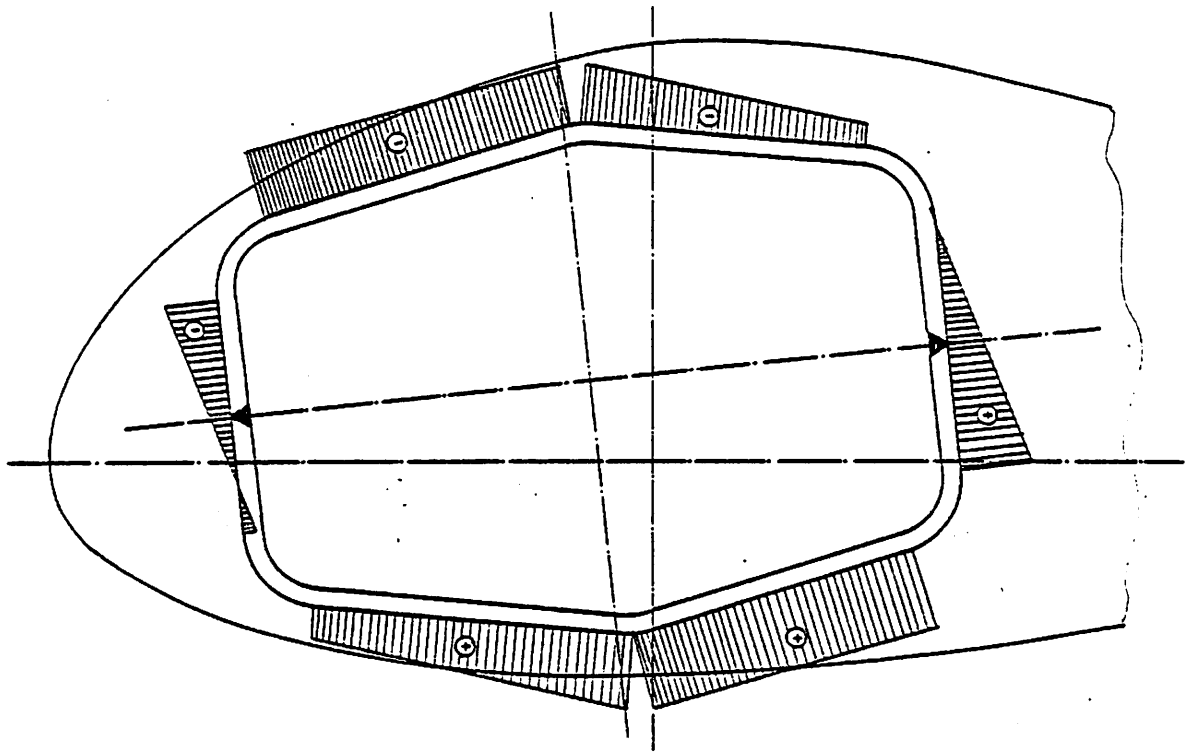

Fig.:5 Stress Distribution in the Spar-Girders

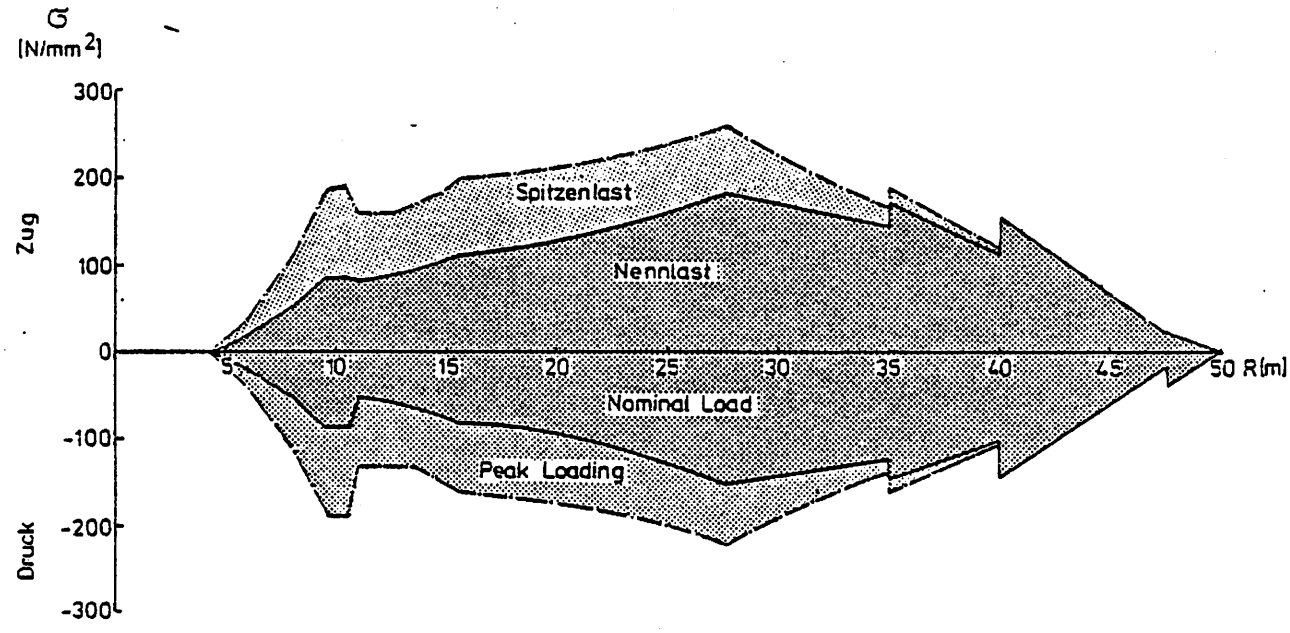

Fig.: 6 Stress Distribution in the Spar

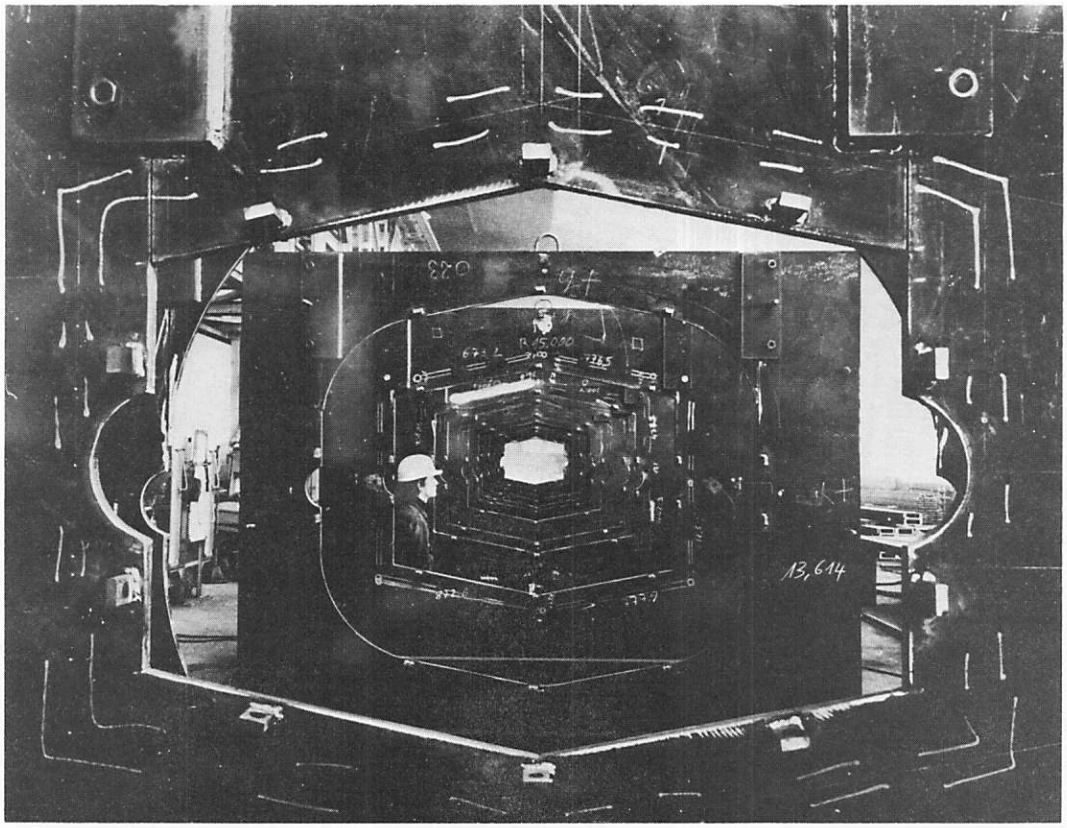

Fig. 7 Assembly Jig

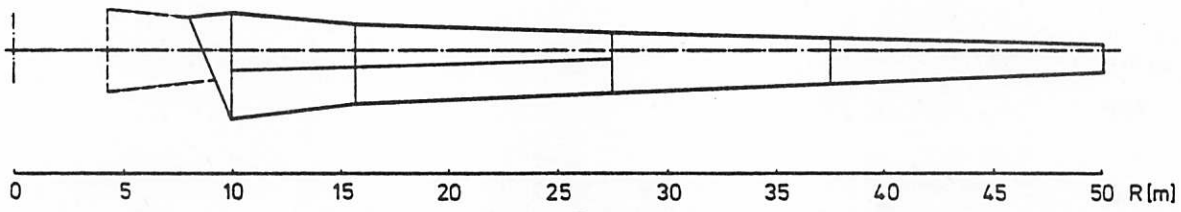

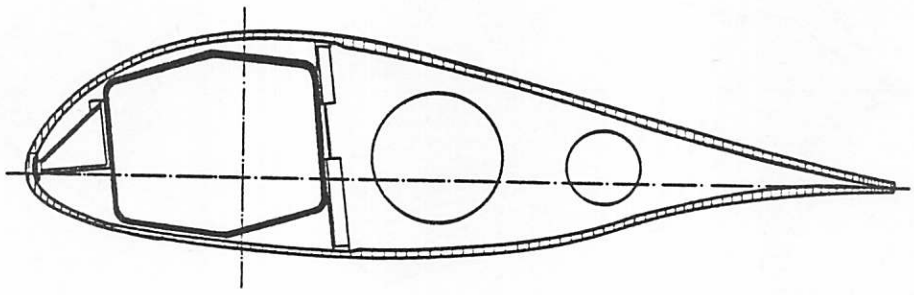

Fig. 8 GFK-Profilierung
GFK-Airfoil

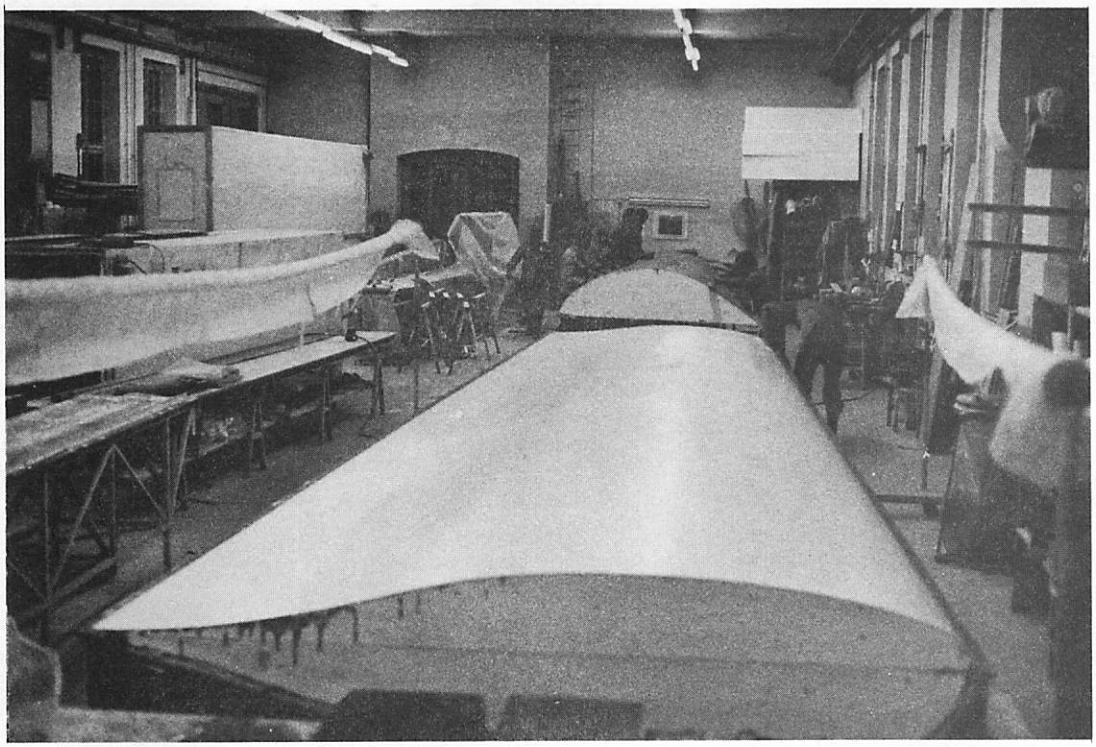

Fig.9 Mould

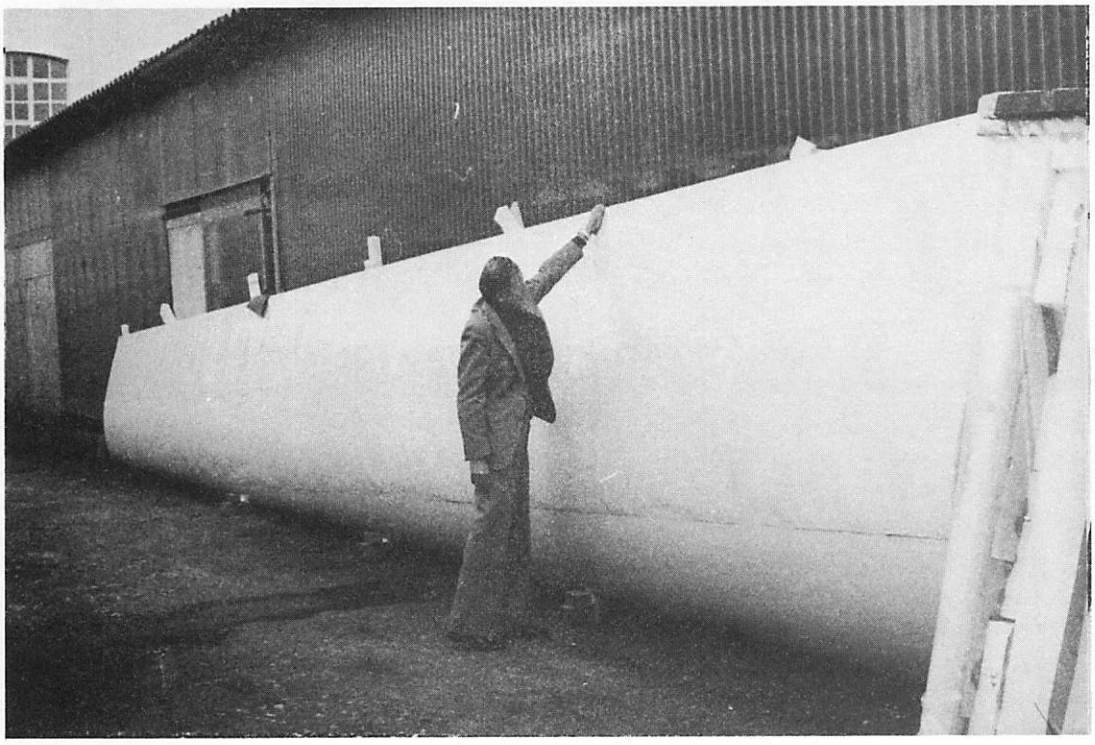

Fig. 10 Master piece

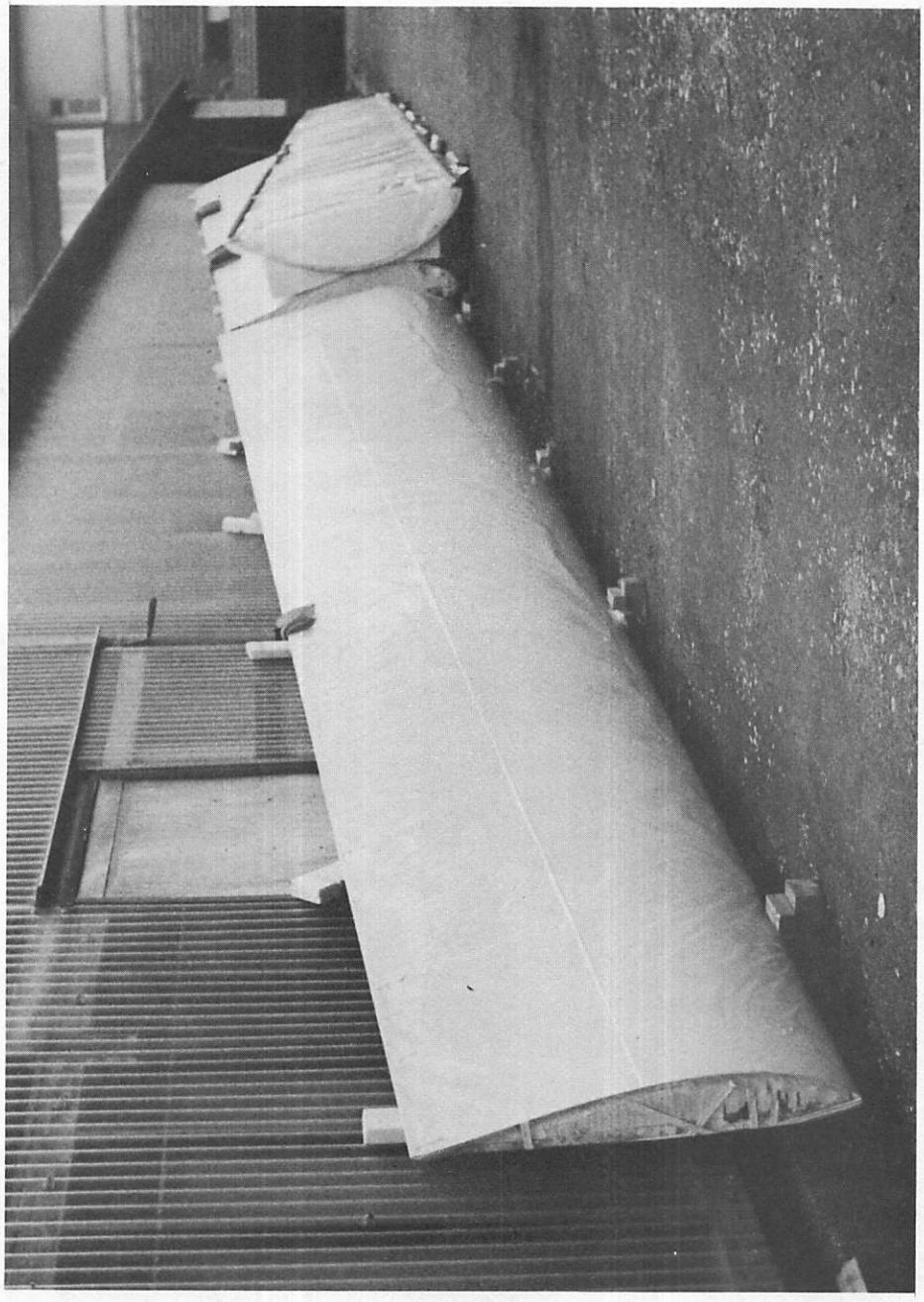

Fig. 10 a Master piece
R = 27,5 - R - 50 m

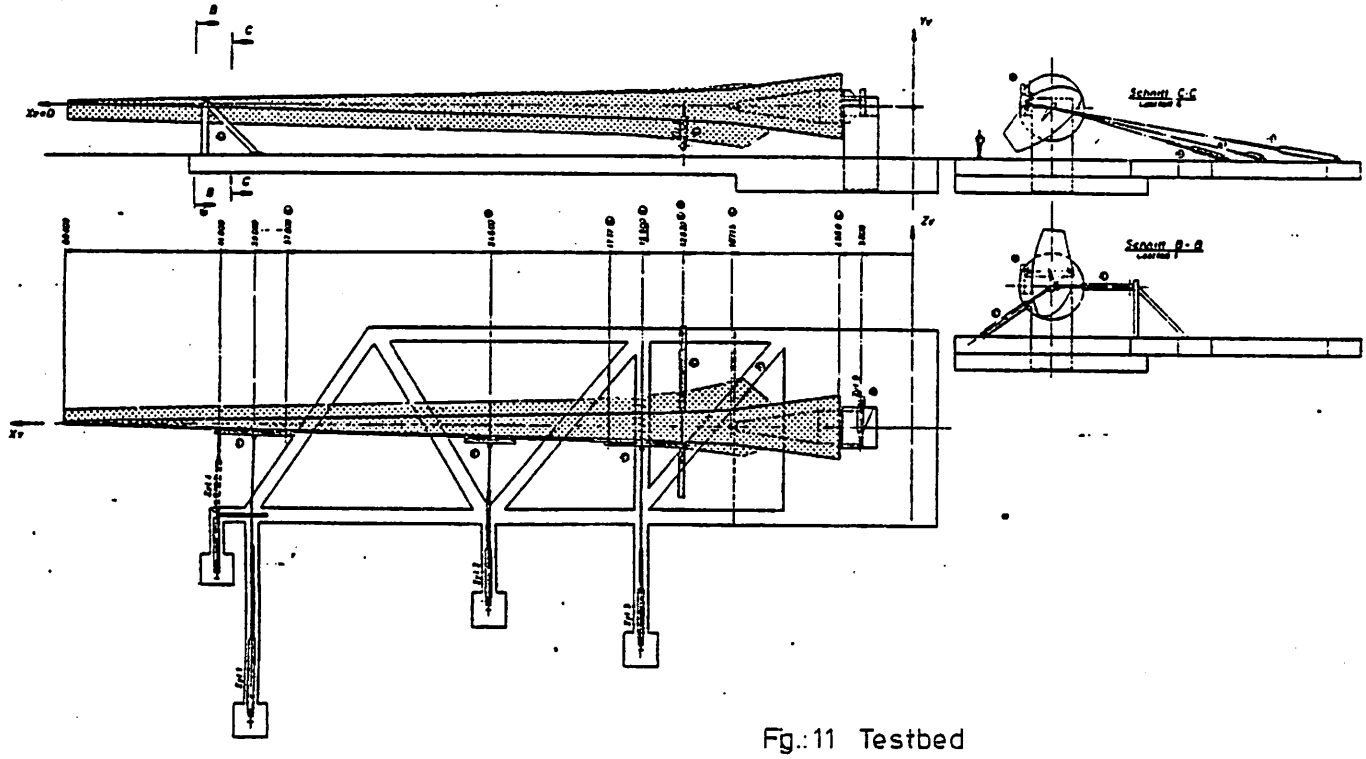

Fg.: 11 Testbed

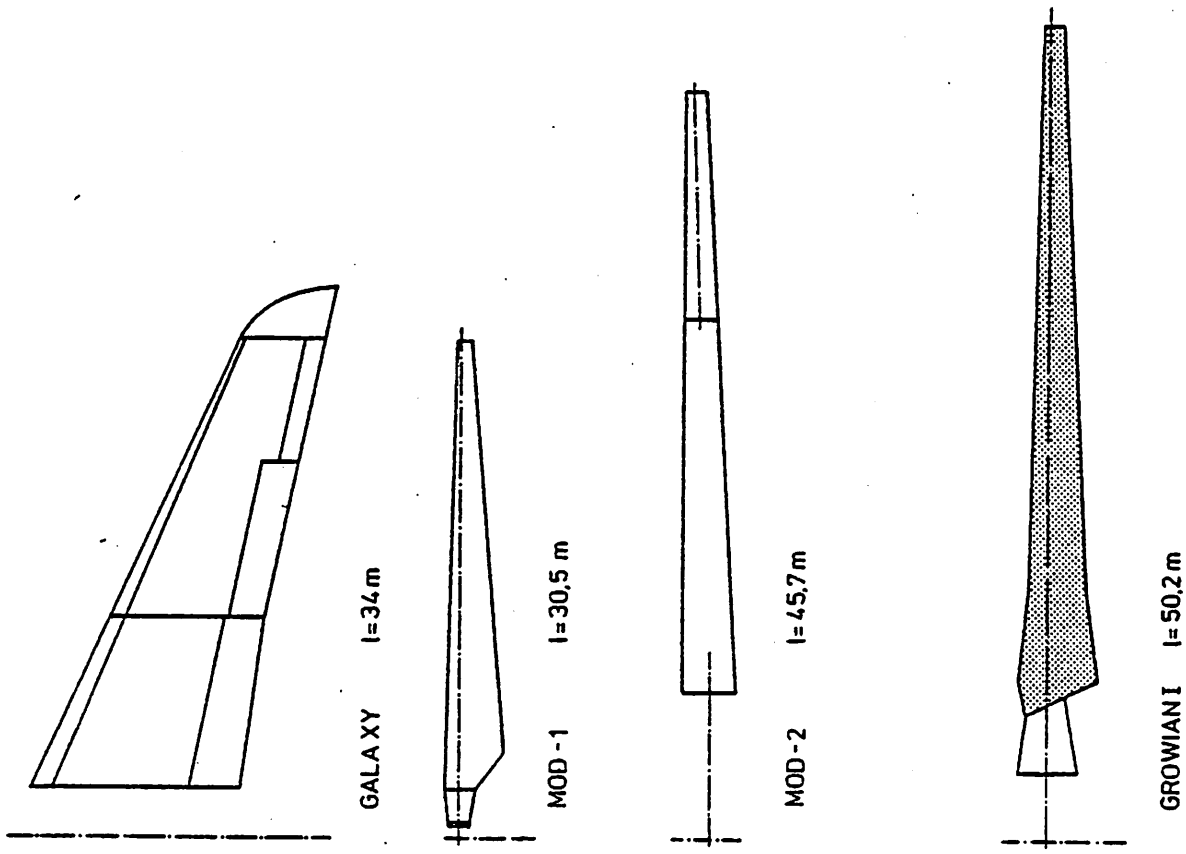

Fig: 12 Size Comparison

GROWIAN
Composite Rotor Blade
Design Concept and Testing

IEA - 4th Expert Meeting
21.4. - 22.4.80 in Stockholm
Sweden

by Dieter Muser

Munich: March 1980

MAN-Maschinenfabrik-Augsburg-Nürnberg
Aktiengesellschaft
N E U E T E C H N O L O G I E
D - 8 München 50 West Germany

1. Technical History

In the preliminary design for GROWIAN I rotor blades five concepts have been in competition (Fig. 1):

- GFRP blade: sparbox and shell GFRP
- CFRP blade: sparbox and shell CFRP
- CFRP steel-blade: from hub to 32 m steel-/GFRP, tip CFRP
- CFRP-steel blade: twisted sparbox steel to 15m/GFRP, tip CFRP/GFRP
- GFRP-steel blade: untwisted sparbox steel, shell GFRP

The different designs were compared in weight, eigenfrequencies, tip deflection under load and costs.
Soon the GFRP blade was thrown out because the costs were higher than those of CFRP blades, depending on too much man hours and too low flapwise eigenfrequencies.

The twisted steel blade with GFRP cowling was also eliminated because the production costs seemed to be to high, too.

Because there are also problems in the zones of force introductions to the bearings the design of a CFRP blade for the "tip" from 15 to 50 m was choosen for further development. But after the tests have been completed, there was no satisfaction in quality control and guarantee of thick CFRP laminates.

So the last concept with untwisted sparbox of steel and an aerodynamic covering in GFRP was winner. This type of blade is presented by Mr. A. M. Thiele.

2. Steel-CFRP blade concept

The design philosophy for this blade and its connections was as follows:

- high stiffness and high mass in the inner part of the blade
- high stiffness and low mass in the outer regions
- force reductions by long distances and well-known flow of forces
- force separation with different bolt directions and bearings

This philosophy originated the concept of figure 2. The hub close part of the blade is fitted to the bearing in a conservative way with a lot of axial bolts. On the other side the lateral loads and flatwise bending moments are carried by two arms with tip bolts while the centrifugal- and edgewise loads are carried by to wide distanced chordwise bolts. (Fig. 3) The same connection is used at radius 30 m, where the blade is separated once more, to allow a road transportation also on narrow roads.

3. Fabrication and Testing

To test this connection and the production of this carbon parts a 7,5 m long test section was fabricated in a glider factory. The sparbox had a total mass of 520 kg. Between point A and B, the finger outside of the profile shell, there is used a solid carbon box (Fig. 4), while a sandwich web construction is used in the shell section between B and C.

Production steps are shown in the following pictures. The base plates, webs and ribs are laminated in different moulds and cured. Afterwards the base plates are bonded to the webs (Fig. 5) and two of this parts are forming the inner web box (Fig. 6). After curing the carbon rovings are layed up, preimpregnated by pulling through a nozzle (Fig. 7). Then the final fabric winding is applicated and the complete sparbox is postcured for 15 hours at 60°C in a heated tent. Fig. 8 shows the test beam before delivering to the test facility.

Besides the static rupture test some dynamic tests at high loads should be performed, because there are only few test results on thick carbon laminates under dynamic loads available. As the deflection at tip of the beam (Fig. 9,10) was about 200 mm, the normal frequency expected by natural loading could not be practised.

Two different load cases were simmulated:

load case 2: Nominal power at nominal windspeed plus 100% gust (12 to 24 m/s)

load case 4 A: Nominal power at cut out windspeed plus 60% gust (25 to 40 m/s)

4. Test results

After installation of the test beam a static test with maximum gust loading was run without loss in stiffness. During the next three weeks the test was undergoing dynamic loading at a frequency of 0.4 Hz or 2,5 seconds per load cycle until 10^5 load cycles were fullfilled.
No damage of the structure was detected.
Also the following 100 cycles at maximum gust loading showed no visible and measureable damage. So the first rupture test started.

At load level 75,1 % of calculated breaking load the bed plate (position B) mid of the beam failed by delamination and rupture of the circumferential fibres wound around the bushing (Fig. 12). This was caused by an asymetric design of the position of the bushing towards the bed plate.

The load introduction was repaired by a simple steel wedge bonded to the compression flange of the beam and pressed against the load frame.

Loaded with only 34% of breaking load, bushing no. A failed because the bearing was not exactly positioned when the test beam has been fixed to the frame after repair. After modification of this part load was applied again and rupture occured at 97,2% of calculated breaking load.

Damage occured in the zone of maximum compression stress rectangular of the fibre orientation, diagonal in the webs and parallel to the fibres in the tension loaded flange towards point C (Fig. 13,14).

The measured strain was multiplied with an experimental gained Youngs modulus to obtain the stress at rupture. Maximum stress in the compression flange was calculated to about 496 N/mm^2 (Fig. 15), while shear stress has been 120 N/mm^2 at maximum (Fig. 16,17). When dynamic load stresses are compared with the ultimate stresses at failure of the test beam the calculated margin of safety 1,2 was reached (Fig. 18). The assumed line of ultimate time dependent stress for handlaminated CFRP seems to be accurate and usefull for further calculations. Caused by a high void content and an unequal resin distribution in laminate cross section, the decrease of the curve is higher than the well-known one of prepreg laminates.

5. Costs

One of the reasons to development of the composite rotor blades was the low expected mass of this blades. Compared with other types (Fig. 19) the value of the CFRP blade is only 40% of the steel version. On the other hand the present manufacturing costs are at a high level (Fig. 20) in comparison to other published datas.
It seems, that there are two different design philosophies: high weight/low cost and low weight/high cost, when prices per unit mass are plotted versus electrical energy output. There is no statement about aerodynamic efficiency of all different blades and other influences of blade mass on dynamic behaviour of the complete wind turbine.

6. Conclusions

The fabrication study and dynamic test of a CFRP-beam in original GROWIAN-size originated following experiences:

- It is possible to manufacture thick CFRP laminates in combined pultrusion-hand lay up technique.

- Allowable dynamic stresses are lower than in common prepreg laminates.

- Costs of CFRP-rotor blades produced in standard technology are to high, depending on high material prices and expensive fabrication methods, but are rapidly decreasing.

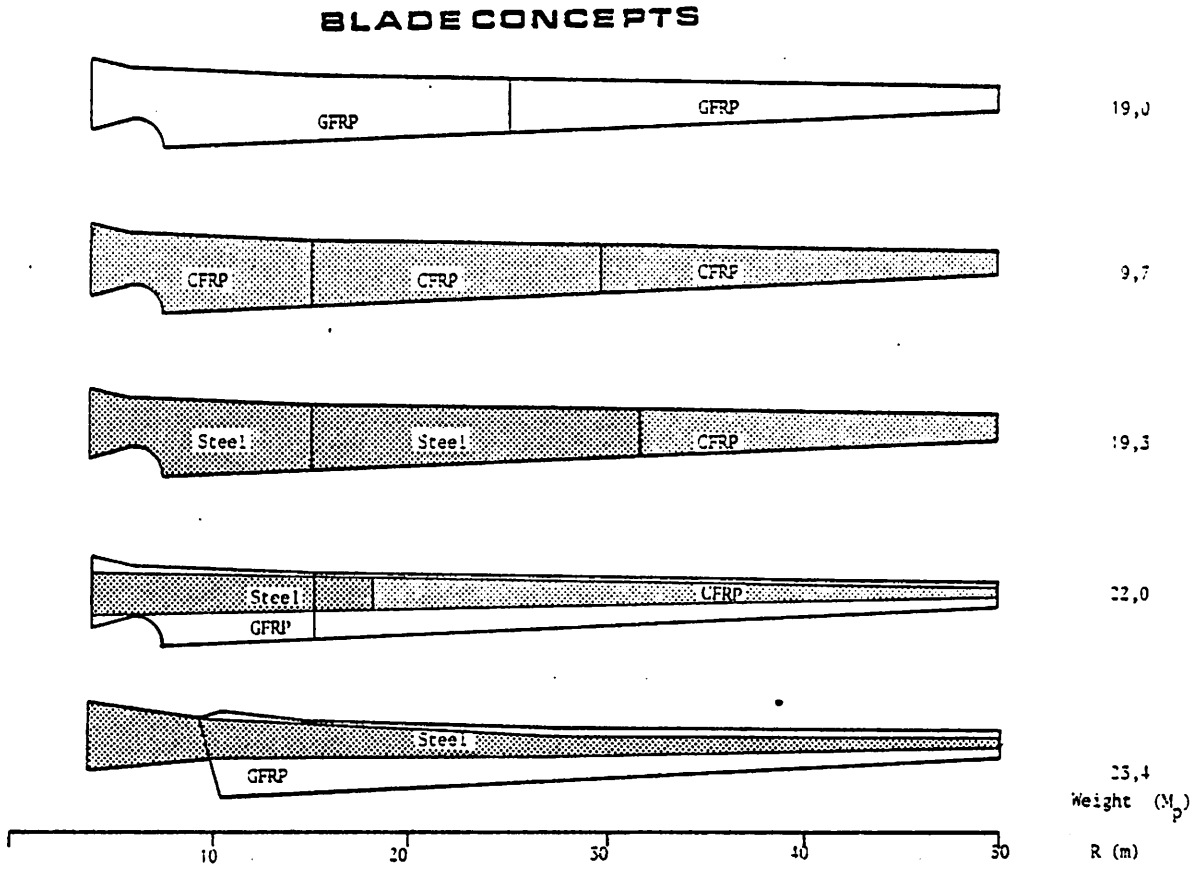

FIG. 1: GROWIAN - Bladeconcept

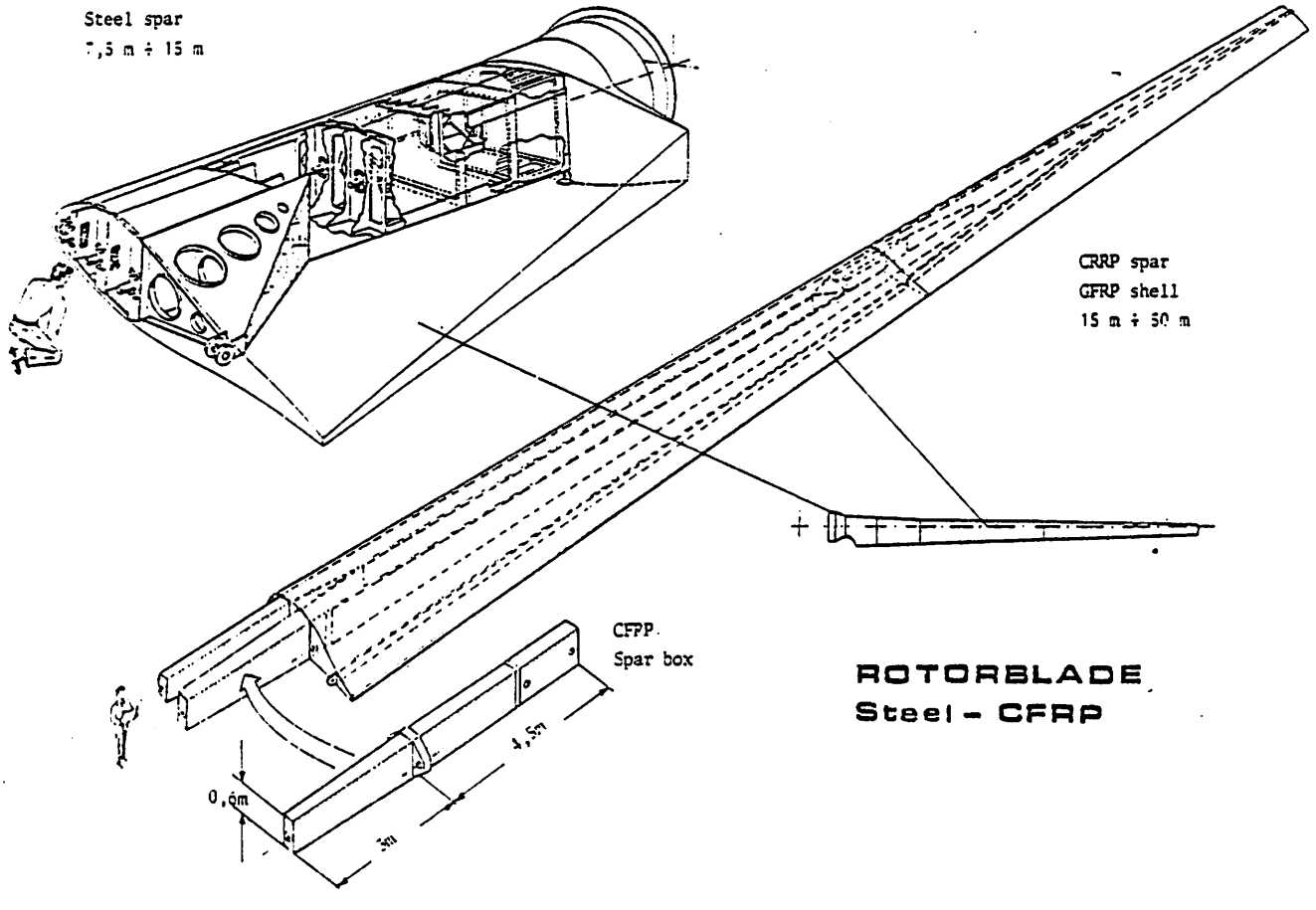

FIG. 2: Steel/CFRP - Rotorblade

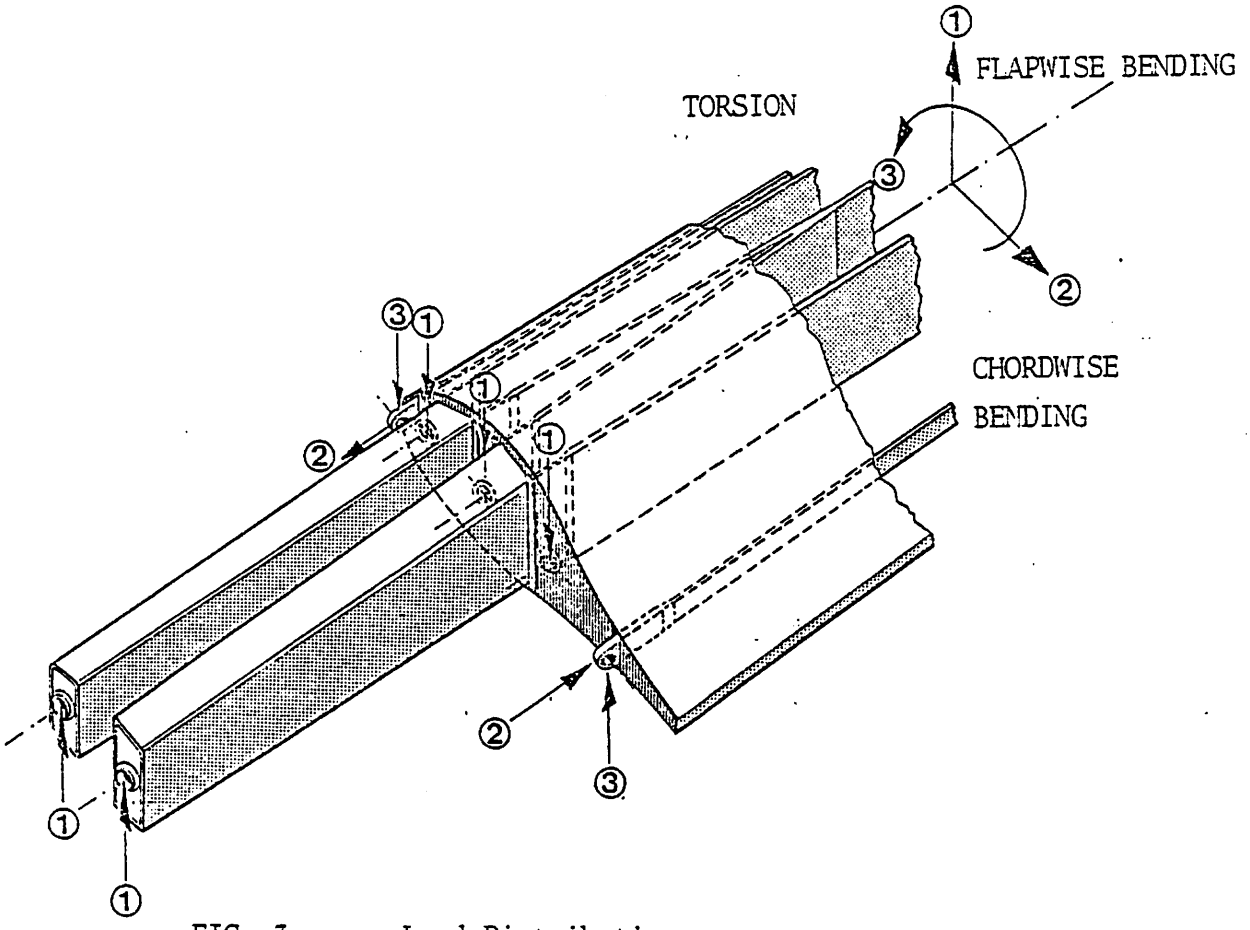

FIG. 3: Load Distribution

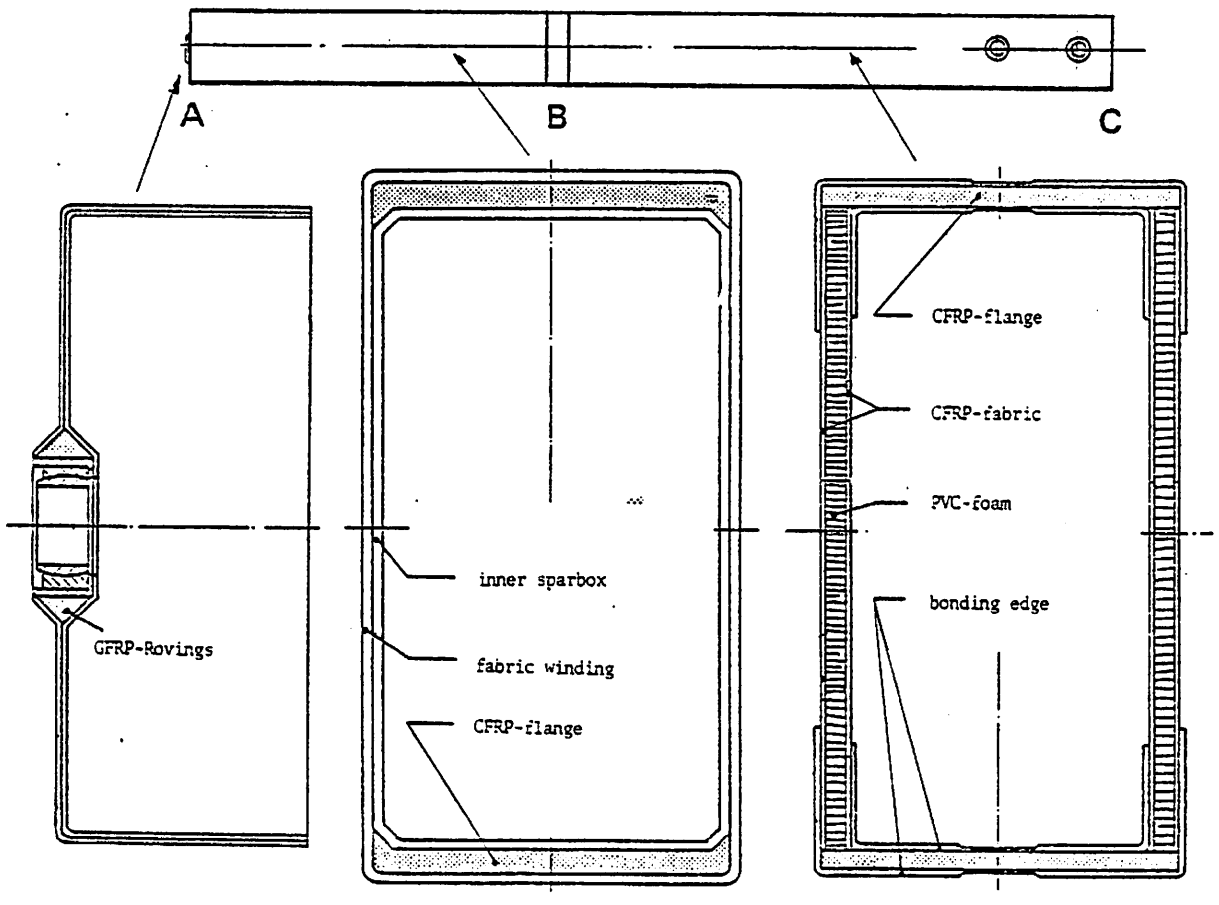

FIG. 4: Cross Section of CFRP-Box Spar

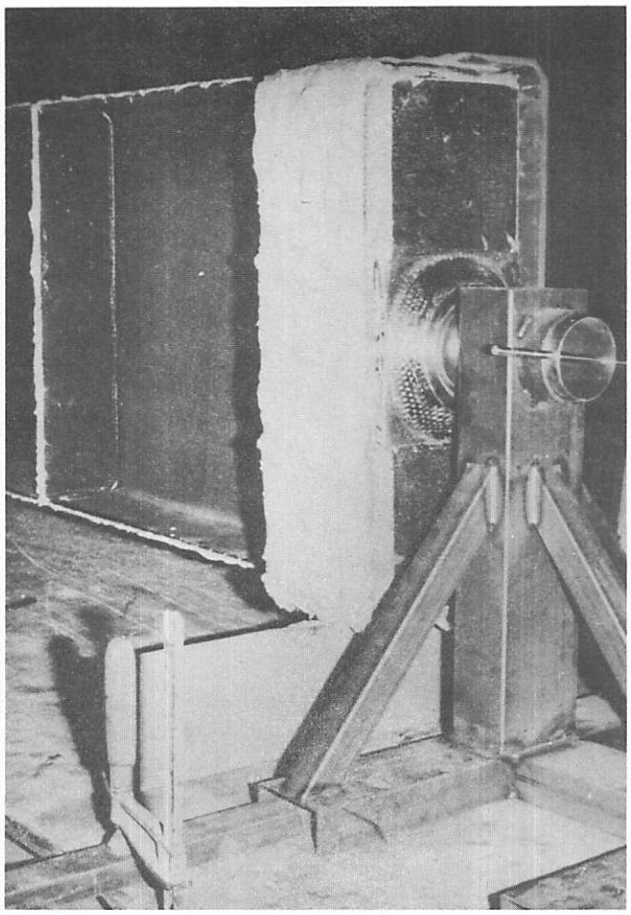

FIG. 5: Base plate "A" before bonding

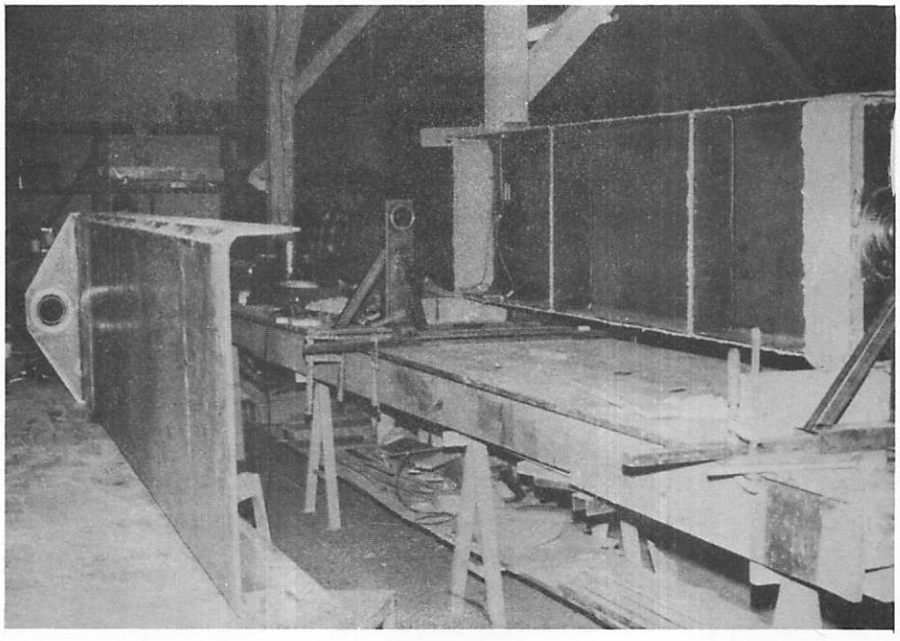

FIG. 6: Base plate "B" bonded into web

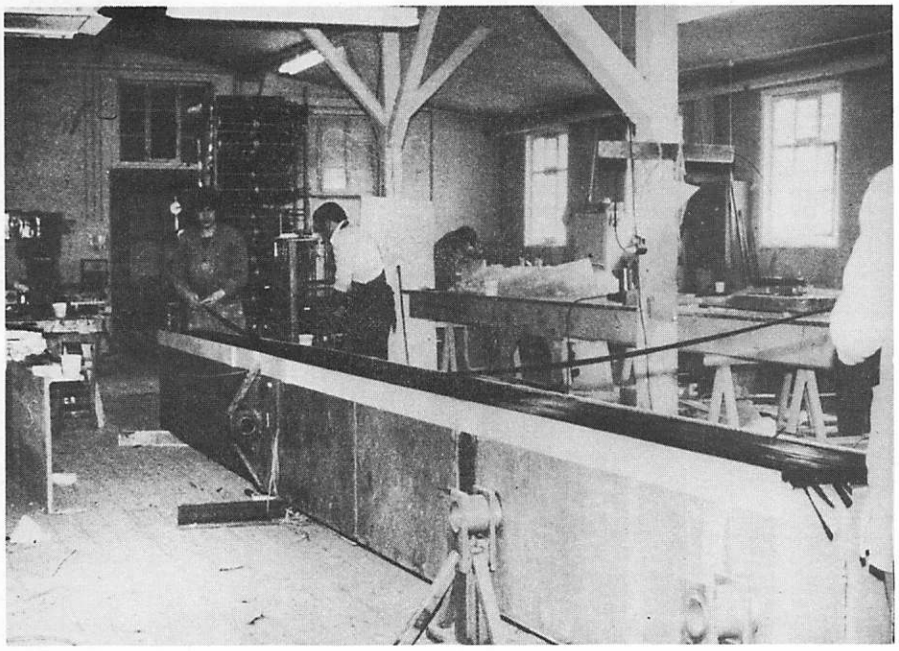

FIG. 7: Fabrication of unidirectional spars

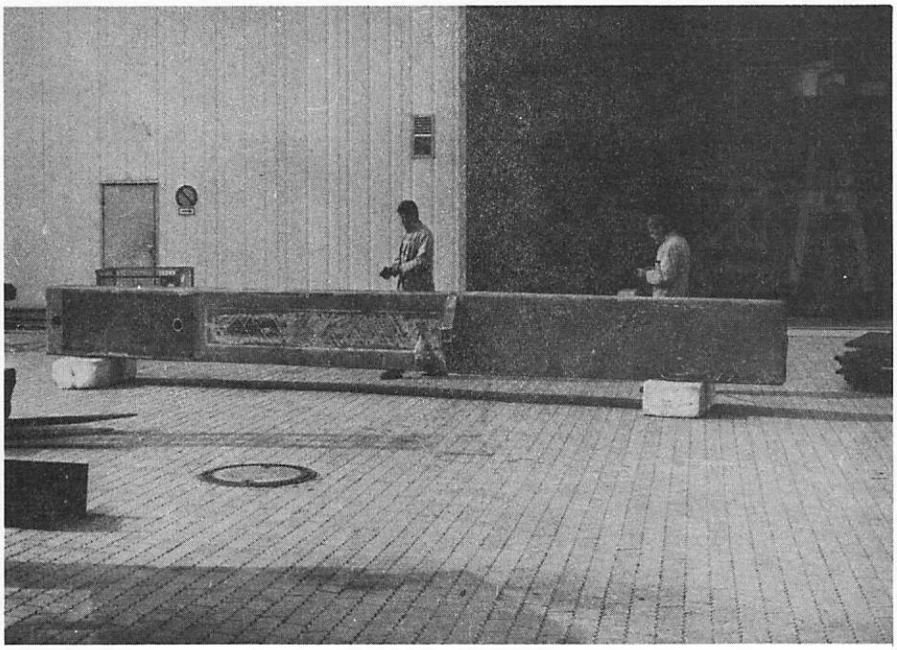

FIG. 8: Complete test beam

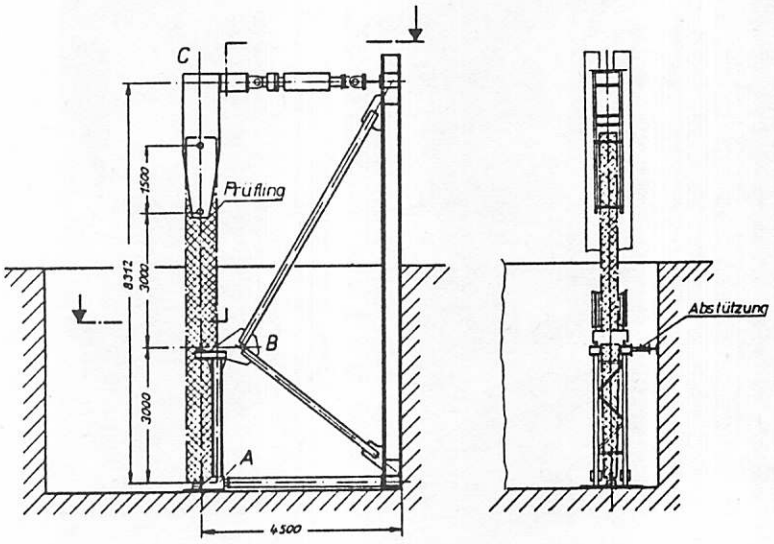

FIG. 9: Test setup, schematic

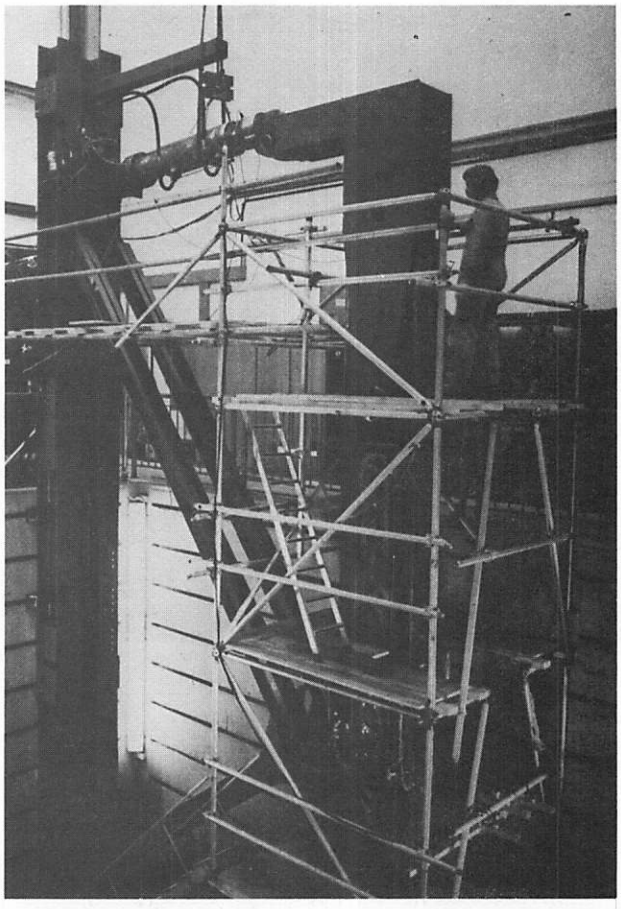

FIG. 10: Test setup

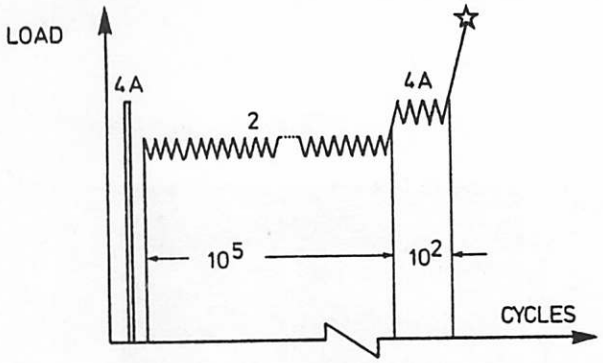

Test no.	Loadcase	Forces A daN	Forces B/2 daN	Bending moment B daNm	Cylinder force C daN
1	Static 4 A	83200	65096	249600	46992
2	2 lower level	60630	47442	181890	34255
	upper level	68525	53620	205575	38715
	$N = 10^5$				
3	4 A Dynamic				
	lower level	68525	53620	205575	38715
	upper level	83200	65096	249600	46992
	$N = 10^2$				
4	Rupture-test	117312	91785	351936	66258

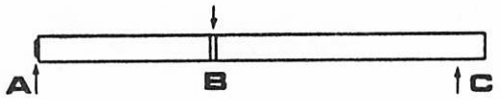

FIG. 11: Test loads

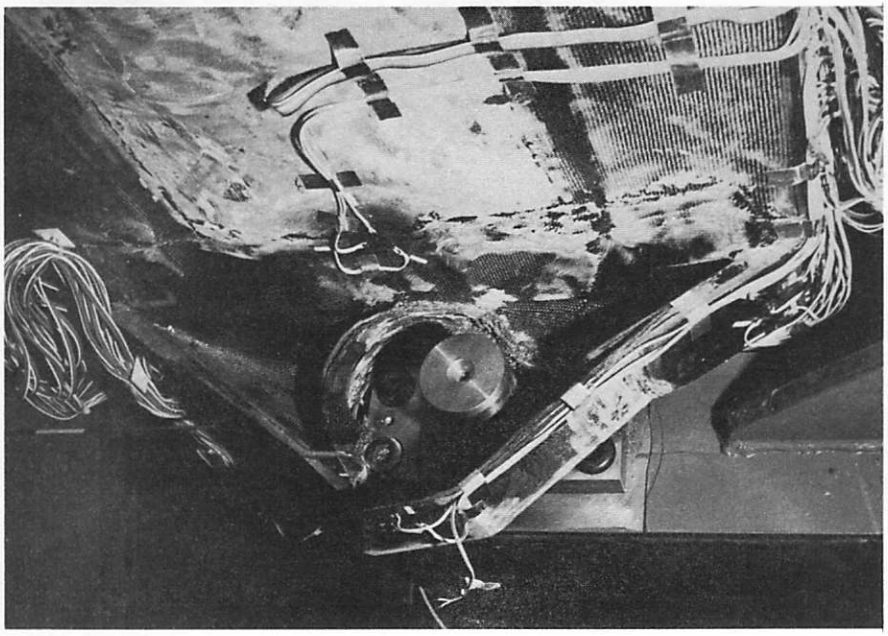

FIG. 12: First Failure, Bed Plate Position B

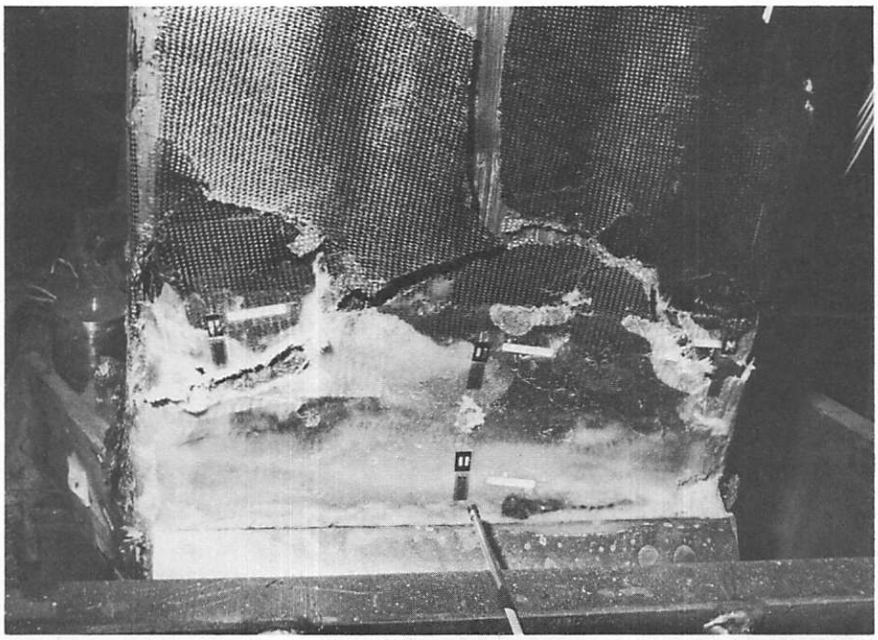

FIG. 13: Failure in Compression Flange

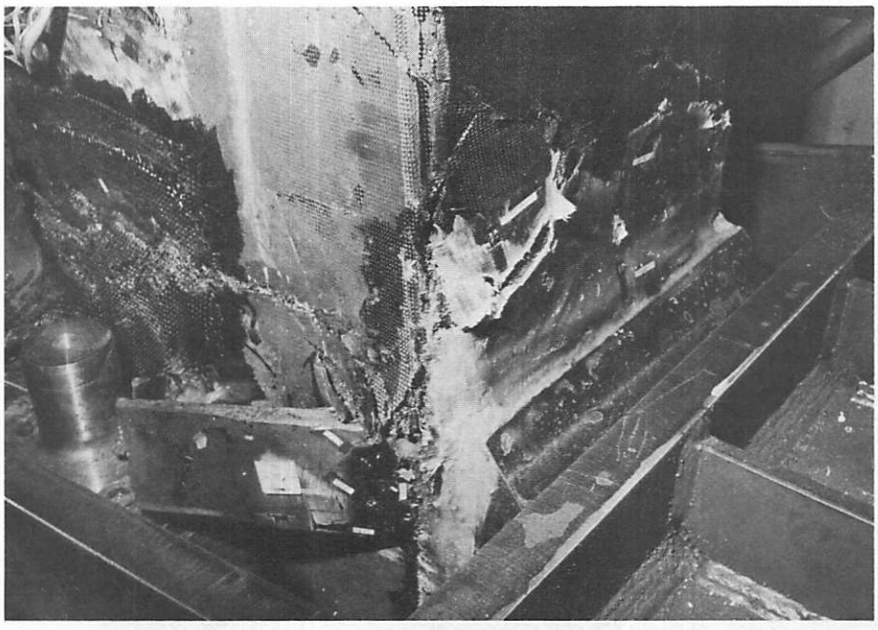

FIG. 14: Failure in the web

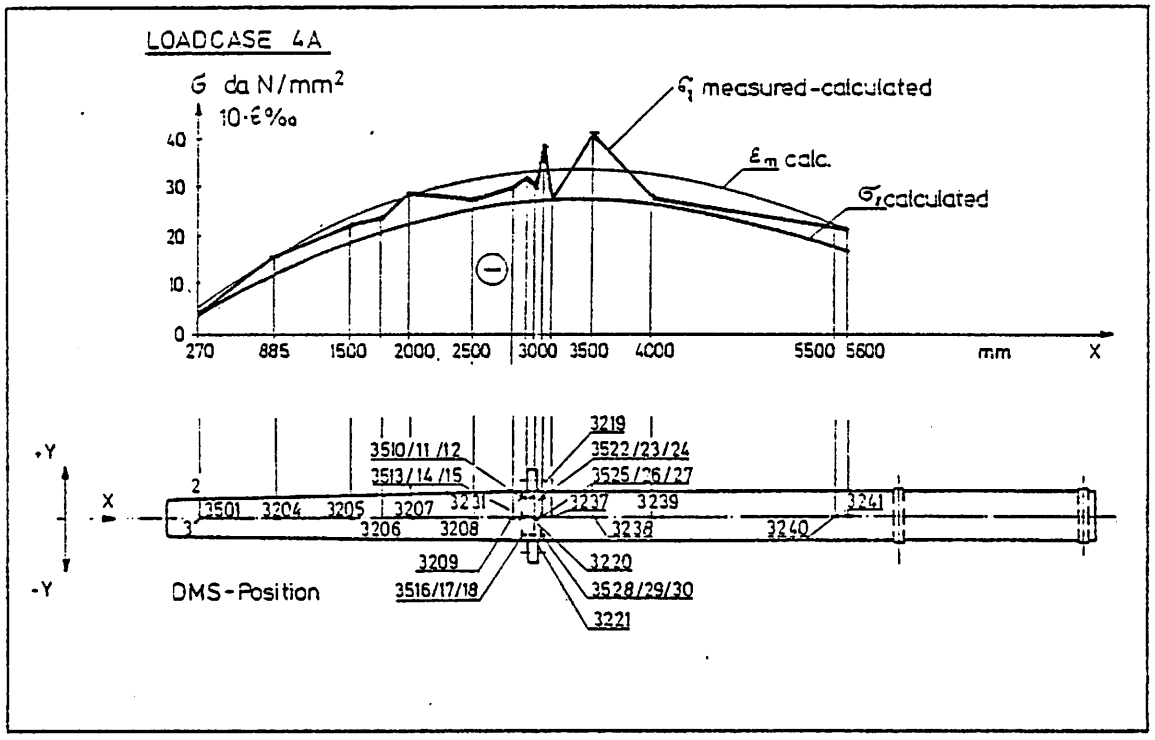

FIG. 15: Stress Distribution in the Compression Flange at Dynamic Load

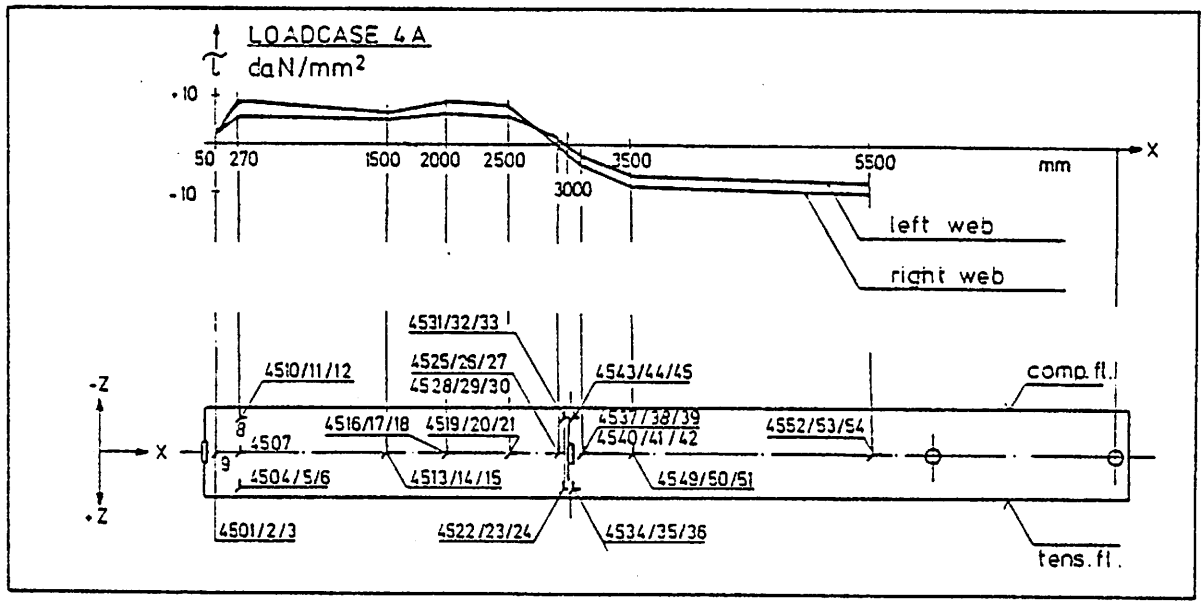

FIG. 16: Shear Stress Distribution in the Web at Dynamic Load

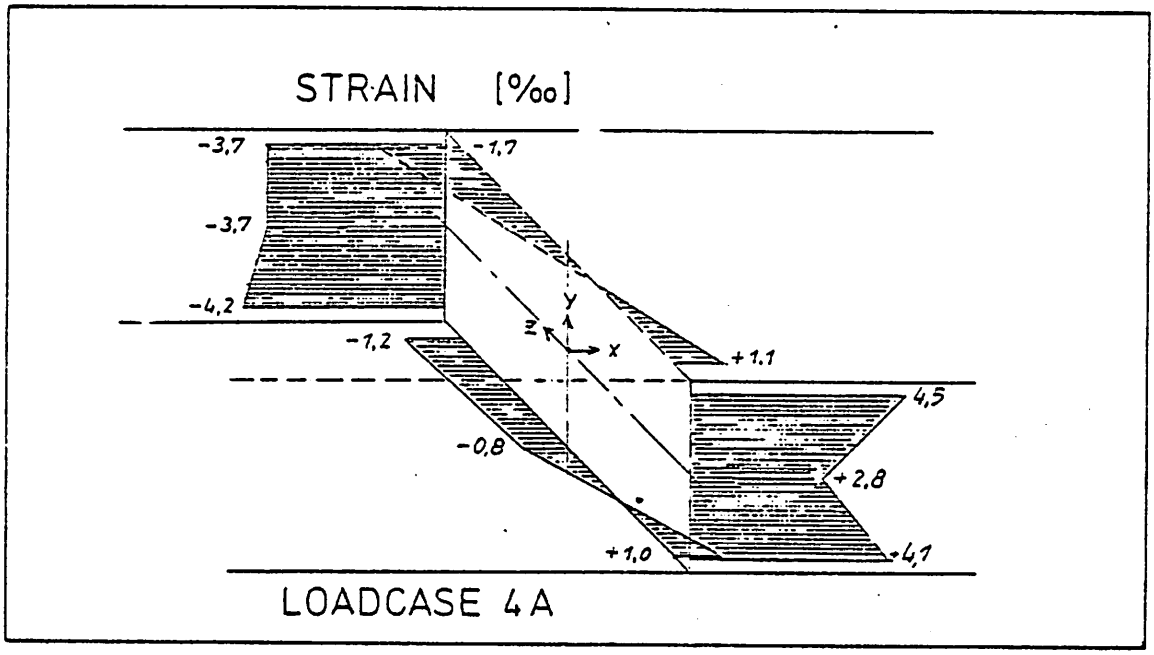

FIG. 17: Strain Distribution at Load Case 4 A
(10^2 cycles)

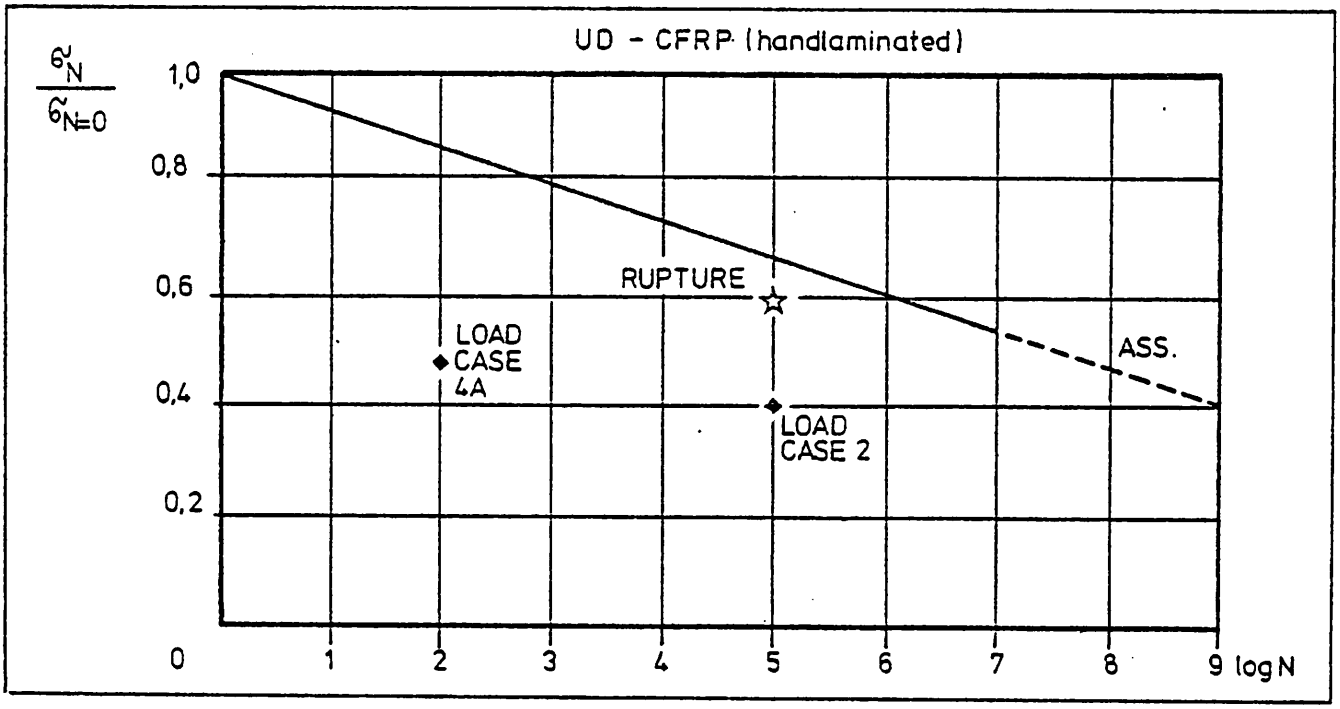

FIG. 18: S-N-curve for hand laminated CFRP

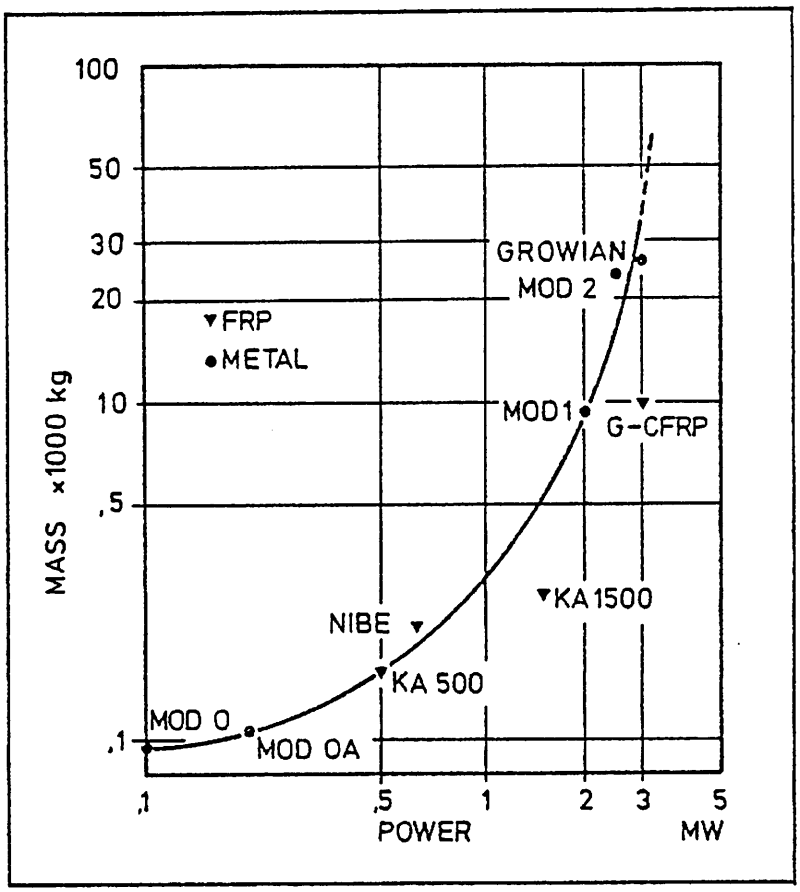

FIG. 19: Mass of Rotor Blades

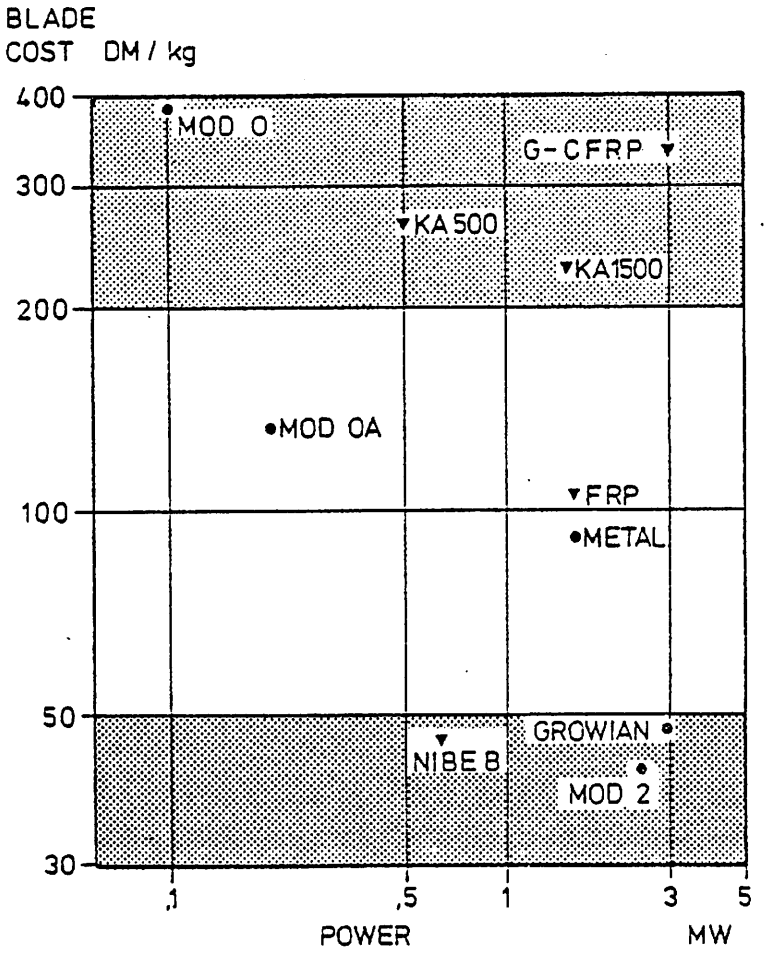

FIG. 20: Relative Blade Costs of Rotor Blades

DEVELOPMENT AND DESIGN OF A LARGE WIND TURBINE BLADE

Dipl. Ing. Michael Hahn*
MBB, West Germany

Summary

A short schedule of the development group and the design-basis developped in the past will be given. The mould-concept is the key for design and manufacturing of large blade-structures, which needs a special surface-definition and structural design.

The blades design and the assembly will be described with all consequences for surface definition, material selection, laminate design, curing procedure and tool design.

A complete survey about the tooling will be given, including mould and heating system, cutting and milling devices.
A short report about the manufacturing of an 11 meter-test section completes the presentation.

* The Paper was presented by H. Bansmir, MBB

1. Introduction

The development of rotor-blades for a large horizontal-axis windmill demants the solution of problems in design and material selection.

Three major problems are typical for large wind-energy units:

a) The big dimensions of the rotor-blade and its complicated aerodynamic shape.
Fig. 1 shows the dimensions of the WEC rotor-blade.

b) The forces acting on the blade and the environmental influences.
The aerodynamic and inertial forces and the environmental influences can be seen in Fig. 2.

c) The extreme requirements which are imposed to the dynamic characteristics of the rotor-blade.
Fig. 3 shows the natural frequencies in bending and torsion, which are very high for such a slender beam.

These three porblems require the development and the application of new technologies.

The material selection, the blade design and the manufacture of a test section, 11 meters in length, for the WEC rotor-blade will be described.

2. Material selection

The dynamic characteristics and the stresses of large rotor-blades are mainly dependent on their masses.
For this reason, materials of high fatigue strength, high stiffness and low mass have to be selected.

Fig. 4 shows the properties of metals and fibre-reinforced composites (FRC). The high specific stiffness and strength of FRC become evident.

These advantages can also be seen when comparing the mechanical properties of cross-sections of rotor-blades of different types of construction.

Three rotor-blades designed for the same contur can be seen in Fig. 5.

Due to the good formability of FRC the structure can be built to the final aerodynamic shape.
That ist why the FRC design provides better stiffness than the metal design.

As to the mass, the strength of the FRC design is higher than the specific strength of the metal design. The margins of safety are higher in FRC than in metal.

There are two additional reasons for the FRC design:

- The good formability of the laminates allows to build rotor-blades of high aerodynamic quality and very different profiles at the tip and the root of the blade.
  Fig. 6 shows the typical profiles of a wind-energy rotor-blade

- The second reason is that it is possible to vary the stiffness of a cross-section with a given contour.
  Since composite designs are mostly very safe in strength, one cannot only chose between different types of fibres, but it is also possible to vary the thickness of the laminates which are to be built up in layers.
  The laminate design of a wind-energy rotor-blade can be seen in Fig. 7.

Thick laminates within the area of big profile thickness and thin laminates within the regions of leading and trailing edges result from the staggering of the layers.

3. Loads and environmental influences

Fig. 8 shows the resultant load of all loads which act on the rotor-blade in operation.

This load is composed of flight loads including bee effects, wind shear and gusts and the inertial forces resulting from the rotation within the gravitation field.

One can see the curve of the safe loads of the FRC rotor-blades. The safety factor is about four. The service-life will be more than 20 years. /See reference (1)/.

Rotor-blades designed in carbon fibre need lightning protections Fig, 9 shows the arrangement of the lightning protection.

Two conductors protect against lightning strikes in the leading edge and the trailing edge.
Within the region of the blade tip the entire surface is protected by thin aluminium mesh. This mesh can conduct away smaller induced charges following the first lightning strike.
Fig. 10 shows the environmental influences.

The elastic surface of the erosion-resistant paint and the compact design of the blade protect from

- erosion
- icing
- moisture
- solar radiation and
- impact of small particles.

FRC has no corrosion.

4. FRC technology for large structures

Since the manufacture of large laminate quantities (more than 1 ton/per blade) require some days , one has to use resins, which have long pot lifes at room temperature.

These resins cure in heated moulds at temperatures above 90°C. To avoid unnecessary thermal stresses, the whole laminate quantity is cured in one cycle.
Fig. 11 shows the manufacture of the BO 105 helicopter rotor-blade.

This hand-laminating method cannot be used for producing large structures. The impregnation of the fabrics in the mould and the use of small roving tapes do last too long.

For big rotor-blades MBB uses prepregs which are cut to size outside the mould.
Fig. 12 shows the lay-up of prepregs in the mould of a wind-eeergy rotor-blade (WEC).

After finishing the lamination the shell is cured under a vacuum-foil.
The curing of the shell is a single-step preocess with slow temperature variation for heating up and cooling down.

Filament winding of a rotor-blade can be seen in Fig. 13 Filament winding is not used, because the mass would increase in relation to the prepreg-technique, the surface and the contour quality would be reduced and the tooling would be more expensive.

The advantages of filament winding are good laminate quality and economical manufacture due to automation.

An experimental set up for the testing of the resin injection method can be seen in Fig. 14.

Dry fabrics are fixed in a closed mould and will be impregnated by resin under low pressure. The advantages are good impregnation, greater independence of the pot life of the resin systems and economical manufacture of higher quantities.

The diesgn and manufacturing of moulds require higher effort and there is a problem of visual inspection of the impregnation process.

5. Mould concept (Fig. 15)

The moulds of big rotor-blades have to be heatable, deflection--free and should be economically produced.
Fig. 16 shows a cross-section of the mould for the WEC rotor-blade. A mould-concept was developed for big structures with a plastically formed steel shell, which is supported by steel frame-work.

The supporting allows as both an adjustment of the mould-hight and a fixation of the shell-twist. The bearings are free for thermal expansion, but they do not change the exact mould position.

Fig. 17 shows a part of the rotor-blade and its development.

The outline of the blade will be numerically defined by means of a computer.
Due to the bending of the moulds made of plates, the outline has to be a surface that can be developed. The loft-lines, which are the control-lines for the bending process, are thus determined.

A completed shell mounted on the underframe can be seen in Fig. 18.

The depth of the profile is about 1.1 m and contour deviations of less than 3 mm could be measured.
The position of the rotor-blade axis is within a tolerance of ± 1 mm. The twist was positioned within 0.1 degree.

The tool cannot be closed. The moulds of the upper shell and the lower shell of the rotor-blade are set in parallel to manufacture the common junction plane with one tool only.

Fig. 19 shows the mould of the upper and the lower rotor.blade shells.
Both moulds have a parallel tolerance of less than ± 1 mm and the twist is 6.7 degrees.

The steel shells can be heated by current-carrying carbon fabrics.
Fig. 20 shows the construction of the heating system.

Two layers of glass-laminate isolate the carbon laminate on both sides.
The heating-system will be laminated directly on the surface of the mould. The electrical contacts to the carbon.cloth at the border of the mould are manufactured out of cupper straps.

A control loop regulates the power to optain the right temperature. The range is from 30°C up to 120°C.
The costs of three different mould-concepts and the best range of application can be seen in Fig. 21.

Milled metal moulds are good for small rotor-blades with high geometric accuracy and big quantities. Moulds made of FRC used both for small parts and for big parts, but they cannot be heated easily and the specific costs increase for big blades.

The moulds made of bent metal panels can be applied cost-efficiently for big parts.

6. Design

Dimensions: (Fig. 22)

length	25.2 m
max. chord	1.1 m

circular cross-section in the attachment area.

Dynamic characteristics:

natural frequencies (rotating)
first modes

flapwise	1.3 Hz
chordwise	1.6 Hz
torsion	15 Hz

Margins of safety:

statically	above 4
fatigue	above 2

The blade consists of two halves (upper and lower halves) which are bonded to each other. A cross-section of the blade is given in Fig. 23.

The skin is made of glass fibre fabric with a fibre orientation $\pm 45^{\circ}$ to the blade-spandirection.
It is both torsion-box and aerodynamic shape.
The upper and the lower skins are connected by glass-laminate caps on the leading and trailing edges.

The flanges are made of unidirectional carbon-fibre (T300) laminate.
They provide tensile strength and flexural stiffness.

The core, machined of PVC does stabilize airfoil geometry uniformly and contributes to shear-load transfer.

The shear web reinforces the rear part of the foam core. The good stabilization of the foam core allows a design with three ribs only: one of them at the inboard end and one at the outboard end of the blade.

The third rib is to transfer the shear-loads from the foam core into the webs of the inboard blade structure. The attachment configuration can be seen in Fig, 24.

In the attachment area the laminate is thickened considerably. The loads are transferred by means of prestressed studs in combination with cylindric nuts, which fit into bores within the thickened laminate.

The laminate is designed for the same coefficient of thermal expansion of the steel rotor-hub and for the required pretension of the studs.

7. Manufacturing technology

The lay-up of the prepregs can be seen in Fig. 25.
The fabrics were cut to size outside the mould while they are protected by two foils.

Fig. 26 shows the lay-up of the thick laminate at the attachment area. The laminate thickness is 90 mm which is needed to support the cylindric nuts.
The adjusting of the PVC foam to the FRC-shell can be seen in Fig. 27.

Freely expanding foams cannot be used because these foams are not available with low density (l.th. 100 kg/m^3) together with sufficient dynamic resistance.

Foam pieces are bonded to the shell by an adhesive which can foam up and fill the soaces between the skin and the pre-cut foam.

The junction plane is machined at the cores of both shells by a special milling device. The milling can be seen in Fig. 28.

The milling device is guided at the mould and machines a twisted plane with the same shape for both rotor-blade parts. At this junction plane the halves are bonded together by an adhesive.

Fig. 29 shows the bonded rotor-blade. The attachment area is not yet machined. The laminate caps at the leading and the trailing edges are already assembled.

The drilling of the attachment-bores can be seen in Fig. 30. The diameters of the bores are 45 mm for the cylindric nuts and 32 mm for the anti-fatigue bolts.

Whereas the 45 mm bores cross the thick laminate, the 32 mm bores are rectangular to them and to the attachment plane. The attachment plane is machined by a diamant-tool.

8. Qualification

Fig. 31 shows the different test specimens which are used for the qualification of the WEC rotor-blade.

The laminate is fatigue-tested and its stiffness is measured. The evaluation of the elastic properties of the foam and its adhesive joints include shear tests as well as tension tests.

The test-specimen simulating the attachment is fatigue-tested to evaluate fatigue strength and information about reductions of the initial stresses in the bolts.

A part of the outer rotor-blade was loaded to ultimate strength in a 3-point-bending-test, to measure the buckling limit of this shell construction.

Finally the natural frequencies of a test section of 11 meters in length and the bending strength are measured in a cantilever test programme.

A complete presentation of all experimental and theoretical evaluations are given in ref. (1).

9. References

/1/ Stress analysis and testing for wind energy rotorblades
H.Bansemir, H.Pfeifer
West-Germany, MBB. DE 133

/2/ Material and manufacturing technology Information 1/80
West-Germany, MBB

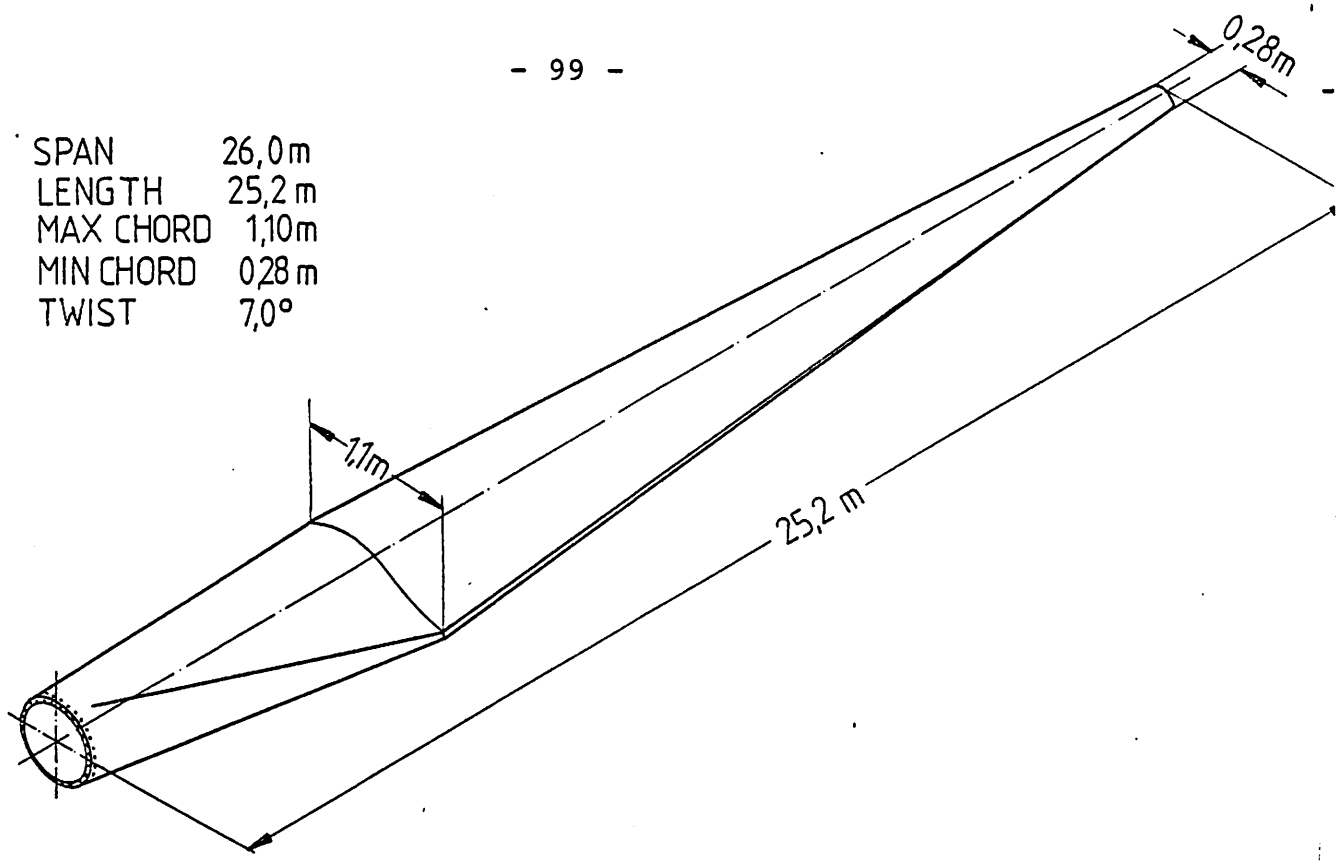

FIG.1
WEC ROTOR-BLADE
PROFILE AND DIMENSION

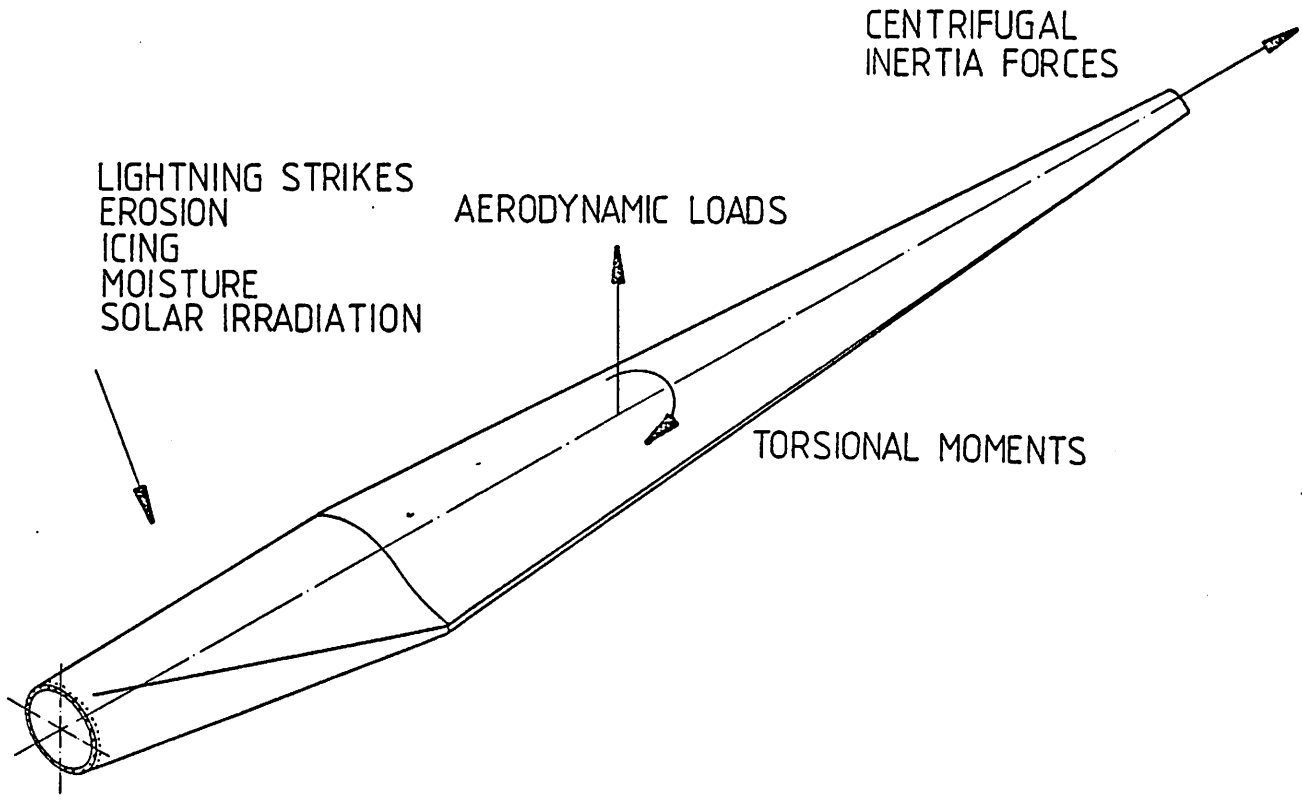

FIG.2
THE FORCES ACTING ON THE BLADE
AND THE ENVIRONMENTAL INFLUENCES

FIG. 3

DYNAMIC CHARACTERISTICS OF THE WEC ROTOR-BLADE

NOMINAL ROTATIONAL SPEED $n = 0{,}6\ s^{-1}$

1. BENDING FREQUENCY FLAPWISE $f_\beta = 1.3\ s^{-1}$
1. BENDING FREQUENCY CHORDWISE $f_\xi = 1.6\ s^{-1}$
1. TORSIONAL FREQUENCY $f_\theta \geq 15\ s^{-1}$

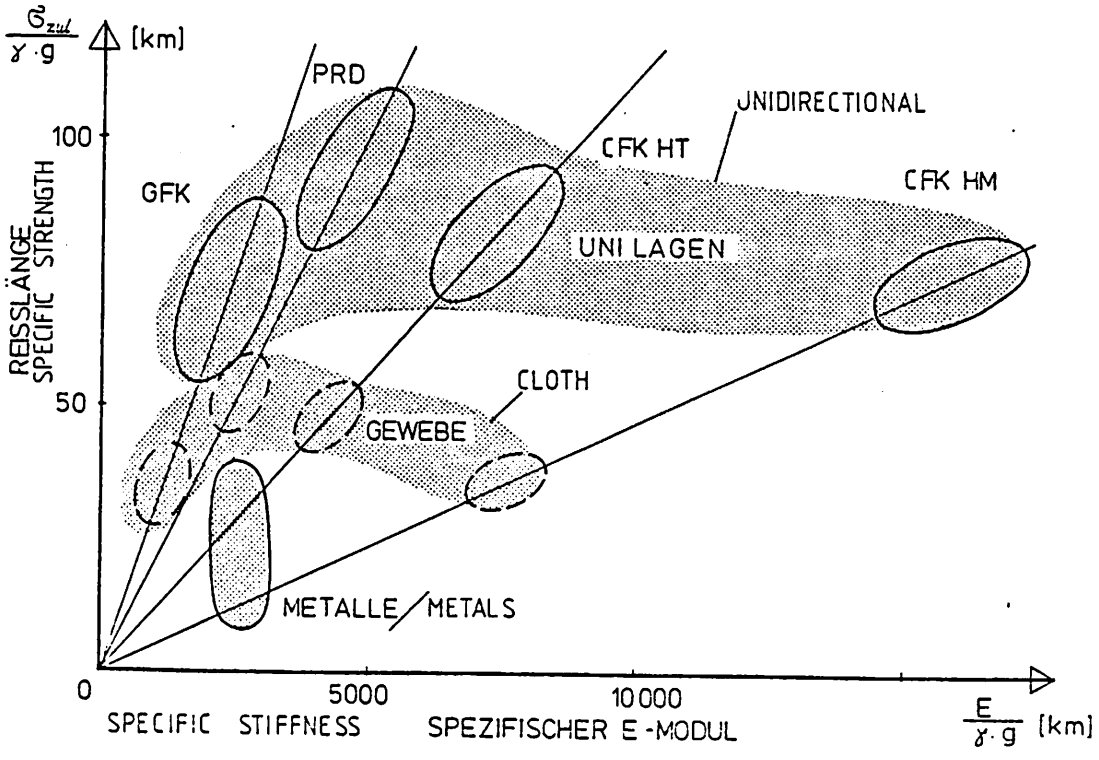

FIG. 4
FESTIGKEIT UND STEIFIGKEIT VON FVW UND METALLEN
SPECIFIC STRENGTH AND STIFFNESS OF FRC AND METALS

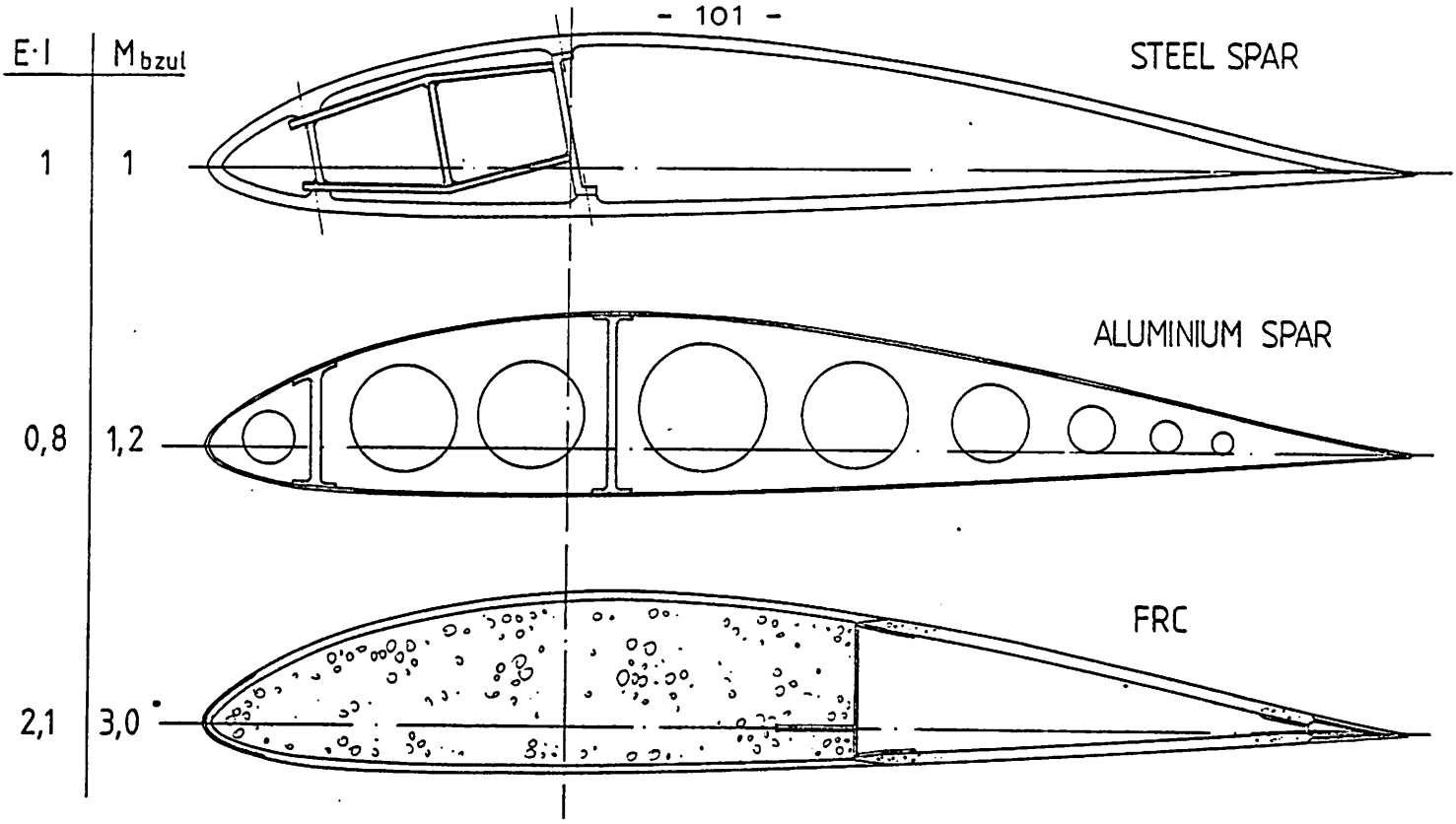

FIG. 5
DIFFERENT ROTOR-BLADE DESIGNS
FOR THE SAME CONTOUR

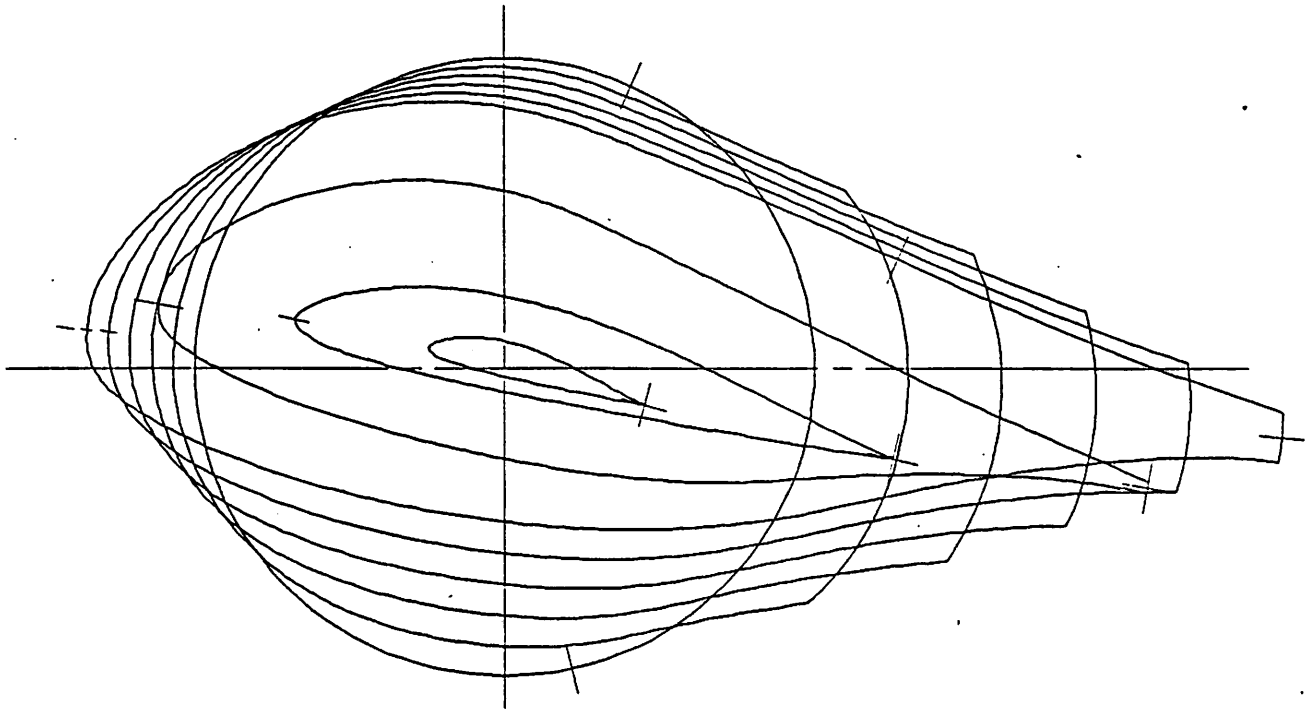

FIG. 6
PROFILE OF THE WEA ROTOR-BLADE

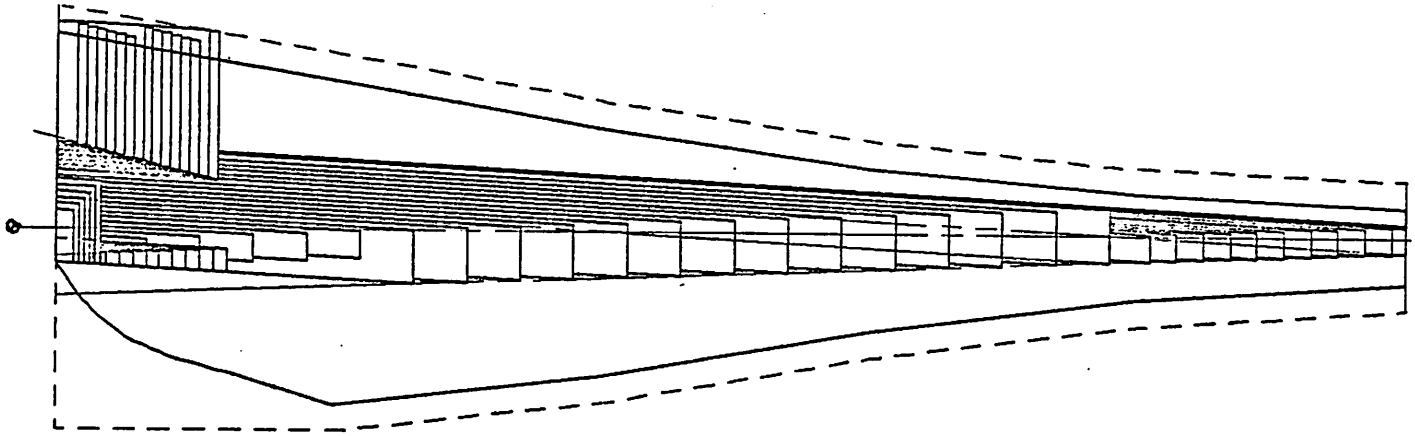

Fig.7 LAMINATE DESIGN OF THE WEC WIND-ENERGY ROTOR BLADE

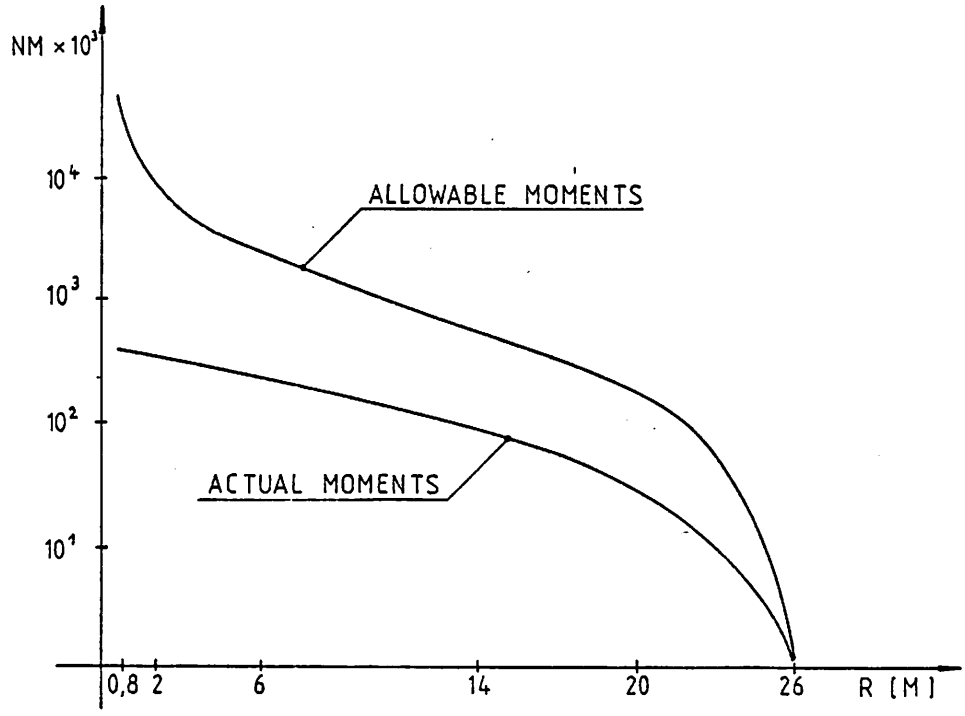

FIG. 8

MARGINS OF SAFETY

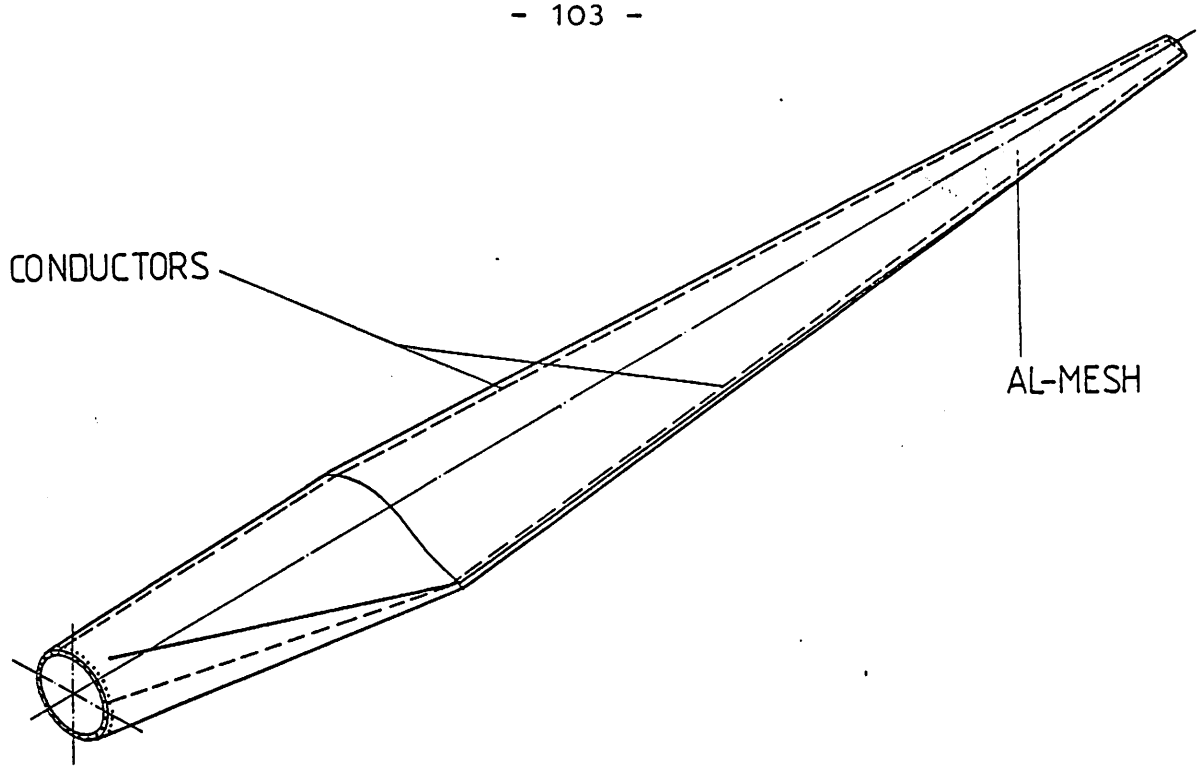

FIG.9
ARRANGEMENT OF THE
LIGHTNING PROTECTION

EROSION
ICING
MOISTURE
SOLAR RADIATION
IMPACT
CORROSION

FIG.10
ENVIRONMENTAL INFLUENCES

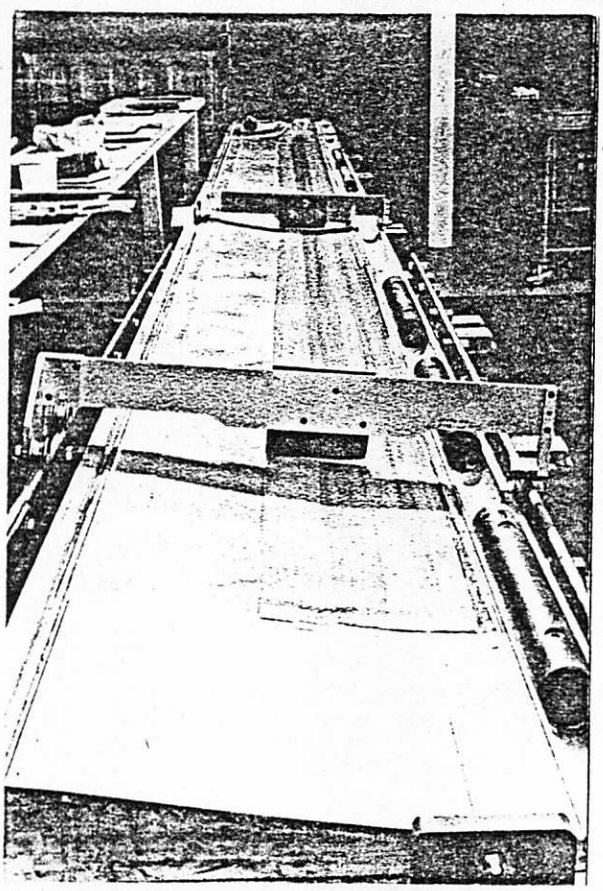

FIG.11 MANUFACTURING OF THE BO 105 ROTOR-BLADE

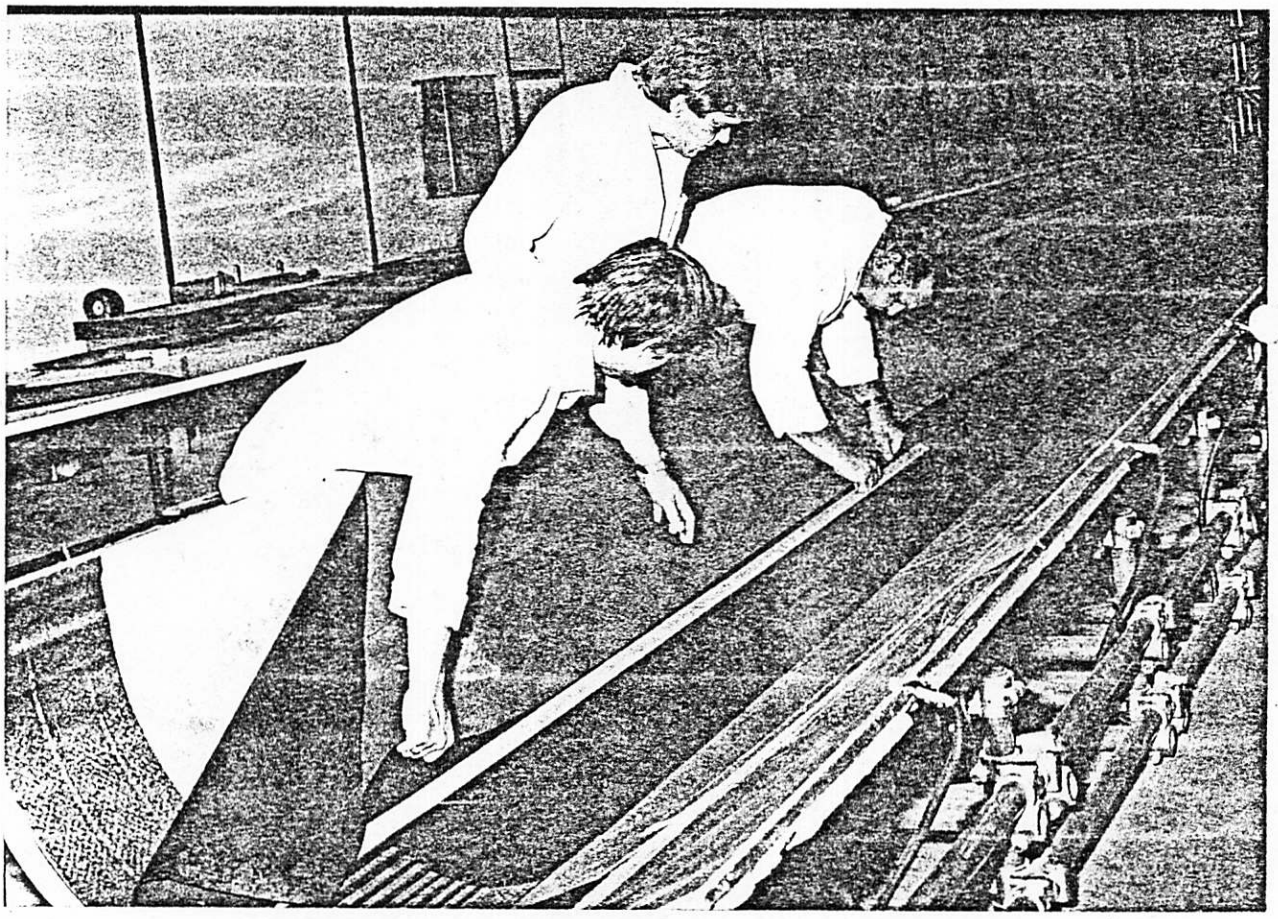

FIG.12 LAY UP OF PREPREGS

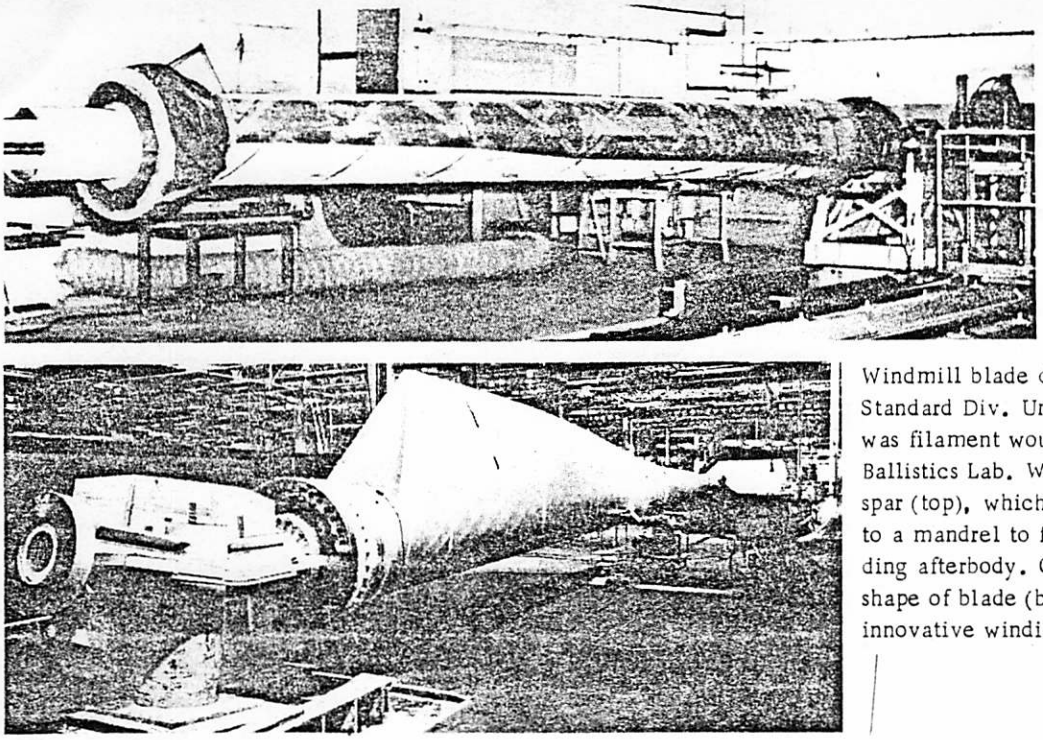

Windmill blade designed by Hamilton Standard Div. United Technologies, was filament wound by Allegheny Ballistics Lab. Wound first is the spar (top), which is then connected to a mandrel to form core for winding afterbody. Overall tapered shape of blade (below) required innovative winding method.

FIG.13 FILAMENT WINDING OF A WIND ENERGY ROTOR-BLADE

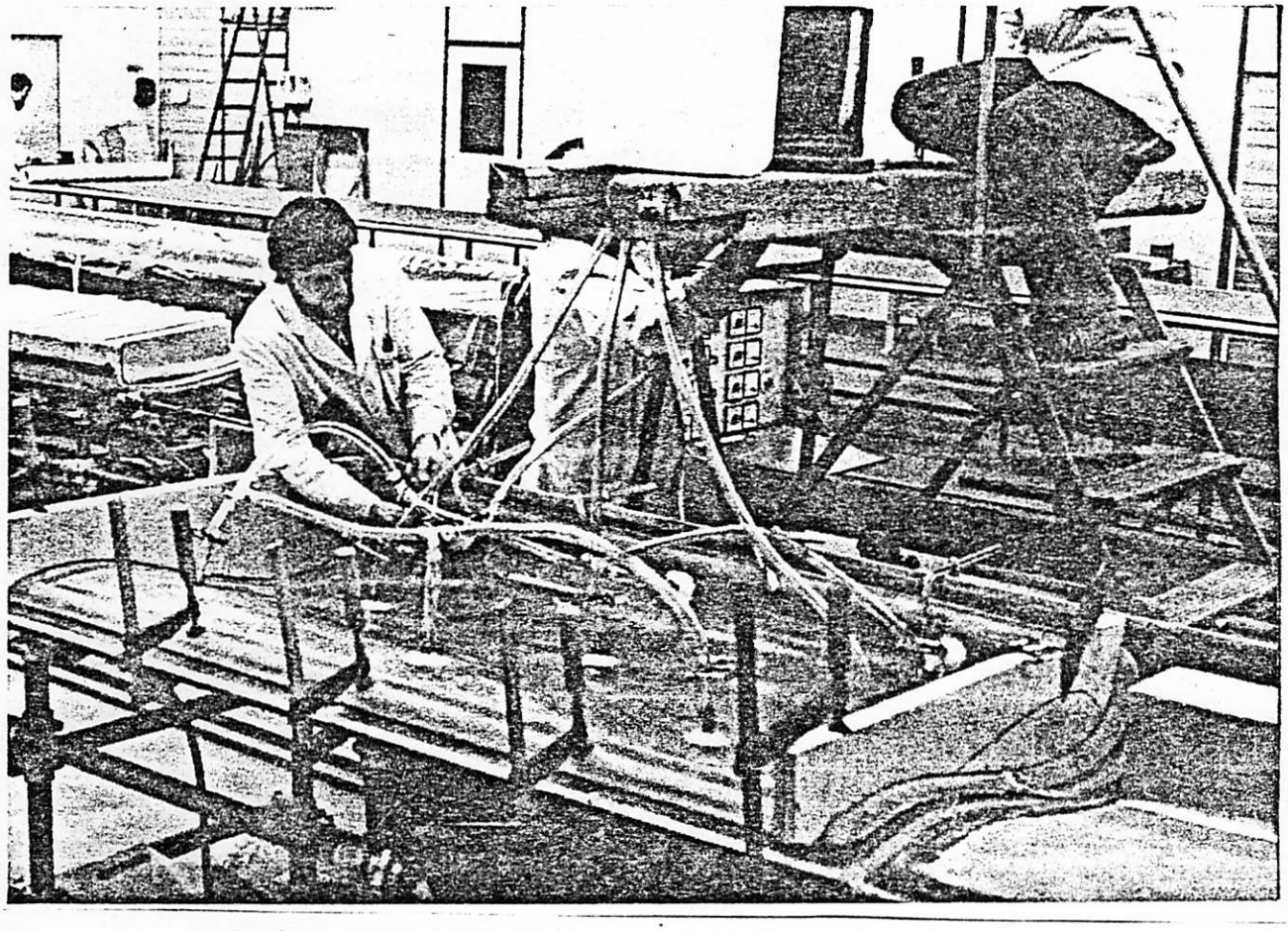

FIG.14 EXPERIMENTAL SET-UP FOR TESTING OF RESIN INJECTION

-HEATABLE
-CONSTANT HEAT-FLUX
-GOOD LOFT-ACCURACY
-LOW COSTS
-SMALL DISPLACEMENTS

FIG. 15
REQUIREMENTS FOR MOULDS
OF WIND-ENERGY-ROTOR-BLADES

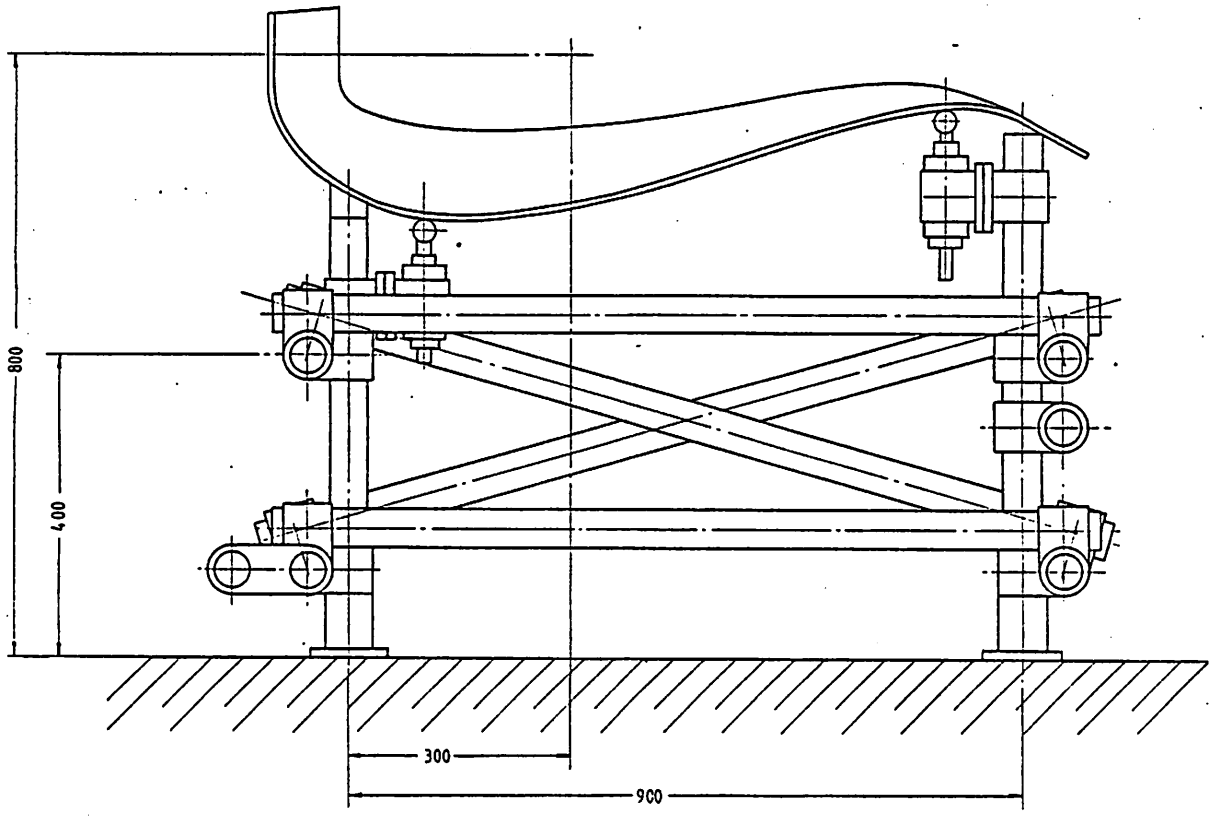

FIG. 16 CROSS-SECTION OF THE WEC MOULD

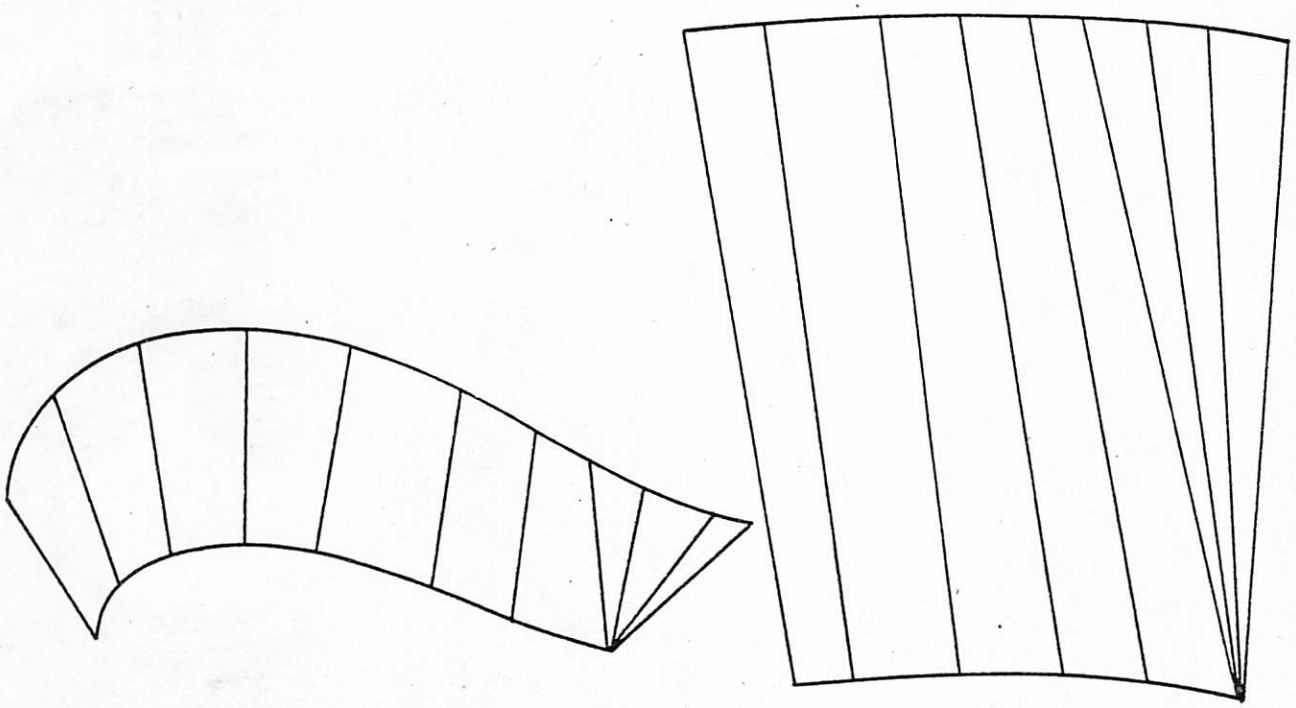

FIG. 17 A DEVELOPABLE SURFACE OF A ROTOR-BLADE SECTION

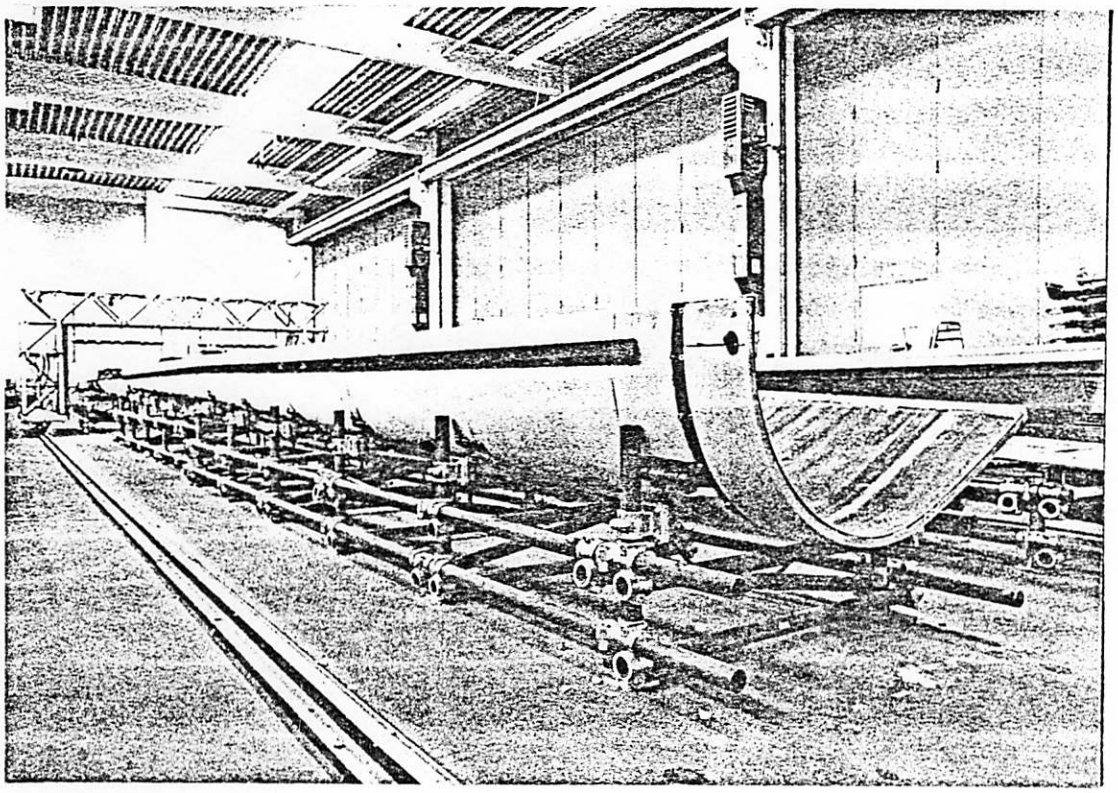

FIG. 18 MOULD MADE OF FORMED STEEL PLATES

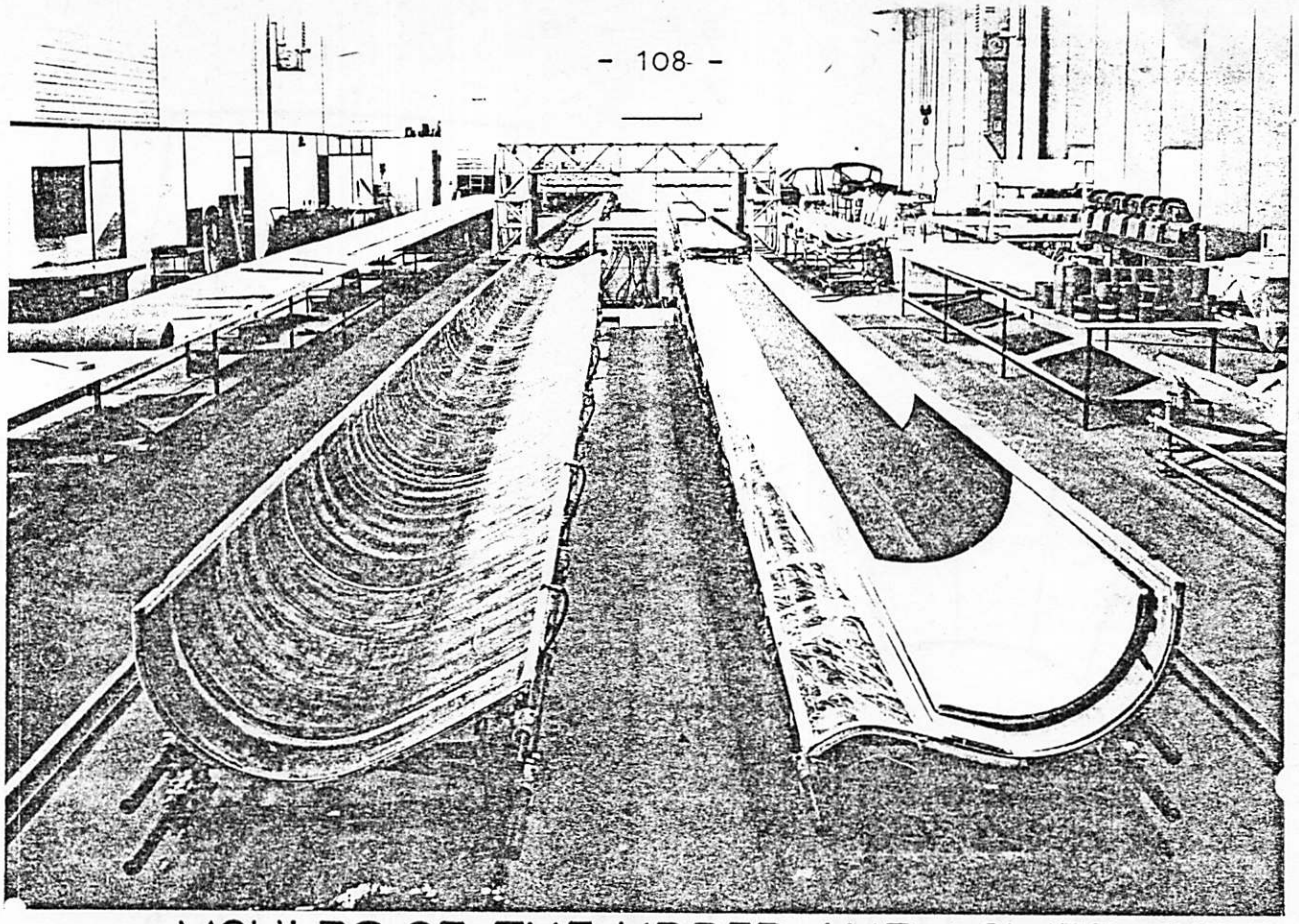

FIG.19 MOULDS OF THE UPPER AND LOWER SIDE OF THE WEC ROTOR-BLADE

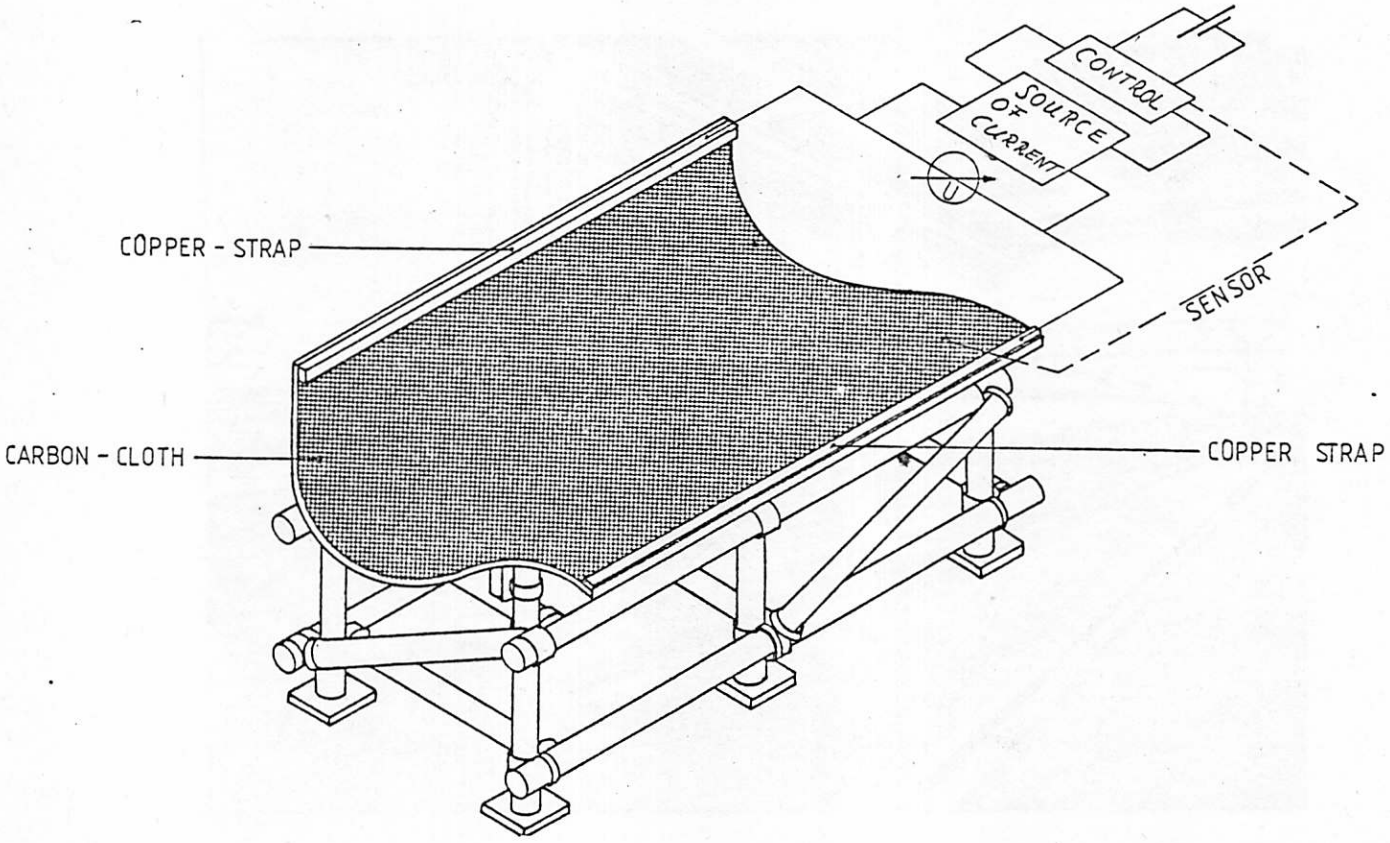

FIG. 20 CONSTRUCTION OF THE HEATING SYSTEM

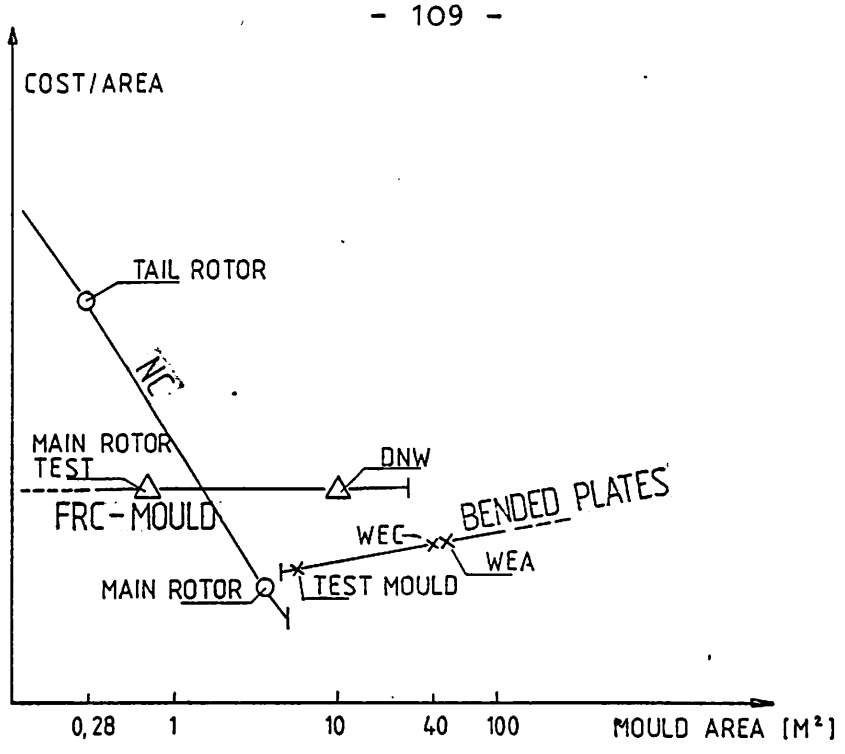

FIG. 21 COSTS PER AREA OF THREE DIFFERENT MOULD-CONCEPTS

DIMENSIONS

LENGTH	25,2 M
CHORD	1,1 M – 0,3 M
CIRCULAR CROSS-SECTION AT THE ATTACHMENT	

DYNAMIC CHARACTERISTICS

NATURAL FREQUENCIES (ROTATING)
FIRST MODES

FLAPWISE	1,3 HZ
CHORDWISE	1,6 HZ
TORSION	15 HZ

MARGINS OF SAFETY

STATICALLY	ABOVE 4
FATIQUE	ABOVE 2

FIG. 22
SPECIFICATION OF THE WEC ROTOR-BLADE

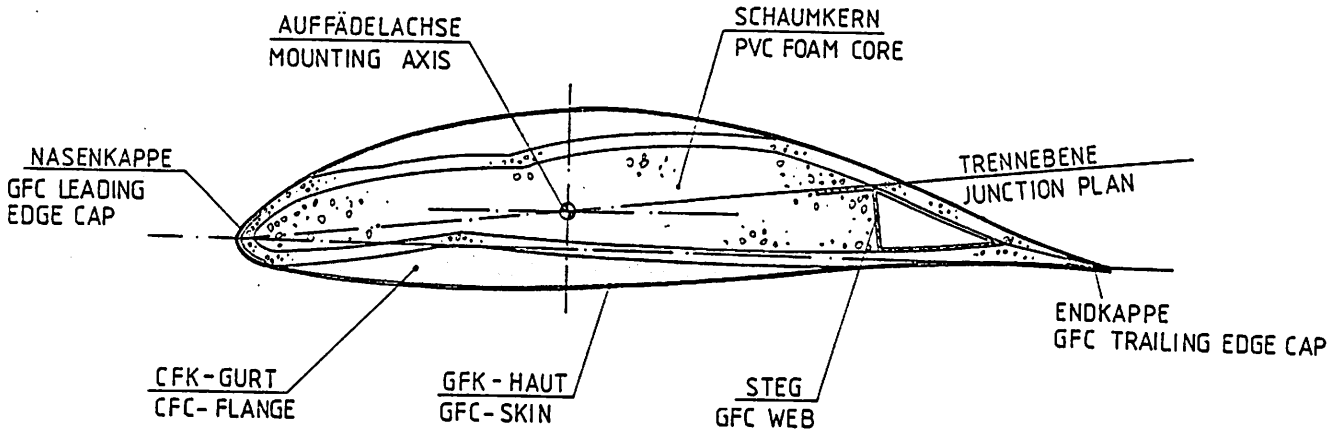

ALL SECONDARY BONDINGS WITH USE OF LIQUIDE (FOAMING) EPOXY ADHESIVE

FIG.23
CROSS-SECTION OF THE
WEC ROTOR-BLADE

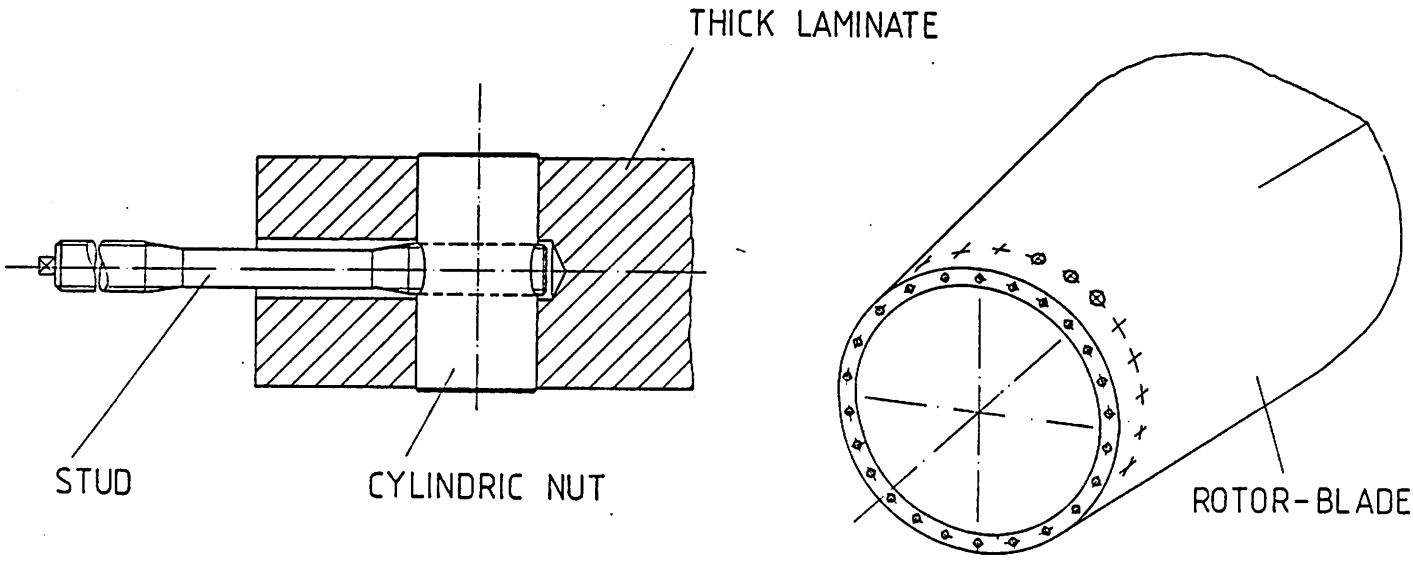

FIG.24
ATTACHMENT CONFIGURATION

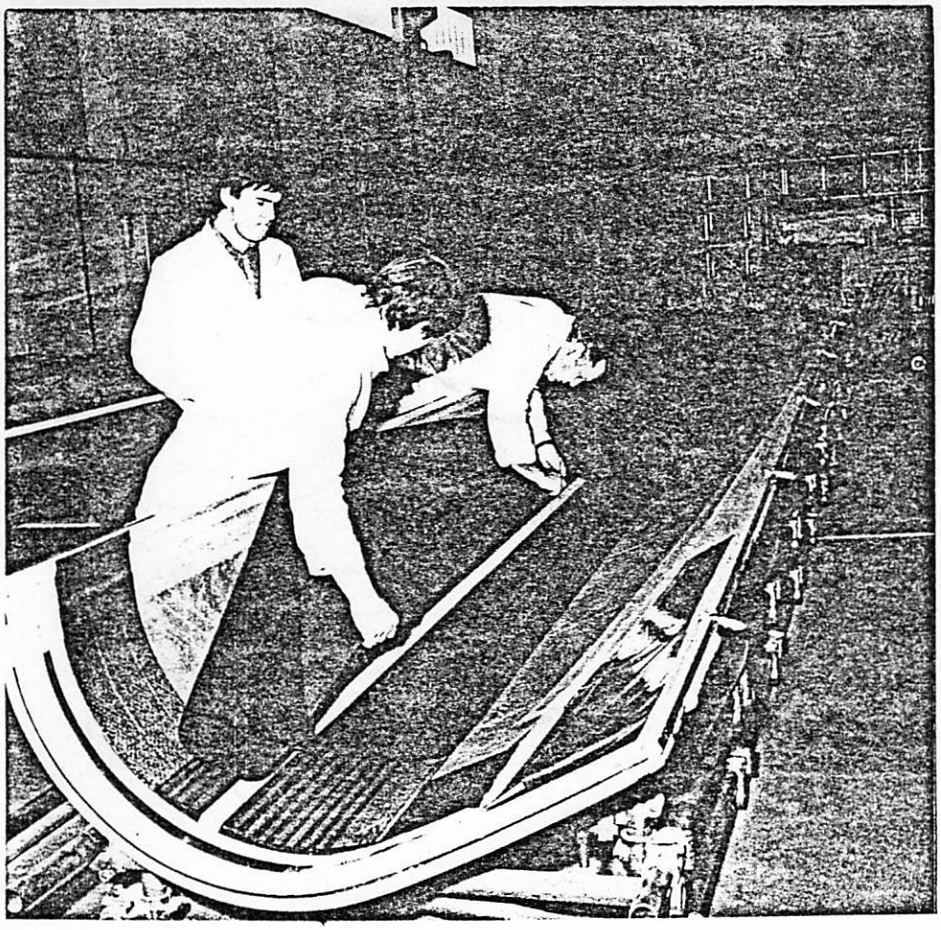

FIG. 25 LAY UP OF THE LAMINATE

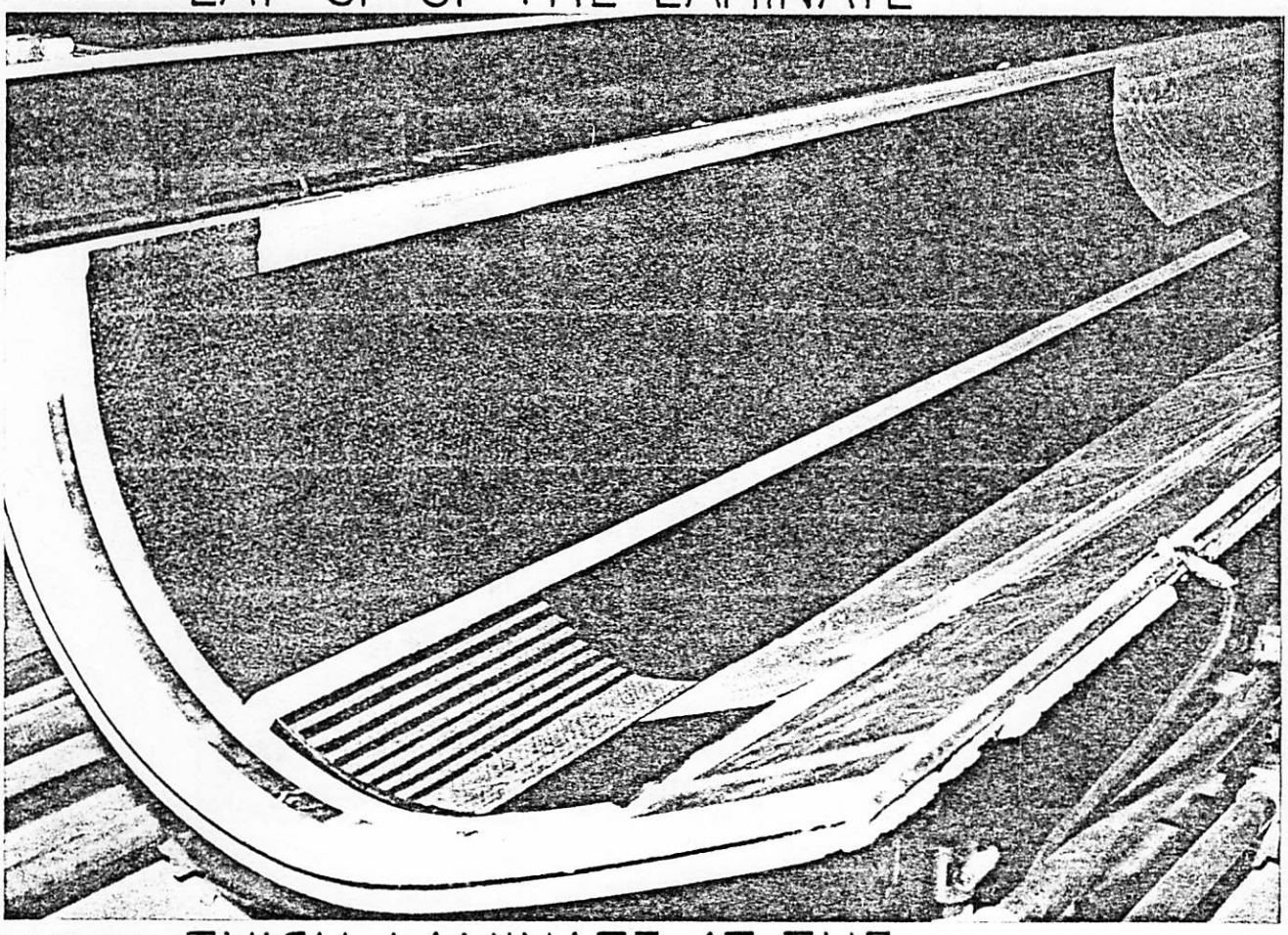

FIG. 26 THICK LAMINATE AT THE ATTACHMENT AREA

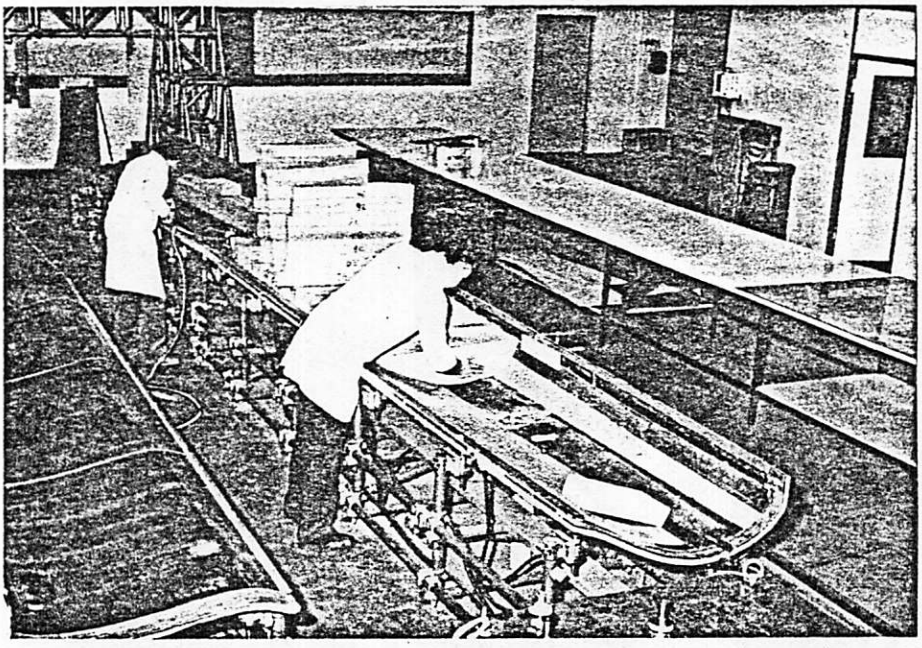

FIG. 27 ADJUSTING OF PVC FOAM

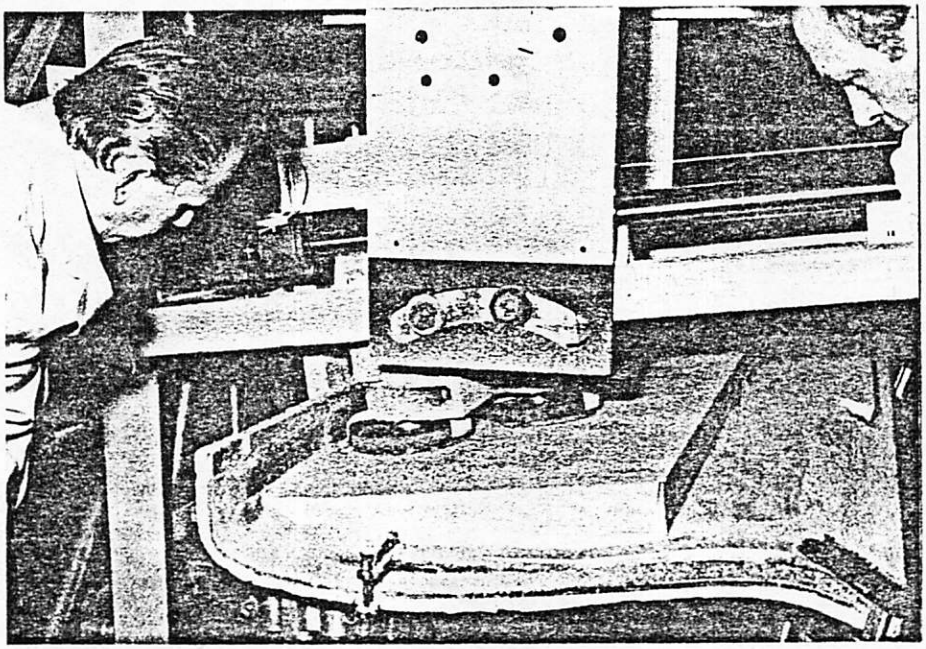

FIG. 28 MILLING OF PVC FOAM

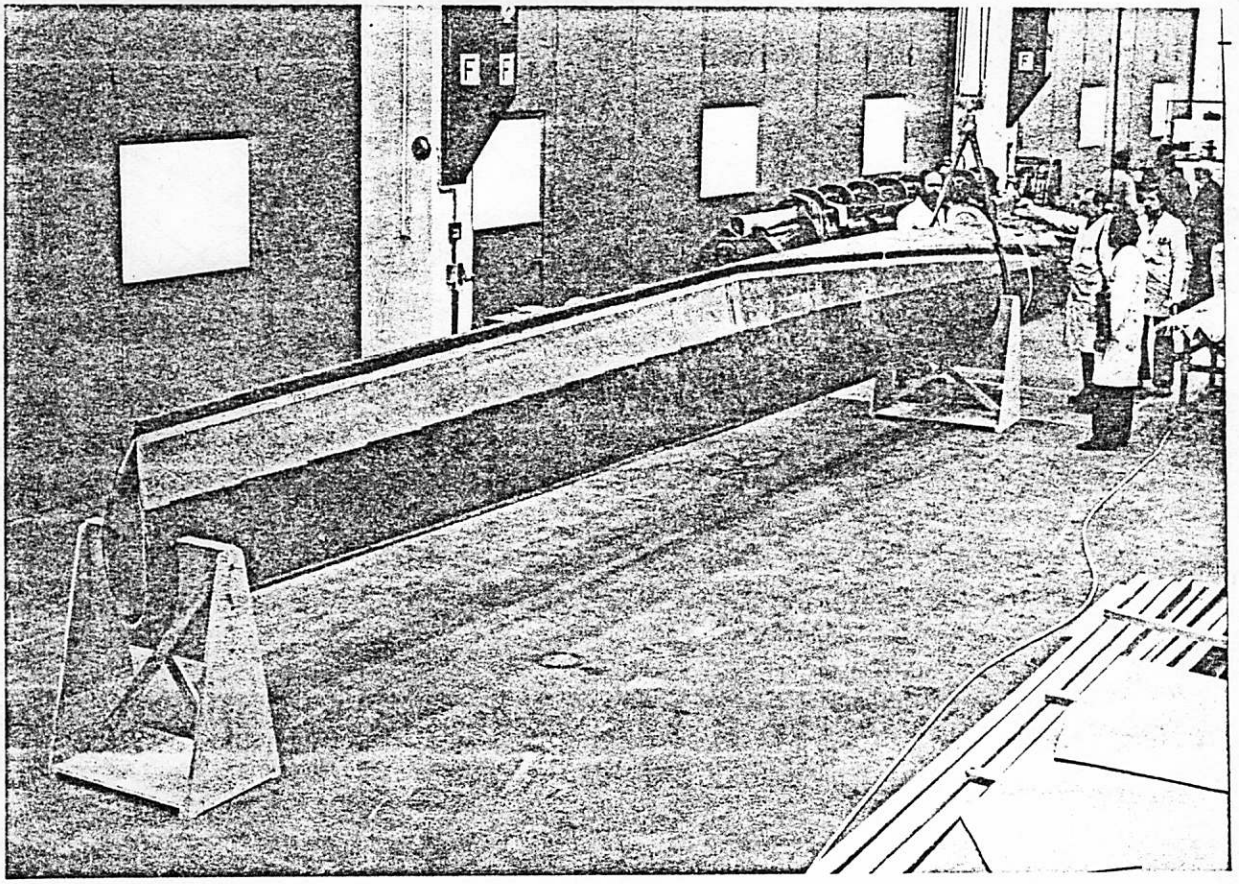

FIG. 29 BONDED ROTOR BLADE (WEC)
11 m TEST-SECTION

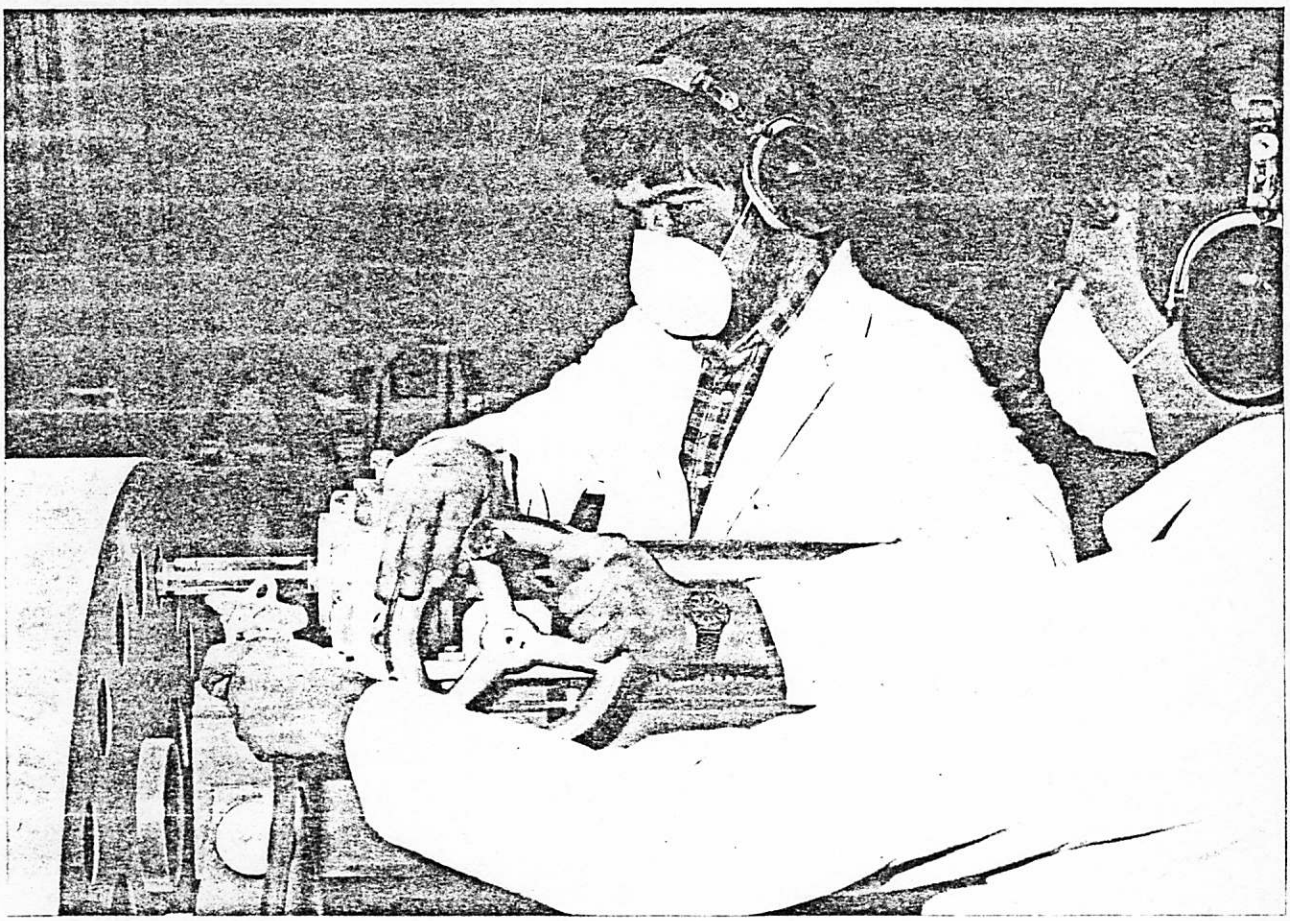

FIG. 30 MACHINING OF THE ATTACHMENT

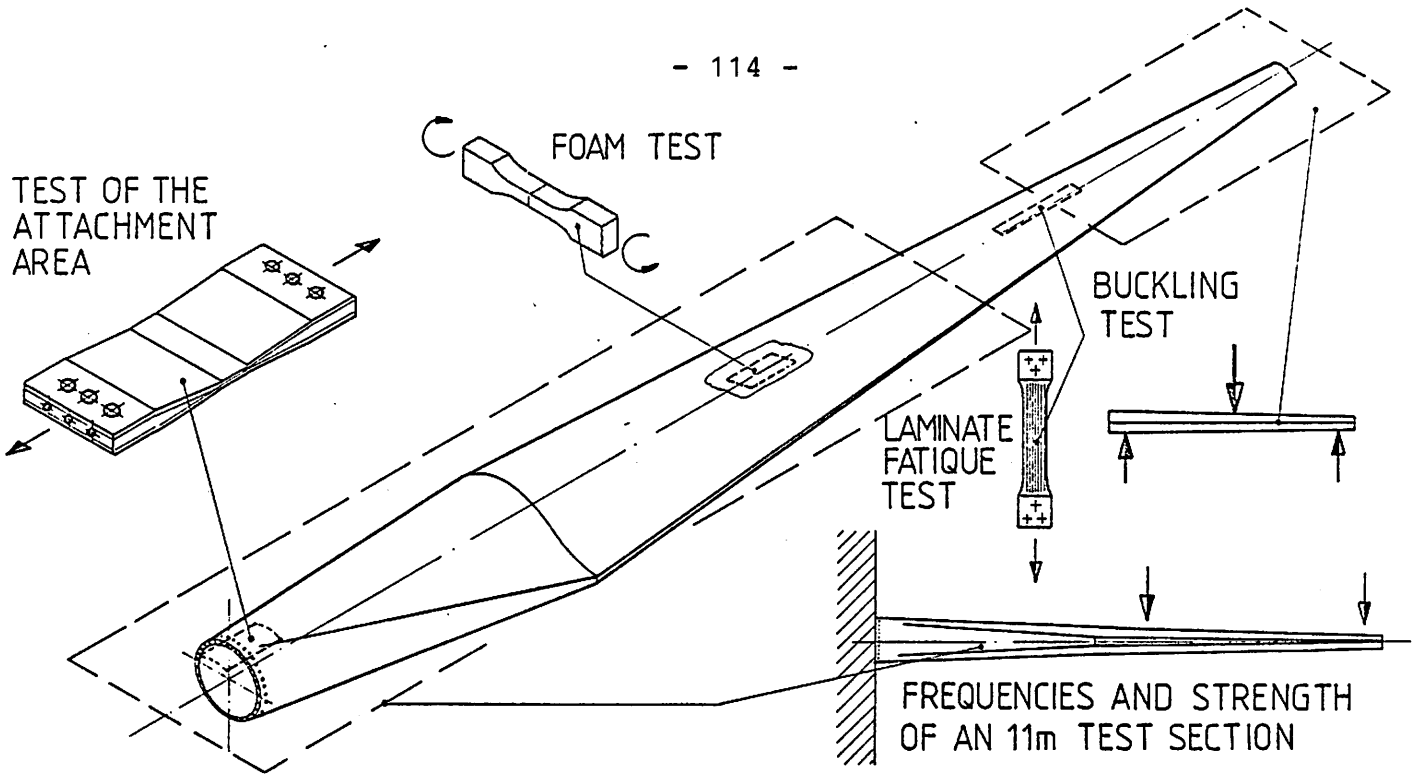

FIG. 31
TEST SPECIMENS OF A WIND ENERGY ROTOR-BLADE

STRESS ANALYSIS AND TEST PHILOSOPHY FOR WIND ENERGY CONVERTER BLADES

H.Bansemir, K.Pfeifer
MBB, West Germany

Abstract

After a short description of the projected wind energy converter blades, some aspects of the analysis are discussed.

Main points of the analysis are the calculation of laminate and cross-section values as well as the overall behaviour of the blade. Special attention has to be paid to the bolted area, and to the tensile stresses in the blade as it is mainly loaded by bending moments.

In addition to the theoretical work, tests are described. Tests are performed in order to obtain basic data of the materials used in the design. Special components such as the bolted area are tested by static and dynamic loads. Finally the strains in the entire blade under load and the eigen frequencies are measured.

Notation

$E_{\parallel}$	[N/mm^2]	Young's modulus in fiber direction
$E_{\perp}$	[N/mm^2]	Young's modulus normal to fiber direction
$\nu_{\parallel\perp}$	[-]	Poisson's ratio
$G_{\#}$	[N/mm^2]	Interlaminar shear modulus
σ	[N/mm^2]	Tensile stress
τ	[N/mm^2]	Shear stress
ϕ_F	[-]	Fiber content by volume
$\alpha_{F\parallel}$	[1/K]	Thermal expansion coefficient of the fiber in longitudinal direction
$\alpha_{F\perp}$	[1/K]	Thermal expansion coefficient of the fiber in normal direction
ϱ	[g/cm^3]	Density
A	[mm^2]	Area

1. Introduction

Since 1978, MBB has developed the WEA project (Wind-Energie-Anlage = wind energy converter) under contract of the German Bundesministerium für Forschung und Technologie (department for research and technology) (see Fig.1). The system operates within the range of 6m/s to 20m/s wind speed. The plant design power of 5 MW is reached at a wind speed of 11.3 m/s at the height of the fan hub. At higher speeds, the generated electric power remains constant by adjusting the blade angle.

At speeds higher than 20 m/s the system is stopped. With a change in wind directions the rotor is automatically "followed up".
MBB has chosen the one blade system for WEA, because of the following reasons:

- simple rotor hub
- low bending moments in flapping at the root of the blade
- easy realisation of stiffness and strength requirements of the blade because of large cross sections
- wider range of tolerance for blade production because of lack of symmetry requirements. That means
- reduced blade costs
- lower demands of the tower

Two other MBB projects are already in an advanced phase.

WEA Demonstrator (WEA Demo)
scale model of the WEA windmill,
rotor diameter about 48 m, single blade rotor

WEC (wind energy converter) (see Fig.2)
rotor diameter 52 m, two blades
electric power 285 kW

MBB produces the blade under contract of Voith, Germany

A test specimen of WEC has already been built. It has the same structure as the production blade but consists only of the section from the root to 11 m. Fig.3 and Fig.4 show the blade in production.

The "know-how" of MBB in producing fiber composite blades is based on experiences from the (see Fig.5):

BO 105 blade
EMMEN wind tunnel blade
rotor diameter 8.5 m

DNW wind tunnel blade
rotor diameter 12.35 m

2. Basic Design of Rotor Blades

A structural member must be able to transfer all forces and moments.
Unidirectional carbon fiber layers in longitudinal direction react both, bending moments and centrifugal forces. Glass fiber fabric ($\pm 45^{\circ}$) transfers the torsional moments as well as the transverse loads. Foam or spars are provided for preventing local bending and for supporting the flapping force.
Fig. 6 shows the typical design of a cross-section.

3. Stiffness Values of a Laminate

For calculating the stiffness values of the different laminates and cross-sections, the characteristic values of the resin and the fibers are needed:

material properties:

resin: $E_B = 3500\ N/mm^2$

$\nu_B = 0.35$

$\rho_B = 1.2\ g/cm^3$

$\alpha_B = 55 \cdot 10^{-6}\ 1/K$

Toray T300 fiber: $E_{F||} = 218800\ N/mm^2$

$E_{F\perp} = 28000\ N/mm^2$

$G_F = 50000\ N/mm^2$

$\nu_{F||\perp} = 0.23$

$\rho_F = 1.78\ g/cm^3$

$\alpha_{F||} = -0.35 \cdot 10^{-6}\ 1/K$

$\alpha_{F\perp} = 12.5 \cdot 10^{-6}\ 1/K$

$\phi_F = 40.5\%$ by volume $\hat{=}$ 50% by weight
(G825-1 fabric, warp direction)

E-glass fiber: $E_F = 70000\ N/mm^2$

$\nu_F = 0.217$

$\rho_F = 2.59\ g/cm^3$

$\alpha_F = 4.8 \cdot 10^{-6}\ 1/K$

$\phi_F = 36\%$ by volume ($\pm 45^\circ$-plies)

$\phi_F = 31.7\%$ by volume $\hat{=}$ 50% by weight
(G825-1 fabric, filling direction)

Conticell C60 foam: $E = 35\ N/mm^2$

$\nu = 0.3$

$\rho = 0.06\ g/cm^3$

By using these values we obtain the elastic properties of unidirectional and multilayer laminates (program VERBUND).

laminate properties:

G825-1 (Unidirectional carbon fiber laminate with 5% glass fibers in filling direction):

$E_x = 86400\ N/mm^2$

$E_y = 7240\ N/mm^2$

$G_{\#} = 2620\ N/mm^2$

$\nu_{xy} = 0.26$

$\nu_{yx} = 0.022$

glass fiber fabric with $\pm 45^\circ$ fiber orientation:

$E_x = 7500\ N/mm^2$

$E_y = 7500\ N/mm^2$

$G_{xy} = 7640\ N/mm^2$

$G_{xz} = G_{yz} = 2330\ N/mm^2$

$\nu_{xz} = \nu_{yx} = 0.61$

4. Calculation of the Cross-Section and Blade Properties

To obtain quick results at the beginning of a blade design, the program MGS was developed. It computes typical cross-section values of multicellular closed shells as stiffnesses, and the positions of characteristic points as center of shear, center of gravity and center of elasticity. In this program, the cross-sections are idealized in beams of constant Young's modulus, shear modulus, thickness and density (see Fig. 7). Calculated results can be seen below.

It is also important to know the overall behavior of a blade. This can be calculated by using the program BALKEN (=beam). It computes the unknown forces and bending under load at any desired cross-section of a blade, which may have varying bending stiffnesses and mass distribution.

For the final static analysis the data of the cross-sections are computed with the more exact finite element program S47. The geometry of a cross-section is split up into triangular and square disc elements for which the material values, calculated by VERBUND (in section 4), are needed (see Fig. 8). Like the program MGS, S47 supplies the bending and torsional stiffnesses as well as the positions of significant points and the principal axes. It also computes the shear stresses for a torsional angle of 1.0 [rad]. The following list shows the comparison of different values computed by MGS and S47 for the cross-section r/R=0.4 of WEA Demo blade.

		MGS	S47	
center of gravity	x	743 [1]	800	mm
	y	55	53	
center of elasticity	x	558	549	
	y	61	64	
center of shear	x	576	509	
	y	59	84	
tensile stiffness		1.24	1.20	10^9 N
bending stiffness in flapping		49.8	48.9	10^6 Nm^2
in lagging		197	179	
torsional stiffness		10.9	12.5	

[1] without foam

It can be seen that most of the values approximately coincide.

5. Calculation of the Stresses

To obtain the safety factors, the resulting stresses and the strains of the blade are calculated by using the program NLBLADE. As input the geometry and the characteristic values of the cross-sections computed by S47 and additional data as mass distribution, tilt angles etc. are needed. The program computes the transverse and normal forces, the moments and the maximum stresses at each cross-section taking into account theory II effects, which are important for blades with large bending.
For static loads, a safety factor of 5 is required and for dynamic loads a value of 2.
If only the maximum bending stresses in flapping or lagging (and not the resulting stresses) are needed, they can be calculated by using the following formula:

$$\sigma_{max} = \frac{M_x \, E_{max_{layer}}}{(EI)_{x\ total}} \cdot y$$

We obtain for the above mentioned cross-section of the WEA-Demo blade in the unidirectional CRC-layers (moments in fig. 9):

$$\sigma_{max} = 93.7 \text{ N/mm}^2 \text{ in flapping}$$

$$\sigma_{max} = 21.0 \text{ N/mm}^2 \text{ in lagging}$$

The ultimate stress of the T300 laminate (ϕ = 40.5% by volume) is:

$$\sigma_B = 1050 \text{ N/mm}^2$$

That means a safety factor of 11.2 in flapping and of 50 in lagging.
It can be assumed that the CRC rovings react the centrifugal force which normally causes low stresses in the windmill blades in comparsion to the other loads:

$$\sigma = \frac{F_{centr.}}{A_{rovings}}$$

Foam or spars and the skin of the blade react the transverse forces Q as a function of the shear stiffnesses:

$$\frac{Q_1}{Q_2} = \frac{(G\ F_s)_1}{(G\ F_s)_2} \; ; \qquad Q_{total} = Q_1 + Q_2$$

$$F_s = \text{thickness x height}$$

which leads to the shear stresses:

$$\tau = \frac{Q}{A} \leq \tau_{allowed}$$

6. Blade Root

Especially in the root section, thermal stresses can be caused by different thermal expansion coefficients of root laminate and steel flange. This can be avoided by using additional $\pm 45^{\circ}$ glass plies or carbon fibers in the circumferential direction.
Fig. 10 shows the connection between the bolts and the hub flange used by MBB for the wind tunnel and wind energy rotor blades. In order to minimize the dynamic loads the bolts are prestressed.
The total stiffness C_F of the flange can be calculated by

$$\frac{1}{C_F} = \sum_i \frac{l_i}{E_i A_i}$$

It is difficult to establish the stressed area in the root laminate between cross bolt and root rib or flange. Normally an equilateral triangle with the upper corner in the center of the bolt is assumed. The stiffness C_B of the bolt is also calculated according to the upper formula. In addition to the initial load, the bolt receives the following share of the dynamic load F_{dyn}:

$$F_{Bdyn} = \frac{C_B}{C_B + C_F} \cdot F_{dyn}$$

Fig. 11 shows the bolt-flange diagram of the WEA Demo blade.

7. Tests

To obtain a good product the following tests are performed:

Test of material properties
- weight
- Young's modulus and ultimate stress by single layer specimens
- ultimate interlaminar shear stress by ILS specimens

Test of structural parts
- Young's modulus of root laminate
- creeping of the bolted structure
- dynamic test of the root laminate
- crumpling test

Test of the entire blade
- eigenfrequencies
- damping
- static loads

8. Test of the Material Properties

To obtain basic data of the used materials, all delivered lengths of fabric have to be tested. At first the weight of an area of 100 x 100 mm is measured with and without resin. Then the number of fibers in the sample are counted and the weight of 10 single fibers is measured.

The fibers should be evenly distributed and straight across the breadth of a prepreg or a fabric. In order to check the qualitiy of the material, single layer specimens are produced out of the fabric and tested (Fig. 12/13). These specimens, which are relatively cheep to produce, give the ultimate stress and the Young's modulus in longitudinal and perpendicular direction of the fibers. The waisted tensile specimens are not used for acceptance test. On an average, these show little higher values of the Young's Modulus and a smaller standard deviation, but they need much more time consuming.
ILS specimens supply the ultimate stress for interlaminar shear. A sample is considered broken when the curve in the diagram showing the relation between force and bending suddenly declines.

9. Test of Structural Parts

In this section the tests of the structural parts are described for the qualification of the windmill blades. Some of the tests have already been performed.

a) Laminate Test

In order to check the quality of thick fiber laminates, a beam is tested having a structure similar to that of the root laminates of the windmills. The elongation is measured by using strain gauges. Then the Young's modulus is compared with the theoretical value.

b) Test of the Root Section (fig.14)

A bolt connection element is tested under static and dynamic load. The used laminate is in conformity with the real blade. The bolts are prestressed with 100 kN. The creep is measured as a function of time. Finally the sample is loaded by a dynamic force of F_{dyn}=250 kN $\pm$ 250 kN up to at least 10^6 cycles. A creep test was already performed for the DNW wind tunnel bolts (fig.15). The initial stress fell to about 90% of the original value. After two weeks, there was no more change.

c) "Crumpling Test"

A fracture test was made with the outer part of a EMMEN wind tunnel blade to obtain the ultimate loads (transverse force in flapping and bending moment) (fig.16/17). The blade was loaded in a 3-point-bending-test. The theoretical crumpling stress was calculated by the following formula:

$$\sigma_{cr} = 0.825\sqrt[3]{E_{UD}E_K G_K} = 273 \text{ N/mm}^2$$

E_{UD} = 76540 N/mm^2 M40A unidir. laminate (CRC)

E_K = 35 N/mm^2, G_K = 13.5 N/mm^2 } Conticell C60 (foam)

The tested ultimate load was a little higher than the theoretical value because the curvature of the outer contour cannot be included in the formula .

To minimize the bending moment, the transverse force was then introduced near one of the two bearings. The expected fracture value was 35 kN; the tested ultimate load was 44 kN

10. Test of the Blade

a) For the WEC project a test specimen was built (fig. 18/19). For testing it was fixed in the horizontal position. The eigen frequencies and the modes were measured up to 200 Hz by using electrodynamic pulsators . After switching off, the damping was measured. The following list shows the first eigen frequencies.

	calculated Hz	measured Hz
lagging	8,9	10,0
flapping	8,6	9,8

b) The static test will be performed in few weeks. A force $F = 10^5$ N is introduced at two sections, first at 5.2 m and then at 10.2 m. By using two force introduction positions we can obtain information about the influence of the shear deformation in bending. The strains are measured by more than 200 strain gauges. Introduced at 10.2 m, the force simulates 2.5 x the maximum possible operational bending moment in flapping and lagging (fig.2o).

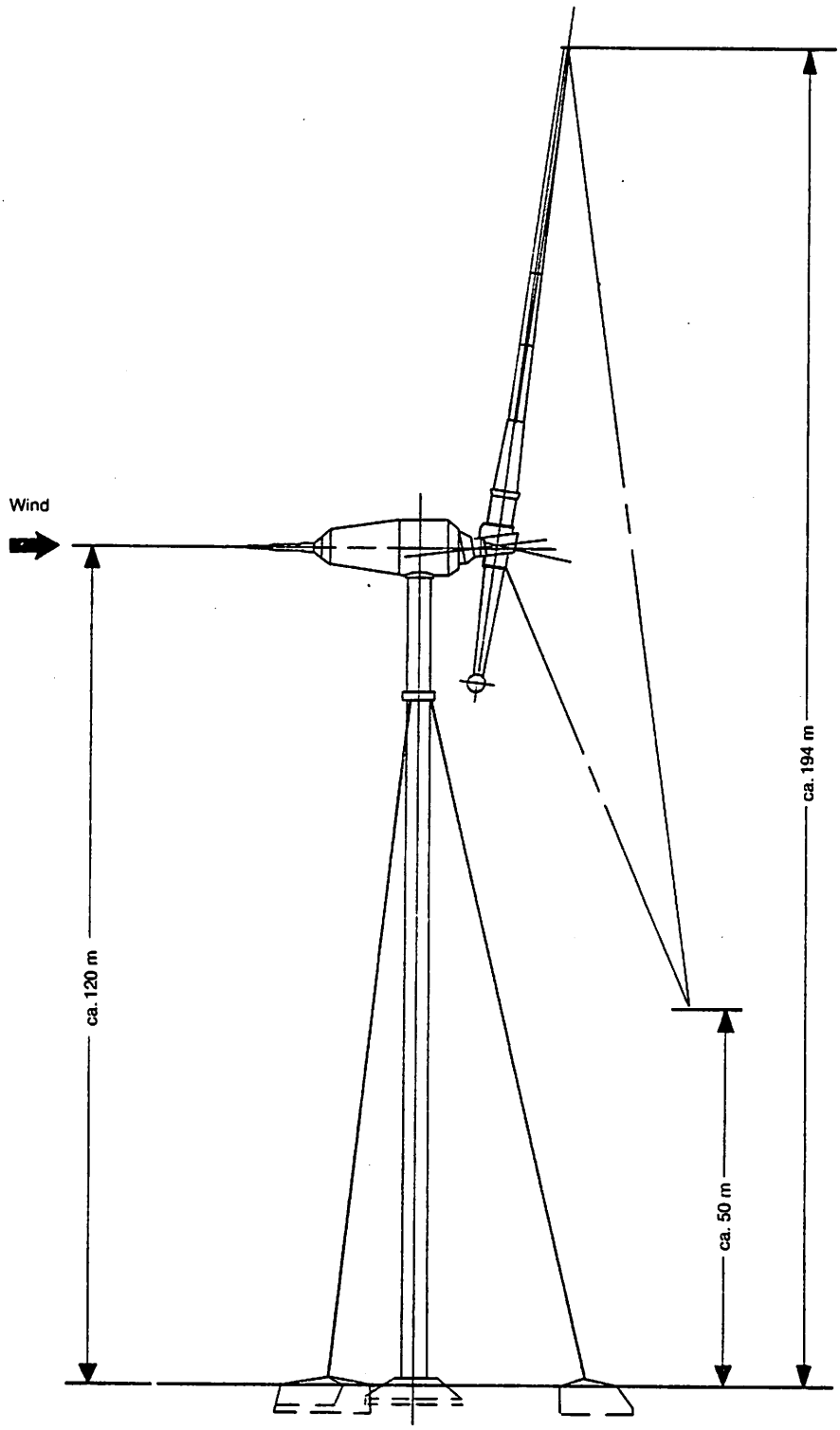

Figure 1:
WEA-Wind Energy Converter
(Wind Energie Anlage)

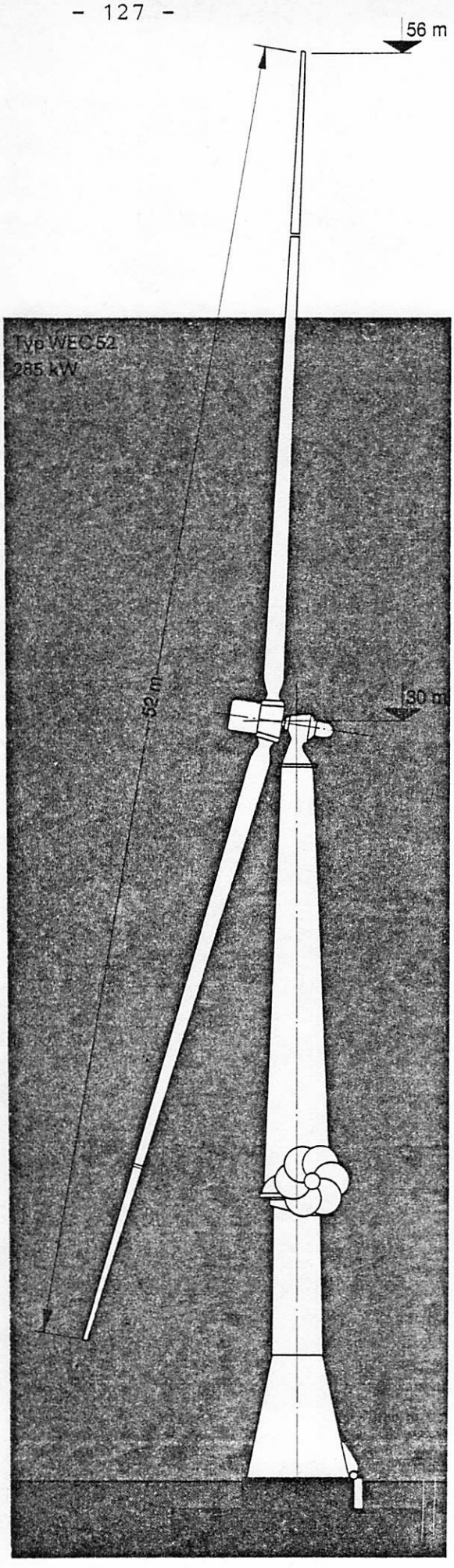

Figure 2:
WEC-Project
(Wind Energy Converter)

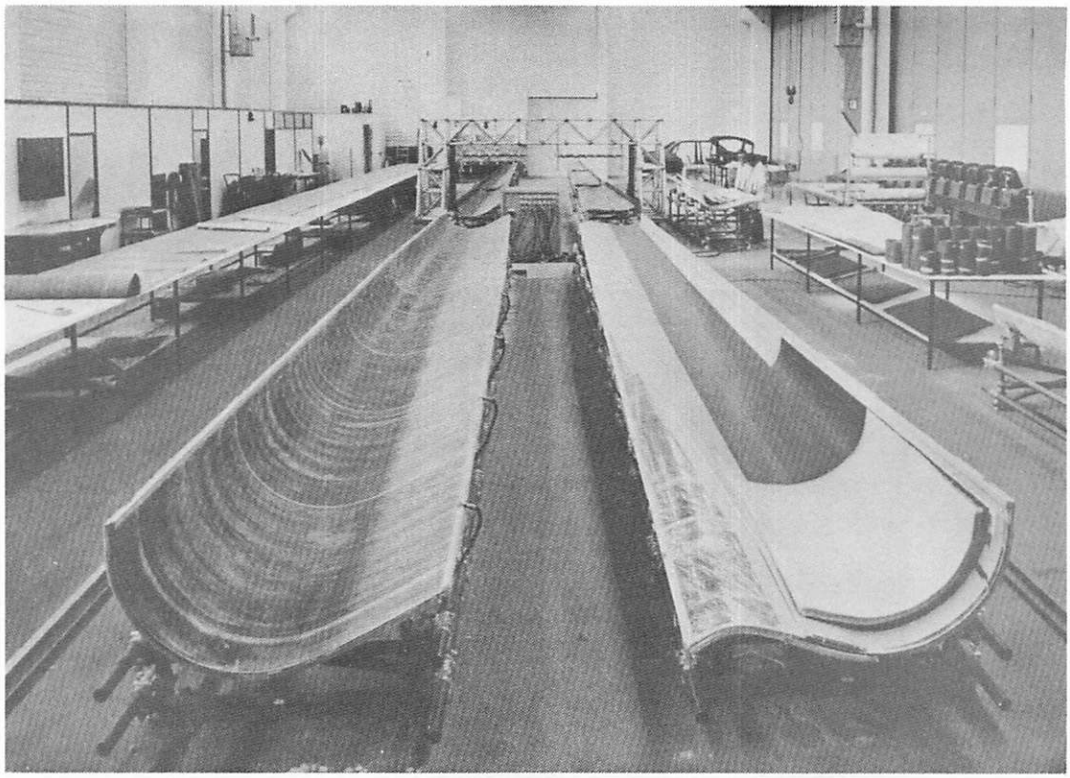

Figure 3: Upper and Lower Shells of WEC

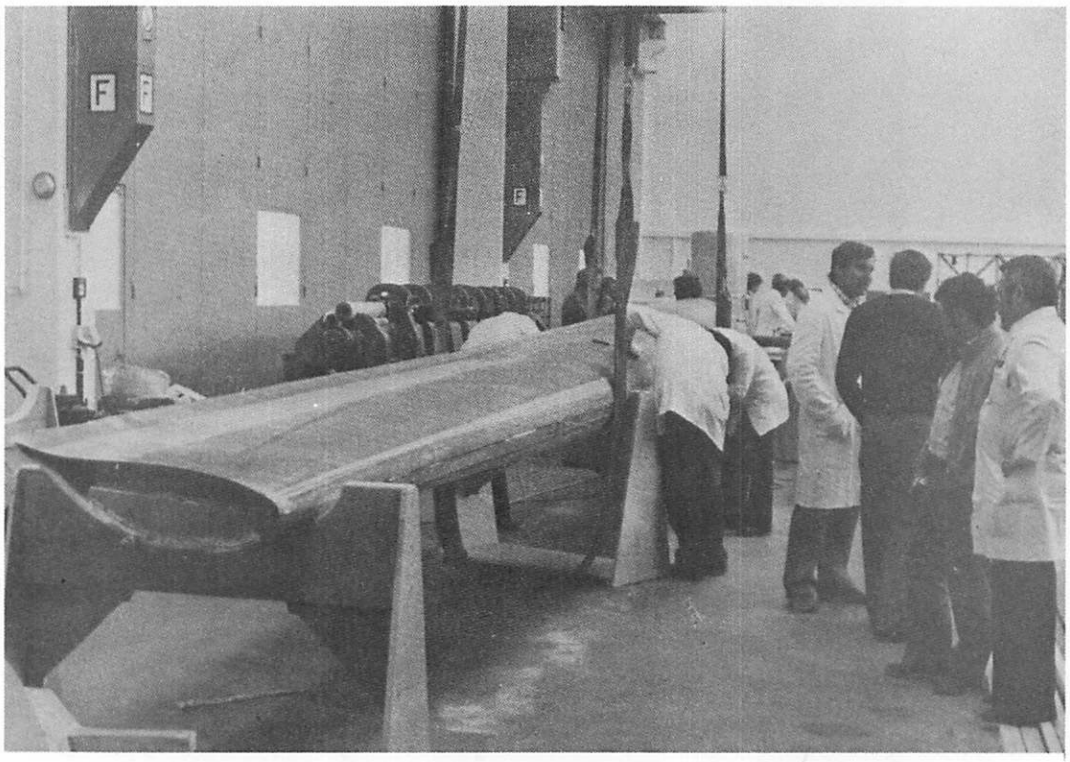

Figure 4: Assembly of WEC Test Specimen

BO 105

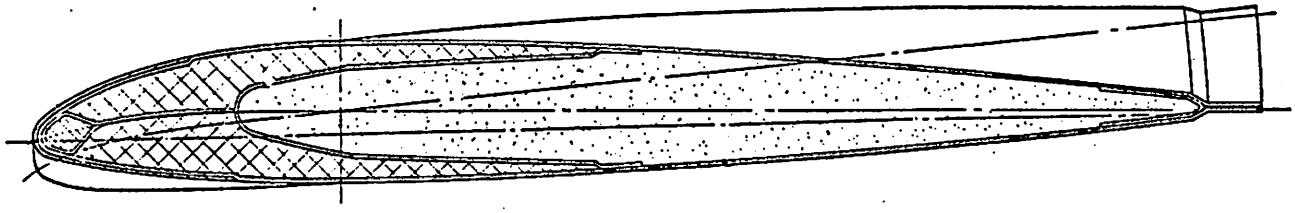

EMMEN wind tunnel

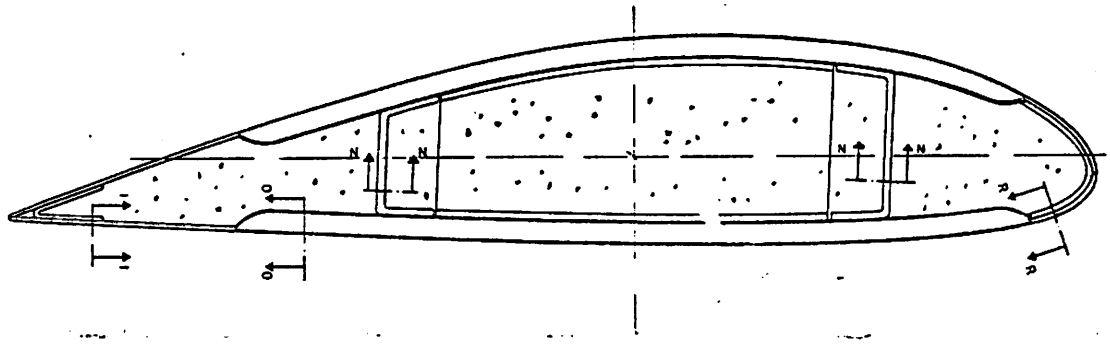

DNW wind tunnel

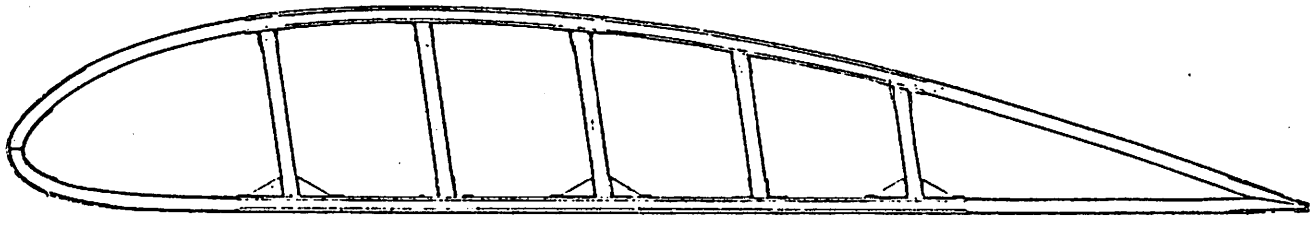

Fig.5: Cross Sections of Blades Constructed up to the Present

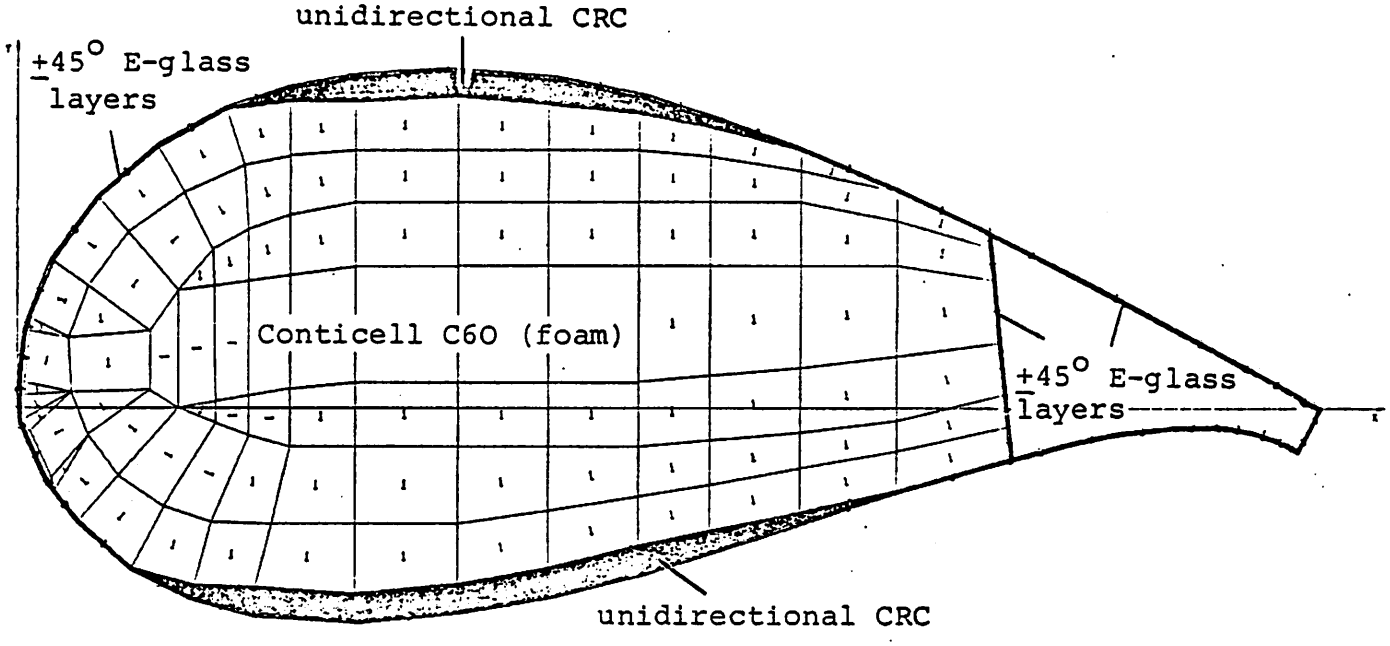

Figure 6: Typical Construction of a Cross Section of a CRC Blade

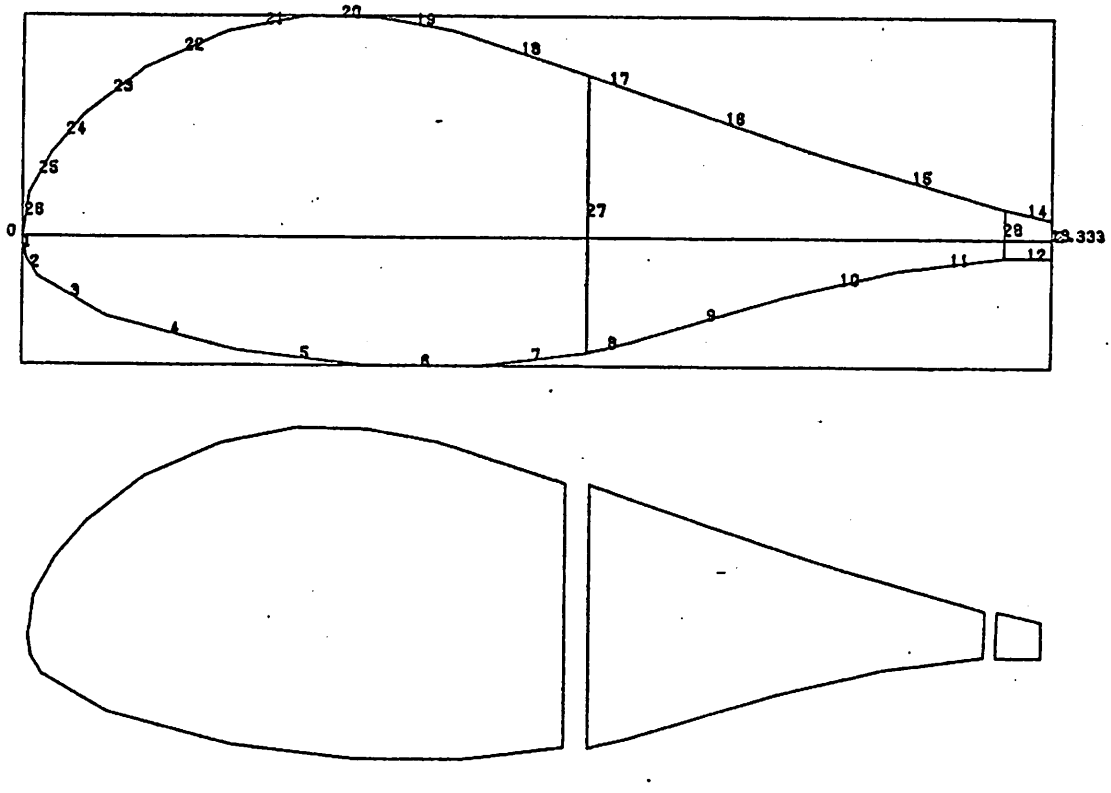

Figure 7: WEA-Demo, Cross Section at r/R = 0,25
Idealized Structure for MGS-Program

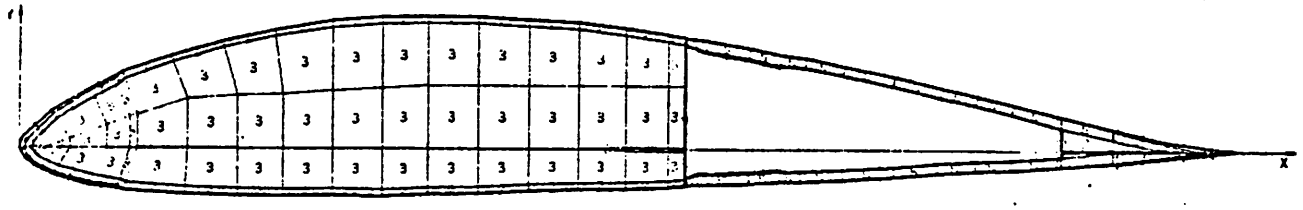

WEA DEMO PROFIL BEI R/RA=0.7

MASSSTAB 1 : 7.5

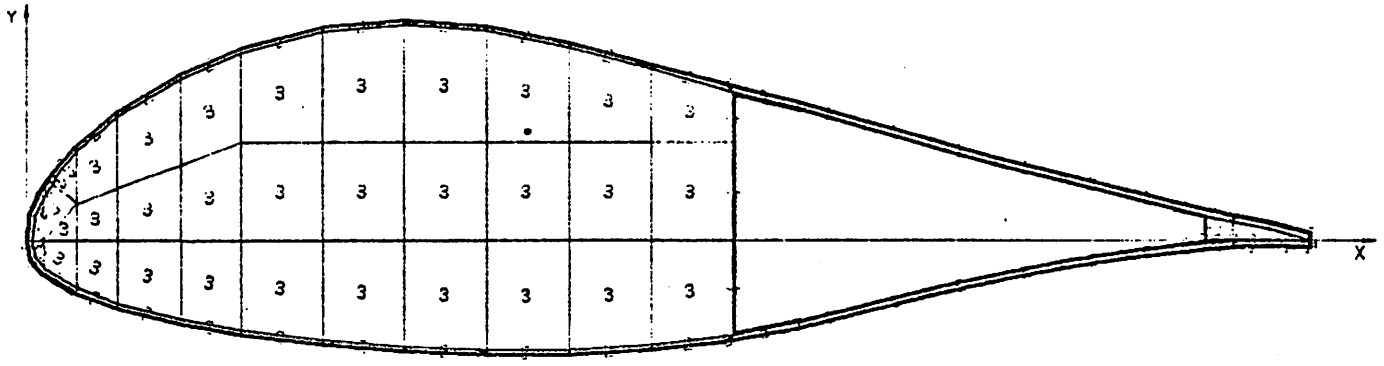

WEA DEMO PROFIL BEI R/RA= 0.4

MASSSTAB 1 : 11.628

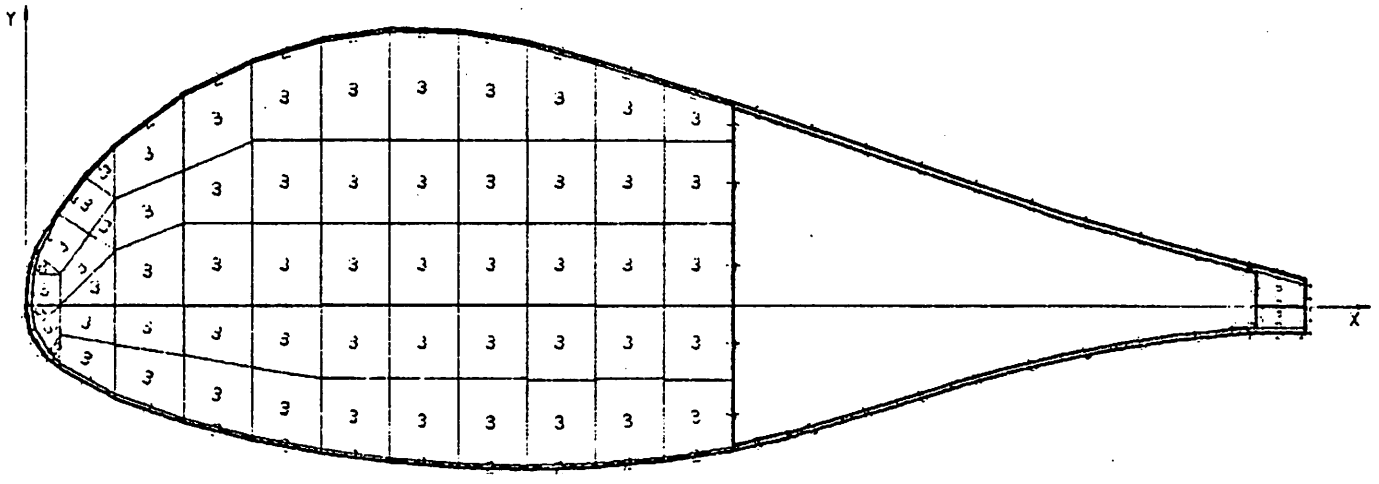

WEA DEMO PROFIL BEI R/RA= 0.25

MASSSTAB 1 : 13.889

Fig.8: 3 Cross Sections of the WEA Demo Wind Energy Converter (different scales)

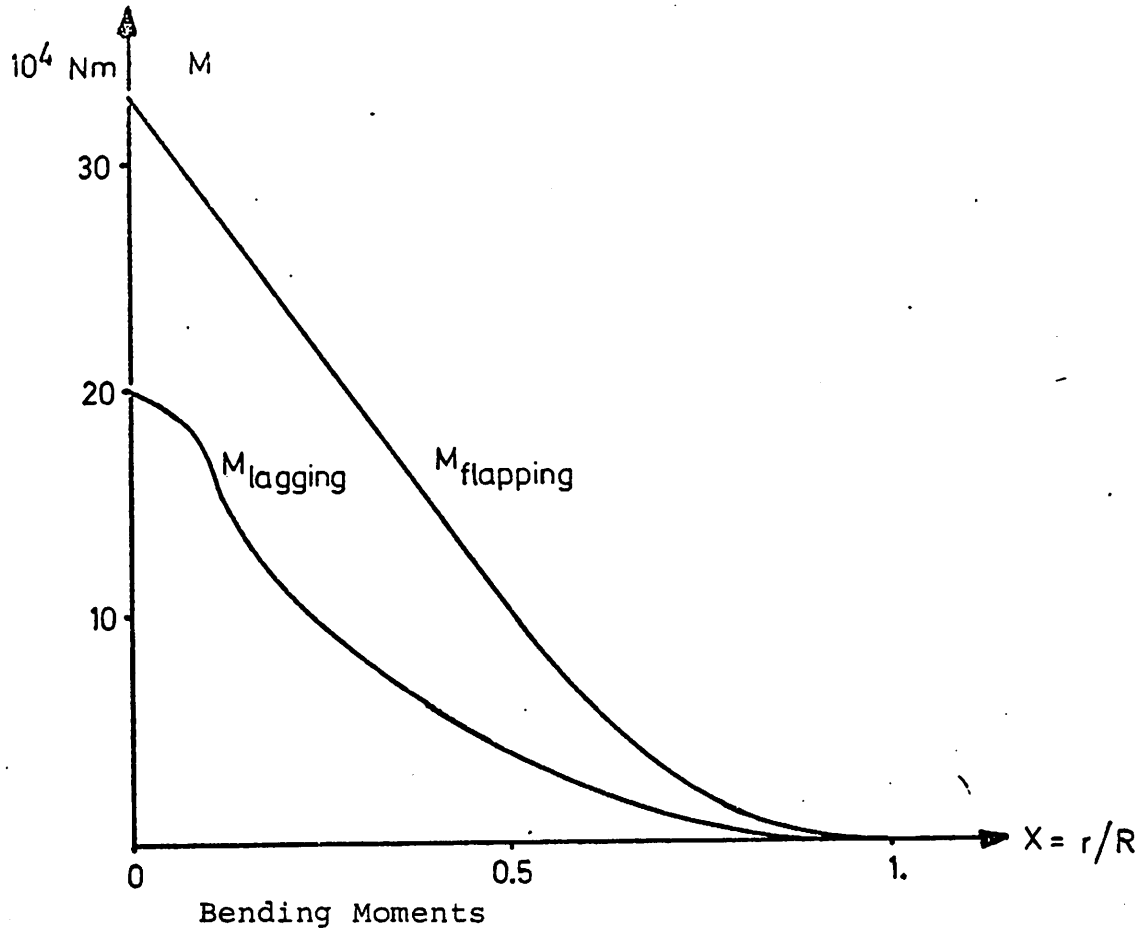

Bending Moments

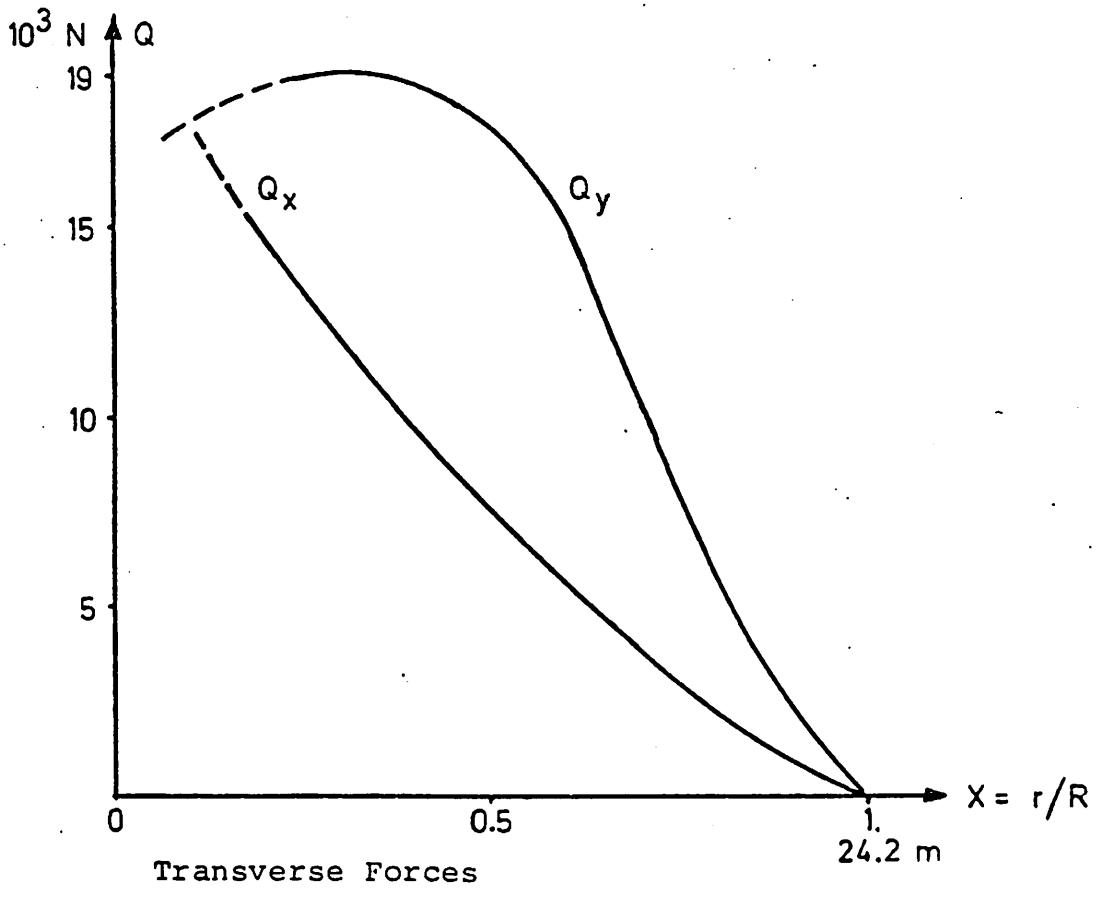

Transverse Forces

Fig.9: Typical Loads for WEA-DEMO Blade

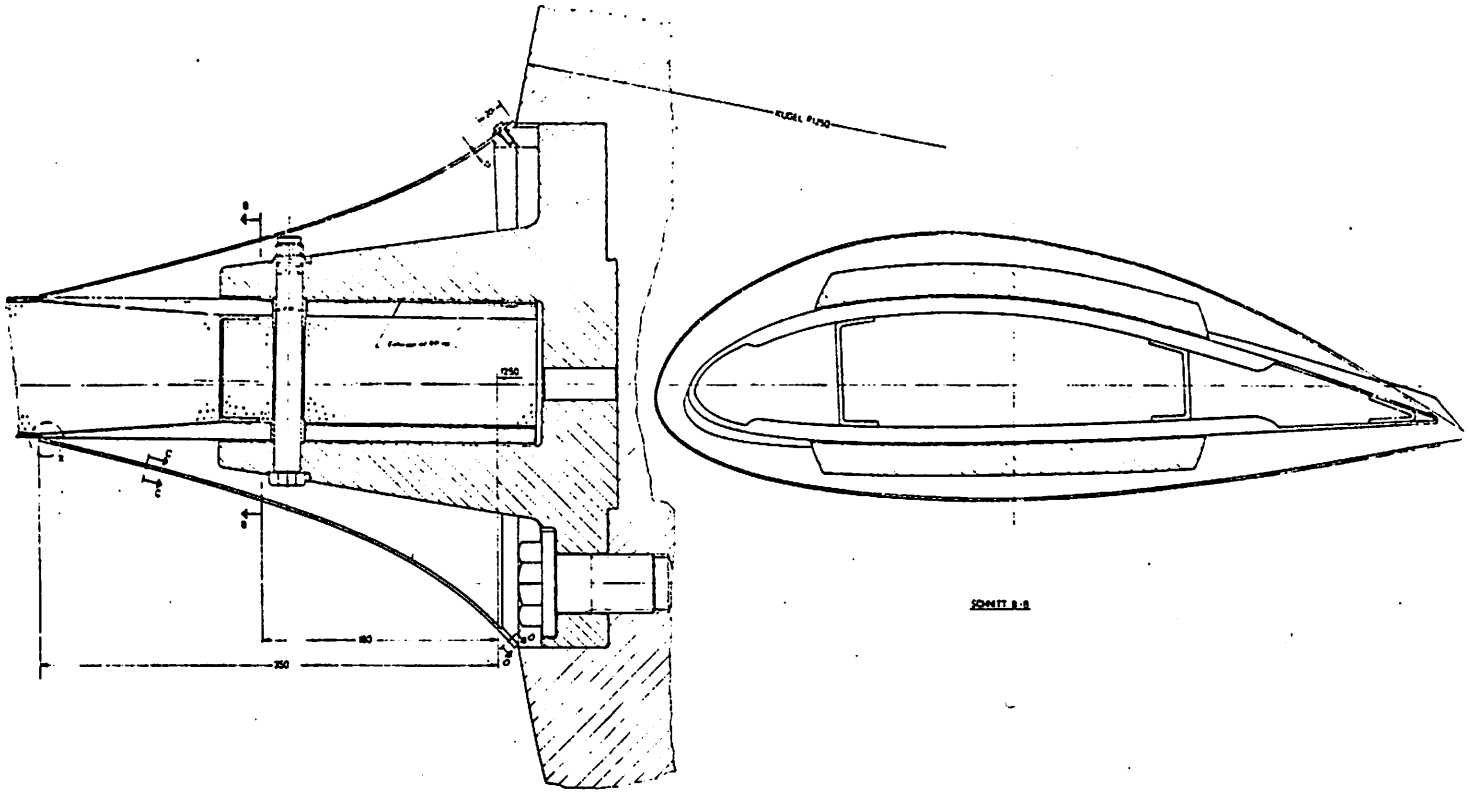

EMMEN Wind Tunnel

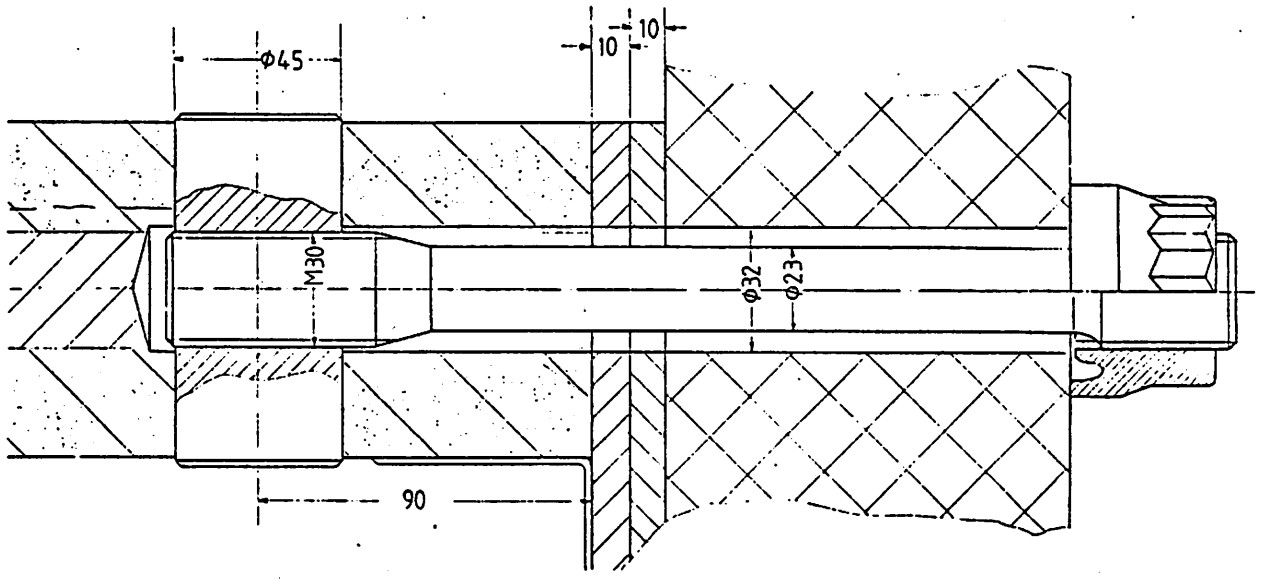

DNW Wind Tunnel

WEA and WEC Wind Energy Converters

Figure 1o: Various Bolt Connections

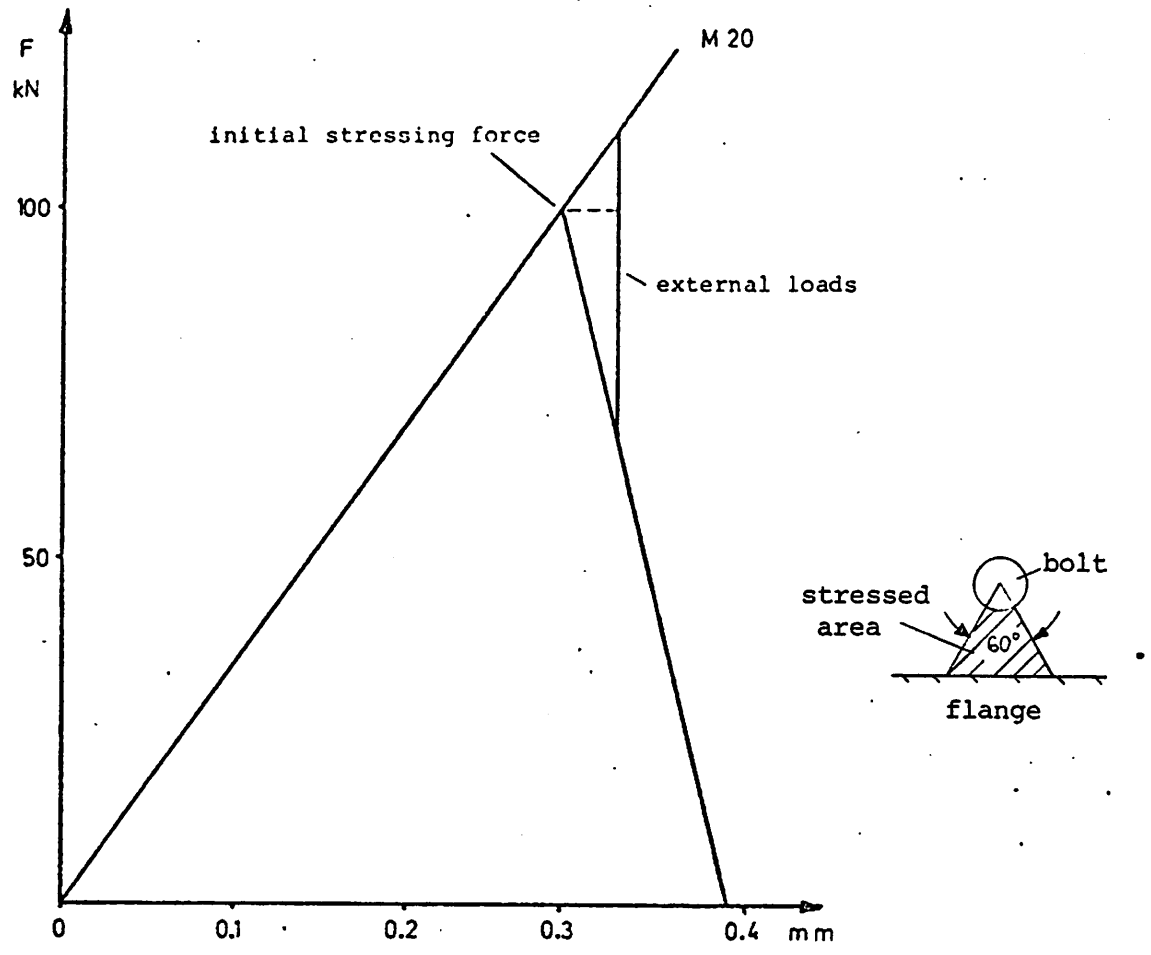

Fig. 11: Rigging Diagram of Blade Bolt Connection for WEA Demo

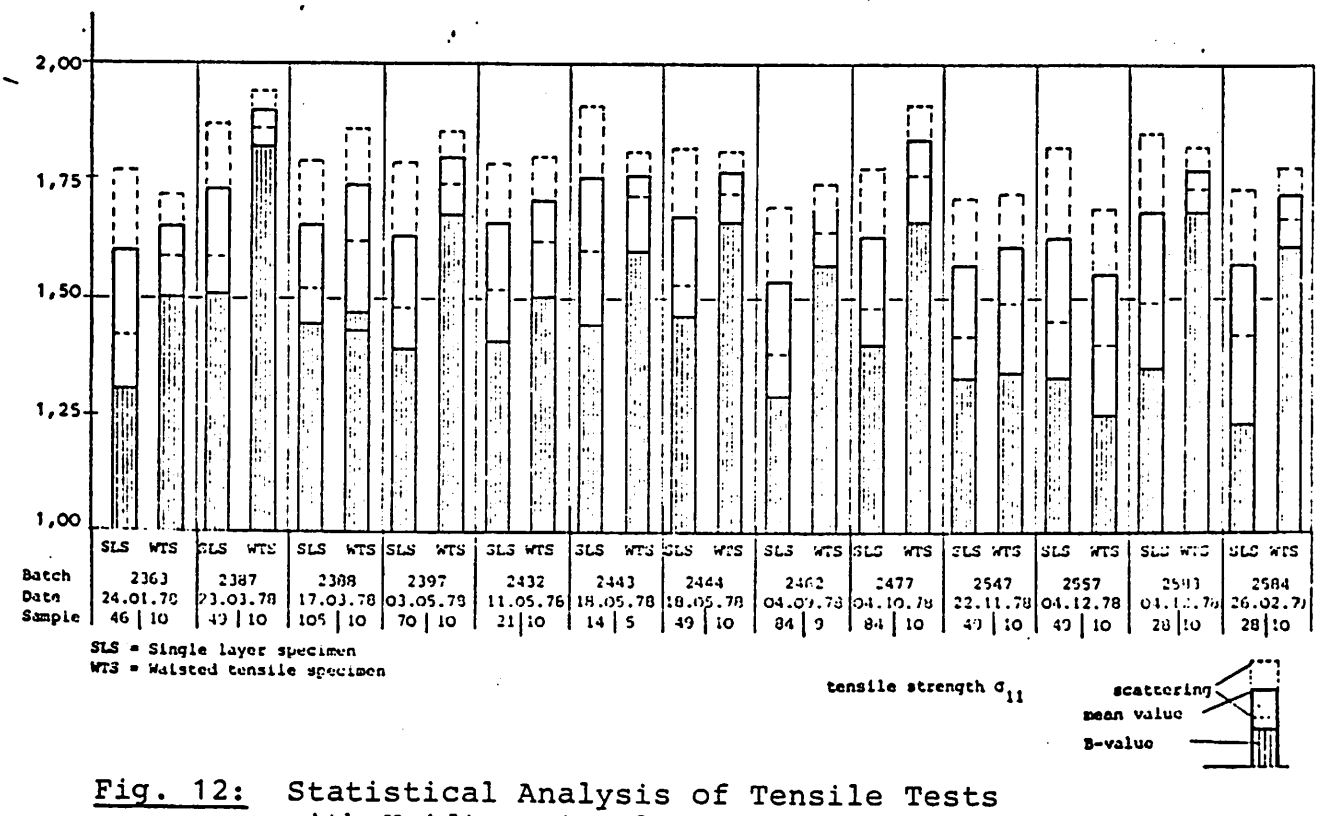

Fig. 12: Statistical Analysis of Tensile Tests with Unidirectional CRC Laminates 914 C

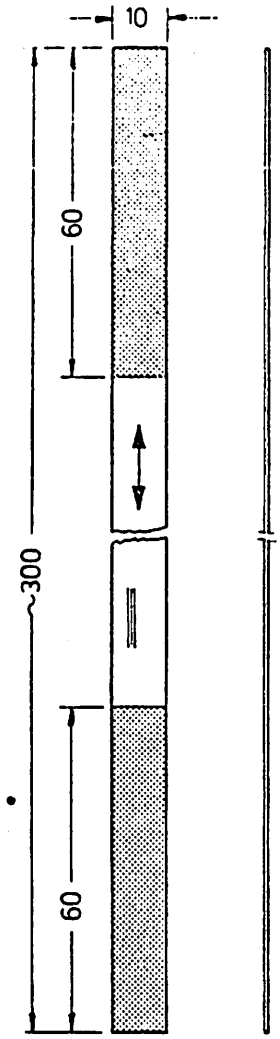

Single Layer Specimen

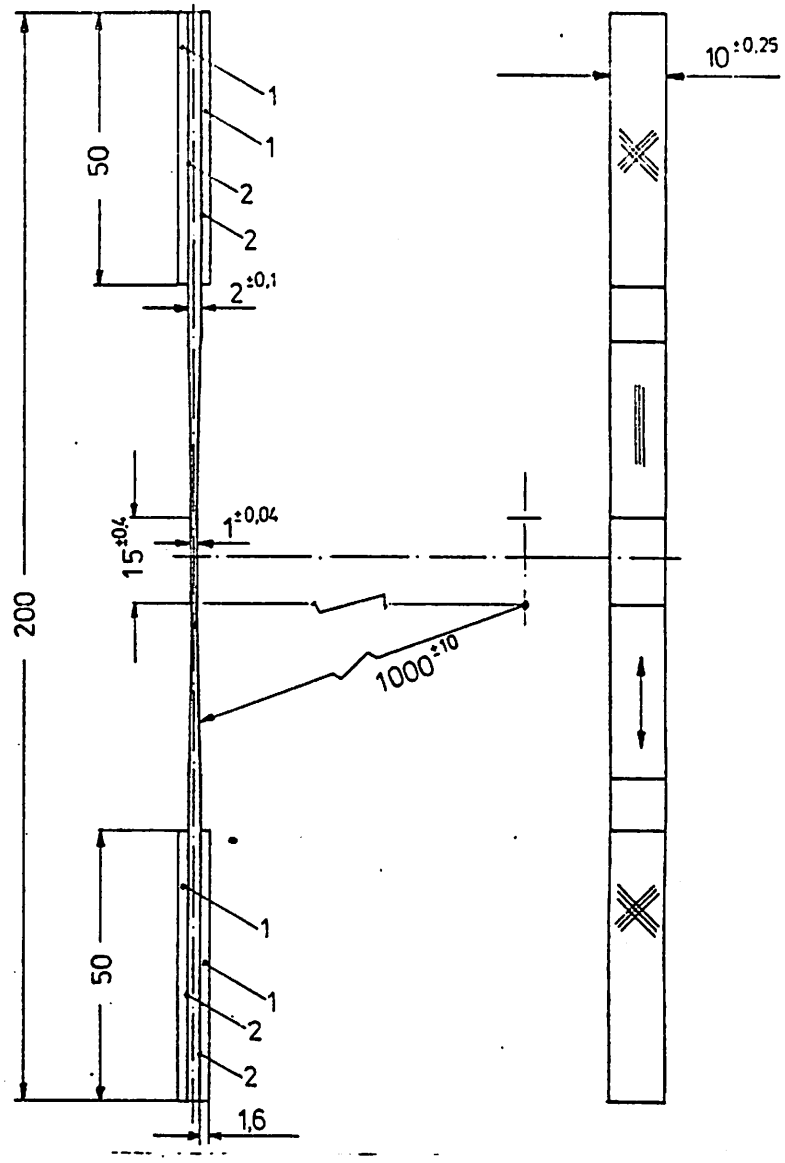

Waisted Tensile Specimen

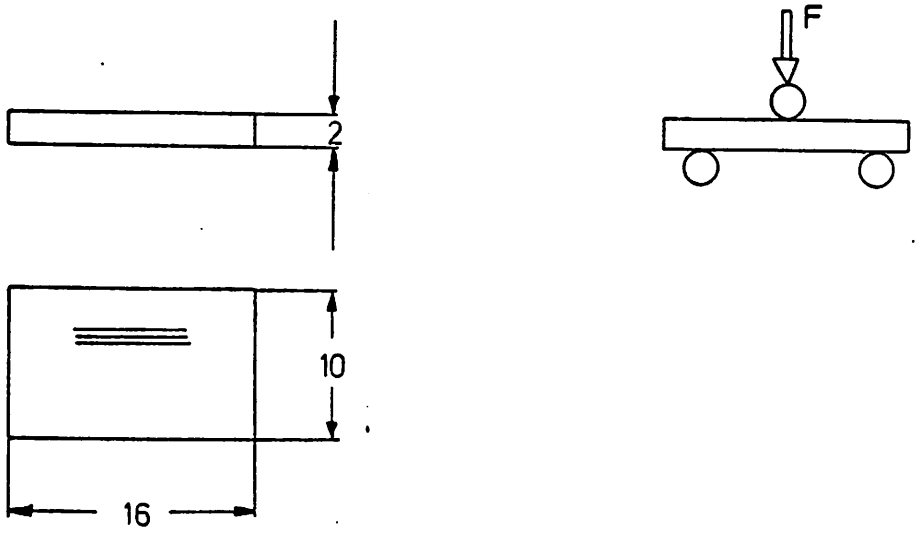

ILS Specimen

Fig.13: Specimens for Testing Material Properties

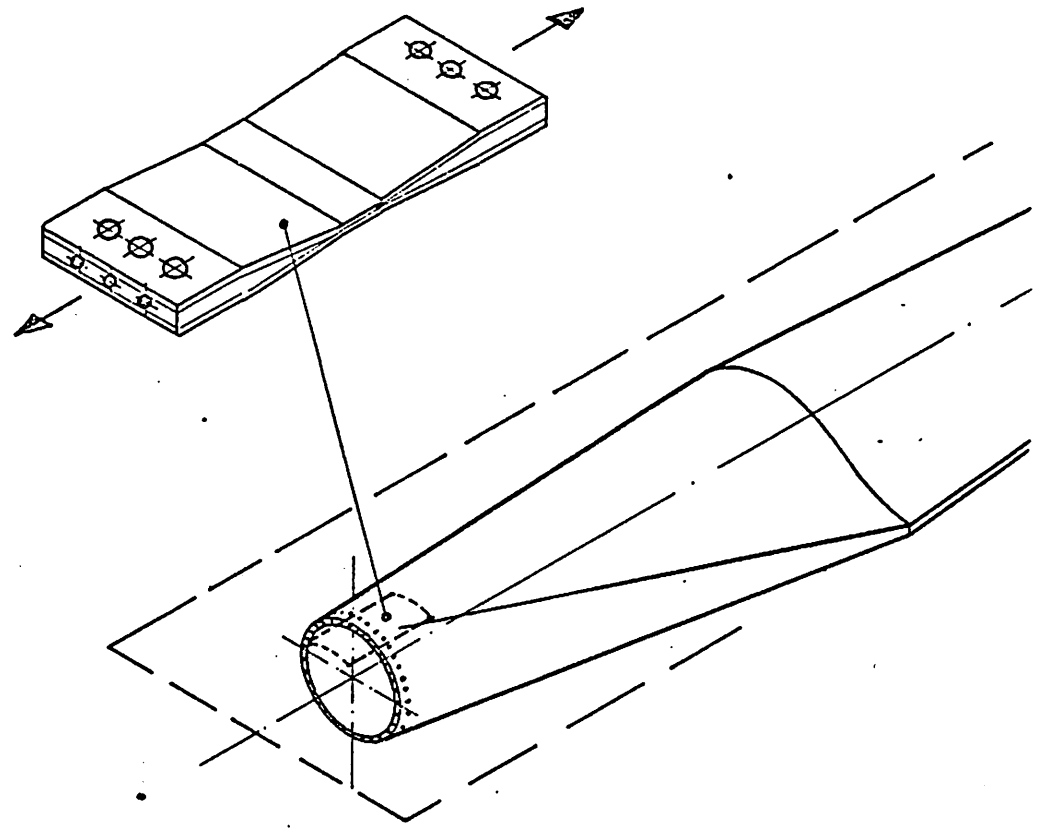

Fig. 14: Test of the Attachment Area

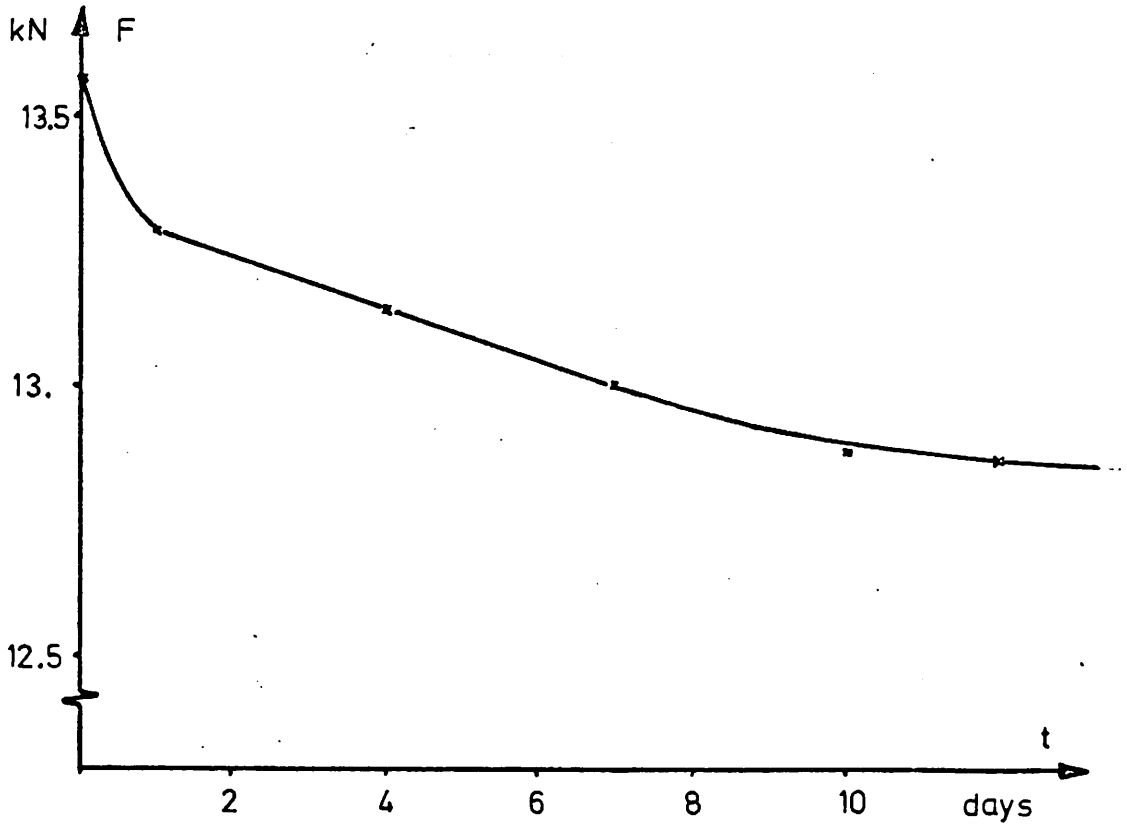

Fig. 15: Measured Diminution of Initial Stressing Force of DNW Bolt

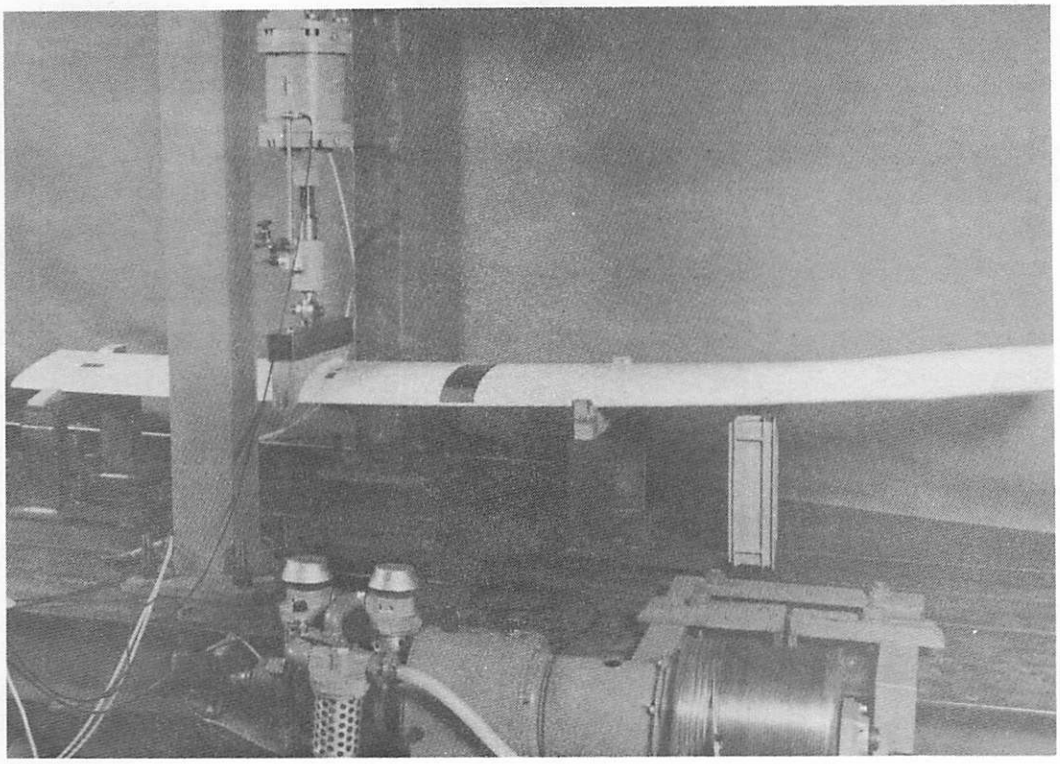

Figure 16: Setup of Crease Resistance Test

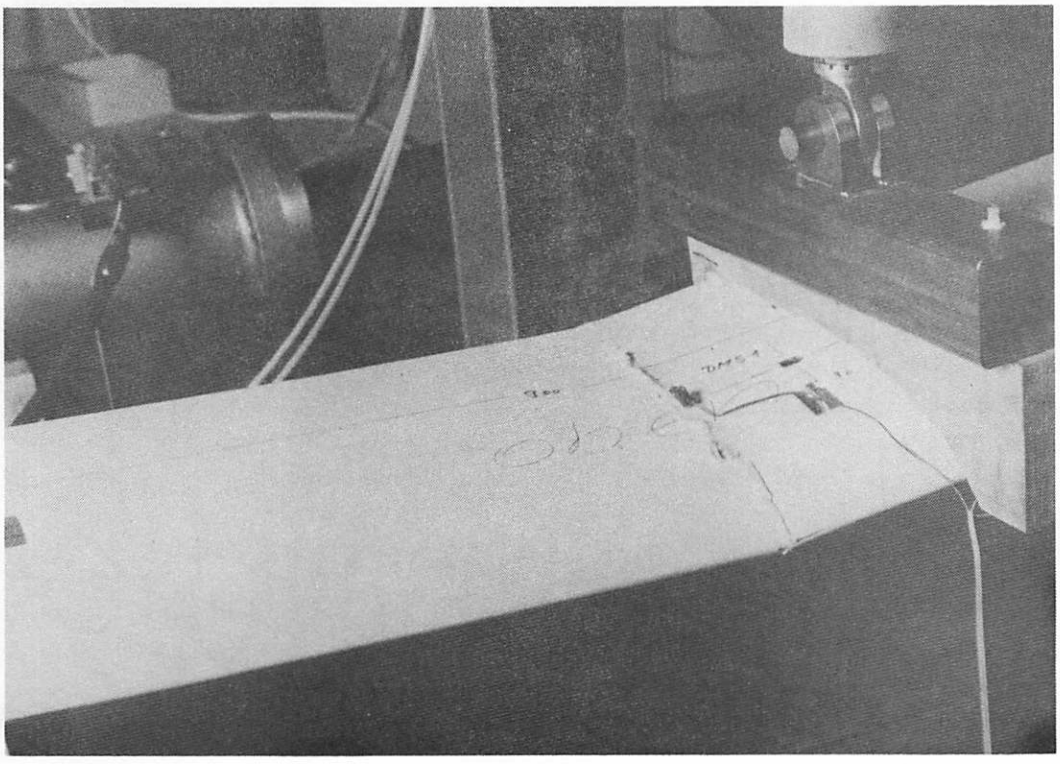

Figure 17: Site of Fracture

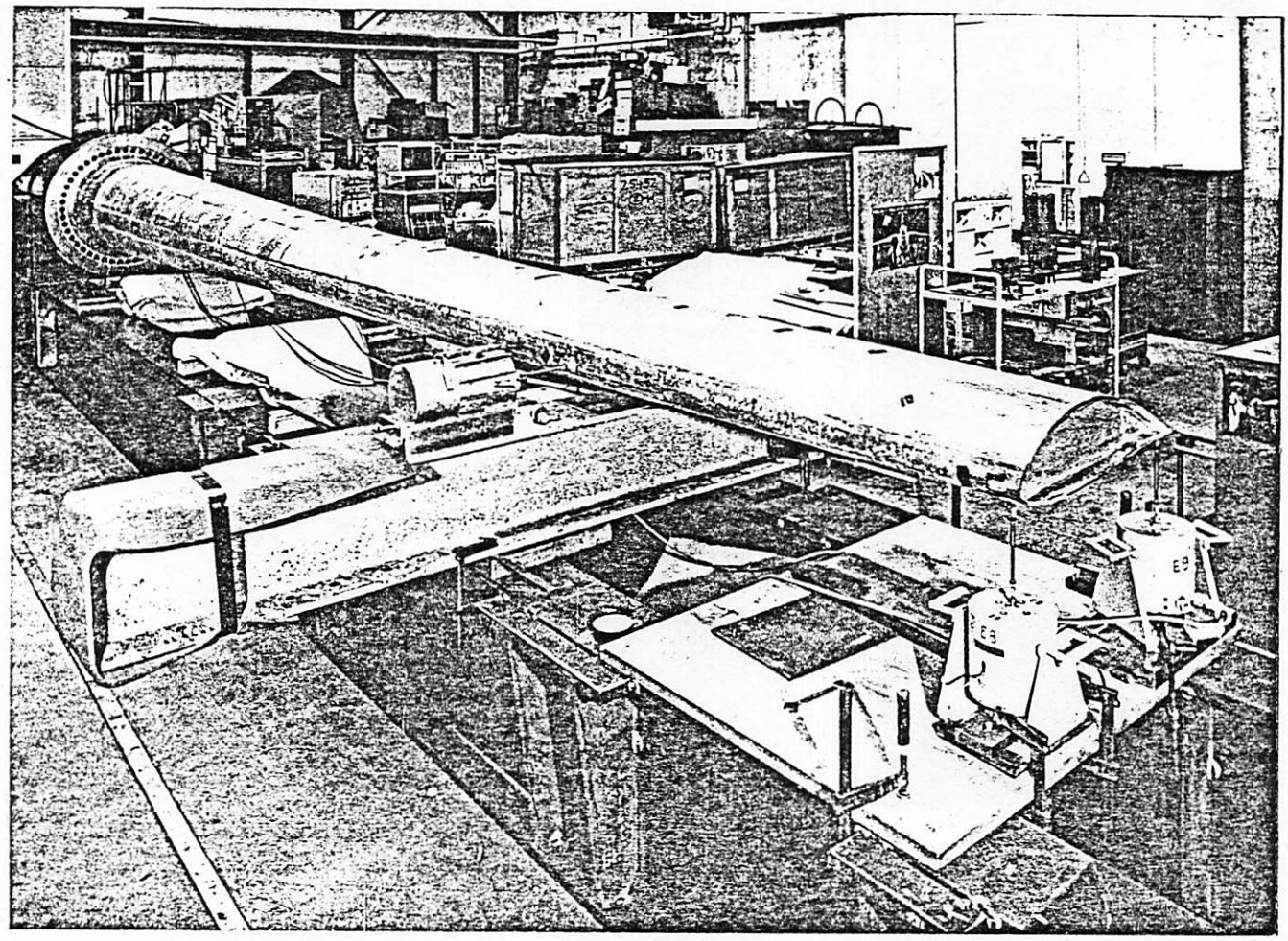

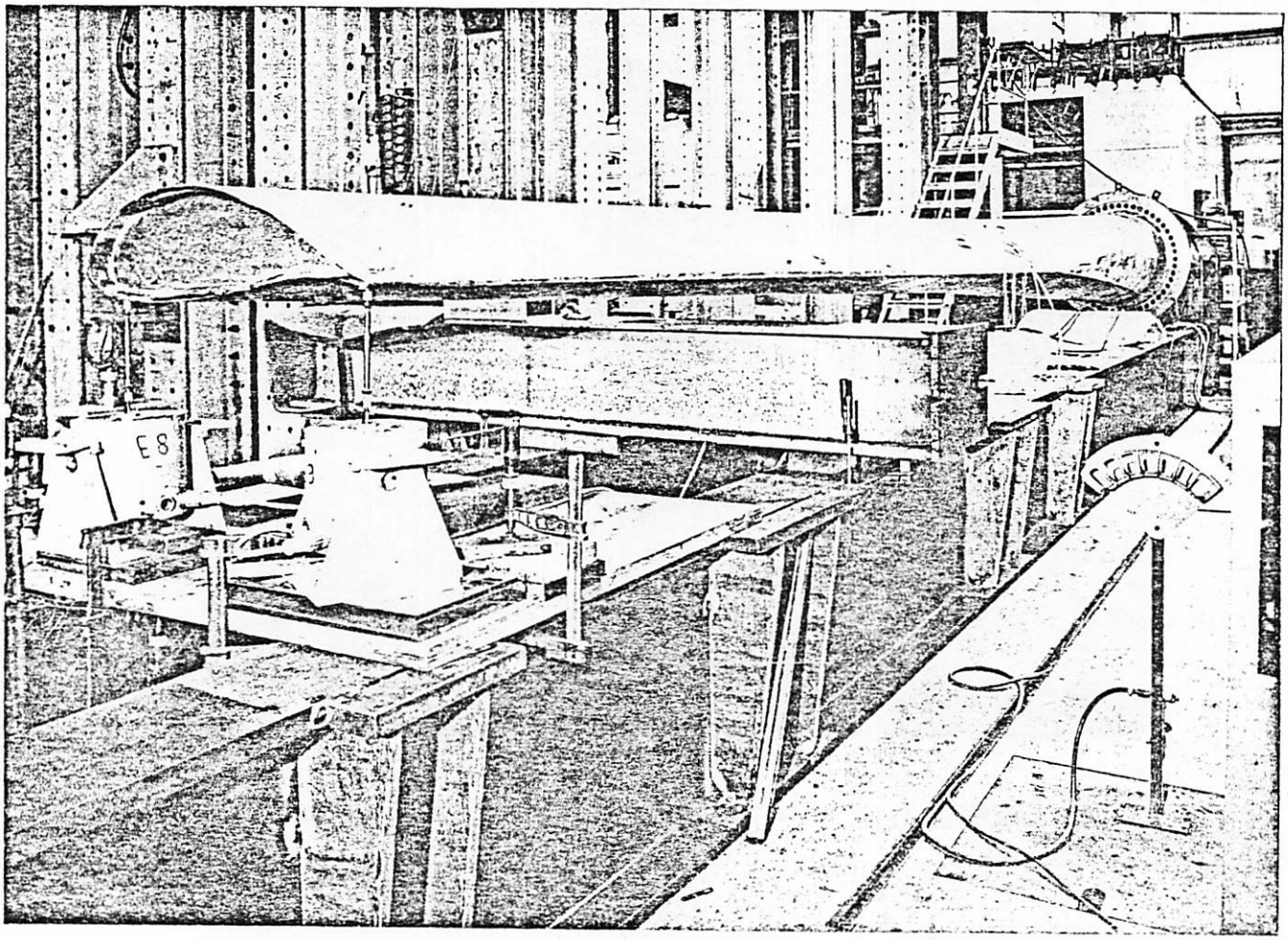

Fig. 18/19: Setup for Frequency Test

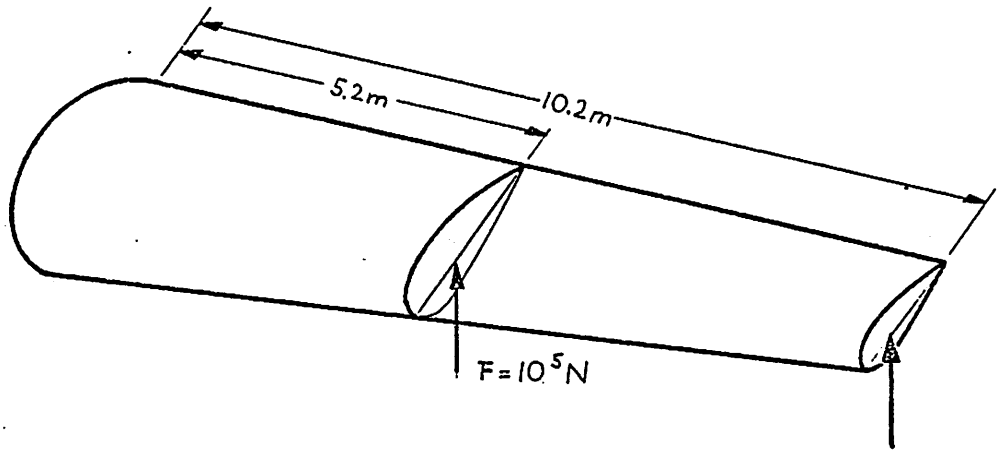

Figure 2o: Bending Test of WEC Specimen

REVIEW OF DOE/NASA LARGE WIND TURBINE BLADE PROJECTS

PATRICK M. FINNEGAN
NATIONAL AERONAUTICS AND SPACE ADMINISTRATION
LEWIS RESEARCH CENTER
CLEVELAND, OHIO 44135

CONTENTS

PRESENTED AT THE IEA MEETING, STOCKHOLM, SWEDEN
APRIL 21 AND 22, 1980

BLADE DEVELOPERS

ALUMINUM

LOCKHEED - 60' - MOD-0, -0A

STEEL SPAR

BOEING - 100' - MOD-1
BOEING - 150' - MOD-2
BUDD CO. - 60' - SR AND T
LERC - 60' - MOD-0

FIBERGLASS

HAMILTON - 60' - SR AND T
KAMAN/SCI - 150' - SR AND T
KAMAN - 100' - MOD-1
SCI - 60' - MOD-0A

WOOD

GOUGEON BROTHERS - 60' - MOD-0A

WTG BLADE CONFIGURATIONS

ALUMINUM (AIRCRAFT WING CONST.; MOD-0, -0A)

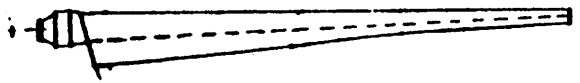

FIBERGLASS (FILAMENT AND TFT WOUND; SR & T)

STEEL/FIBERGLASS (UTILITY POLE AND SPOT WELDED SPAR; MOD-0, SR & T)

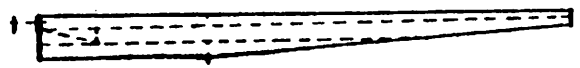

WOOD (BOAT HULL CONST; SR & T)

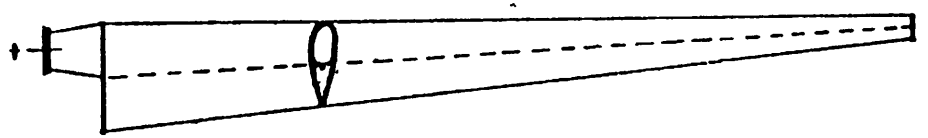

STEEL (WELDED SPAR, BONDED SS & FOAM TE; MOD-1)

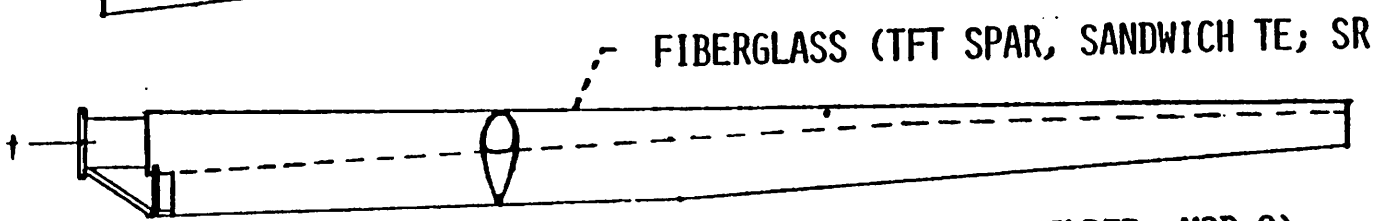

FIBERGLASS (TFT SPAR, SANDWICH TE; SR & T)

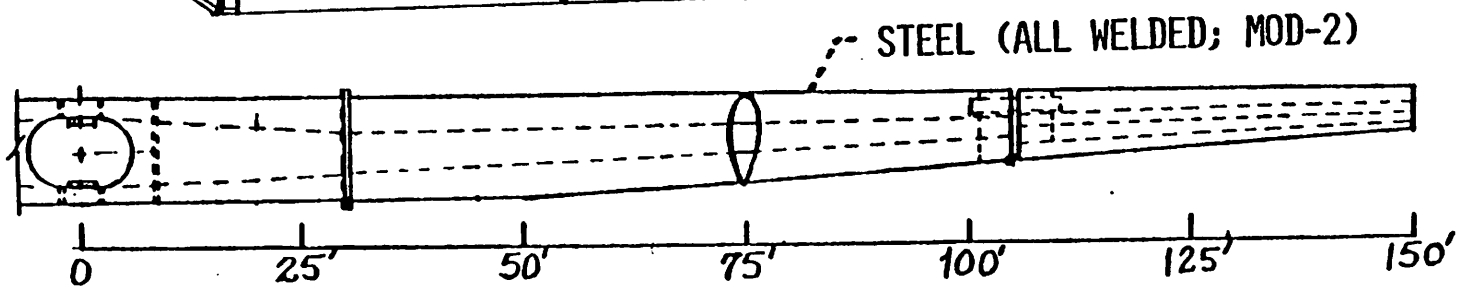

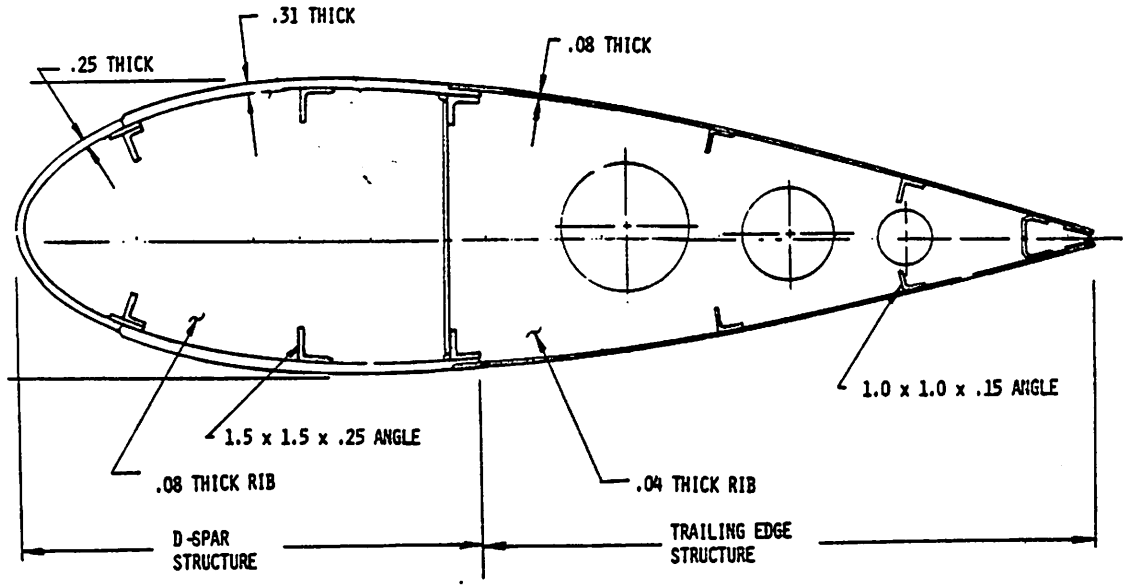

TYPICAL CROSS SECTION

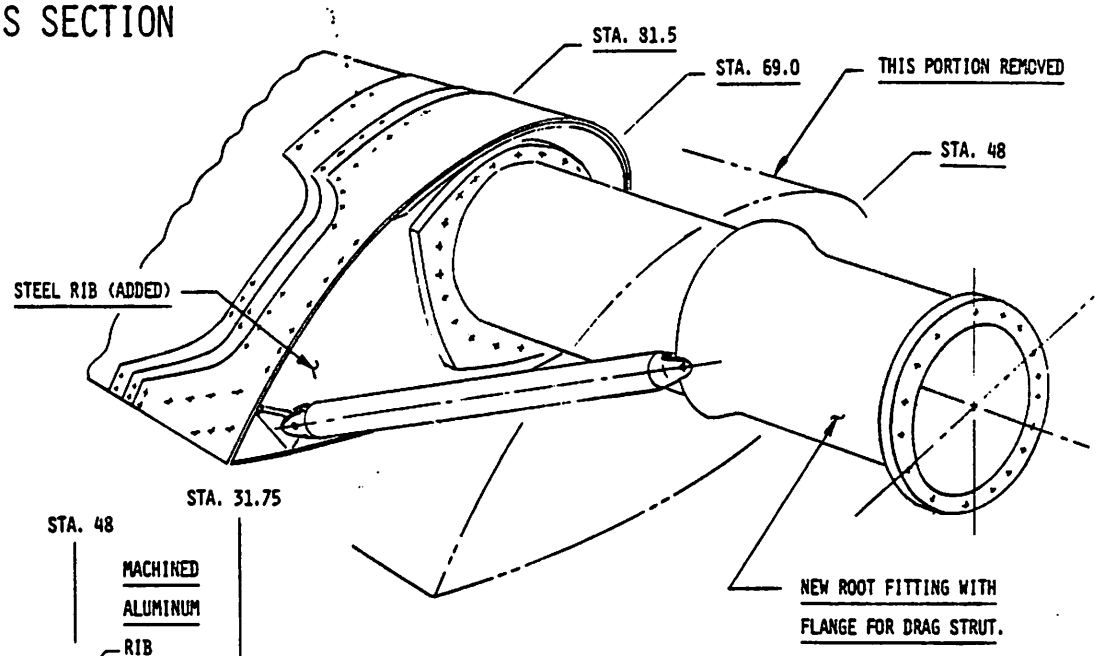

ALTERNATE ROOT END CONFIGURATION

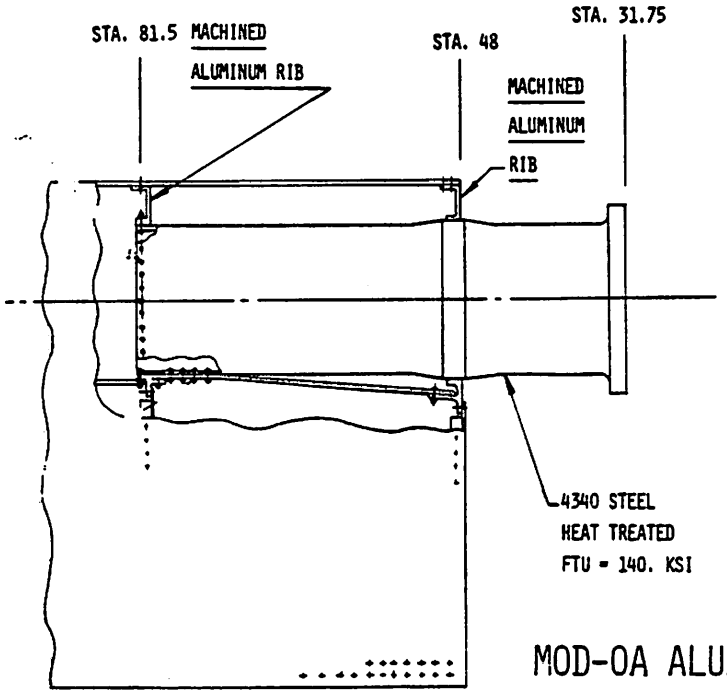

MOD-0A ALUMINUM BLADE ROOT END

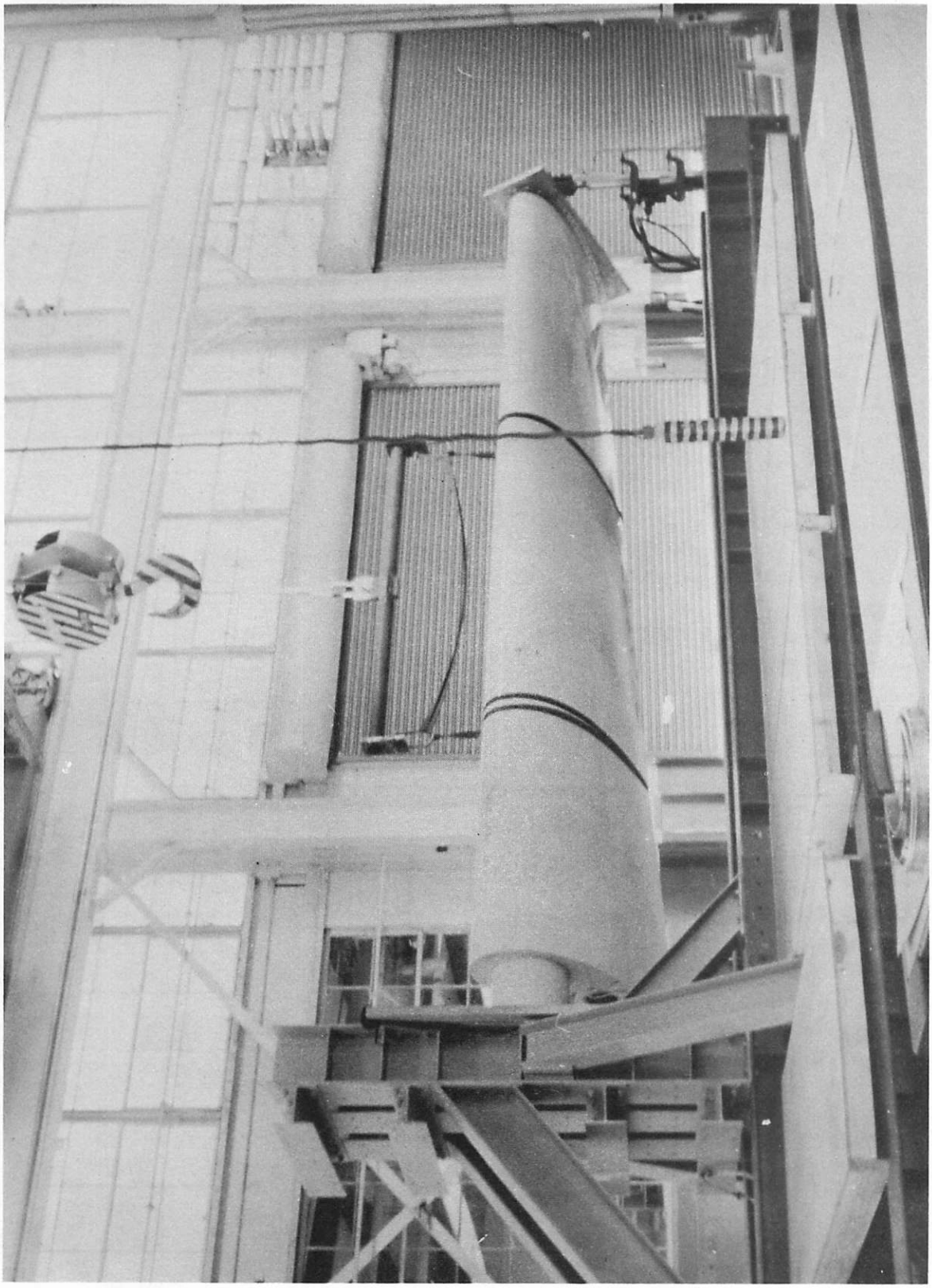

20 FOOT LONG FULL SCALE ROOT END FATIGUE TEST OF MOD-OA ALUMINUM BLADE

FATIGUE TEST - MOD-OA BLADE

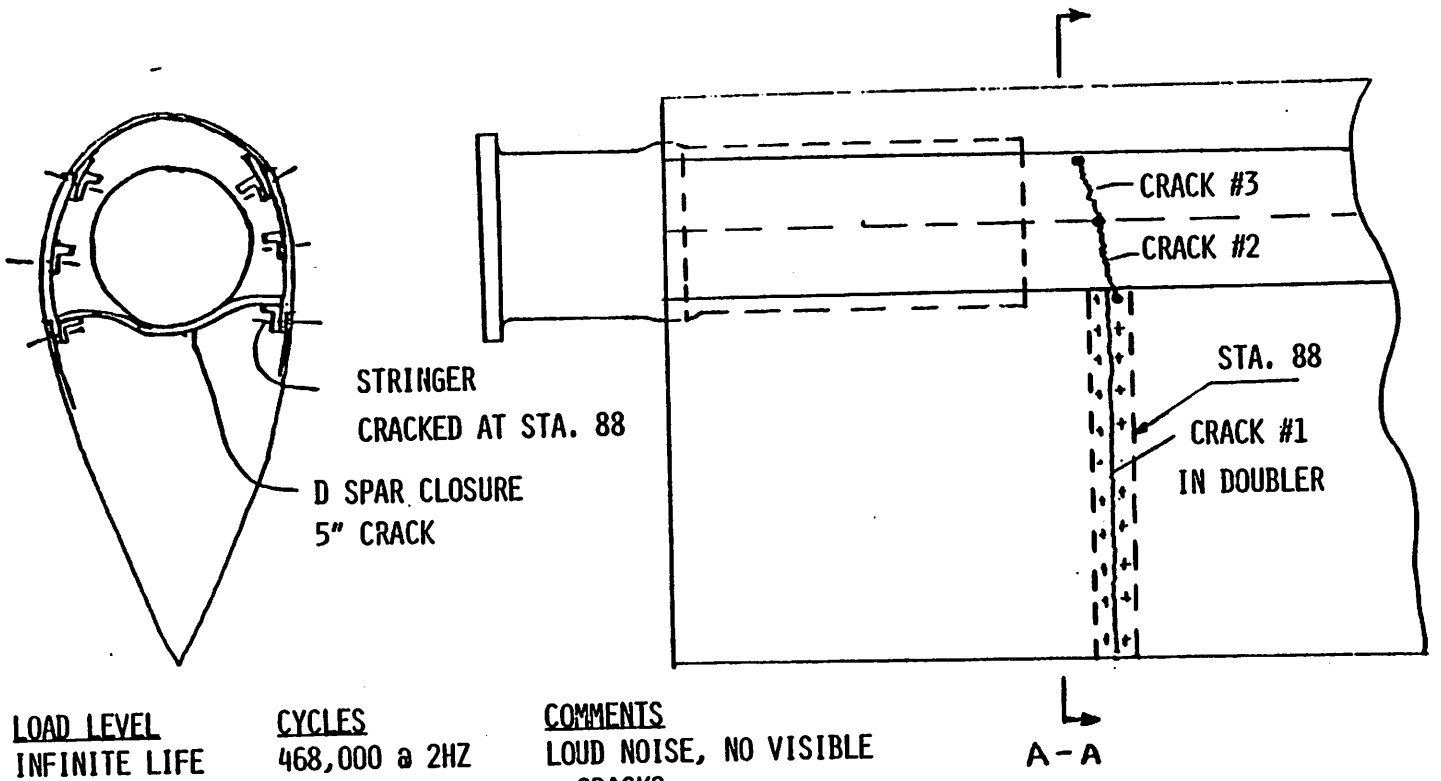

LOAD LEVEL	CYCLES	COMMENTS
INFINITE LIFE	468,000 @ 2HZ	LOUD NOISE, NO VISIBLE CRACKS
103,200 FT # @ STA. 80	920,000	LOUD NOISE. NO VISIBLE CRACKS
	1,000,000	CRACK #1
40 MPH CUTOUT	2,000	LOUD NOISE, CRACK #2
135,000 FT # @ STA. 80	9,000	LOUD NOISE, CRACK #3

4-10-80
PMF

STEEL BLADE CONCEPTS BEING DEVELOPED

- SIZE -- 60, 100, AND 150 FEET
- BUTT AND SPOT WELD
- STRUCTURE
  - -- ALL STEEL AND STEEL SPAR
  - -- STEEL SPAR
    - -- FORMED PLATE AND WELDED
    - -- UTILITY POLE TECHNOLOGY
    - -- SPOT WELDED STAINLESS SHEET, ANGLES, & CHANNELS
  - -- AFT PANELS
    - -- WELDED STEEL
    - -- STAINLESS BONDED TO SPAR, FOAM SUPPORTED
    - -- FIBERGLASS, SEGMENTED, FOAM SUPPORTED
    - -- DOPED FIBERGLASS ON PLYWOOD RIBS
  - -- HUB
    - -- CARRY THROUGH
    - -- BOLT ON
- CONTRACTORS
  - -- BOEING, BUDD, LERC WITH UTILITY POLE MFG

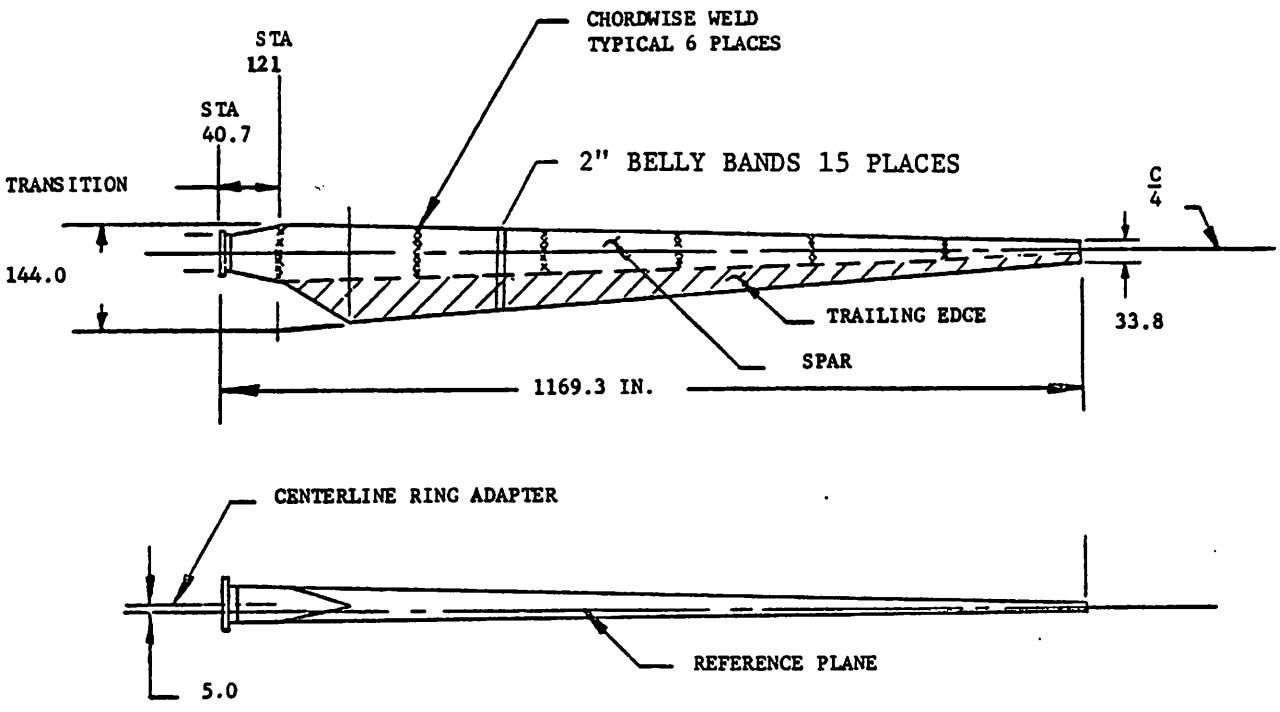
STA
121
STA
40.7
TRANSITION
144.0
CHORDWISE WELD
TYPICAL 6 PLACES
2" BELLY BANDS 15 PLACES
C/4
TRAILING EDGE
33.8
SPAR
1169.3 IN.
CENTERLINE RING ADAPTER
REFERENCE PLANE
5.0

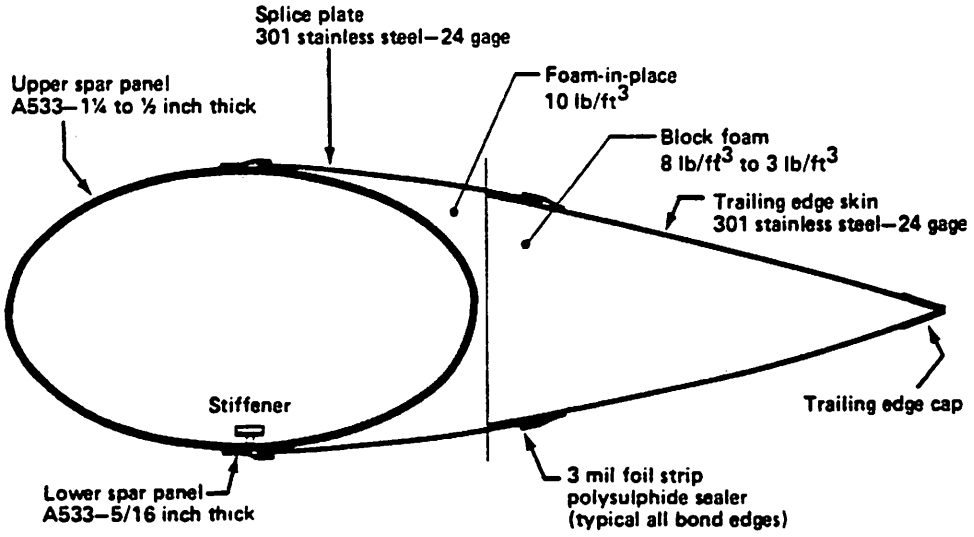
Splice plate
301 stainless steel—24 gage
Upper spar panel
A533—1¼ to ½ inch thick
Foam-in-place
10 lb/ft3
Block foam
8 lb/ft3 to 3 lb/ft3
Trailing edge skin
301 stainless steel—24 gage
Stiffener
Trailing edge cap
Lower spar panel
A533—5/16 inch thick
3 mil foil strip
polysulphide sealer
(typical all bond edges)

MOD-1 Blade

MOD-1 100 FOOT STEEL SPAR BLADE

- USE AISC FOR FATIGUE ALLOWABLES
  -- DEVELOP QUALITY CONTROL TO ASSURE DEFECTS WITHIN MARGINS
- CRACK PROPAGATION RATE VERIFIED BY TEST. CRACK DETECTOR RESPONSE PROVIDES SAFETY MARGIN.
- BUCKLING DESIGN VERIFIED BY 15 FOOT FULL SCALE TEST
- TRAILING EDGE TO SPAR JOINT IS MOST INNOVATIVE FEATURE
- WEIGHT AND HUB MOMENT DIFFICULT AND EXPENSIVE TO ACHIEVE
- MEASURED LOADS WITHIN DESIGN MARGINS

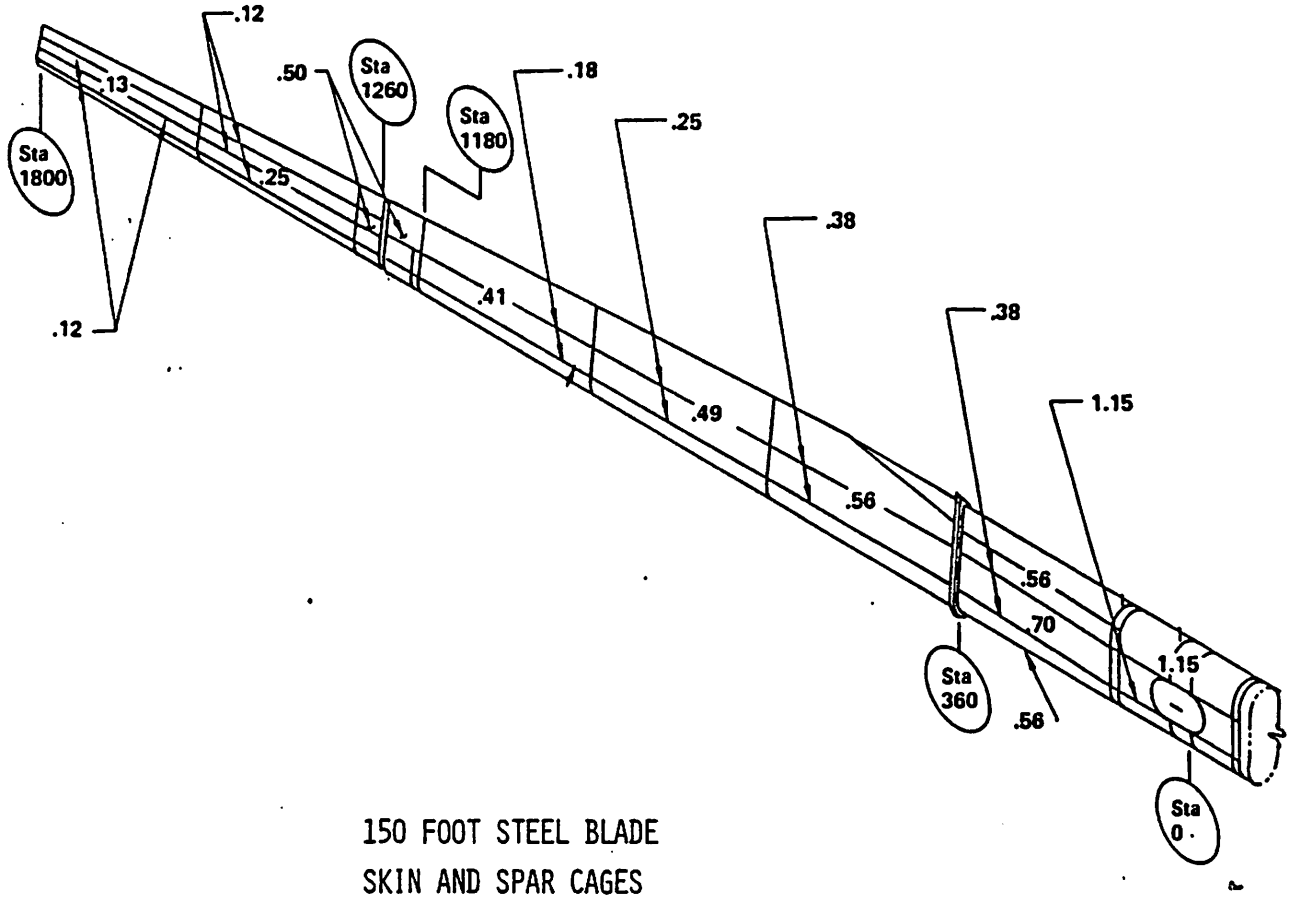

150 FOOT STEEL BLADE
SKIN AND SPAR CAGES

MOD-2 150 FT TIP CONTROL BLADE

- USE AISC FOR FATIGUE ALLOWABLES
  -- DEVELOP QUALITY CONTROL TO ASSURE DEFECTS WITHIN MARGINS
- CRACK PROPAGATION RATE VERIFIED BY TEST. CRACK DETECTOR RESPONSE PROVIDES SAFETY MARGIN.
- BUCKLING DESIGN VERIFIED BY 30 FT FULL SCALE TEST
- VERIFY TIP SPINDLE DESIGN BY TEST
- IN FUTURE DESIGNS IMPROVE TIP STRUCTURE
  -- LIGHTER--BETTER AIRFOIL SURFACE

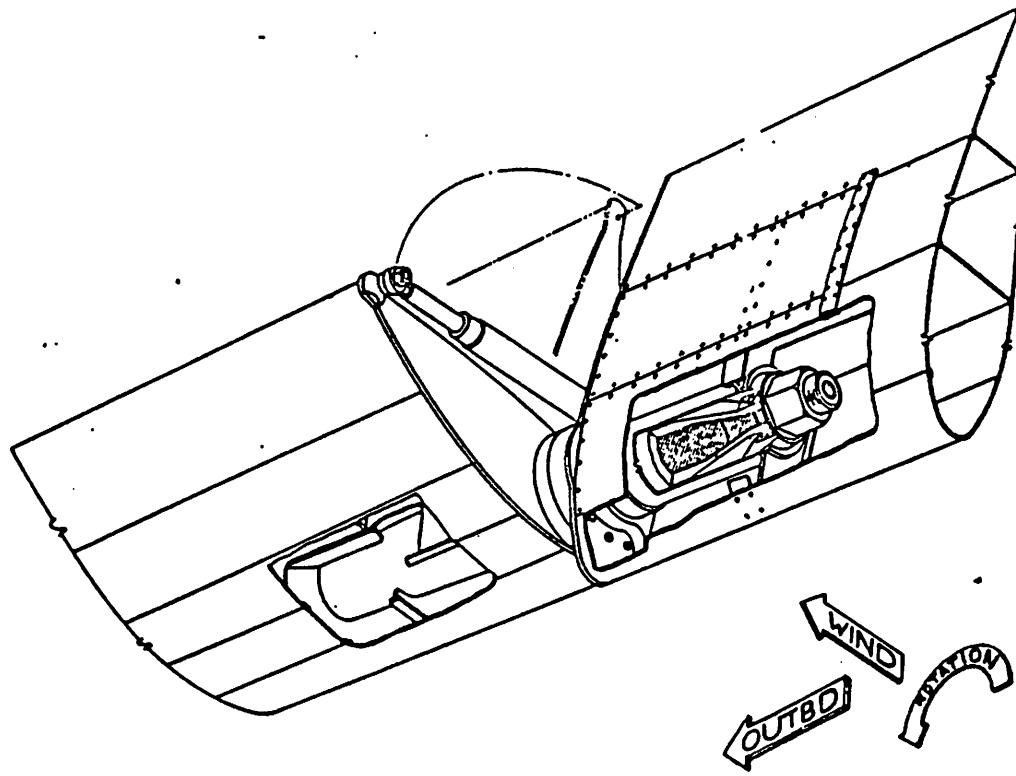

TIP CONTROL SPINDLE - 150 FOOT STEEL BLADE

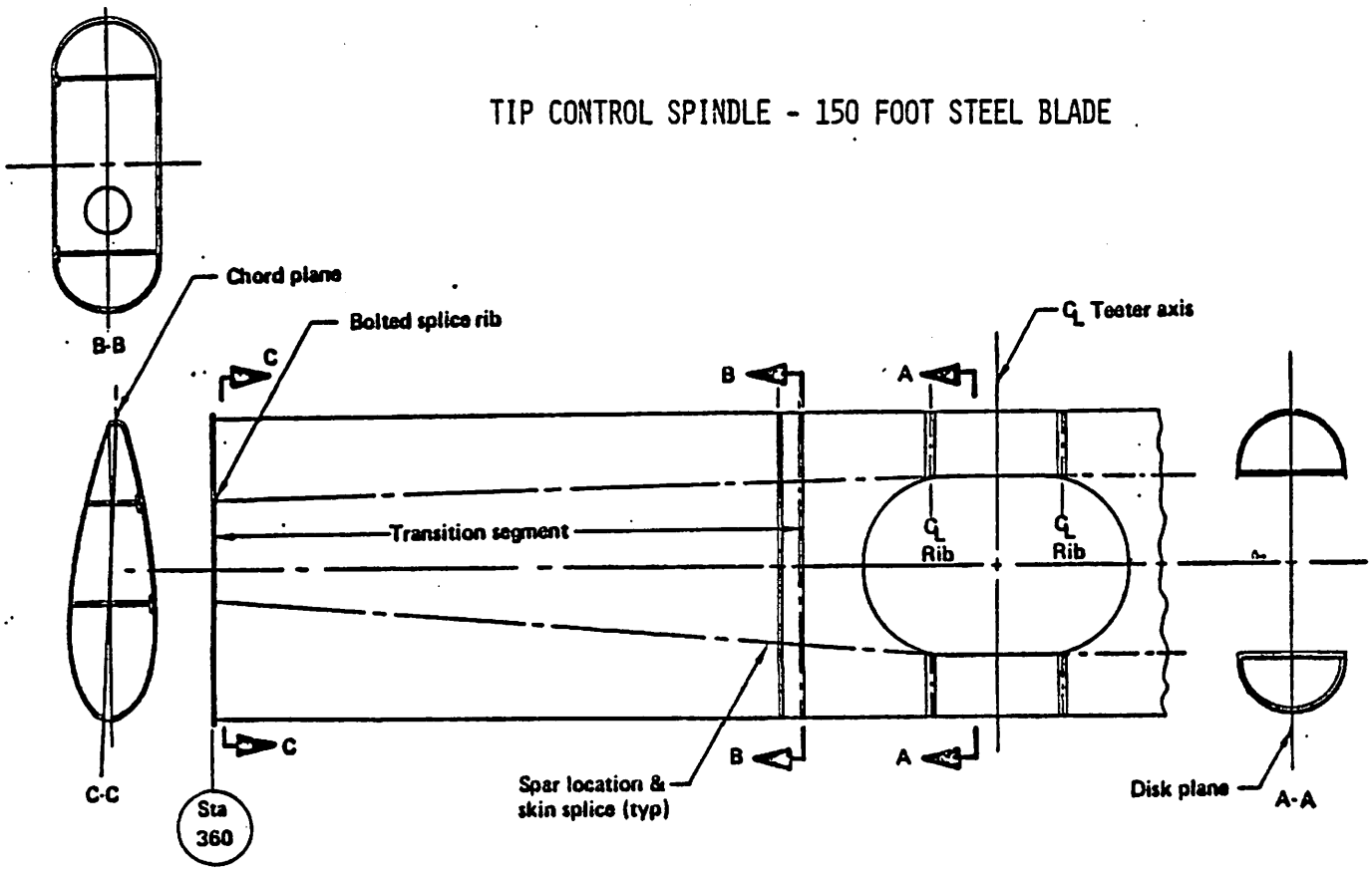

ROOT END 150 FOOT STEEL BLADE

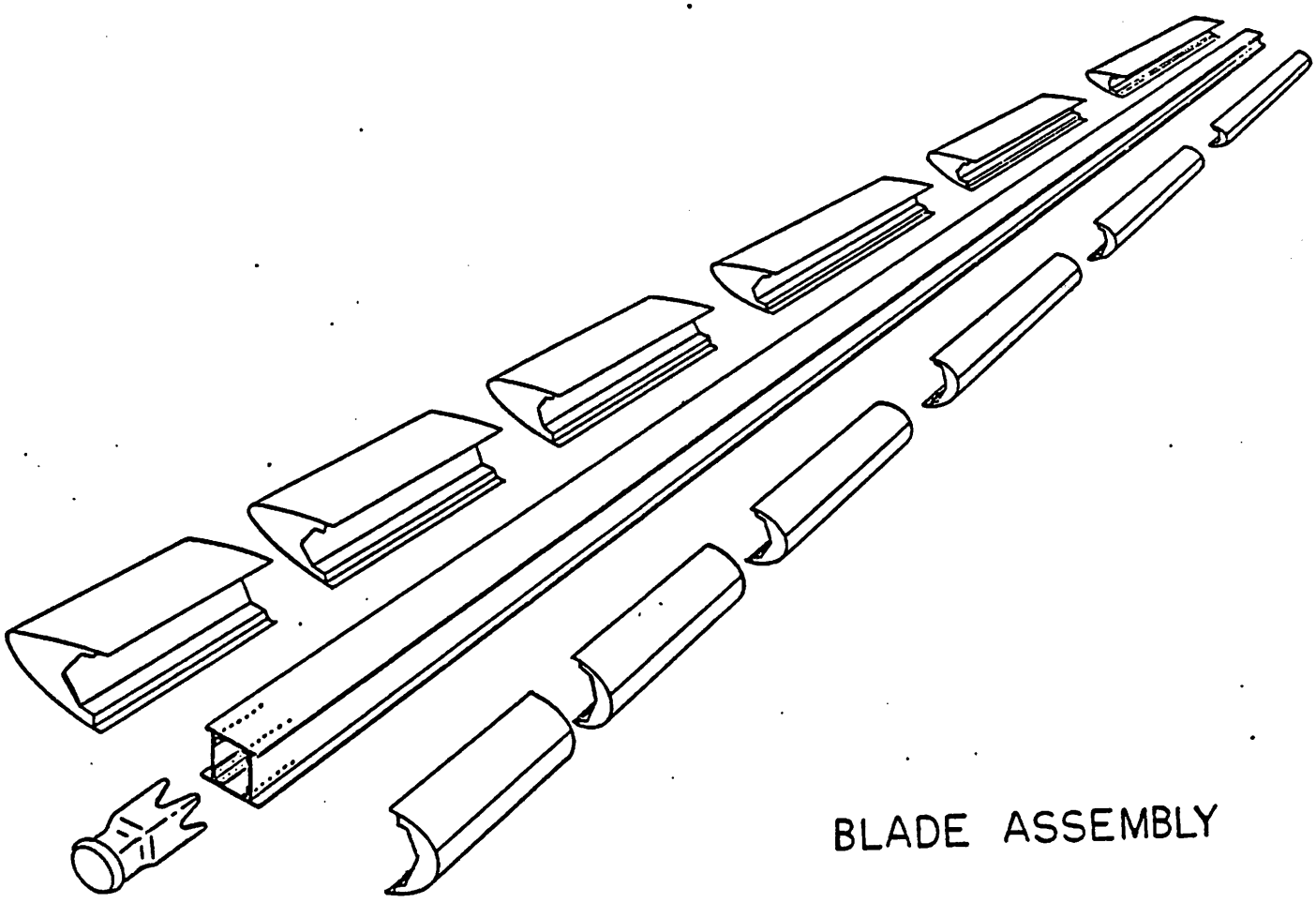

BLADE ASSEMBLY

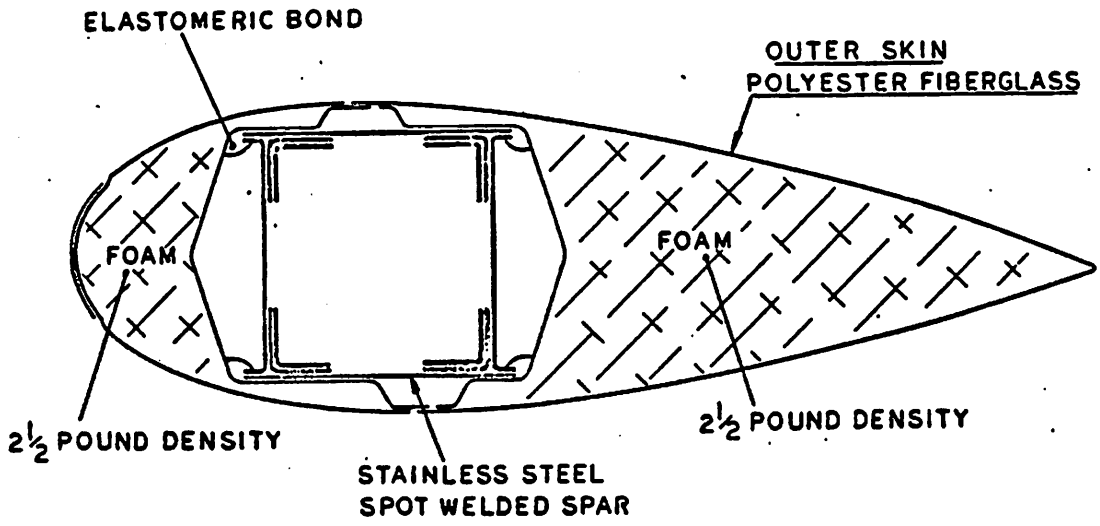

SECTION

SPOT WELDED STEEL SPAR BLADE

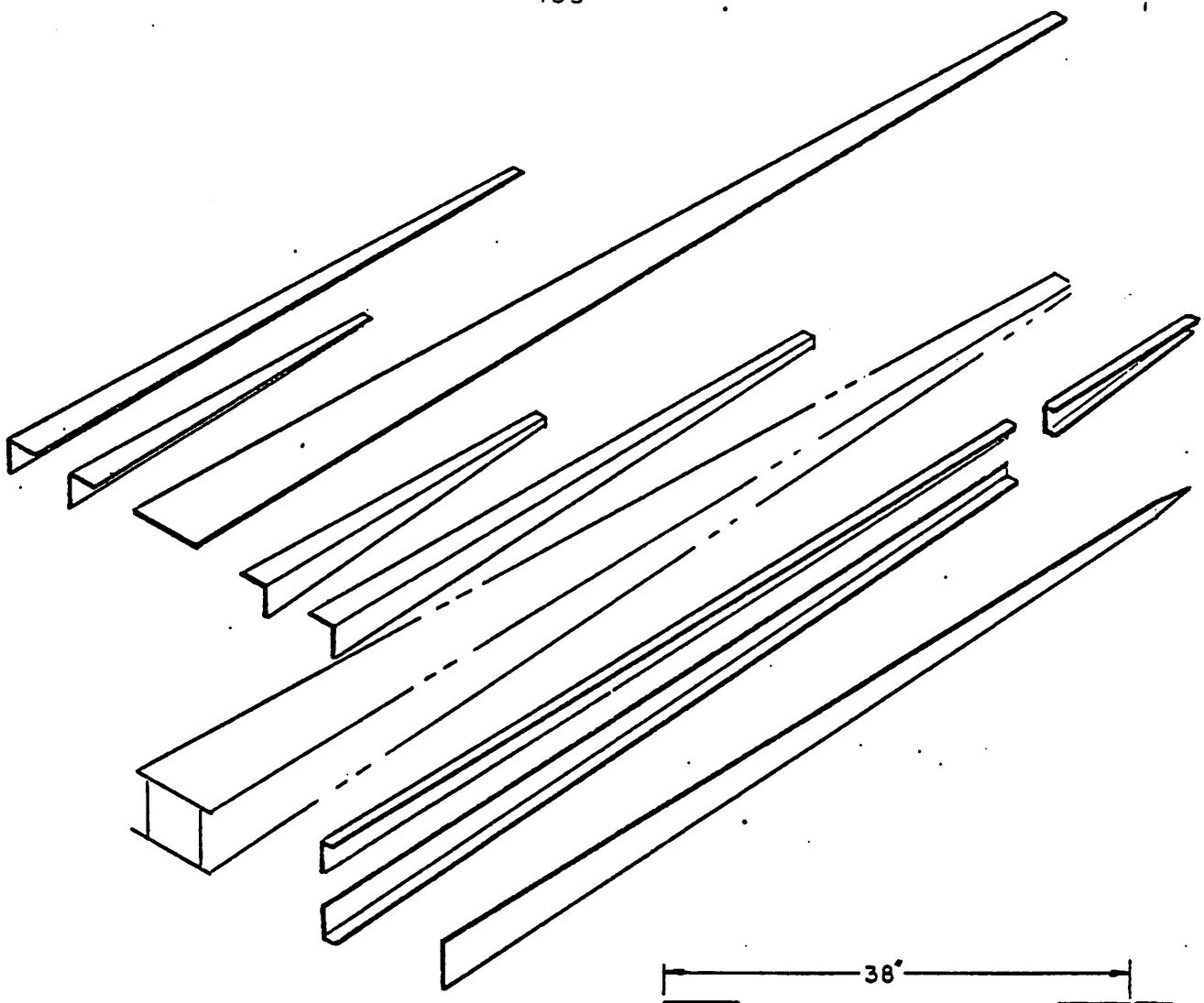

EXPLODED VIEW
OF STAINLESS
STEEL SPAR

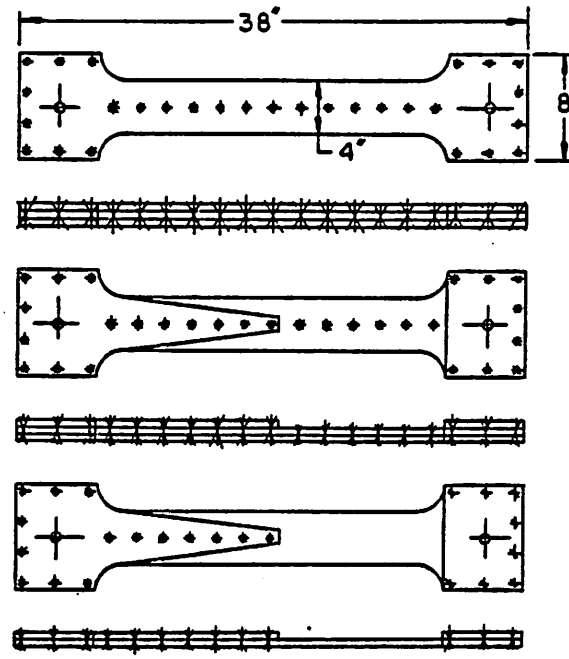

FULL SCALE TEST ELEMENTS

SPOT WELDED STEEL SPAR BLADE

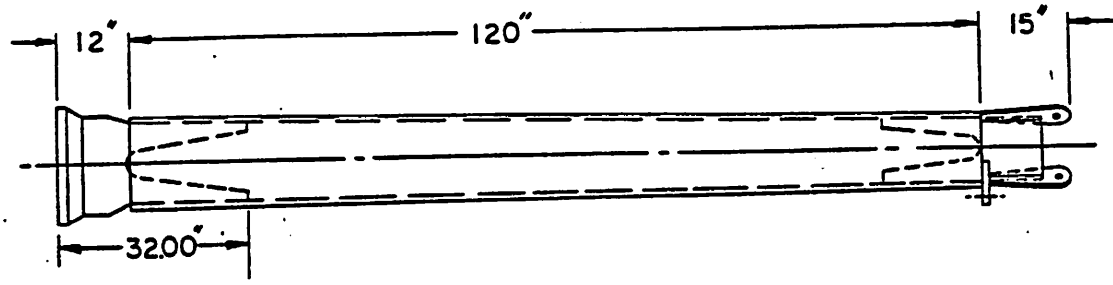

TEST SPECIMEN

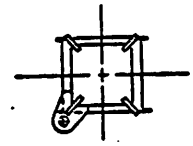

FULL SCALE TEST SPECIMEN OF
SPAR AND ROOT END FITTING

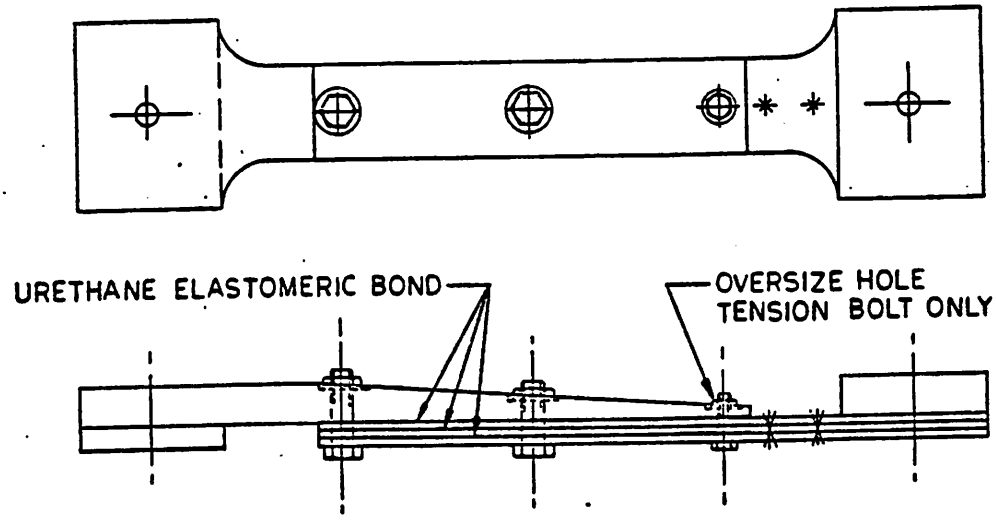

FULL SCALE TEST ELEMENT ROOT END

SPOT WELDED STEEL SPAR BLADE

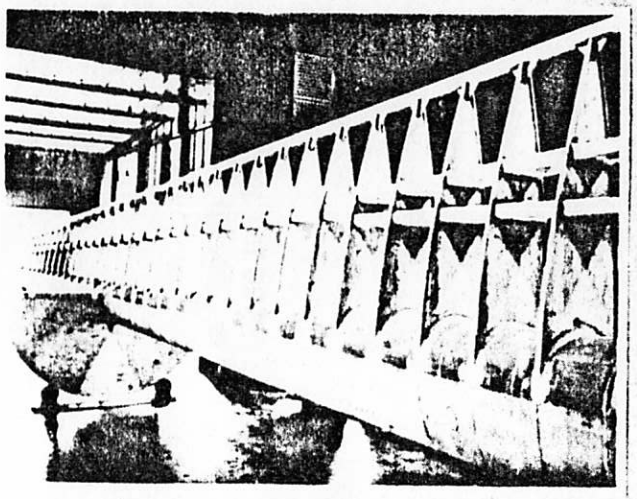

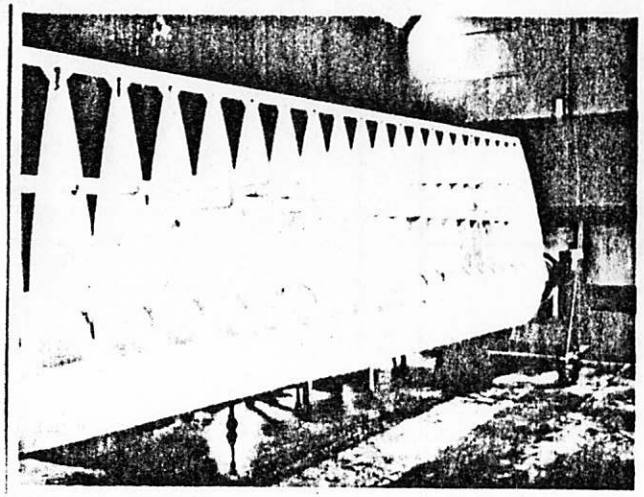

FABRICATION

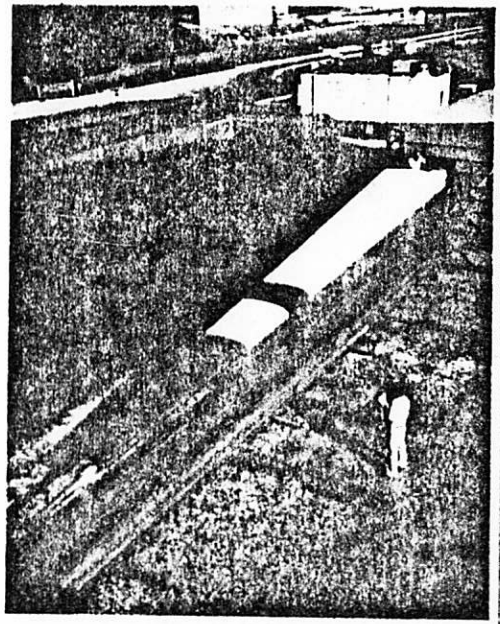

LOADS APPLICATION

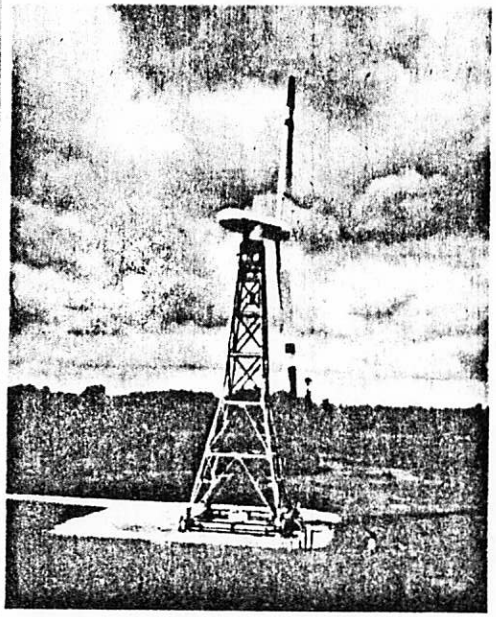

INSTALLATION ON MOD-0

PHASES OF CONSTRUCTION OF UTILITY POLE BLADES.

Part		Test no.	Yield stress (0.2%), psi	Ultimate tensile stress, psi	Tensile elong., %
Spar	Flange	1	35,000	59,000 [a]	38 [a]
		2	28,400 [a]	59,600	50
	Weld, flange/pipe	1	35,900	64,600	7 [a]
		2	37,600 [a]	61,600 [a]	7
	Weld, pipe/pipe	1	54,700	79,700 [a]	16 [a]
		2	50,000 [a]	79,800	16
		3	53,900	81,000	16
Extension piece		---	80,000 [b]	107,000 [b]	

[a] Allowable value

[b] Estimated from hardness of RC 22 MATERIAL PROPERTY DATA

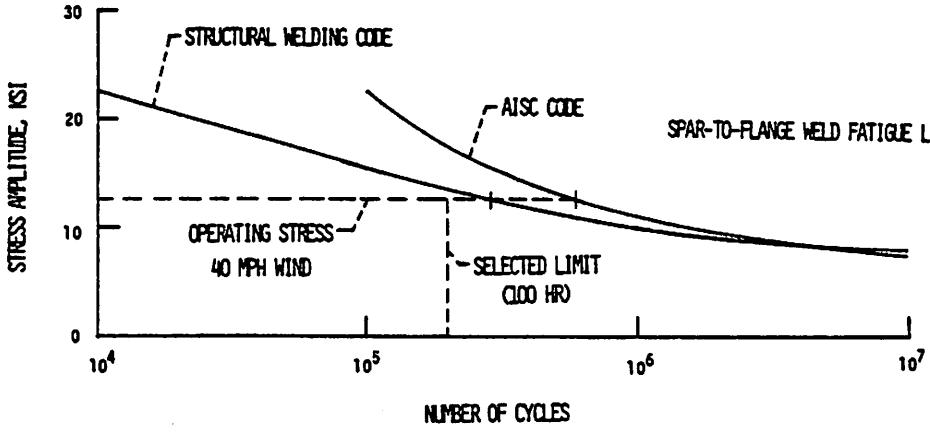

SPAR-TO-FLANGE WELD FATIGUE LIFE ANALYSIS.

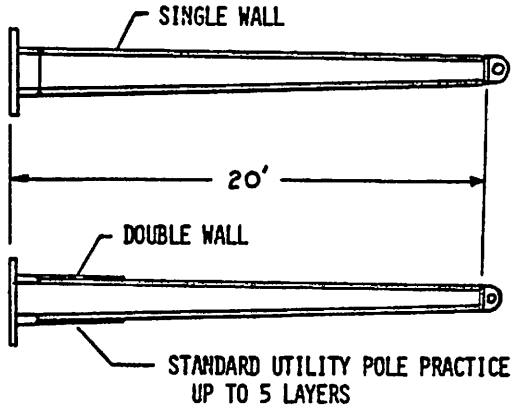

FULL SCALE FATIGUE TEST SPECIMENS OF UTILITY POLE SPAR AND ROOT END

FIBERGLASS BLADE CONCEPTS BEING DEVELOPED

- SIZE -- 60, 100, AND 150 FEET
- FILAMENT AND TAPE WOUND
- ROTATING MANDREL AND RING WINDER
- AFT PANELS
  - -- FIBERGLASS/HONEYCOMB PANELS/FOAM SUPPORTED
  - -- WOUND ON REMOVABLE AND FOAM AND MANDRELS
  - -- PREFORMED HONEYCOMB PANELS
  - -- ONE AND TWO CELLS
  - -- WITH AND WITHOUT SPAR TO T.E. JOINT
- ROOT END
  - -- BOLT ON
  - -- WOUND AND BOLTED
  - -- WOUND WITH MECHANICAL INTERLOCK
- CONTRACTORS
  - -- HAMILTON STANDARD, HERCULES, SCI, KAMAN

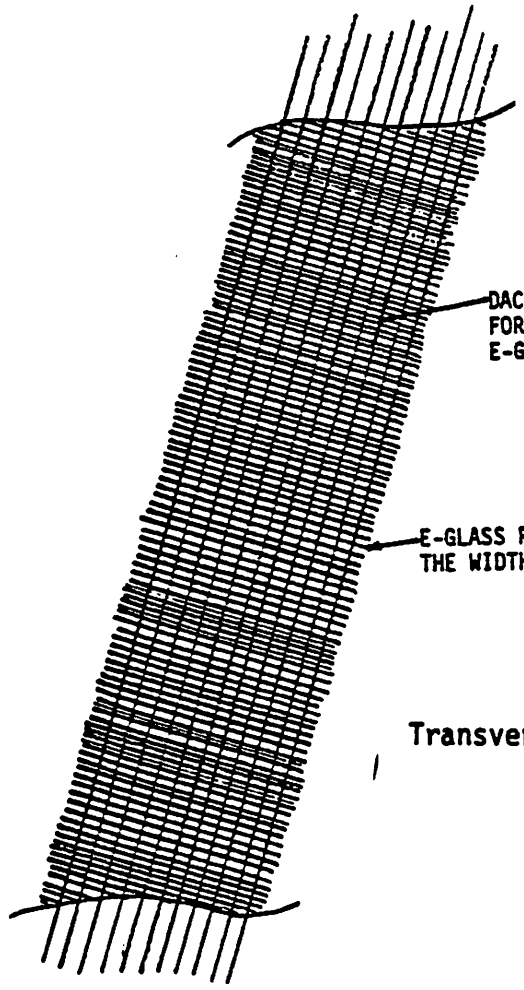

Transverse Filament Tape (TFT).

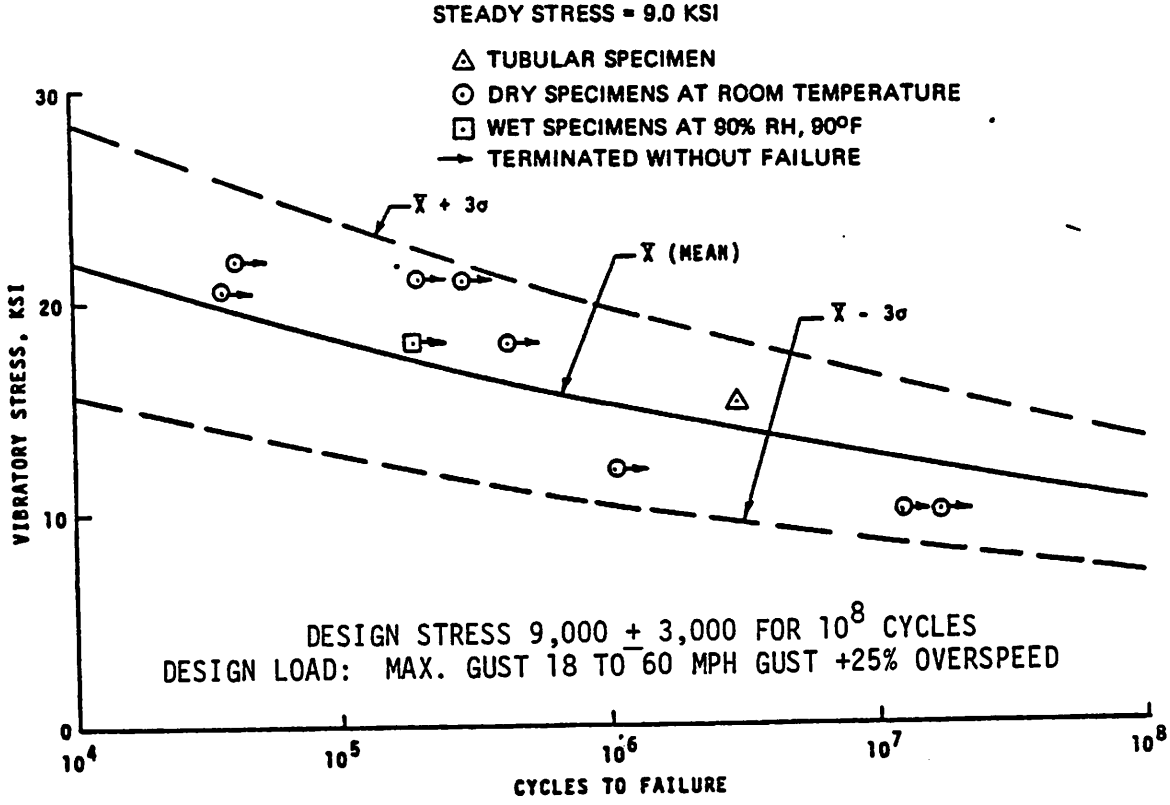

TFT Laminate Fatigue Characterization.

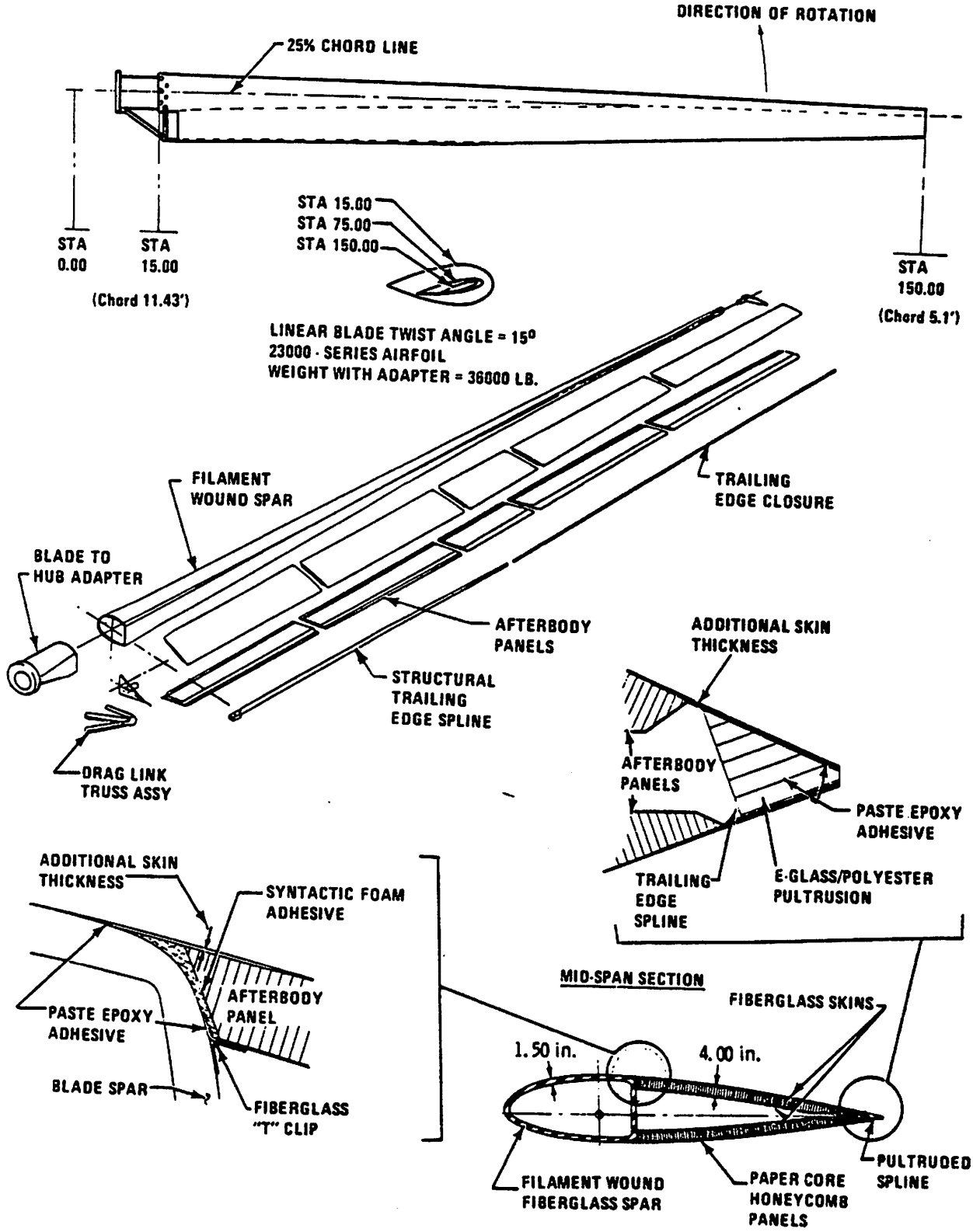

150 Foot Wind Turbine Blade Assembly Details.

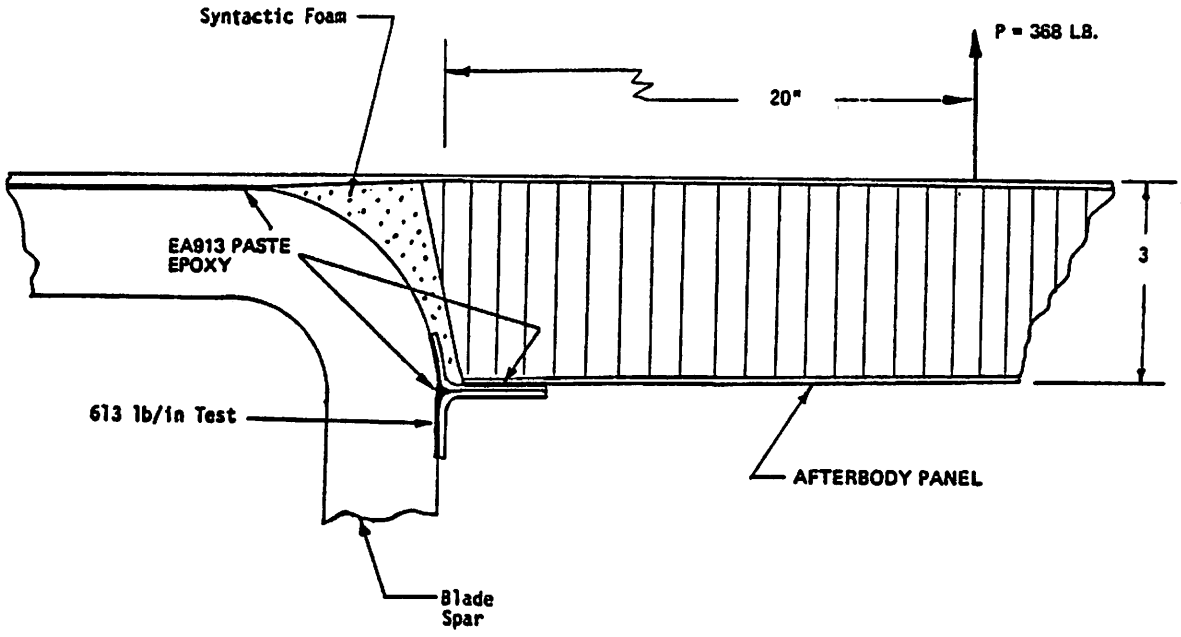

Sub-element Test of Afterbody Panel to Spar Attachment.

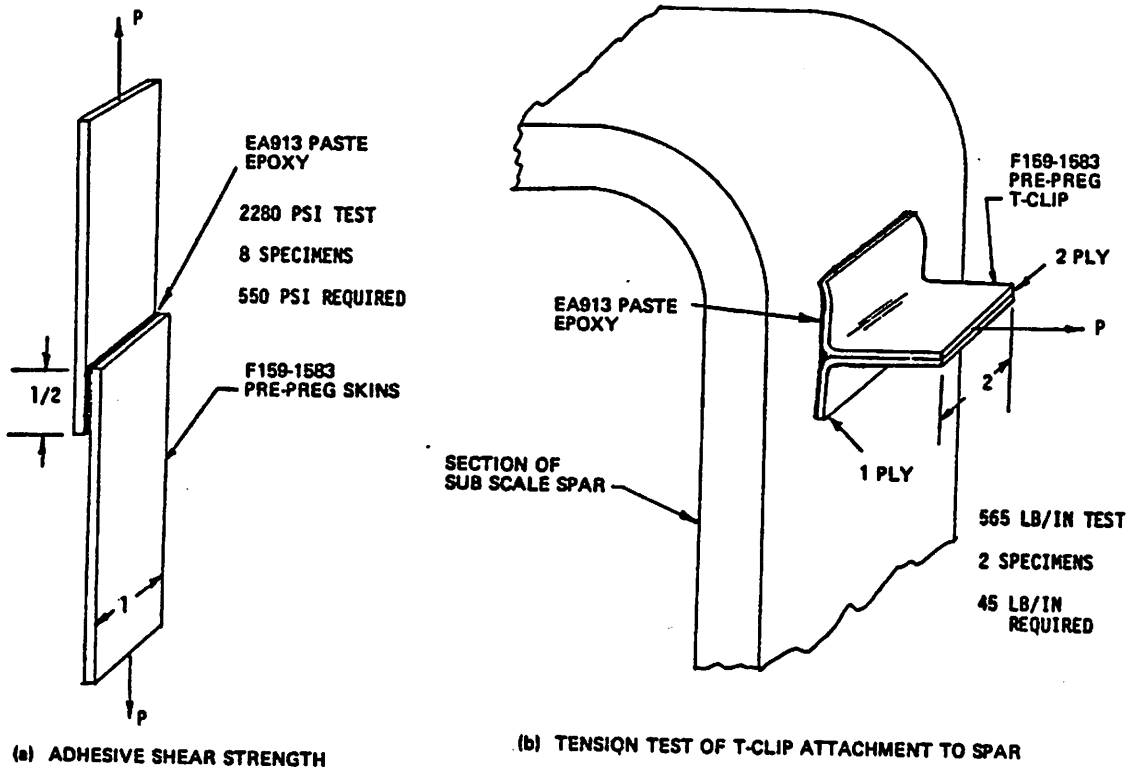

Sub-element Tests of Skin-to-skin Bond Lines and T-clip-to-spar Bond Lines.

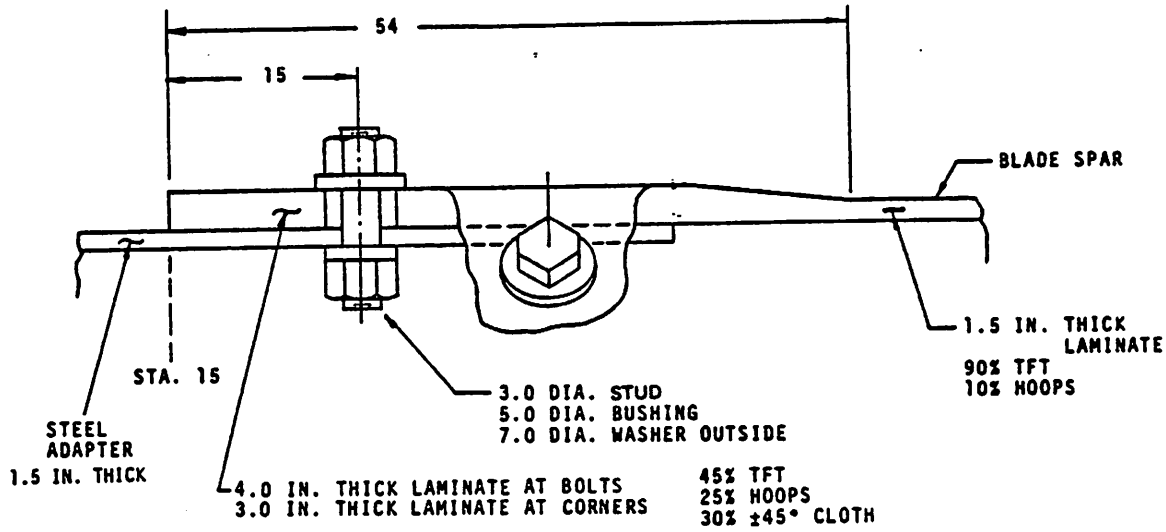

Blade Root End Adapter Attachment Detail.

DESIGN LOAD: MAX. GUST 18 TO 60 MPH GUST +25% OVERSPEED, 10^8 CYCLES
FATIGUE TESTS: 4 SPECIMENS, 10^7 CYCLES, AT MAX. GUST LOAD

TEST	NUMBER OF SPECIMENS	AVERAGE STRENGTH	REQUIRED STRENGTH
Afterbody skins, tensile strength	4	51,000 psi	10,000 psi
Skin to core bond tensile strength	2	175 psi	10 psi
Afterbody skins bond adhesive lap shear	8	2,280 psi	550 psi
T-clip to spar attachment (detail) tensile strength	2	565 lb/in.	45 lb/in.
T-clip to spar attachment (subassembly) tensile strength	1	613 lb/in.	45 lb/in.
Afterbody panel to spar attachment shear strength of syntactic foam	2	117 psi (core failure)	32 psi

ALLOWABLES FOR AFTERBODY STRUCTURES
150 FOOT FIBERGLASS BLADE

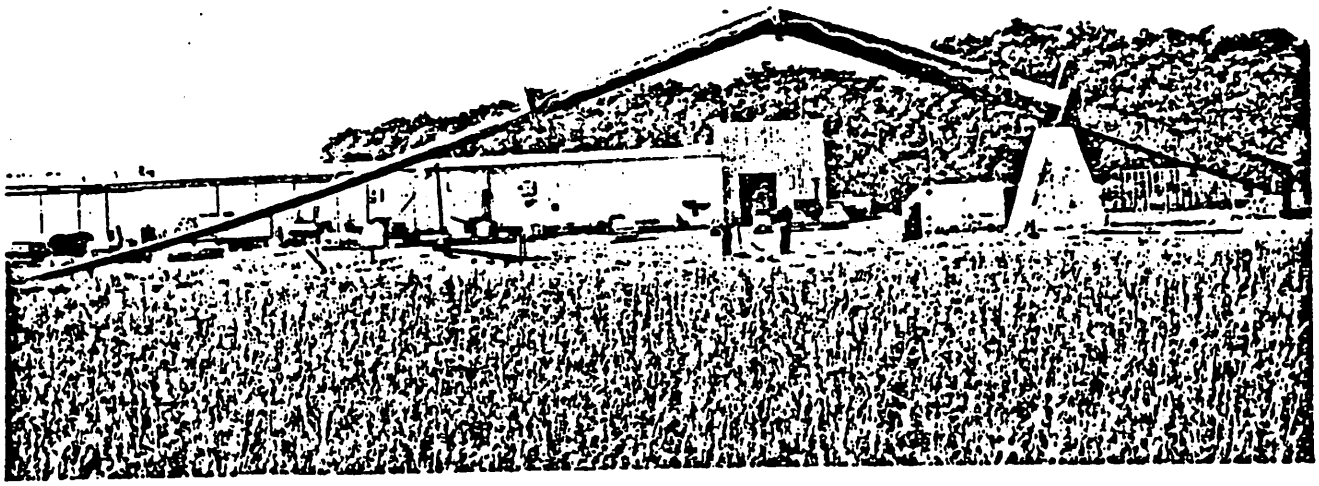

BUCKLED AT 9% ABOVE DESIGN LIMIT LOAD
DESIGN LIMIT = HURRICANE WIND LOAD

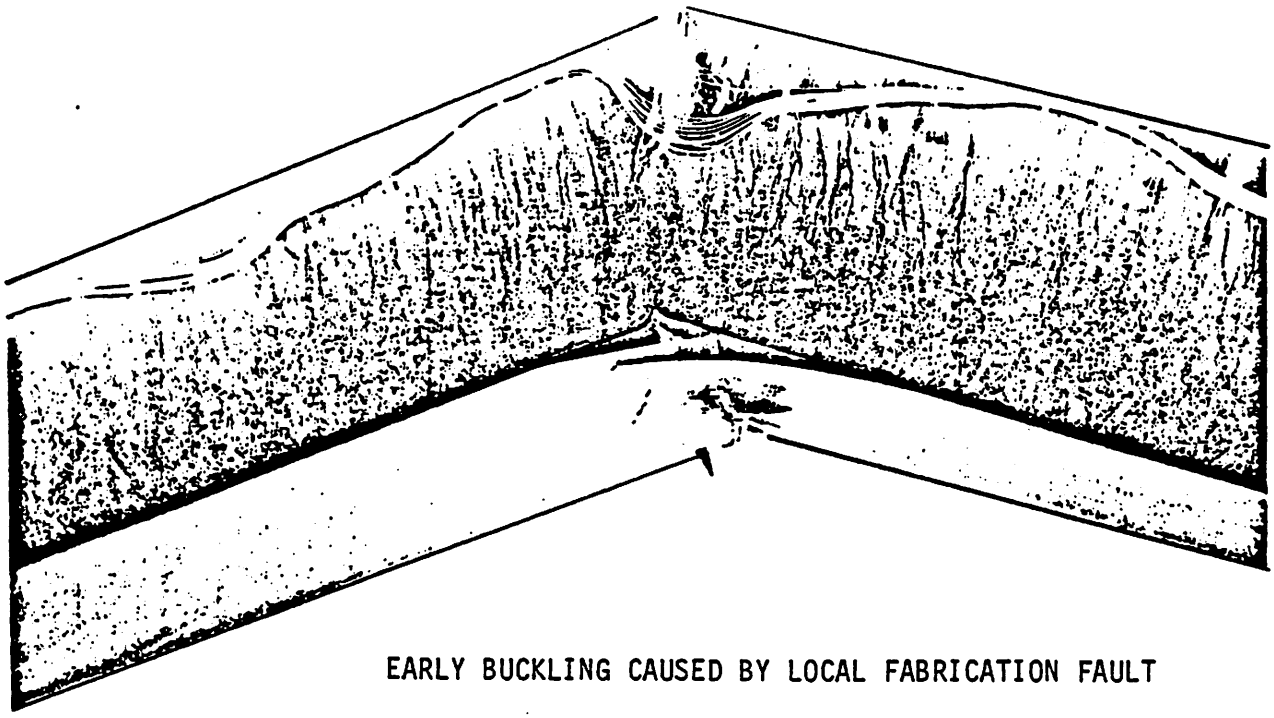

EARLY BUCKLING CAUSED BY LOCAL FABRICATION FAULT

150 FOOT FIBERGLASS BLADE BUCKLING TEST

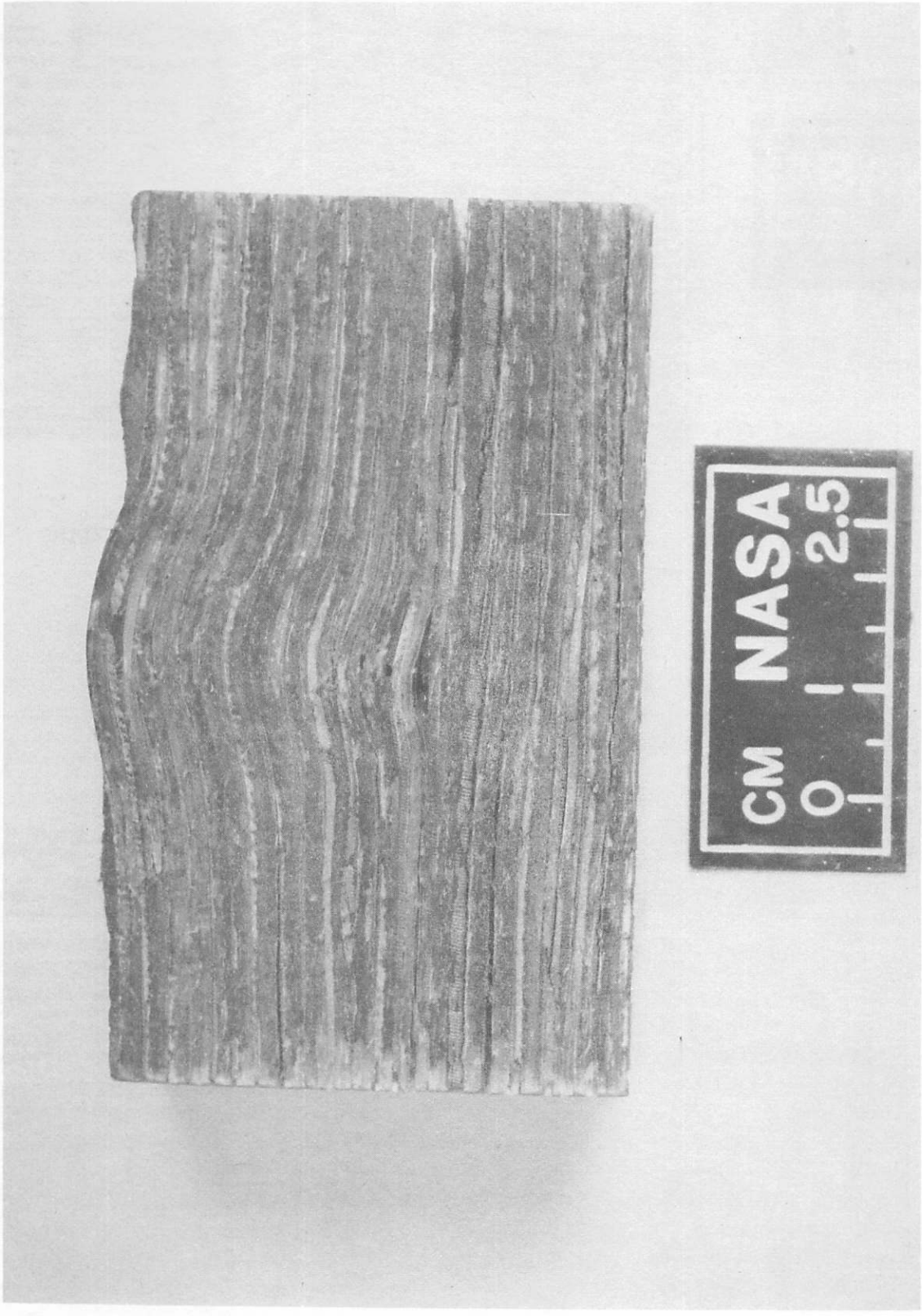

FABRICATION FAULT IN 150 FT FIBERGLASS BLADE

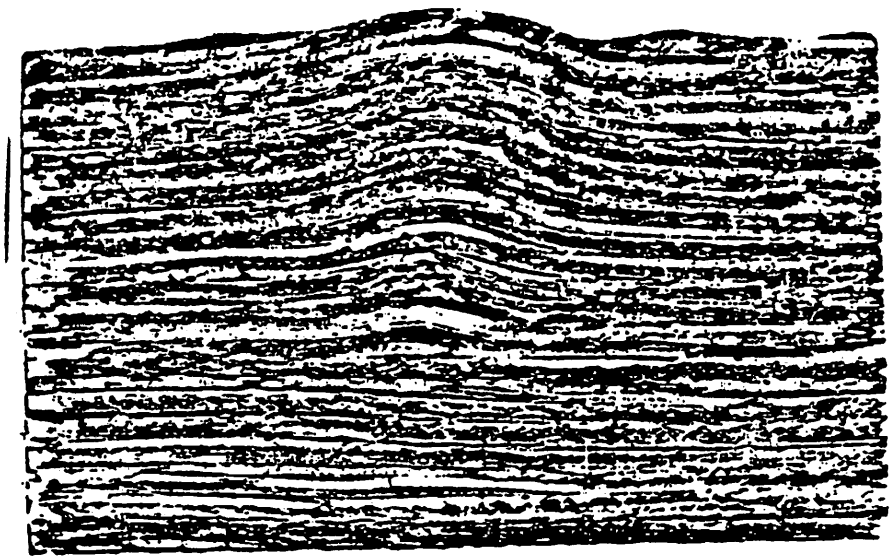

FABRICATION FAULT THAT CAUSED EARLY BUCKLING

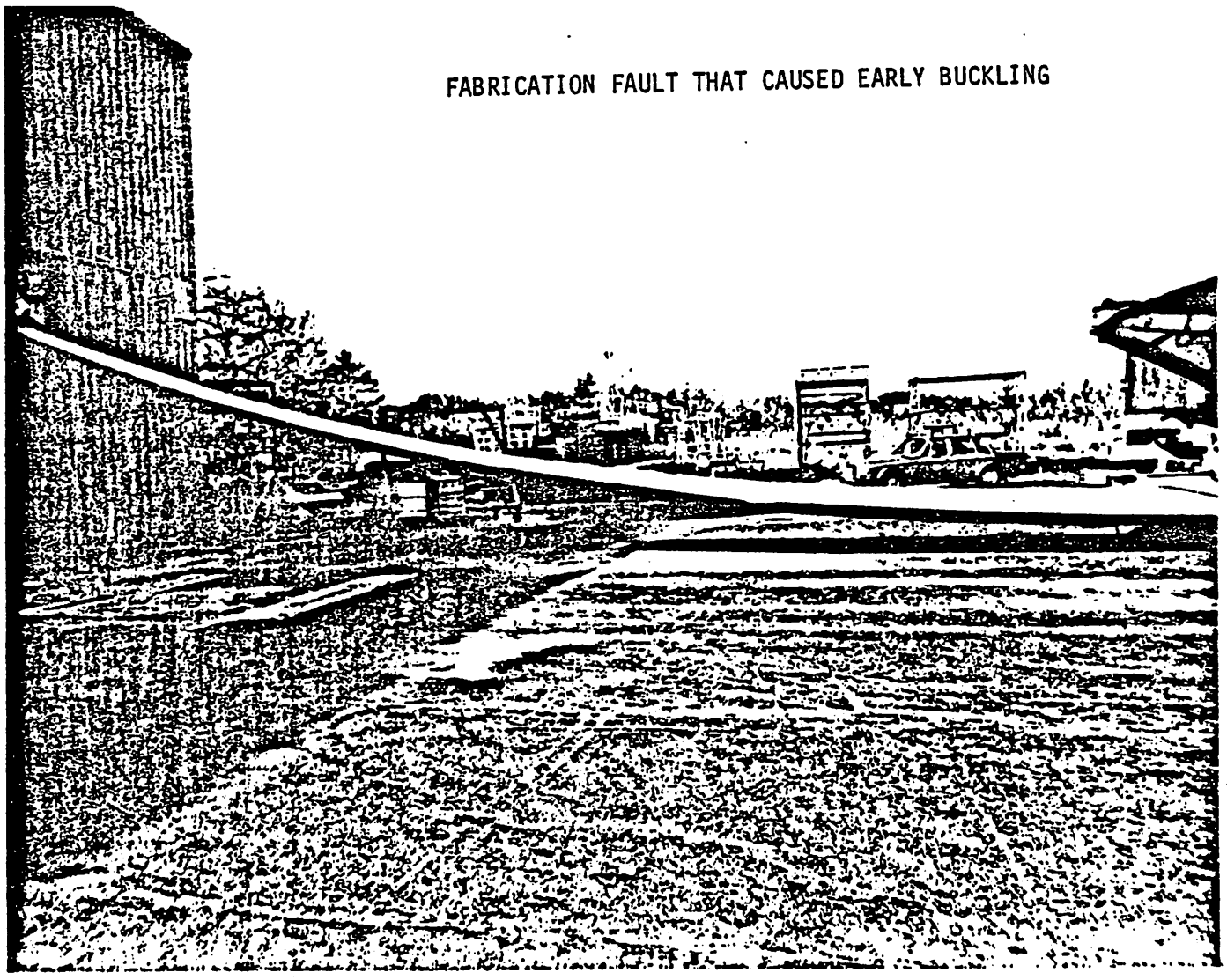

OUTBOARD 100 FEET DID NOT CONTAIN FAULTS TESTS TO 1.5 TO 2.8 TIMES DESIGN LIMIT LOAD WITHOUT FAILURE

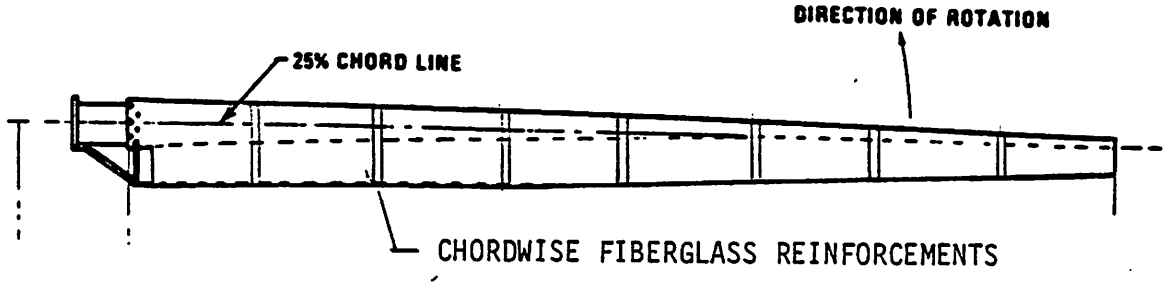

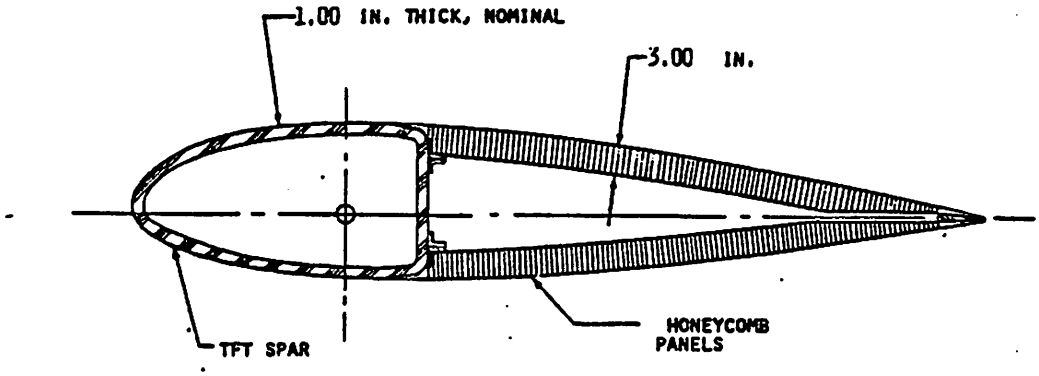

TYPICAL BLADE SECTION

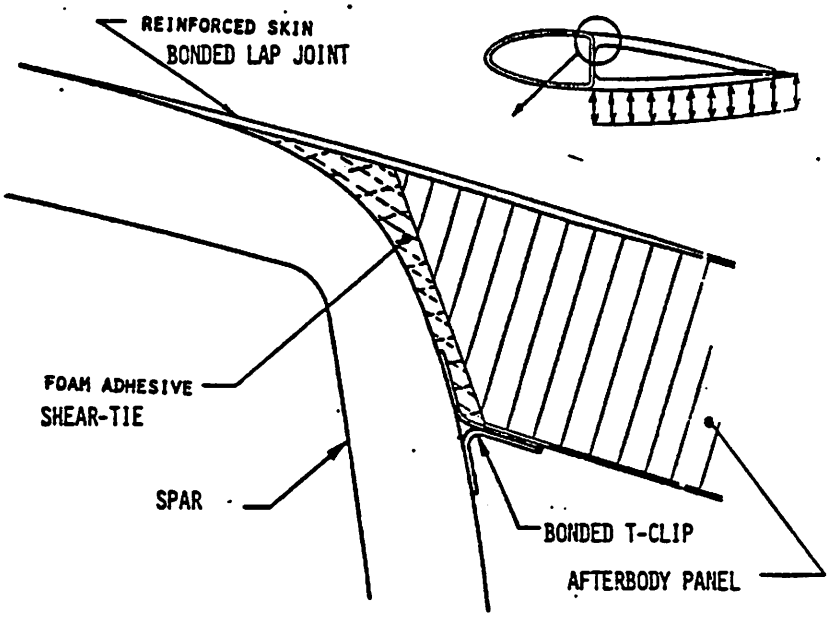

SPAR-TO-AFTERBODY SPLICE - FULL SCALE FATIGUE SPECIMEN

10^6 CYCLES AT OVERLOAD CONDITION

SPAR/AFTERBODY FATIGUE TEST

100 FT. FIBERGLASS BLADE

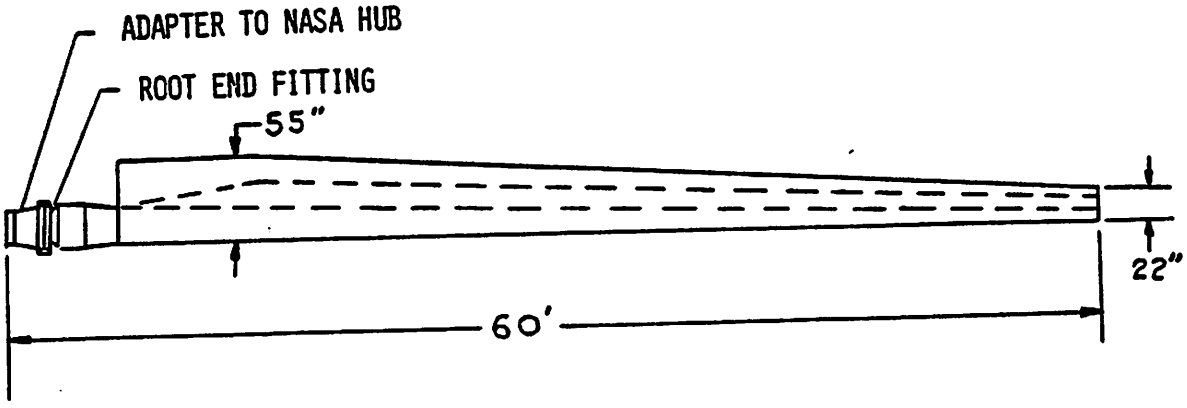

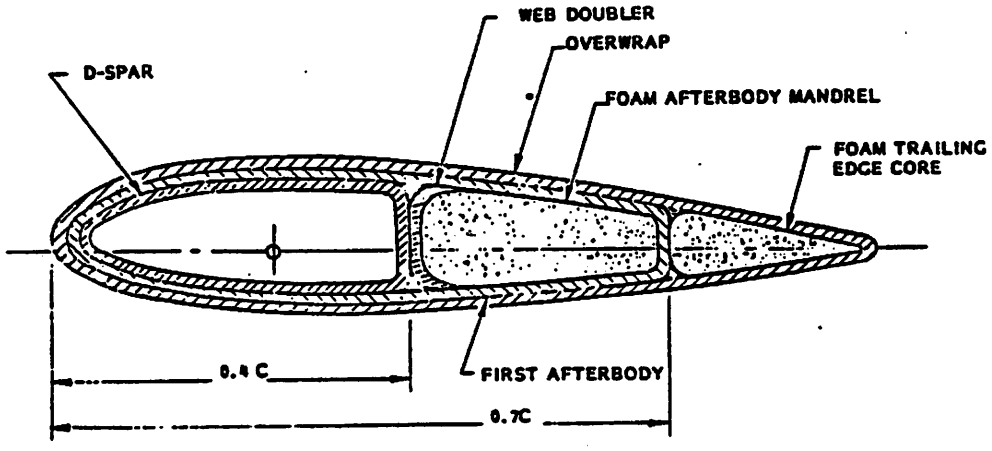

TYPICAL CROSS-SECTION

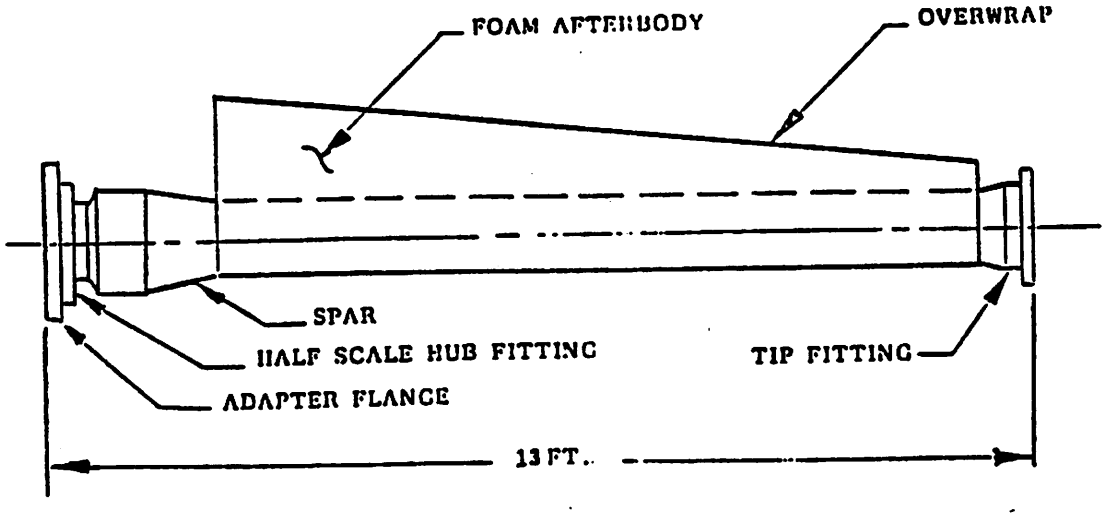

HALF-SCALE HUB JOINT FATIGUE TEST SPECIMEN

60 FOOT COMPOSITE BLADE

GOUGEON - WOOD BLADE DESIGN

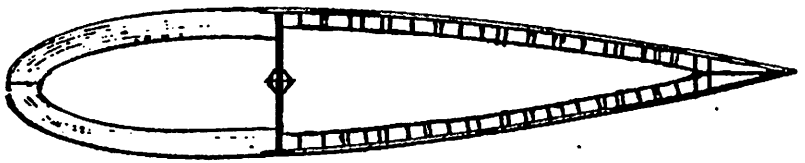

Blade Cross Section

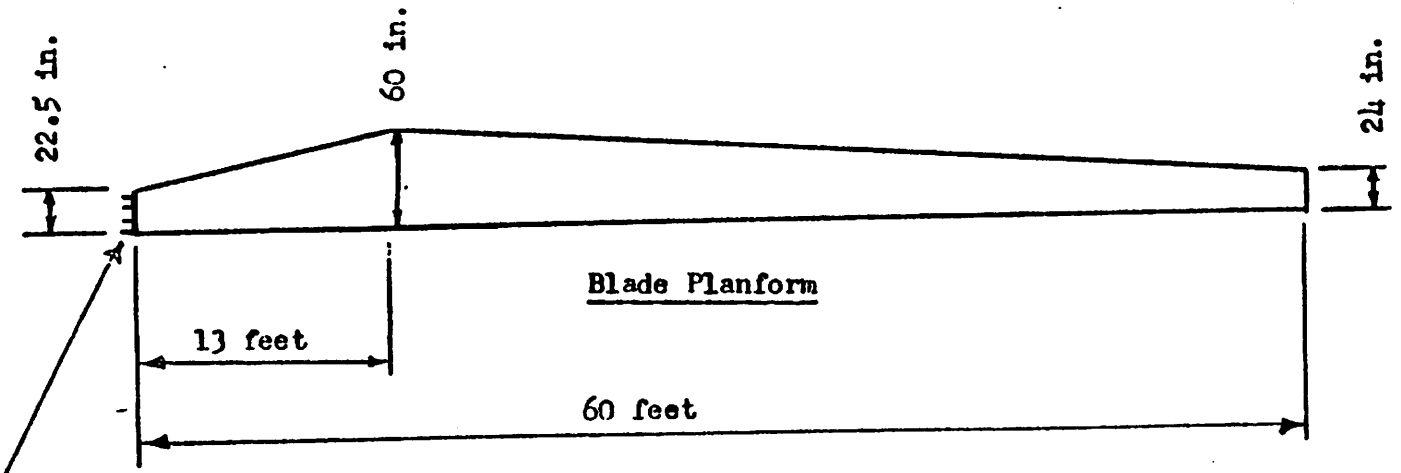

Blade Planform

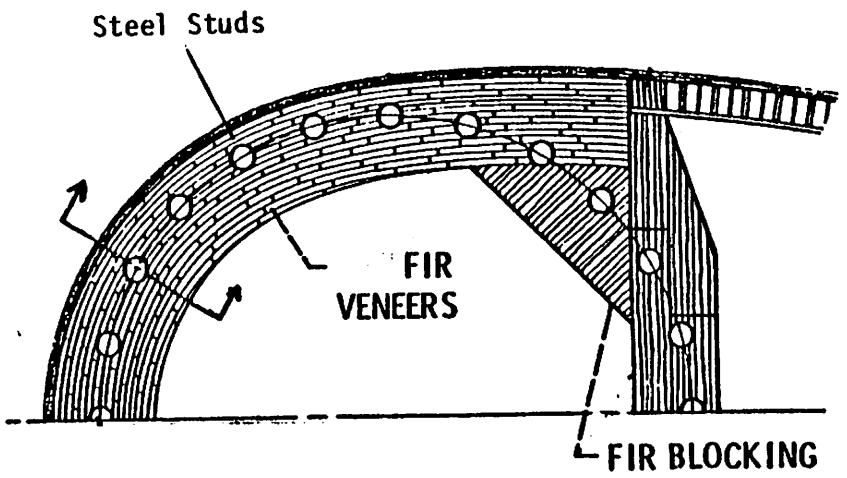

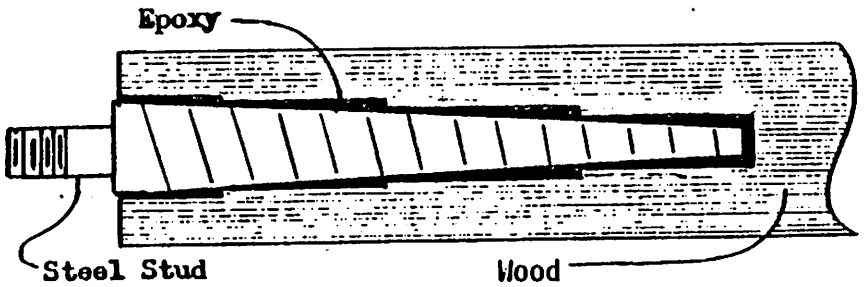

Blade-to-Hub Attachment Method

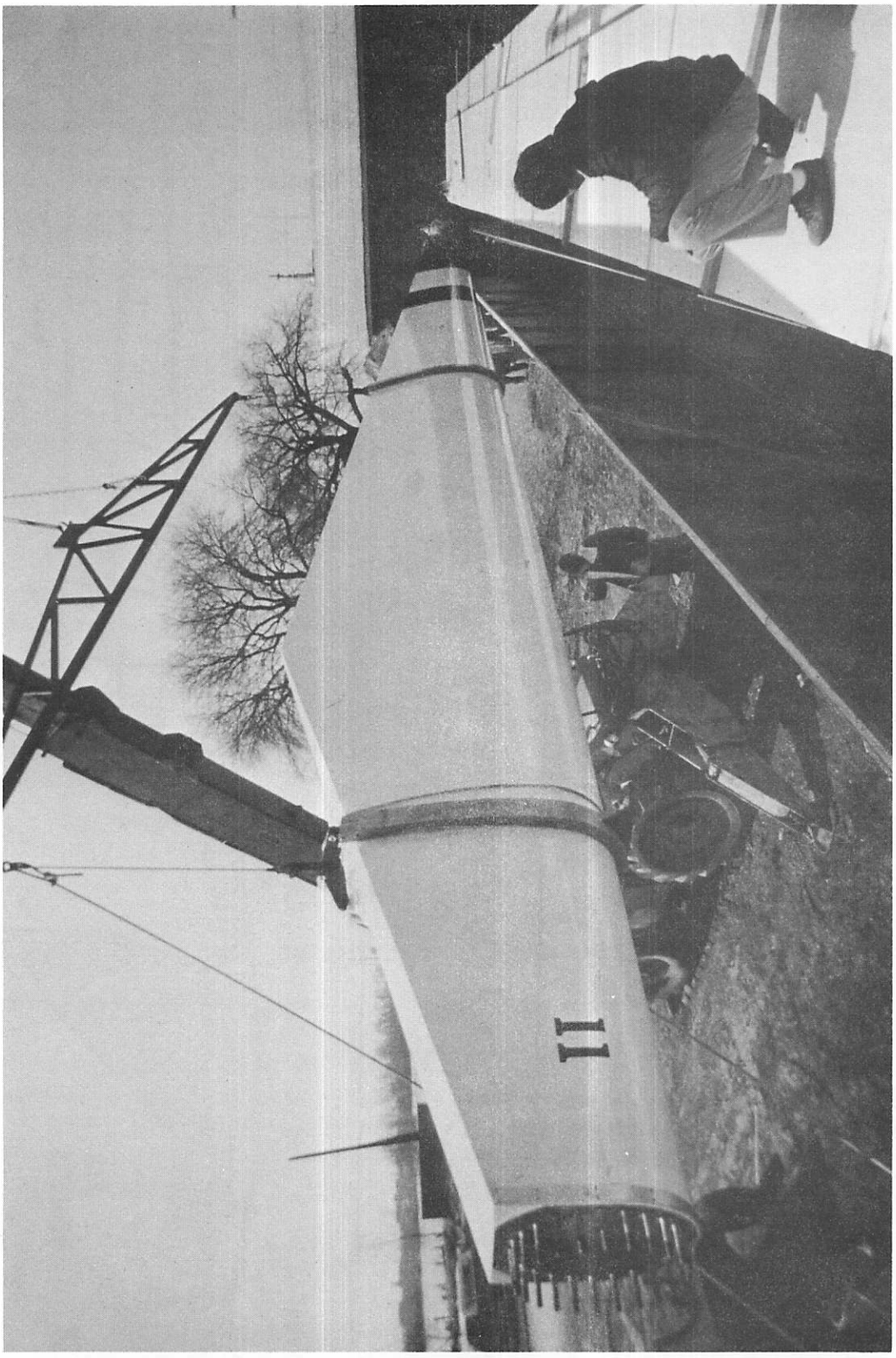

60 FOOT WOOD BLADE FABRICATED BY GOUGEON BROS., INC.

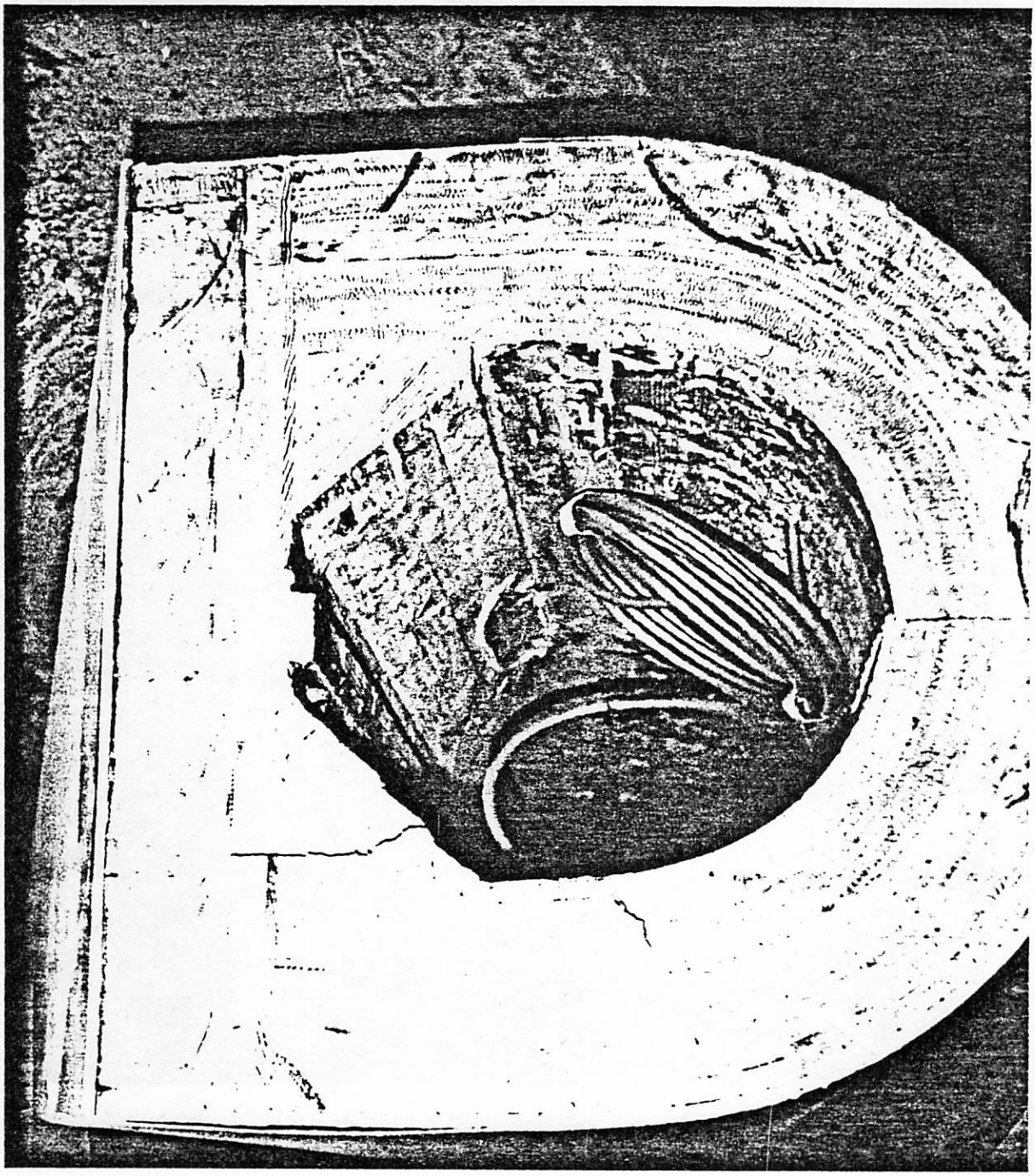

ROOT END OF 60 FOOT WOOD BLADE AFTER ROUGH TRIM CUT.

"D" THICKNESS 4.75 INCHES

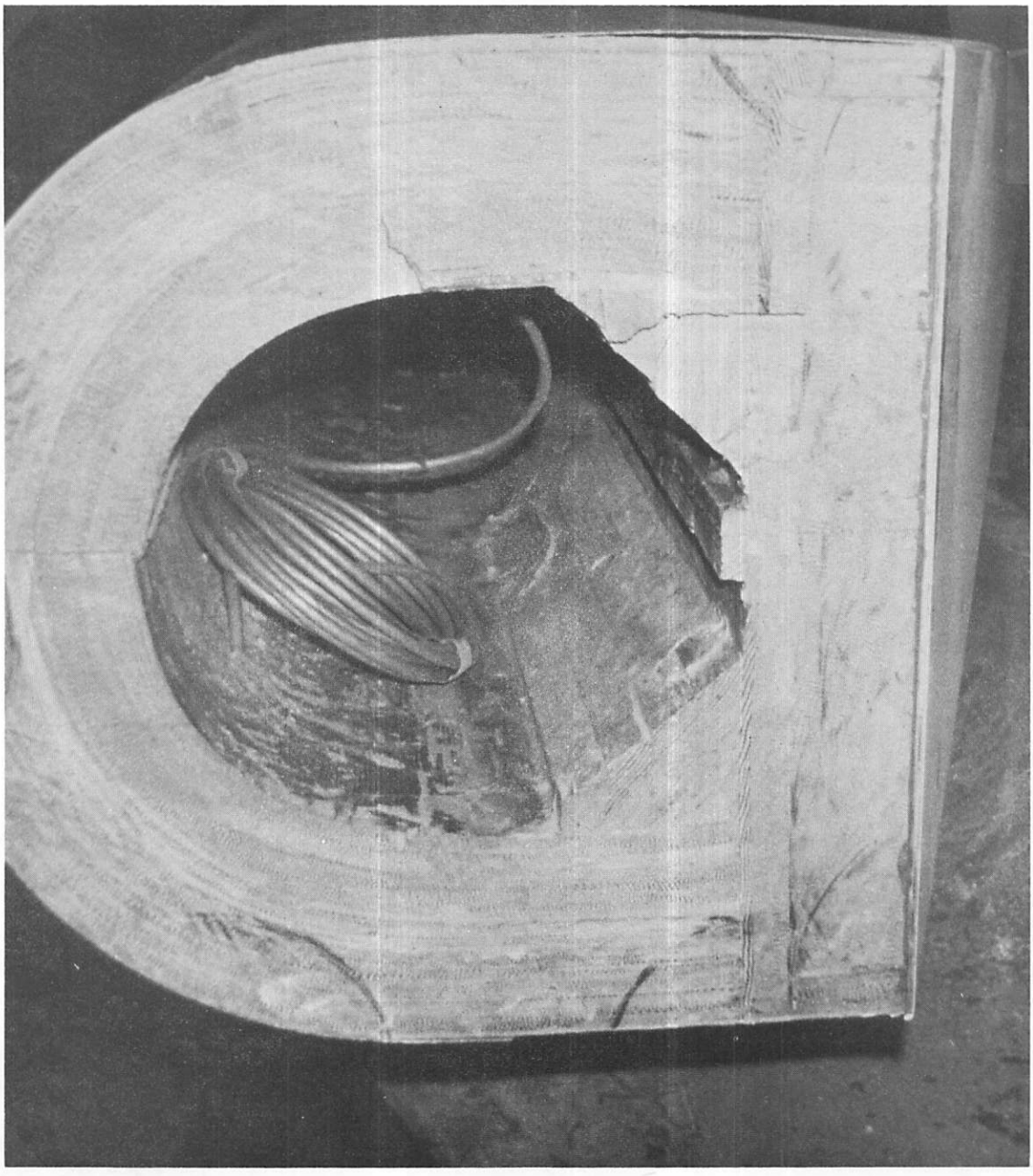

ROOT END OF 60 FOOT WOOD BLADE AFTER ROUGH TRIM CUT.
"D" THICKNESS 4.75 INCHES

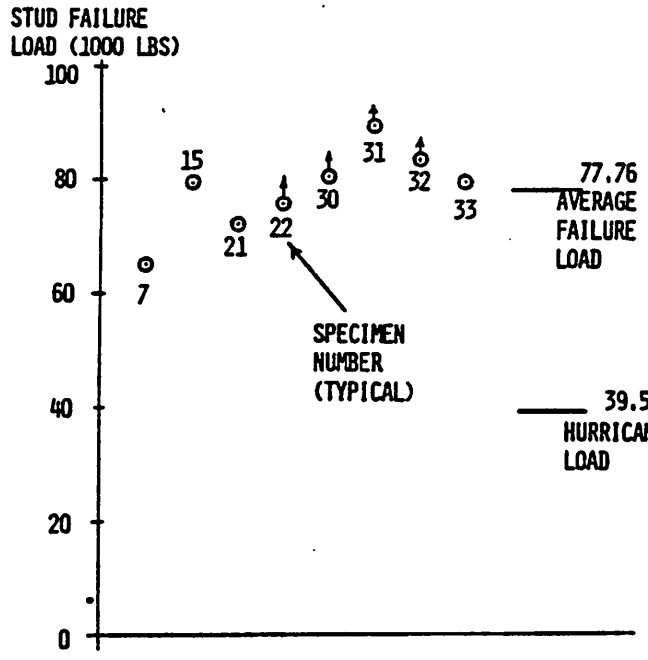

60 FOOT WOOD BLADE - MAXIMUM STUD LOADING CAPABILITY

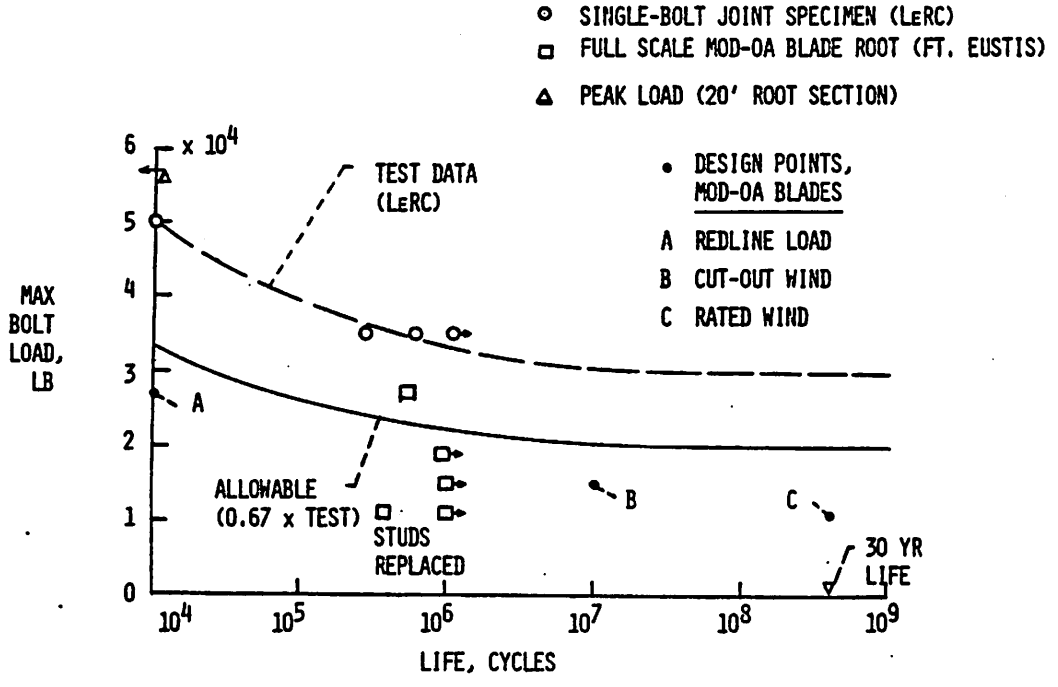

FATIGUE DATA FOR BOLT-TO-WOOD TENSION JOINTS
FABRICATED BY GOUGEON BROS., INC.

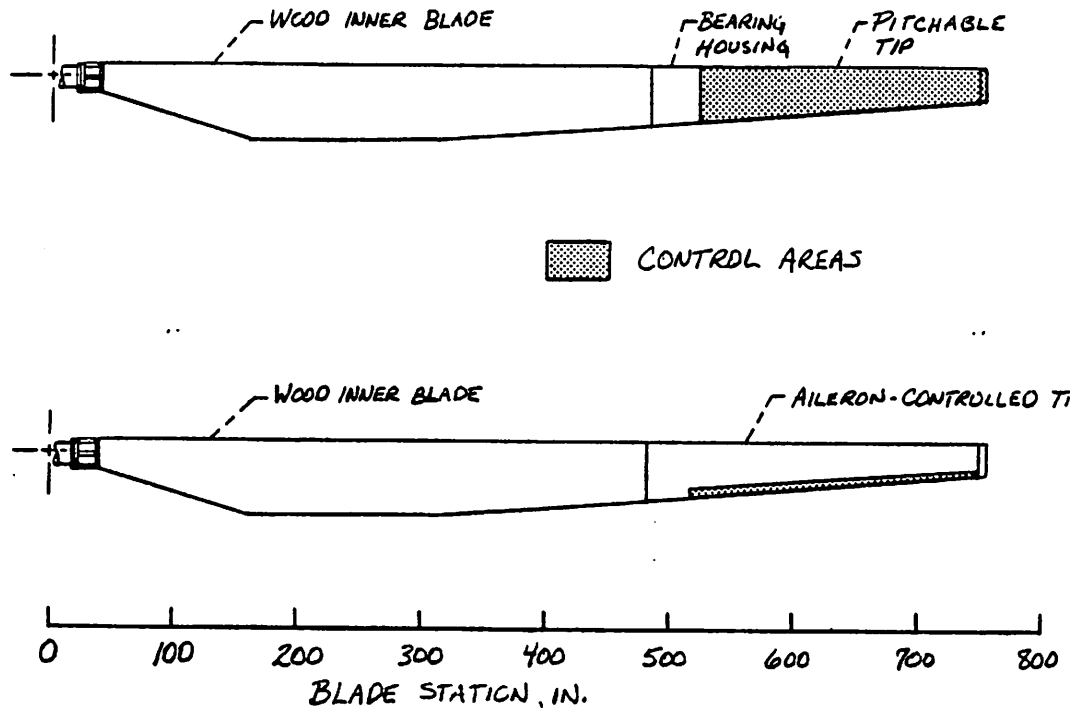

COMPARISON OF TIP-CONTROLLED AND AILERON-CONTROLLED BLADE PLANFORMS

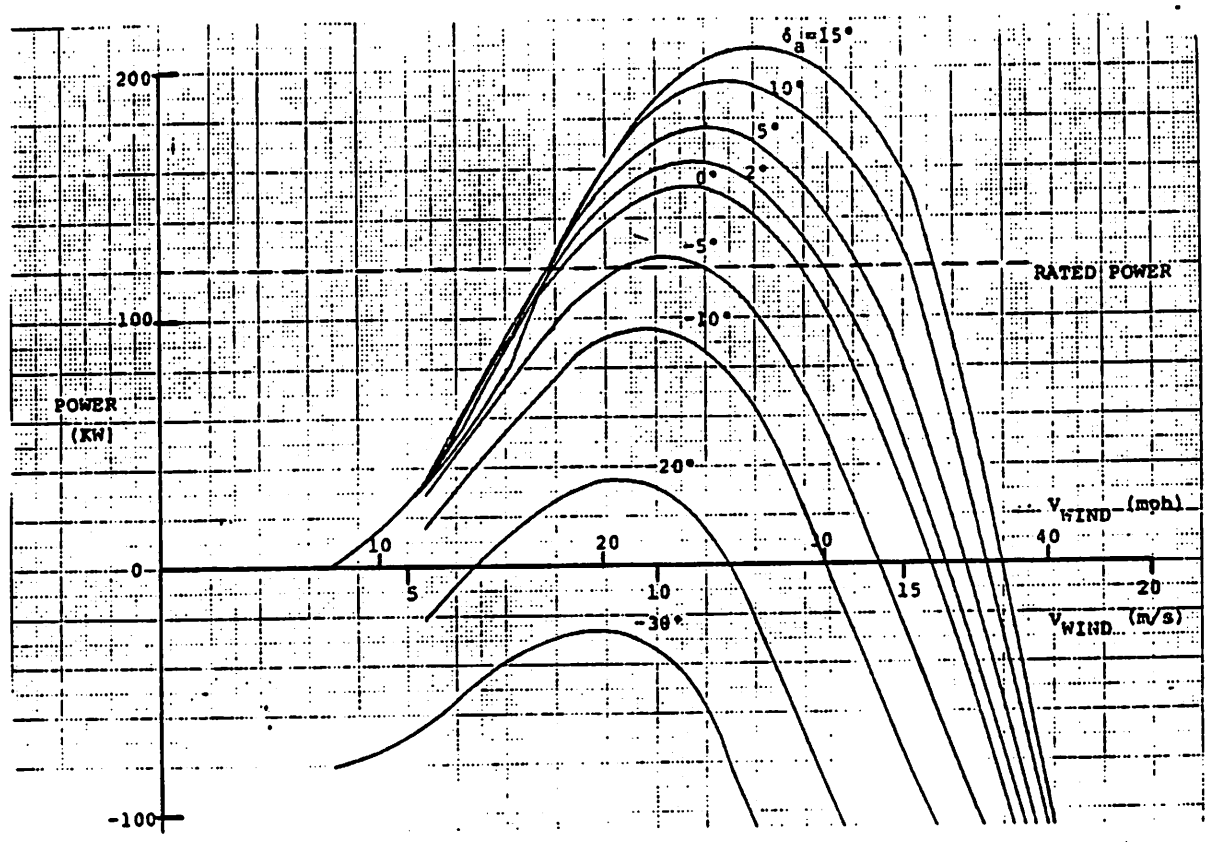

ROTOR POWER VS WIND SPEED FOR VARIOUS AILERON DEFLECTION ANGLES AT 33 RPM

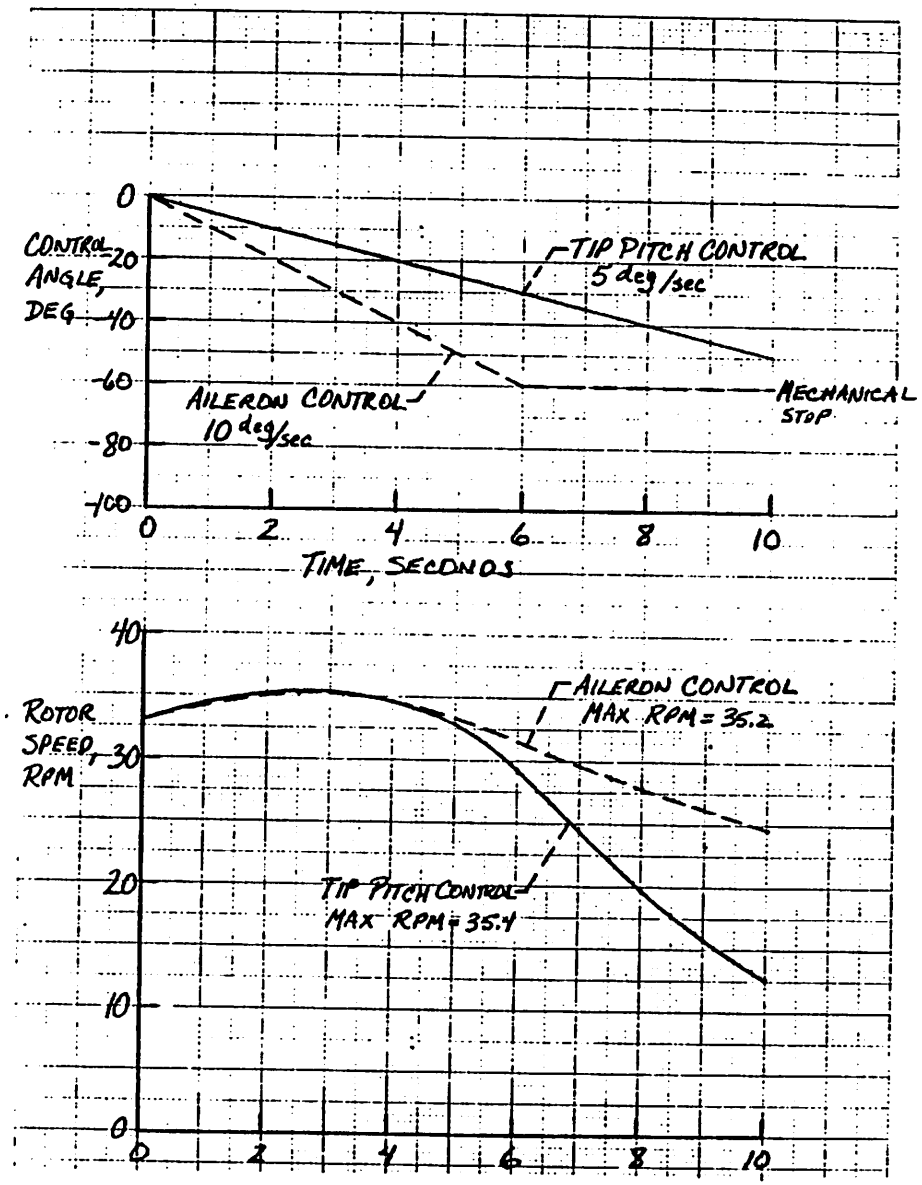

COMPARISON OF OVERSPEED CONTROL WITH AILERON AND TIP PITCH CONTROL

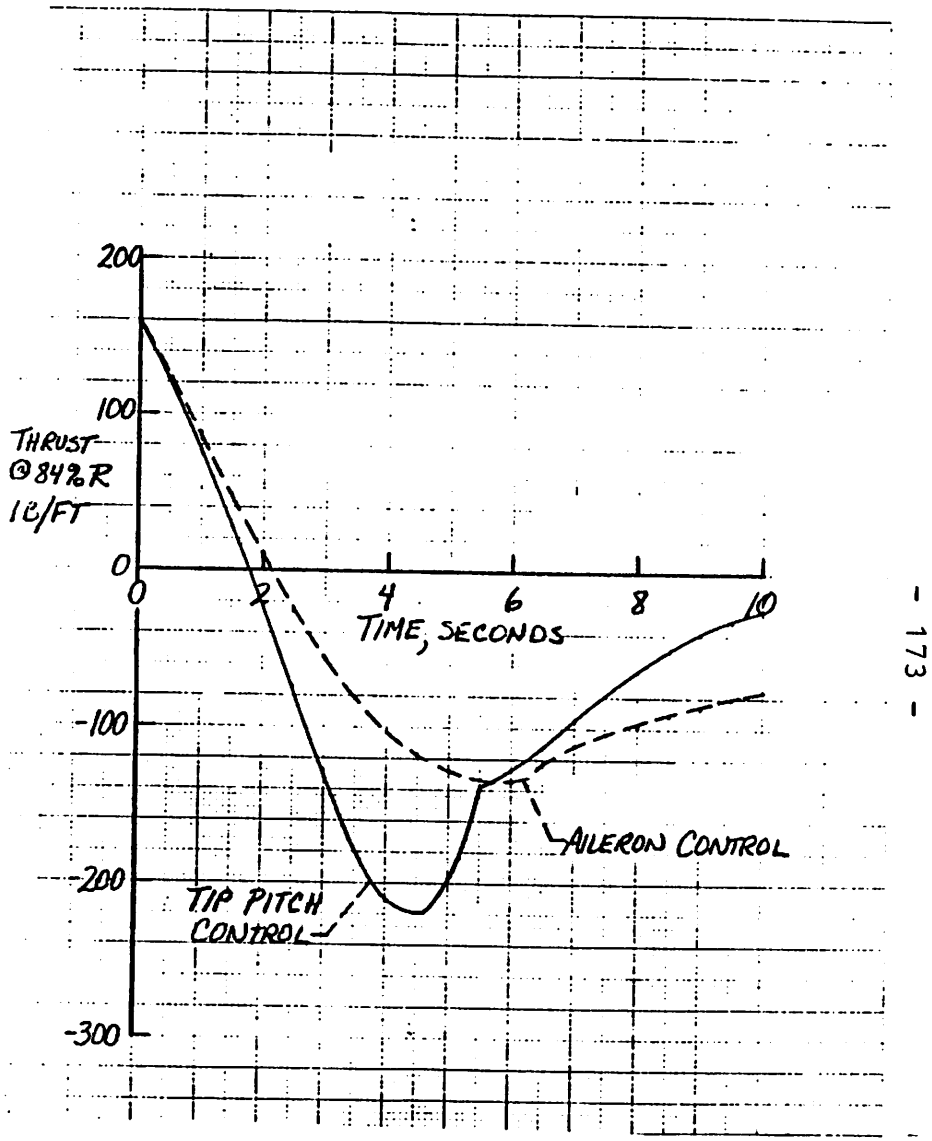

COMPARISON OF THRUST LOADING DURING OVERSPEED WITH AILERON AND TIP PITCH CONTROL

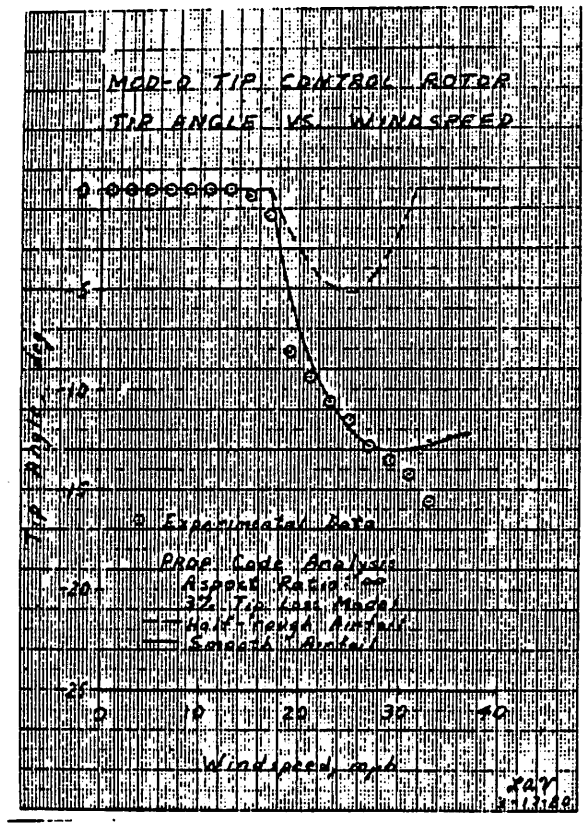

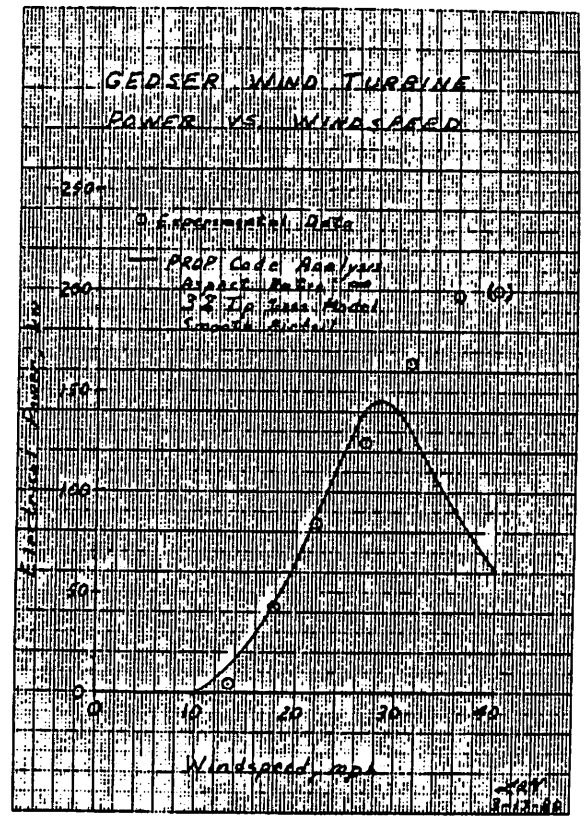

INFINITE LENGTH BLADE ANALYSIS AND EXPERIMENTAL RESULTS

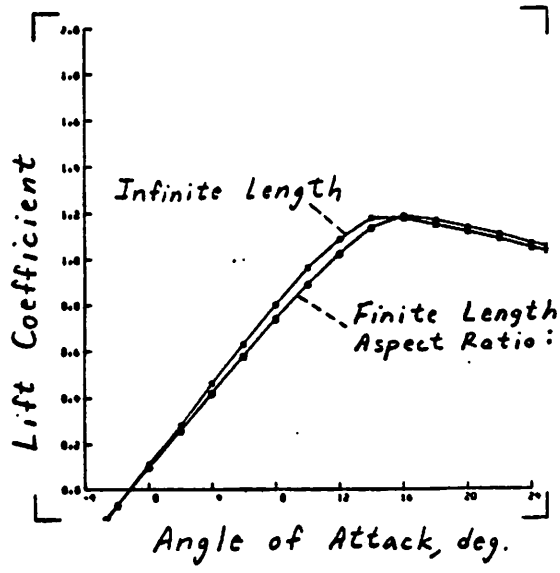

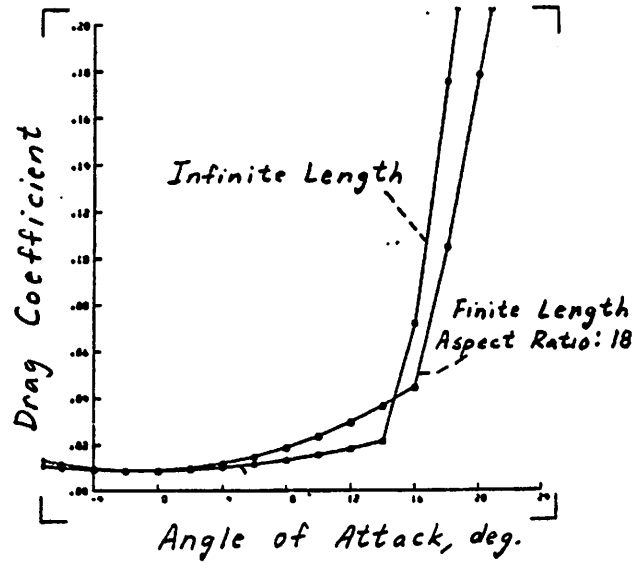

23024 AIRFOIL CHARACTERISTICS (MOD-0) FOR INFINITE AND FINITE LENGTH BLADES

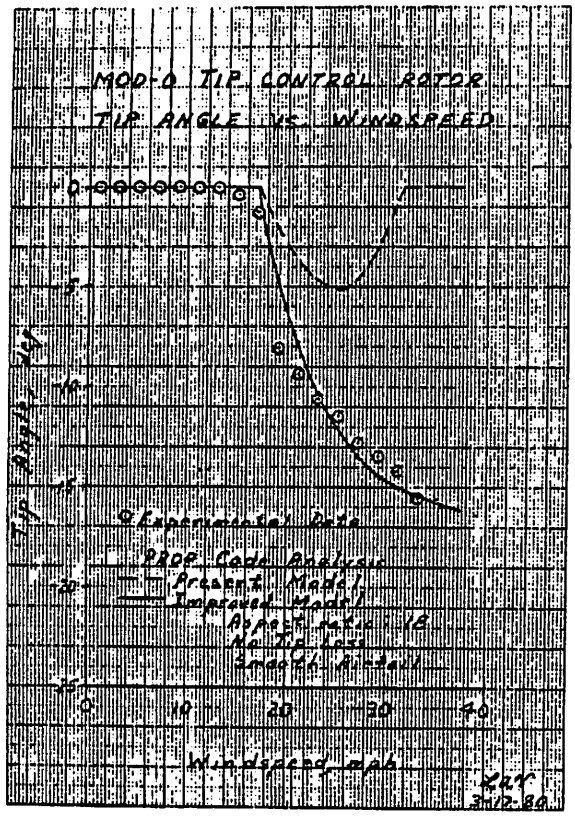

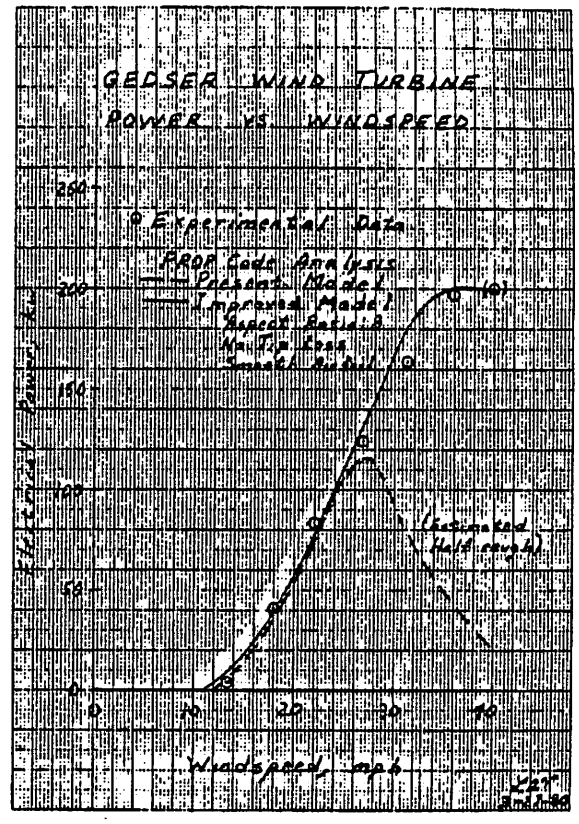

FINITE LENGTH BLADE ANALYSIS AND EXPERIMENTAL RESULTS

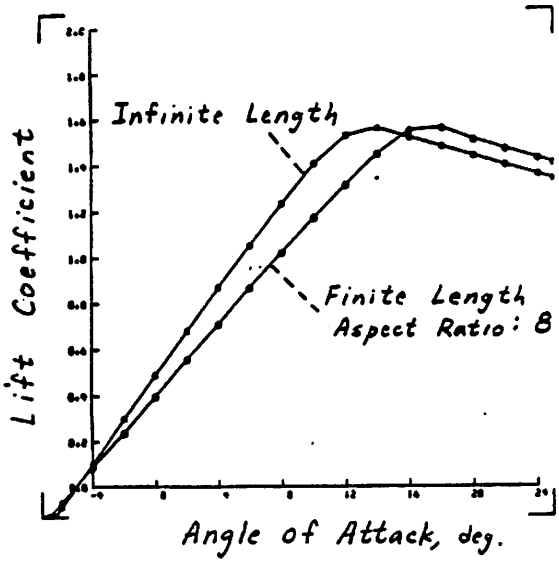

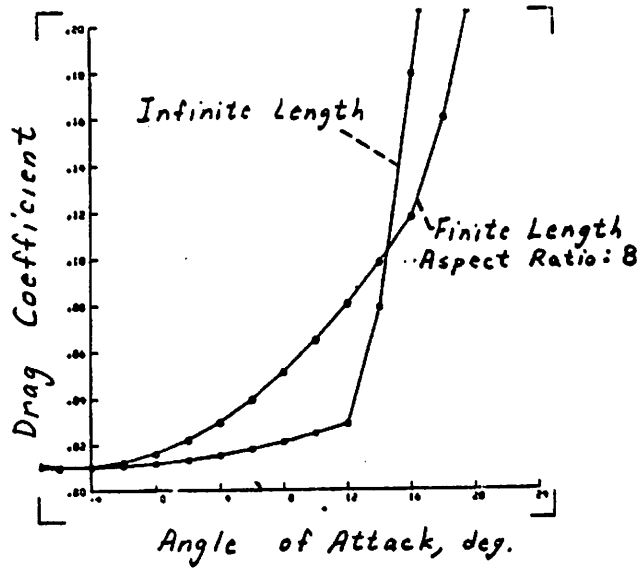

CLARK-Y AIRFOIL CHARACTERISTICS (GEDSER) FOR INFINITE AND FINITE LENGTH BLADES

SOME DESIGN ASPECTS OF THE KMW/ERNO/VFW WIND TURBINE ROTOR BLADE

by

K. Wieland
A. Nowag

Presented at an IEA-Expert Meeting at Stockholm on the 21th April 1980.

Abstract: The report describes roughly the KMW/ERNO WTS-system and its design philosophy.

The requirement for 30 years life time demands very carefull design work and material selection in order to achieve a fatigue safe design especially if a welded steel construction is chosen. Load assumptions and load cycles are discussed. Dimensioning load cases are described and related to the total potential of material cyclic life.

1. Introduction

In 1979 the cooperating companies KMW (Sweden) and ERNO/VFW (Germany) received a Swedish government contract to develop and built a horizontal axis wind energy converter in the 2 - 3 MW class. KMW acting as the program leading firm is responsible for tower, machinery (Gear, Generator) and hub, and ERNO/VFW is responsible for the rotor blades as well as for the entire system dynamics. Fig. 1 gives an impression of the entire system. Some design data is presented in table I.

The WTS consists of a two blade turbine of 75 m diameter which is mounted to a concrete tower of 85 m height. 2 MW rated electrical power shall be achieved at 12,5 m/s wind speed.

2. Design philosophy of the rotor blades

During the tender phase for this project in 1978 investigations have been performed to develop the design philosophy for the entire system and specially for the blades.

Alternatively to other known designs the rotor shall run upwinds to avoid negative effects from the tower shadow. The blades therefore had to be designed stiff. Fig. 2 shows the result of an evaluation of the blade deflection using different blade materials. The glass reinforced plastic blade shows a deflection at the tip of about 6 m which was unacceptable for upwind rotor operation due to foreseen blade/tower interference.

Fig. 3 summarises the arguments which had to be belanced.

The resulting configuration is described in fig. 1 and table I.

- o Two blade rotor running upwinds
- o Rotor and Hub rigid design
- o Stiff steel reinforced concrete tower

For the construction of the blades different materials have been considered for selection:

1. Fibres: Glass
   Aramid
   Carbon

2. Light Metal: Aluminum
   Titan

3. Steel : different alloys

The table II gives a survey of the material properties.

Selection criteria were:

- o specific tensile strength
- o specific E-modul (stiffness)
- o endurance (fatigue resistance)
- o material cost
- o manufacturing cost
- o development cost and risk.

Fibres

Fibre materials clearly show the highest specific tensile strength, whereas with regard to the specific stiffness, the carbon/aramid combination or the pure carbon fibre only can compete with steel.

Disadvantages for fibres are resulting from cost, namely

- o high material cost (specially for carbon)
- o high manufacturing cost with great quality assurance effort
- o high development cost in order to provide a statistic basis for material values with respect to the long life behavior for a period of at least 30 years.

  Experts cannot give any endurance guarantees for load cycle numbers higher than 10^7. (A WTS should survive more than 10^8 load cycles).

Aluminum

Two qualities of aluminum have been considered:

Alloy 7075T7351,	high tensile strength, non weldable
Alloy AlMg5,	weldable

For reasons of statical and fatigue loads the weldable Al-alloy AlMg5 will reach the same weight as a box beam out of steel. As plate thicknesses of 30 mm must be used for the box, the welding would be very expensive and reducing the reliability extremely.

The disadvantages therefore are:

- o Problems in production (forming and welding)
- o Difficulties in delivery of plates of the required thickness
- o Material costs.

A rotor blade made of the high tensile strength alloy would offer advantages as the blade weight might be reduced by appr. 30 %. But this would also correlate to:

- o Reduction of stiffness by 30 %
- o Remarkable increase in costs for production and material (totaly riveted construction)
- o Difficulties in delivery of the material

Titanium

The titanium alloy requires very high material and manufacturing cost and has therefore been removed from further discussion.

Steel

The steel materials show the highest specific stiffness. Further advantages are:

- o Material price
- o Manufacturing cost (conventional welding methods in accordance with specified working processes)
- o Availability of statistically secured material characteristics
- o Low development risk.

Merely the low specific tensile strength is to be regarded as a disadvantage.

Result of material investigation

Since high stiffness requirements were imposed on the rotor blades aiming on a very rigid rotor, a steel construction only was suitable for the load carrying box beam. Economic considerations lead in this case to the same conclusion. For the secondary structure (leading and trailing edge) the least expensive fiber offered itself - the glass fiber. The low stiffness is of no importance in this case. However, the higher material costs are compensated by the lower costs for manufacture of these strongly molded parts.

3. Blade design

Following the material selection for the load carrying structure of the blade the construction principle was developed. See fig. 4 .

The structure of the blade is devided into a torsion box (primary structure) made from steel and into leading and trailing edge parts (secondary structure) made from GRP which form the aerodynamic shape of the profile. The surface of the steel torsion box itself is part of the aerodynamic surface of the blade.

The torsion box is a combined welded/riveted steel structure which is stiffened by ribs.

Carefull corrosion protection shall be applied because of the very negative influence of corrosion to the fatigue problem. The inside of the torsion box is therefore ventilated by the centrifugal forces when the rotor is running.

4. Design aspects for high endurance qualities of the rotor blade

The Swedish Board for Energy Research has defined a number of load cases in the technical specification for the project, which are based on experience of theoretical data, meteorological measured data and experimental data.

These load cases combined with the requirement for 30 years life time of the system generate an engineering problem which centers around the fatigue aspects of material and design elements.

Fig. 5 gives a summary of the most important load cases. The diagram shows the number of load cycles to be taken into account as well as the stress levels between the various cycles have to be calculated.

It should be pointed out that the WTS control system will influence the load levels for cases 1 and 5 in fig. 5 . Except for an emergency braking the system shall be brought to stop in a soft manner to avoid high negativ stress level peaks for case 5 . This can easily be achieved by the respective computer software of the control system.

During the start procedure the blade has to be pitched from the feathered position ($\approx 90^{o}$) to the operating pitch position. Pitch angle values from around 90^{o} - 45^{o} generate high stress levels in some critical parts of the blade load carrying structur due to the fact that the high bending moment from the blade weight acts in the plane of lower stiffness. These loads can also be deminished by adequate start-control.

Having chosen a welded steel torsion box for the blade we had to follow the rul es for welded construction as defined by the Swedish welding code.

Fig. 6 shows a diagram taken from StBK-N2 describing the permissible stress amplitudes with respect to cycle number and welding quality (K_x-factor). You may find similar values in the building codes of other countries as well as especially in the German area. The diagramm shows indirectly the difficulty to achieve a low weight but healthy design. The design loop is described in fig. 7 . As the weight is the main dimensioning parameter but is parallel influenced by aerodynamic loads one gets a very sensitive design circle.

Finally all material life using load cycles have to be cumulated.

The diagrams in fig. 8 and fig. 9 show for the two different areas $< 10^7$ and $> 10^7$ load cycles the relation of the different load cycles.

Load cycles 3, 5 and 6 are cumulating life usage, portional described in fig. 8. Load cycles 2 and 4, which are normal operating cases, have to be calculated for infinite endurance.

The portion of weight loads and aerodynamic loads for these cases is shown in fig. 9.

To keep weight down one has carefully to define details in the design, to avoid critical points in the welded structure. It should be aimed to achieve an overall welding K_x factor not greater than 2 which seems feasable in a good workshop.

Summary

It can be shown that a WTS-rotor blade made from welded steel will sufficiently do its scheduled work for many years, if the dangerous areas known for such machinery are carefully investigated.

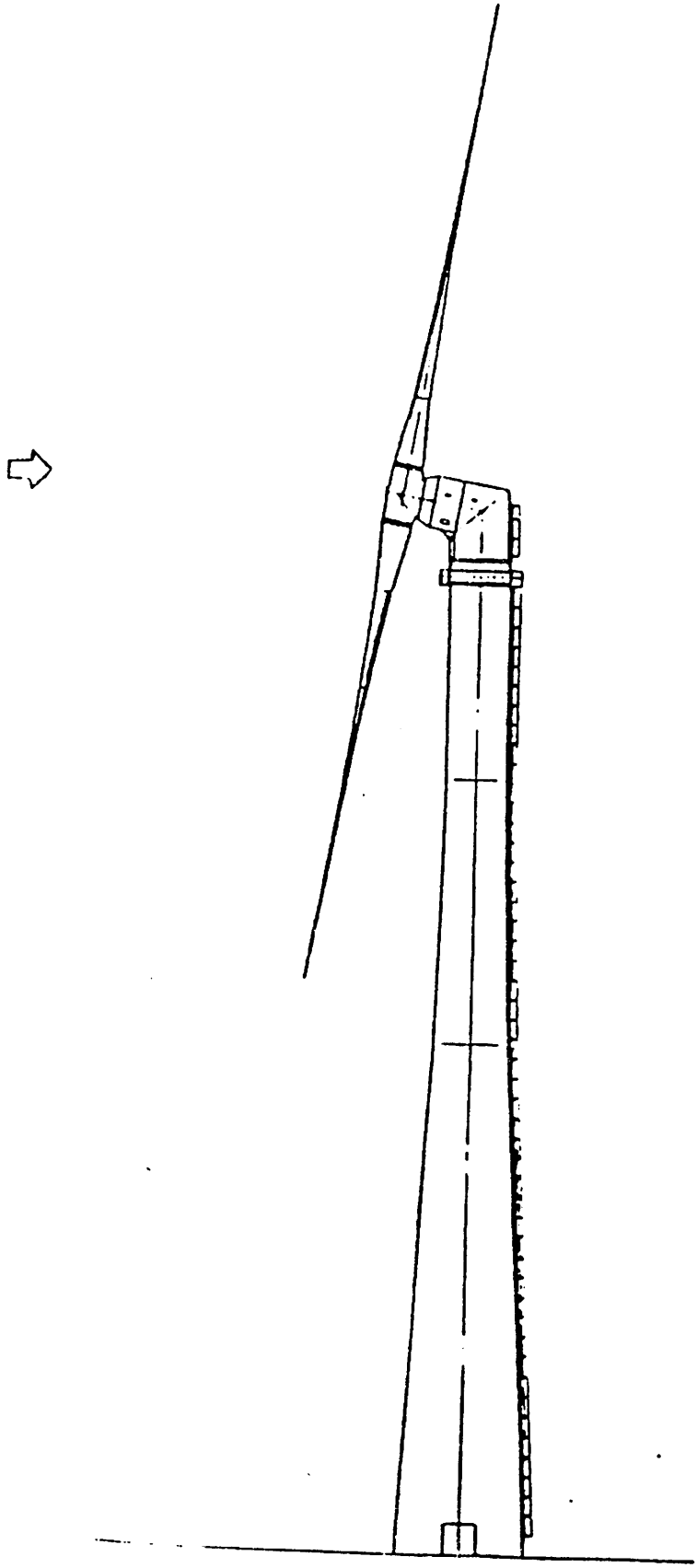

KMW/ERNO/VFW WIND ENERGY CONVERTER

FIGURE 1

WTS DESIGN DATA

WINDTURBINE

Blade number	2
Position	upstream
Diameter	75 m
Pitch control	yes
Rotor speed	25 rpm
Blade material	Steel/GRP

NACELLE

Yaw positioning	yes

MACHINERY

Type of gear	Planet/bevel gear
Generator	asynchronous
Generator speed	1500 rpm

TOWER

Material	Concrete, steel reinforced
Height	85 m
Diameter (top)	4,5 m

PERFORMANCE

Lowest windspeed	6 m/s
Highest windspeed	21 m/s
rated power at 12,6 m/s	2 MW
Energy production/year	6,7 GWh estimated

TABLE I

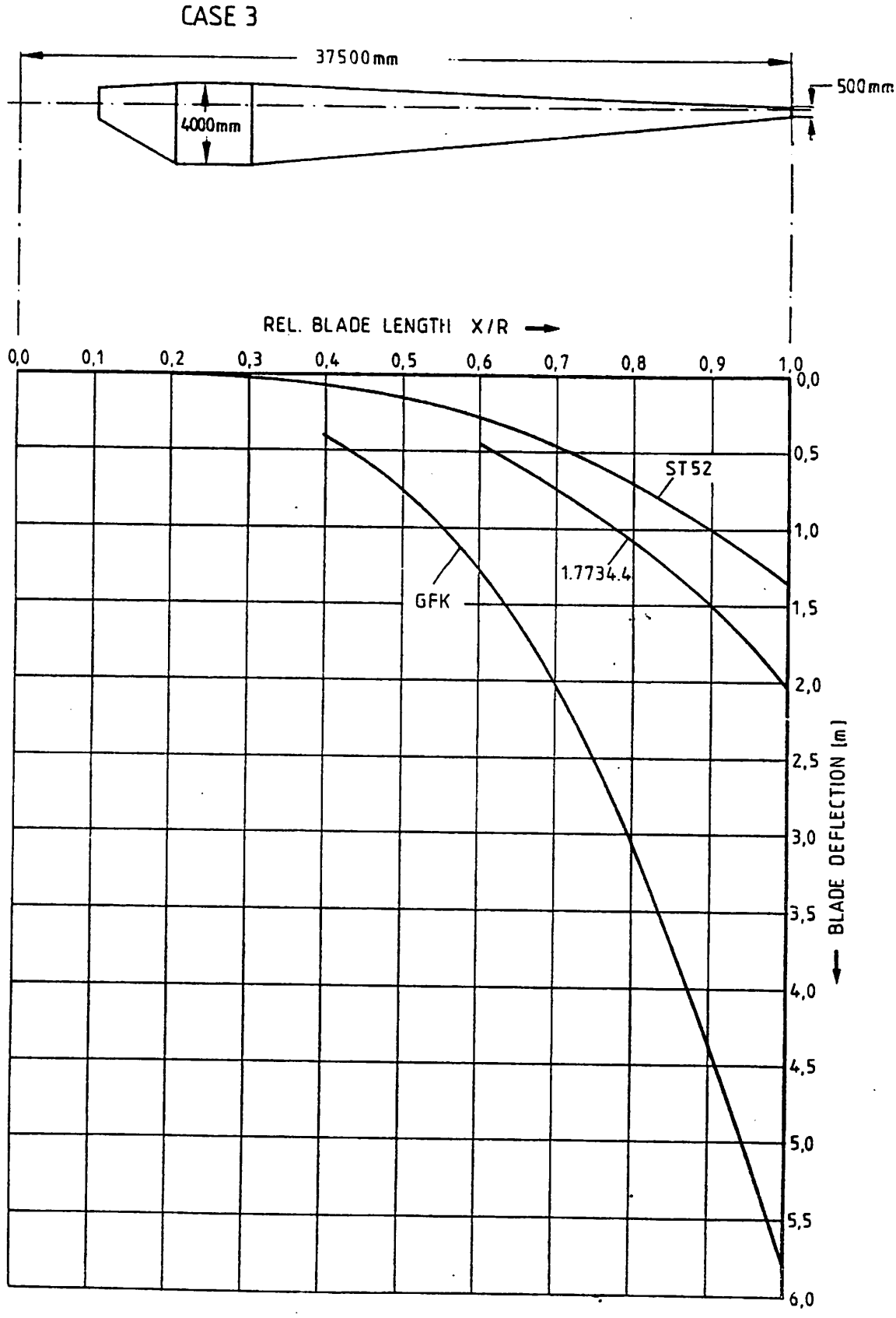

Blade deflection for different materials

FIGURE 2

Table II : COMPARISON OF MATERIAL CHARACTERISTICS

MATERIAL	γ g/cm^3	σ_t N/mm^2	σ_C N/mm^2	E_t KN/mm^2	E_C KN/mm^2	SPEC. TENSILE STRENTH σ_t/γ km	SPEC. E-MODULE E_t/γ 10^3 km	ULTIMATE ELONGATION %	$\pm\sigma_a$ R=0,5 10^7 Cycles N/mm^2	MATERIAL PRICE Relative ST52
FIBRES										
FASERN										
E-Glass	1,7	420	440	15	14	24,7	0,9	3,5	35	~15
Aramidfibre	1,25	450	120	24	12	36	1,9	2,5		
Ar.F + Carb. 50 % 50 %	1,35	500	240	33	23	37	2,6	1,7		
Carbon	1,40	550	500	44	42	39	3,1	1,3	100	400
7075T7351	2,7	480		70		18	2,6	7	40	~ 8 - 10
AlMg5	2,7	236		70		8,7	2,6	9	20	
Titan-Log 3.7164.1	4,5	900		110		20	2,4	8		~ 50 - 70
Steel										
1.7735.4	7,85	680		210		8,7	2,7	12	70	~ 3,5
ST52	7,85	510		210		6,5	2,7	22	60	1

EP-MATRIX, 40 Vol.%

WARP AND FILLINGS 1:1

DESIGN PHILOSOPHY

SHORT REALIZATION TIME

LONG LIFE TIME

no experiments. proven technology only

LOW COSTS / HIGH ENERGY

LOW MAINTENANCE

EASY REPAIR

GROWTH POTENTIAL

"A running WTS is better than a broken high sophisticated one"

FIGURE 3

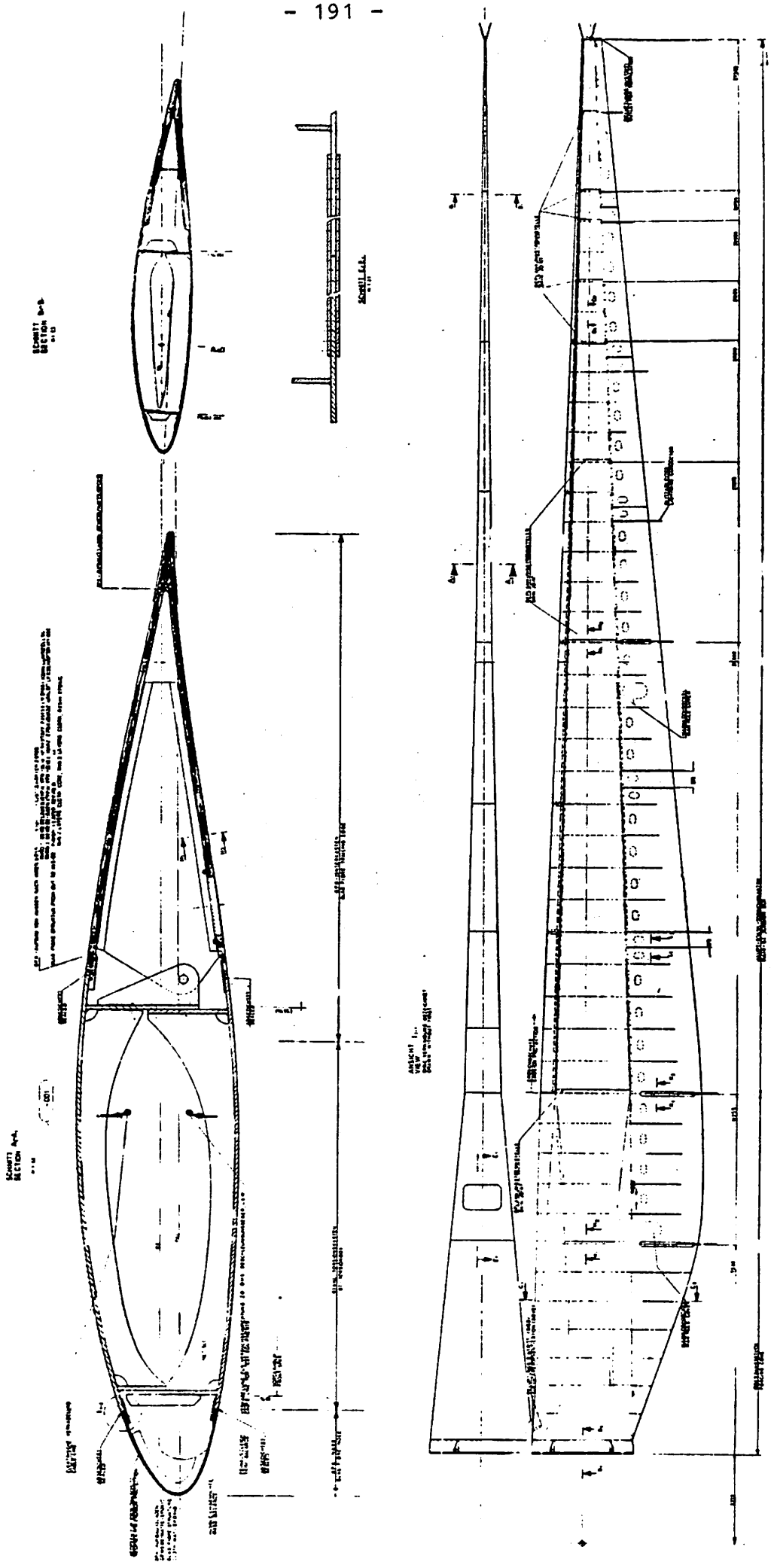

FIGURE 4 Blade Design

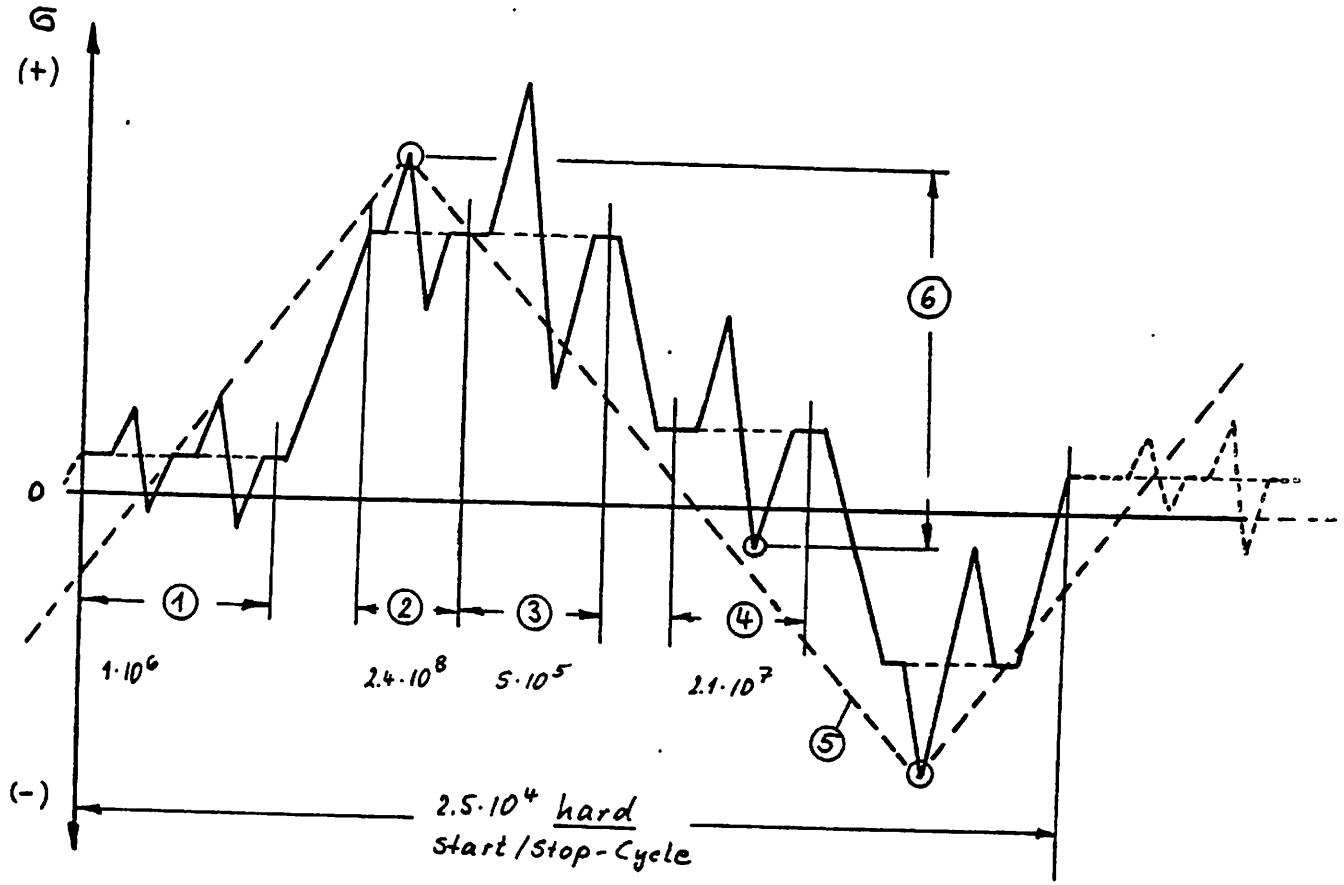

①	Blade feathered	90° blade ∢ 45° " "
②	Normal Operation	12.55 m/s
③	High Wind Shear	12.55 m/s
④	Normal Operation	21.1 m/s
⑤	Start / Rotation / Stop - Cycle	
⑥	Gustload e.g.	V = 17 ± 4 m/s

Summary of Load Cases

FIGURE 5

3: 3 K

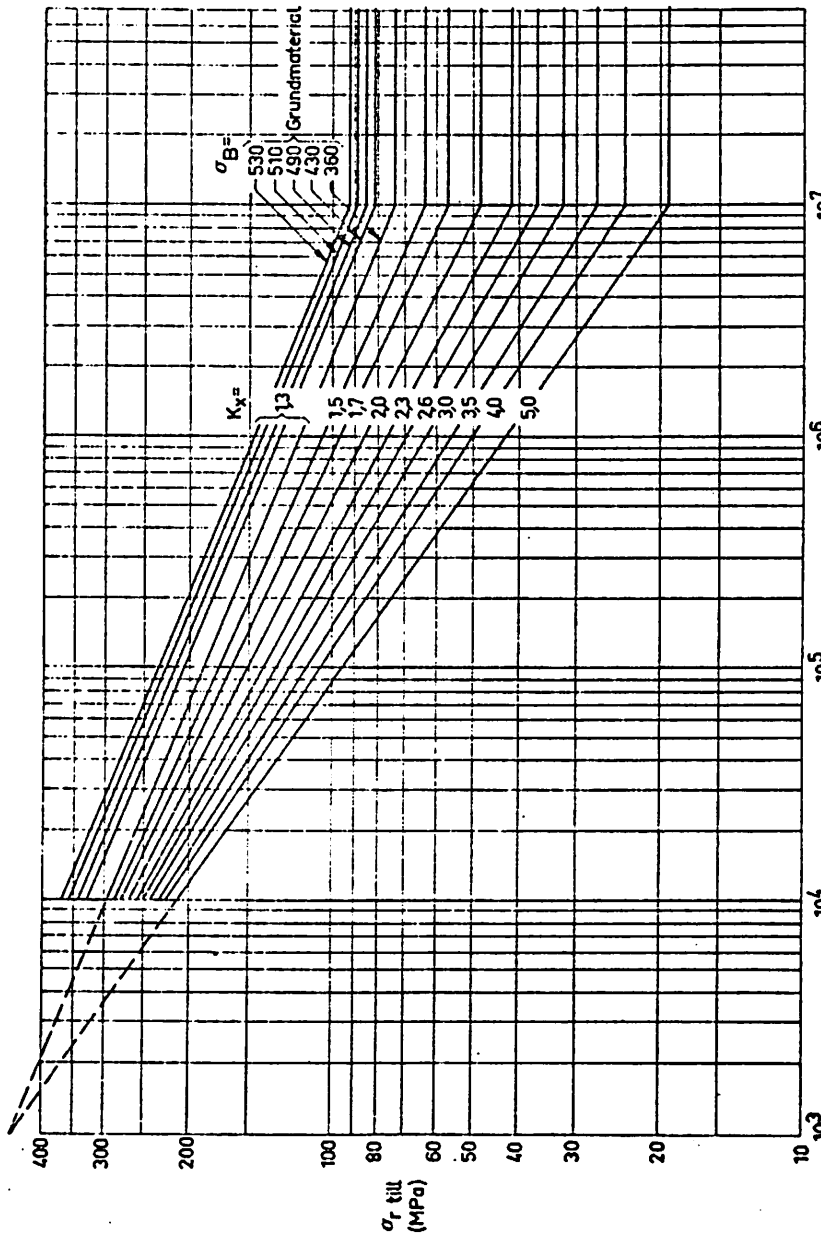

Fig 3: 32b K Tillåten spänningsvidd $\sigma_{r\,III}$ vid $\rho = 1$ (jfr tabell 3: 32)

Ref: Swedish Welding Code (SIBK - N2)

FIGURE 6

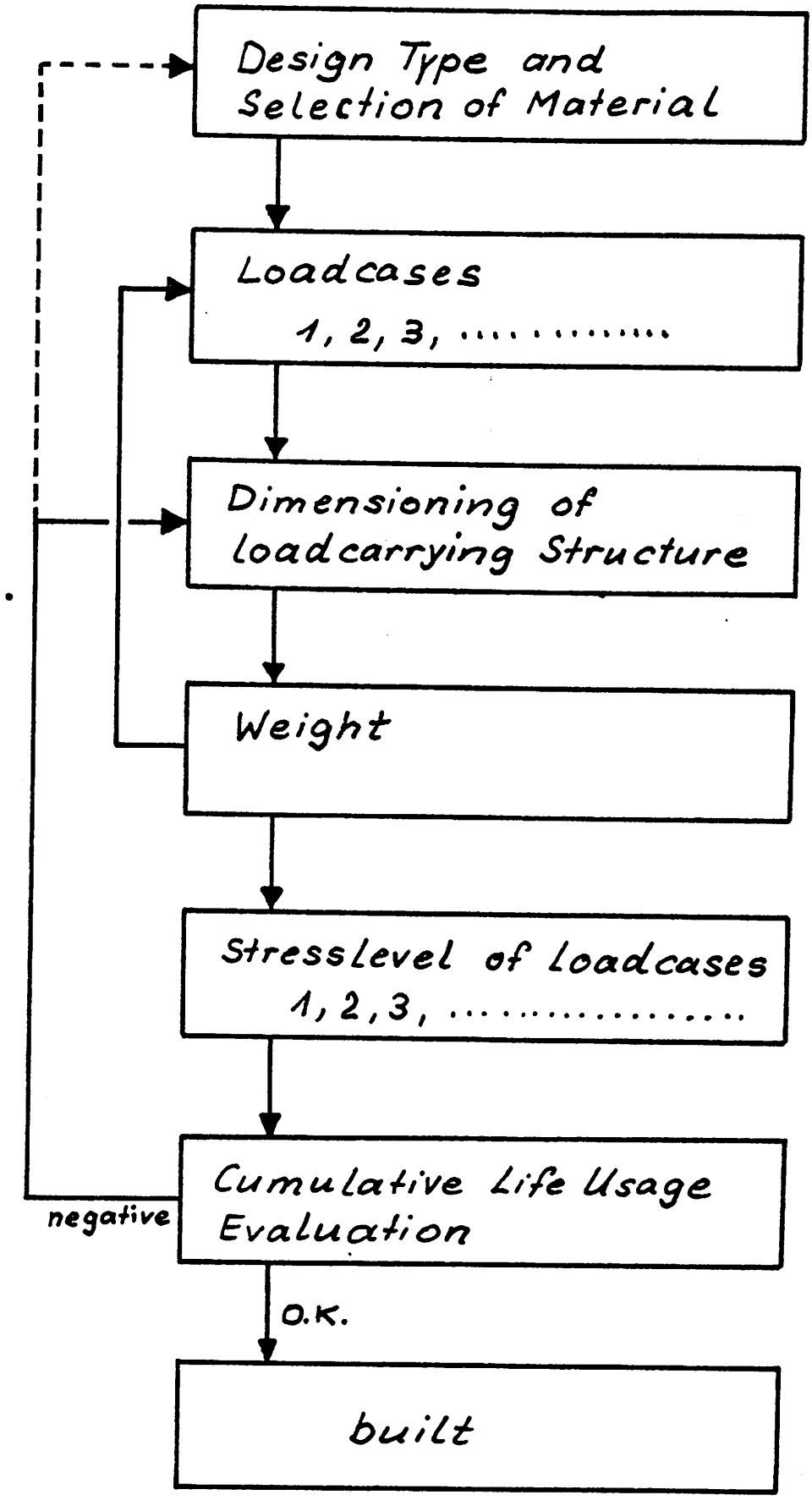

Design Loop

FIGURE 7

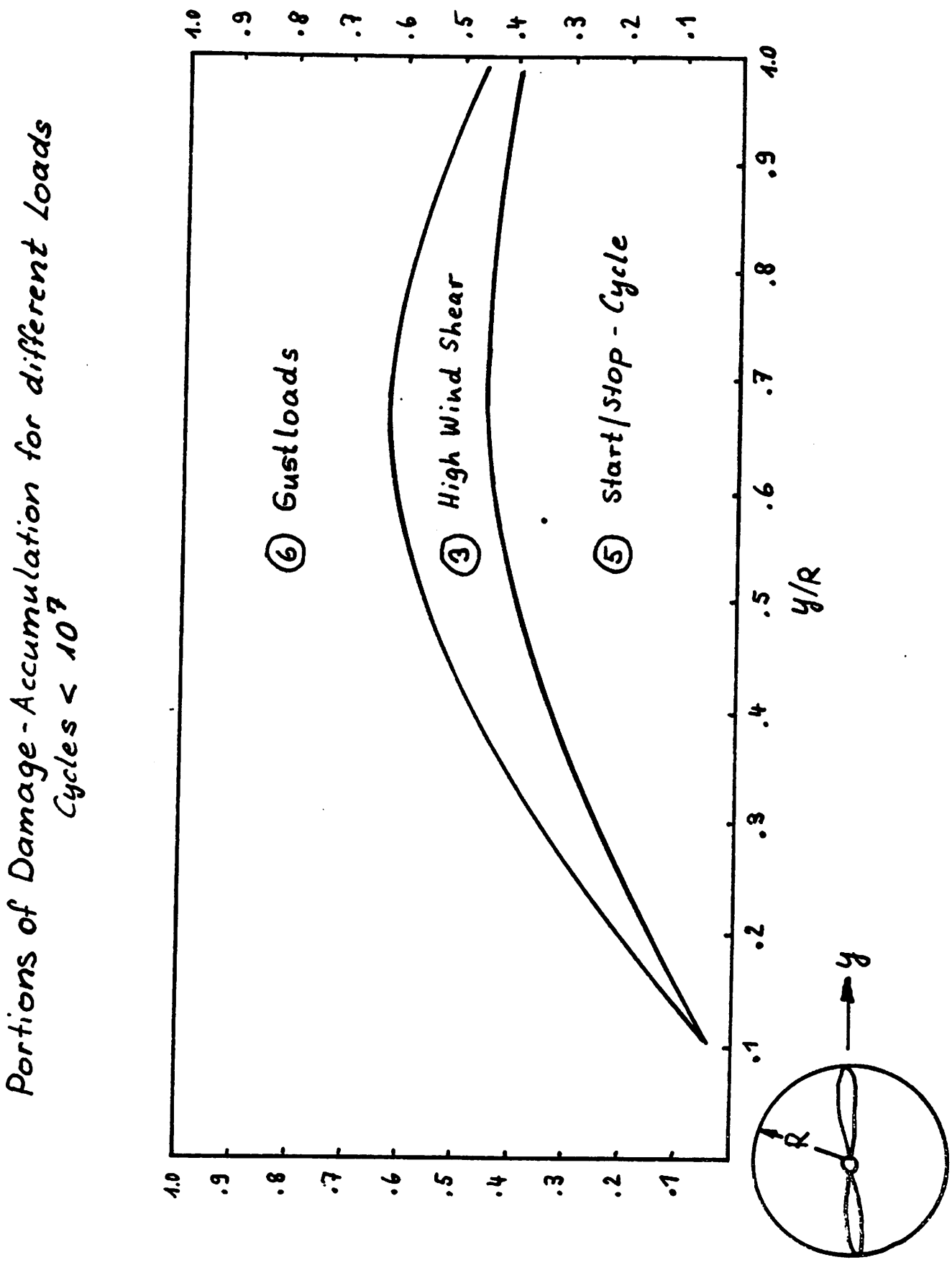
Portions of Damage-Accumulation for different Loads
Cycles < 10^7
⑥ Gust loads
③ High Wind Shear
⑤ Start/Stop-Cycle
y/R
1.0
.9
.8
.7
.6
.5
.4
.3
.2
.1
R
y

FIGURE 8

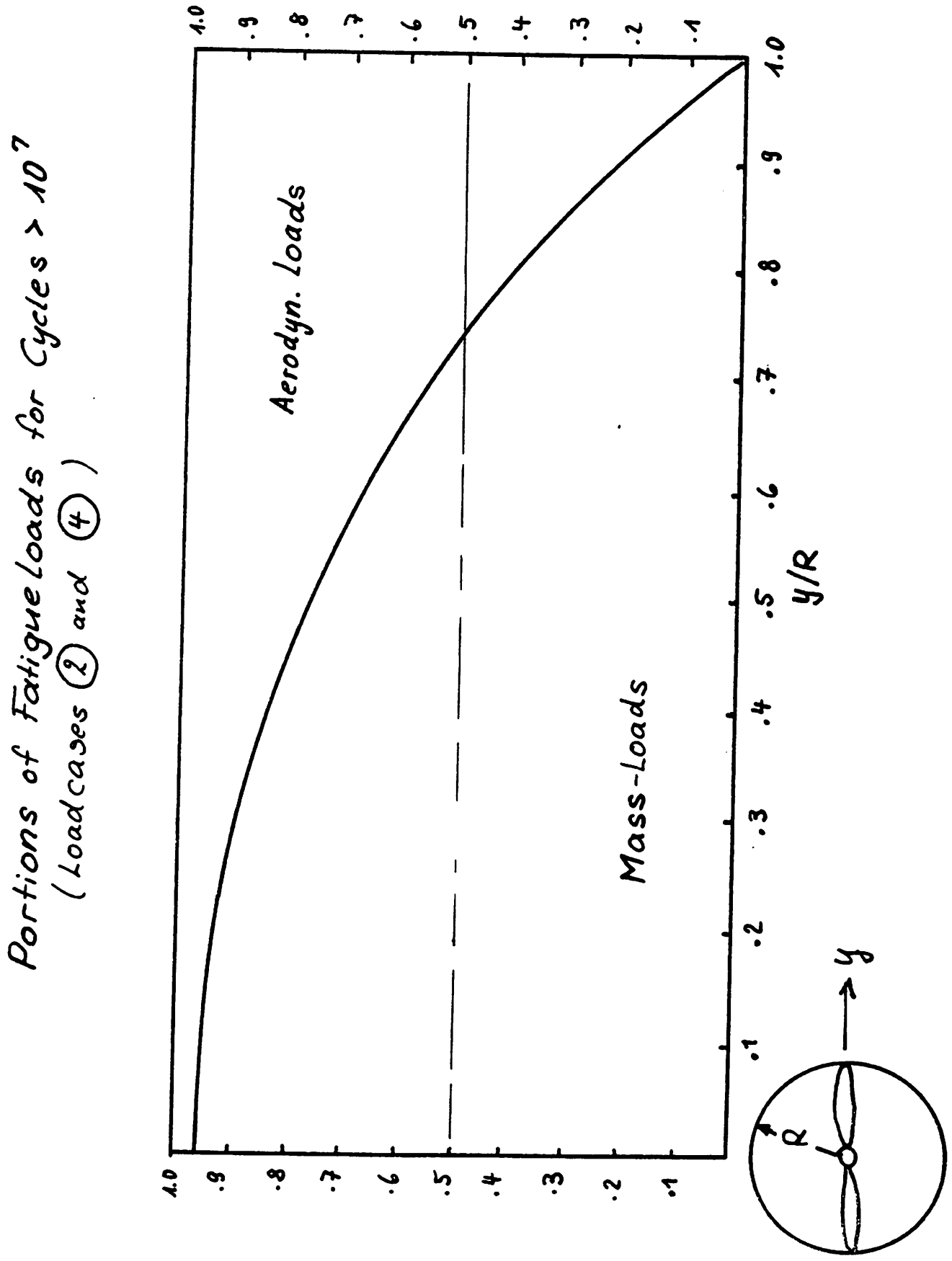
Portions of Fatigue loads for Cycles > 10^7
(Loadcases ② and ④)
Aerodyn. loads
Mass-Loads
y/R
1.0
.9
.8
.7
.6
.5
.4
.3
.2
.1
y
R

FIGURE 9

Combined Effects of Deterministic and Random Loads in Fatigue Design

André Raab

Contents:

1. Introduction

Blades of high power wind turbines belong to the largest rotating machine elements ever made. Their service life is limited by fatigue, which may be combined with corrosion.

Fatigue evaluation consists of several steps:

1. A preliminary design is developed.
2. Loads expected during service life are forecasted.
3. Deflections and stresses are determined using the dynamics and material properties of the turbine.
4. The probability of failure is evaluated comparing statistics over the forecasted stress fluctuations with laboratory test results.
5. If necessary, the preliminary design is modified and the whole procedure is repeated.

The outlines of this method are generally valid in machine design. Problems which are specific for wind turbines arise in the second and fourth step; how to forecast the loads and how to estimate the frequency of their occurrence?

2. Loads on the blade

Deterministic loads	Random loads
Gravitational	Exceptional start
Centrifugal force	Exceptional stop
Mean wind force	Wind gust (turbulence)
Normal start	Interaction of random events and tower passage
Normal stop	
Interaction of deterministic events and tower passage	

The classification of loads in two groups is somewhat arbitrary. The occurence of wind is random, but here we work with the distribution of expected wind velocities during service life and suppose, that this is known from meteorological statistics.

To give an idea, some examples of stress diagrams are shown know:

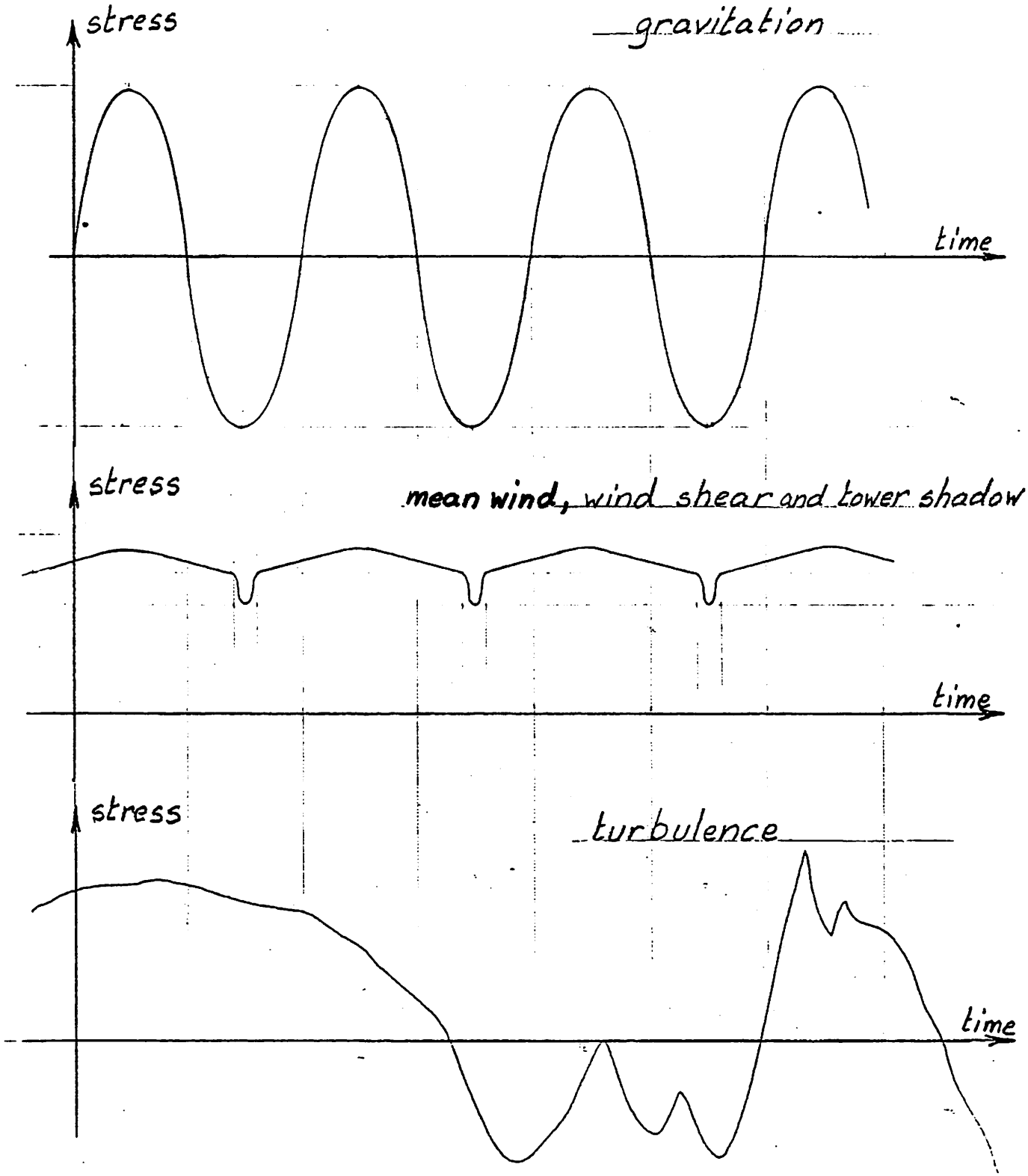

Fig. 1.

The reason for deviding the loads in two categories is that deterministic loads can be calculated in a straightforward manner, whereas the magnitudes of the random loads at given instants are undetermined; thus the treatment of random loads require probabilistic and statistical methods.

It is quite natural to calculate partial fatigue damage caused by deterministic forces and that caused by random forces separately and eventually add them to obtain the total damage, using some cumulative damage theory. This will result in underestimation of the damage, which will be shown now.

3. The linear cumulative damage theory

The purpose of the method is to evaluate fatigue at variable amplitude loading on basis of experiments which are made at constant amplitude loading. The Palmgren-Miner rule is the simplest and most well-know representative of the cumulative damage theories.

Let the fatigue life to failure at [a] constant amplitude stress of S_i be N_i and the actual number of cycles at this stress be n_i, then the partial damage is assumed to be

$$D_i = \frac{n_i}{N_i}$$

In an actual case various stresses S_i; $i = 1,2 \ldots m$ occur n_i times, in any order of succession. The sum of the partial damages, the total damage

$$D = \sum_{i=1}^{m} \frac{n_i}{N_i} \geq 1$$

is the condition of failure.

Values of N_i corresponding to the given values of S_i are taken from the Wöhler (S-N) diagram, which is based on numerous constant amplitude laboratory tests. This diagram is usually plotted using

logarithmic scales on both axes, giving a slightly non-linear curve. As a first approximation, it may be substituted by a straight line corresponding to the equation

$$NS^b = c$$

Inserting the values of N_i evaluated with the aid of this equation in the previous one we obtain the total damage

$$D = \frac{1}{c} \sum_{i=1}^{m} n_i S_i^b$$

The theory as outlined above has several shortcomings, from which we disregard now and postulate, that it is a true description of the actual fatigue mechanism. However, fatigue evaluation may lead to erroneous results which will be shown next.

4. The coincidence of loads

The crucial point is that we do not know at which instant a wind gust with an assumed intensity actually takes place. It may or may not coincide with some of the deterministic loads, for example with the maximal bending moment caused by gravitation or with the interaction of the tower passage with the main wind load.

As an example let us investigate the case of two stress amplitudes S_1 and S_2 (they are always positive by definition); their numbers of cycles are n_1 och n_2, respectively. The total damage is

$$D = \frac{1}{c}\left[n_1 S_1^b + n_2 S_2^b \right]$$

What happens now if a part of these stresses occur at the same instant? Say that this coincidence takes place p times. Then S_1 occurs only $n_1 - p$ times, S_2 only $n_2 - p$ times and the combination $S_1 + S_2$ occurs p times resulting in a total damage of

$$D = \frac{1}{c}\left[(n_1-p)\ S_1^{\,b} + (n_2-p)\ S_2^{\,b} + p\ (S_1+S_2)^b\right]$$

$$= \frac{1}{c}\left[n_1 S_1^{\,b} + n_2\ S_2^{\,b}\right] + \frac{p}{c}\left[(S_1+S_2)^b - S_1^{\,b} - S_2^{\,b}\right]$$

Here the last term can be expanded using the binomial theorem giving

$$D = \frac{1}{c}\left[n_1 S_1^{\,b} + n_2\ S_2^{\,b}\right] + \frac{p}{c}\left[\binom{n}{o} S_1^{\,b} + \binom{n}{n} S_2^{\,b} + \right.$$

$$\left. \binom{n}{1} S_1^{\,b-1}\ S_2 + \binom{n}{n-1} S_1 S_2^{\,b-1} + \ldots - S_1^{\,b} - S_2^{\,b}\right]$$

$$= \frac{1}{c}\left[n_1\ S_1^{\,b} + n_2\ S_2^{\,b}\right] + \frac{p}{c}\left[n S_1^{\,b-1}\ S_2 + n S_1 S_2^{\,b-1} + \ldots\right]$$

The first term in the last row represents the total damage in case that no cycles coincides, as given above. We see that the total damage becomes always greater when some cycles coincide, because the second term in the last row is always positive. This result was proved using the Palmgren-Miner rule, but it holds as well for any other cumulative damage theory. It only depends on the fact that partial damages are not proportional to the stresses, which is a property of construction materials, not of the particular damage theory which we have chosen.

5. The interaction of stresses due to different loads

As we have seen, a unified treatment of all kinds of deterministic and random loads is necessary.

When evaluating fatigue damage due to stress cycles which take rise from different sources, the probability, that some cycles coincide in time, should be evaluated. Partial damages may not be added, if this probability is different from zero (within some permissible error).

Though direct addition of partial damages may not be admitted, a weighted sum might give good results. Thus we are led to the choice between two methods:

(i) Loads (or stresses) are computed as functions of time and added prior to fatigue evaluation. This method will be called simulation (i.e., computation of the time history of the process).

(ii) Statistical properties of different sorts of loads are evaluated separately. When considering fatigue, account of their interaction is taken by probabilistic methods. This procedure will be called the probabilistic interaction method.

6. Fatigue evaluation using simulation

A scheme of the procedure may be as follows:
First, aerodynamic forces are calculated. They depend on the

- specified mean wind velocity at the height of the hub
- wind shear (the difference of mean velocities at different heights)
- turbulence (irregular departure of wind speed components from local mean valus)
- tower shadow (periodic interference with the tower).

Having chosen an appropriate aerodynamic theory (no claims of linearity are posed) local wind speeds and forces along the blade are determined. A special problem in this context is the simulation of turbulence, which will be treated later.

Next, the mass forces due to gravitation and rotation are added and then the sum is inserted into the equations of motion of the blade (or possibly into the dynamic equations of a greater system, which may consist of blade, nacelle, tower and control system). These equations are solved by direct integration in the time domain or by using normal mode decomposition (the latter seems to be more economical). Stresses are computed as functions of time, giving the sample functions for the statistical evaluation of fatigue.

If the length of these sample functions is sufficient, statistics can be made by counting processes such as

- level crossing count
- peak count
- range count
- rain flow count.

These methods are amply documented in the literature on fatigue.

If the sample functions are too short (because of economical reasons), the distribution of peaks should be estimated. However, this is a more difficult and uncertain method.

The procedure described above is repeated for different values of the mean wind velocity. Using estimates of the expected mean wind velocitites during the stipulated life time of the wind turbine, the total fatigue damage can be computed.

Simulation has the advantage, that the dynamics of very complex systems may be treated. Its drawback is the necessity to combine several computer programs and run them extensively, in order to obtain the great amount of data which is needed for statistical evaluation; a sort of brute force method.

7. Turbulence simulation

Wind velocity fluctuations can be described in two manners:

- as a stationary stochastic process
- as a succession of descrete wind gusts.

In the first case one point energy density spectra and two point coherence and phase spectra are specified. These spectra are obtained from anemometers placed at fixed points in space. On the other hand, points of the turbine blades move on vertical circles. If the sensor is moving along a circular path, wind fluctuations can be considered as a periodic stochastic process.

Simulation means to construct by mathematical methods a time function representing the fluctuating part of the wind, having the prescribed spectra.

Two ways of simulation are known

- digital filter techniques
- matrix methods.

Digital filter techniques for simulation were proposed by Shinozouka and Sato Ref 1 and 2 and applied for the case of flight vehicles by Perlmutter (see chapter 14 by Fichtl, Perlmutter and Frost in Ref 3).

Matrix methods were originated by J.N. Franklin (1965). Our current work in Sweden is an extension of this method to the case of a periodic multivariate process. In this way we simulate the turbulence as per cieved at points moving with the rotating turbine blade. For further details see Ref. 4.

The concept of descrete wind gust was used in several decades. Its application on wind turbines was recently proposed by Frost, Long and Turner, Ref. 5.

8. The probabilistic interaction method

This is a new concept and its details are not elaborated yet. Two formulations may be proposed:

- when summing damages, weighting factors are used, which depend on the probability of interaction of the corresponding stresses.
- random and deterministic loads are subdivided in groups and the probability of their mutual interaction is evaluated. This gives the expected numbers of load cycles, valid for such interactions. The corresponding stresses are computed and a conventional application of some cumulative damage theory completes fatigue evaluation.

The question of weighting factors is theoretically complicated and little is done in this context as yet.

The subdivision of loads in groups and evaluation of their interaction is the best of the presently known methods, apart from simulation. However, it is heavily depending on the skilfulness of the individual, who specifies the groups and the conditions for the combination of loads. Loads should be combined taking regard to their dynamical effects. This is difficult to estimate and different trials ought to be tested with the aid of computer programs, which show the transient motions of the wind turbines at these combinations.

9. Conclusions

Separate treatment of various loads in fatigue evaluation leads to weak design. Correct results can be obtained by simulation and by a probabilistic interaction method.

Work on simulation is currently going on at the Aeronautical Research Institute of Sweden in collaboration with SIKOB, Engineering Consultants. Final results will be reported later.

References

1. M. Shinozouka and Y. Sato: Simulation of Nonstationary Random Process. Am. Soc. of Civ. Engrs. - J. of Struct. Div. EM1(1967) Feb. Paper 5105. pp.11-40.

2. M. Shinozouka: Simulation of Multi-variate and Multi-dimensional Random Process. J. of Acoustical Soc. of Am. June 1978.

3. W. Frost and T.H. Moulden: Handbook of Turbulence. Plenum Press 1977.

4. A. Raab: Combined Effects of Periodic and Stochastic Loads on the Fatigue of Wind Turbine Parts. FFA - The Aeronautical Research Institute of Sweden. Technical Note AU-1499 Part 6. Stockholm 1979.

5. Frost, W., B.H. Long, and R.E. Turner: Engineering handbook on the atmospheric environment guidelines for use in wind turbine generator development. NASA Technical Paper 1359, December, 1979.

DESIGNING FOR FATIGUE PREVENTION

Thomas M. Zajac*

Before starting my talk, I want to read two short paragraphs from a lecture by Bo K. O. Lundberg, published as FFA Report 76 Stockholm 1958, entitled "Some Proposals for Evaluating Fatigue Properties of Airplane Structures".

> "The famous Swedish poet Esaias Tegnér (1782-1846), professor in the Greek language, when once involved in an academic controversy concerning the merits of a new grammar in the Greek language, written by a contemporary scholar, made a statement about this grammar which can be translated as follows:
>
> > "The grammar admittedly contains both much that is true and much that is new; what is true, however, is not new, and what is new is not true."
>
> It is my belief that any one requested today to present a paper on the subject of aircraft fatigue runs a great risk of being the target of criticism of the same severe nature as that offered by Tegnér. The reason for this is, on one hand, that such a multitude of articles surveying the contemporary aircraft fatigue problem have been written during the last few year that, easy as it would be to make a lot of true statements, in still another review of the fatigue situation, such statements are unlikely to be scientifically new. On the other hand, the fatigue problem, besides being very obscure, is at present still so controversial that it is very difficult indeed to produce anything that is not only new but at the same time is indisputably true."

* Chief of Materials and Structural Integrity
Hamilton Standard Division
United Technologies Corporation

What Mr. Lundberg believed was true then, I believe is still true today. Since I have no new information, I can only hope that you will find some interesting information that might stimulate your thinking on this complex subject. Since the blade is one of the most critical unlimited fatigue life structures in a wind turbine, I will exhibit some results from many years of structural experience with unlimited fatigue life aircraft propeller blades. This experience has largely influenced the evolution of a design limit concept and design features in the Hamilton Standard wind turbine blade.

Against this background, let me proceed to Exhibit 1 which presents the design for fatigue prevention expression in its most elementary form, i.e. the appropriate strength must be equal to or greater than the actual stress. The next two exhibits look at each side of this equation.

Exhibit 2 lists the main sources of loading which must be evaluated, which then must be translated into stresses which these loadings induce in various regions of the structure. The stress analysis must consider the adequacy of the theoretical method to obtain elastic stresses and plastic strains. When theoretical uncertainty exists, appropriate experimental analyses should be applied.

Exhibit 3 attempts to list the major factors which bear on the strength side of the expression, with the focus being on fatigue strength. It is still not uncommon to find that designers deal with the fatigue strength question on the basis of handbook data obtained from laboratory specimen test results. Realistically, these data generally represent the basic fatigue capabilities of the material in a particular form and heat treat condition.

Actual fabricated components, exposed to particular environments, life requirements, and other factors such as maintenance repairs, number of samples in service, and risk considerations present a most difficult and challenging problem to the designer in assessing what fatigue strength limit to design to. The significant effect that some of the factors listed have on full scale structural component fatigue behavior, and how Hamilton Standard addresses the fatigue strength design limit, will be addressed in future exhibits.

Exhibit 4 presents a typical stress-cycles diagram. Small scatter is indicated for data generally associated with the static strength region of the diagram. Increased scatter is indicated in the low cycle fatigue region of the diagram, and large scatter is indicated for the high cycle fatigue or unlimited life region. Wind turbine structures span the entire range of the stress-cycles diagram; however, information in this talk will focus on the unlimited life region. This is the region where all of the items in Exhibit 3 have their most significant effect and it is the region for which aircraft propeller structural experience has been accumulating for forty years. Over the projected life span of thirty years for a wind turbine, simple calculations indicate accumulation of several hundred million significant stress cycles in a blade. In a mere ten thousand hours of aircraft operation, representing only several years of commercial service, aircraft propellers accumulate over six hundred million significant stress cycles. Therefore, the wind turbine blade fatigue and unlimited life considerations are very much akin to the aircraft propeller blade.

Exhibit 5 shows a typical solid metal smooth and notched laboratory fatigue specimen. Many thousands of such specimens have been tested over the years, and voluminous resulting data are published in the literature.

Exhibit 6 compares the typical laboratory specimen in size and shape scale relationship to a typical simple one-piece solid aluminum propeller blade.

Exhibit 7 depicts some of the damage inflicted on a solid aluminum propeller blade in a normal service environment. The inset picture from the tip portion of the blade shows common erosion and gouging damage in the blade surface. The inset picture from the middle portion of the blade shows intergranular stress corrosion attack that can result from aggressive chemical and moisture environments. The inset picture from the inboard retention fillet area of the blade shows fretting of the surface due to strain differential motions between the blade surface and its mating steel raceway ring. These are only three of the service operating environmental factors that can result in severe reductions in the high cycle fatigue strength of the blade. This damage cannot be prevented. However, the effects of the damage can be and are mitigated by inducing deep compressive residual stress layers in the blade fillet and the major blade surface areas by cold rolling and shot peening, along with appropriate periodic inspections and maintenance.

The essence of Exhibits 5, 6, and 7 is displayed in the composite of Exhibit 8. The upper band encompasses the fatigue test results from many hundreds of laboratory specimens. These specimens, like the smooth version shown in Exhibit 5, were manufactured from cut up sections from actual heat treated solid aluminum alloy propeller blade forgings. The lower band encompassed

the fatigue test results from testing a large number of actual full scale production finished propeller blades of the same aluminum alloy. The bottom dashed line represents an appropriate design limit for this particular propeller blade with prescribed inspection and maintenance. If consideration was given to operating this structure in the unlimited life region without attention to inspection and maintenance, the design limit would be reduced substantially.

In a somewhat parallel display, Exhibit 9 presents only the low boundary of the laboratory specimen fatigue data for a moderate strength low alloy steel used in fabricating hollow steel core/shell propeller blades. In this instance, a preformed steel shell is brazed onto a flattened hollow steel core. The edge cavities between the core and the shell and the central core cavity are filled with a moderate density sponge rubber material for support against local plate vibration and section shear flow. The low boundary, encompassing the results from fatigue testing a large number of full scale production blades, shows the large strength reduction in the fabricated structure compared to the basic material fatigue behavior.

This particular propeller blade was introduced into service shortly after World War II on large commercial and military aircraft. Relatively early service cracking resulted in substantial additional testing of blades as-received from service use. Rather gross reductions in fatigue strength are indicated by the low boundary for blades containing service inflicted damage in the form of gouges and dents. A further reduction, continuing at very high numbers of cycles, is indicated by the low boundary for blades which exhibited corrosion damage from internal moisture entry. It should be pointed out that blades using this same basic steel spar which is corrosion protected with a thin electrodeposited plating system, covered with an

adhesive bonded fiberglass reinforced epoxy shell and filled with a closed cell low density urethane foam, have developed an excellent service record. This configuration provides excellent corrosion protection for the principal load carrying member -- the central steel spar, and the external shell is extremely insensitive to gouge damage, moisture, and it does not dent.

Exhibit 10 relates to a painfully learned experience dealing with the stress side of the expression in Exhibit 1. The sketch depicts the general dimensions of the inboard region of a large one-piece hollow steel propeller blade.

Early samples of this monocoque blade were commited to propeller-engine-test stand running for functional and performance type evaluations. One blade fractured during this testing, the separation occurring in the transition region between the inboard round section and the airfoil section. Subsequent laboratory experimental stress analysis revealed that stresses in this transition region were substantially higher than expected due to local secondary structural action. This lesson was learned prior to the availability of finite element analysis techniques, but points out the importance of knowing the stresses and employing experimental measurement techniques where analysis may not be adequate.

The next two exhibits show methods developed and employed for fatigue testing large sample sizes of full scale propeller structures into the high cycle, unlimited life region. Exhibit 11 shows a method of fatigue testing multiple samples of full scale propeller blades.

In the case shown in the right hand side of the picture, six blades are being tested at a resonant frequency. By small tip mass tuning, each blade vibrates

at the resonance frequency of the test assembly and is stressed at a common vibratory stress level. The assembly may be tested for up to several hundred million cycles. If no distress is observed after detailed inspection, the assembly is returned to test at a higher stress level. This procedure is continued until fatigue cracking is produced. As one blade fails, a dummy blade is inserted in its place and the testing is continued.

At higher modes of vibration, peak stresses are produced in the outer region of the blade. The first fundamental mode produces peak stresses in the inboard region of the blade. By cutting off the tip portion of the blade, peak stresses can be simulated in the inboard region at test frequencies two to three times that of the full length blade, thus shortening the test time. Further, in a similar four blade setup, tips of adjacent blades can be drawn towards each other, producing a steady bending stress in each blade. A vibratory stress is superimposed on this steady stress, at resonance, using this same test equipment. Over the past forty years, nearly two thousand full scale propeller blades and blade sections have been fatigue tested, some to as many as three hundred million cycles at a given stress level.

The left hand portion of this exhibit shows multiple stacking of specimens on similar equipment. Adhesively bonded tab/base bar specimens are tuned and tested in flexure at a constant stress level. Basic material data can be accumulated on large sample sizes in relatively short times.

Exhibit 12 shows a full scale propeller hub/blade retention assembly being fatigue tested. In this case, the test bar replacing the blade has a retention and inboard shank region identical to the propeller blade. Internal

wedge/preload provisions enable applying and maintaining a simulated centrifugal load. Cyclic bending loads are superimposed on the hub/retention assembly by rotating tip unbalance masses. These tip masses can be phased to simulate any vibratory mode, in any direction, on any multi-arm assembly.

The types of full-scale testing described have been conducted on production and on service exposed structures. Some of the results of this testing were shown in Exhibits 8 and 9. It is important to emphasize at this point the dramatic reductions in high cycle fatigue strength, the unlimited life region, that must be adequately considered in designing large critical structures for fatigue prevention in service environments.

In an effort to focus critical attention on the subject of fatigue behavior of structures, Hamilton Standard organized for and evolved the design limit concept nearly twenty years ago. This is depicted in Exhibit 13. Organizationally, a discreet group is responsible for gathering and evaluating all externally developed fatigue data, developing and analyzing all internal fatigue test data on specimen and full scale structural components, conducting all laboratory development, and service fatigue fracture investigations, and integrating product service experience. This same group issues design limits to the Design Room for all components for the prescribed material, fabrication, environment, and life and maintenance requirements. Conceptually, the designer can stress his structure up to the design limit. Safety factors are not applied by the designer to the strength side of the expression in Exhibit 1 since the <u>design limit</u> accounts for the structural performance of the component and embodies a very low probability of failure.

The next Exhibit, 14, displays some of the more important design features of the Hamilton Standard wind turbine blade. The material system for the blade is fiberglass in an epoxy resin matrix. This material system is very insensitive to environmental factors and damage as they relate to unlimited life fatigue performance. The blade design features a two-cell monolithic structure, entirely fabricated by filament winding. The steady tension load is carried by the full cross-sectional area of the blade. The bending loads are carried primarily by the leading edge cell, which can also easily carry the torsional loading.

The nominal fiber layup orientation is $\pm 30°$ to the blade axis, however, material properties are carefully balanced for maximum weight reduction. This orientation results in material properties and a cell geometry that has buckling resistance greater than the loads impressed on the rotor. No internal or supplementary supports are required to provide an adequate buckling margin.

The width and wall thickness of the leading and trailing edge cells are varied along the blade length to provide smooth distributions of major and minor bending moments of inertia, torsional capacity, and blade mass. In the inboard region, the trailing edge cell tapers off to transfer its minor loading unformly and progressively to the leading edge cell which is integral with the retention. This minimizes stress concentrations which can be very detrimental in a high cycle fatigue environment. Detailed finite element alalysis of the trailing edge cell termination has confirmed the efficacy of this concept. Also, the dominant load carrying leading edge cell has no abrupt section changes which eliminates undesirable secondary structural action stressing. No joints, which can present critical fatigue problems, are involved in the blade area of the structure.

The centrifugal and the bending loads in the blade must be transmitted to a central hub structure. This is accomplished through a retention consisting of an inner and an outer steel ring, the outer ring being eventually bolted to the hub. The most effective way of transferring the loads from the fiberglass resin blade structure into these steel rings is by double overlap shear shown in Exhibit 15. This type joint eliminates the bending and related peel associated with single overlap shear type bonded joints. The steel rings are tapered to provide for a more efficient joint, reducing the strain concentration at the outboard ending of the rings. As a conservative design feature, a totally redundant load path is provided by a series of line-reamed and bonded bolts also shown in Exhibit 15. Both the adhesive bonded joint and the bolted joint are fully capable of carrying the blade loads into the steel rings independently.

Finally, it should be mentioned that the blade is protected from erosion and ultraviolet damage by an externally applied urethane coating. Lightning damage protection is provided by a metal system consisting of an aluminum tip cap, and leading edge, trailing edge, and chordwise aluminum foil strips. The edge strips extend from the tip cap and connect to the external steel retention rings. Foil is also wrapped as an extension of the outer steel ring to provide a cone of at least 30° to protect the inner ring. This system has been demonstrated to maintain the lightning charge externally and protects the entire blade from lightning damage.

In closing this talk, the next three exhibits list the major steps that must be followed for designing for fatigue prevention. Exhibit 16 lists the first three steps as design <u>requirements</u>. These are, namely:

1) The best assessment of the service loadings that will be imposed on the structure.

2) Realistic evolution of the environment and the life requirements.

3) An assessment of appropriate maintenance, which must be practical to accomplish.

Exhibit 17 lists the next three steps that are involved in the actual design execution. These steps are:

1) Selection of the materials and processes for the structural component.

2) An adequate theoretical stress analysis, supported by experimental analyses on early simulated sections as needed.

3) Establishment of component design limits to satisfy the loading, environment, life requirements, and maintenance.

The last series of steps are presented in Exhibit 18 and cover the critical verification steps. These are:

1) Large scale component fatigue testing as required. This covers either actual full scale components, sections thereof, or appropriate large simulations.

2) Measure loads on the structure in all types of actual operating conditions and environments.

3) Final stress vs. strength comparison. These final stresses are either measured in discreet areas during the load measurements mentioned above, or are recalculated if loads are different from those initially established. The final strength is obtained from the large scale component testing and reassesses the design limits originally provided. If this final strength is equal to or greater than the actual stress, the elementary expression in Exhibit 1 is satisfied, and a trouble-free structural component should result for its defined life.

TZ:ms

Ex. 1

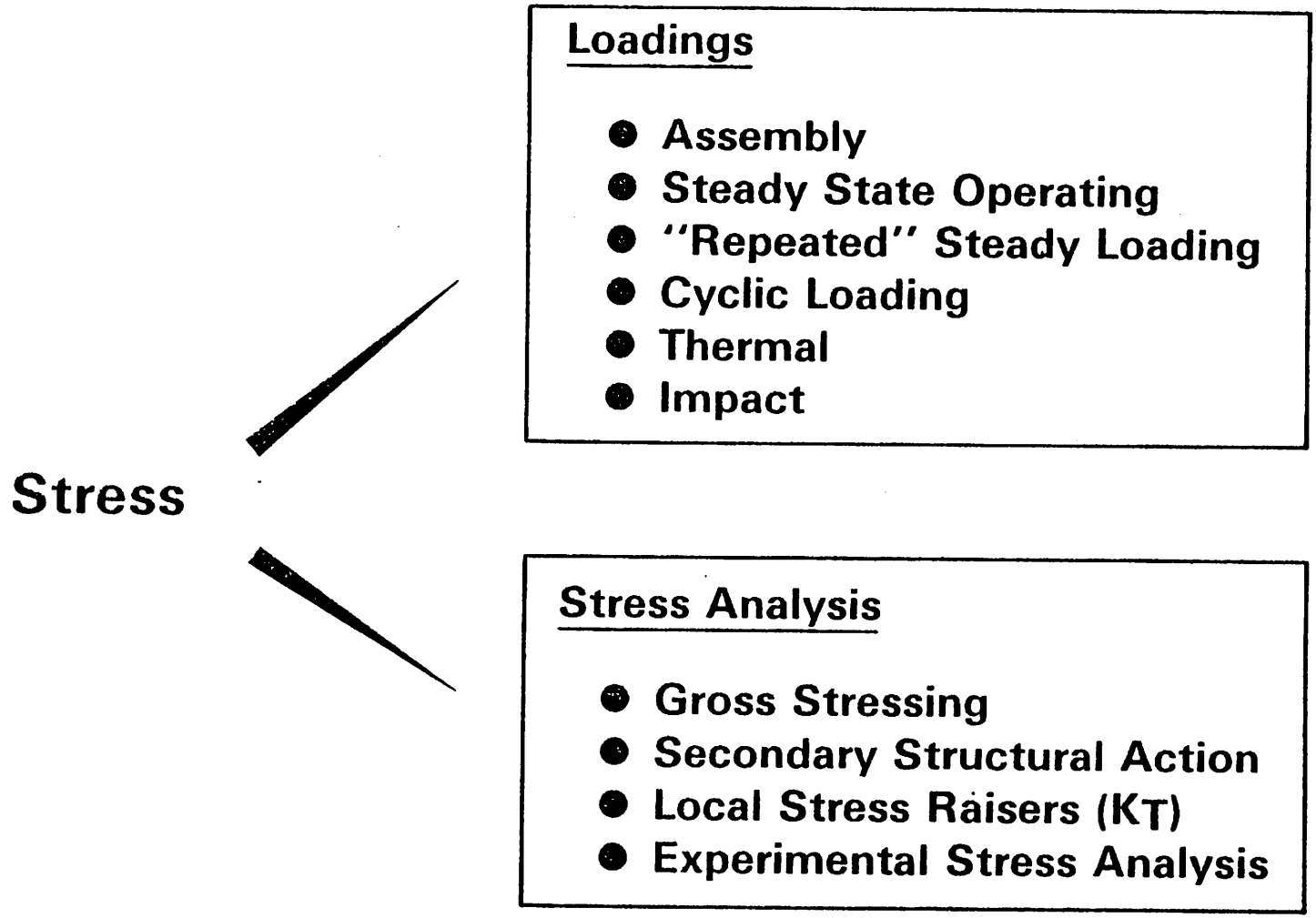
Stress
Loadings
Assembly
Steady State Operating
"Repeated" Steady Loading
Cyclic Loading
Thermal
Impact
Stress Analysis
Gross Stressing
Secondary Structural Action
Local Stress Raisers (KT)
Experimental Stress Analysis

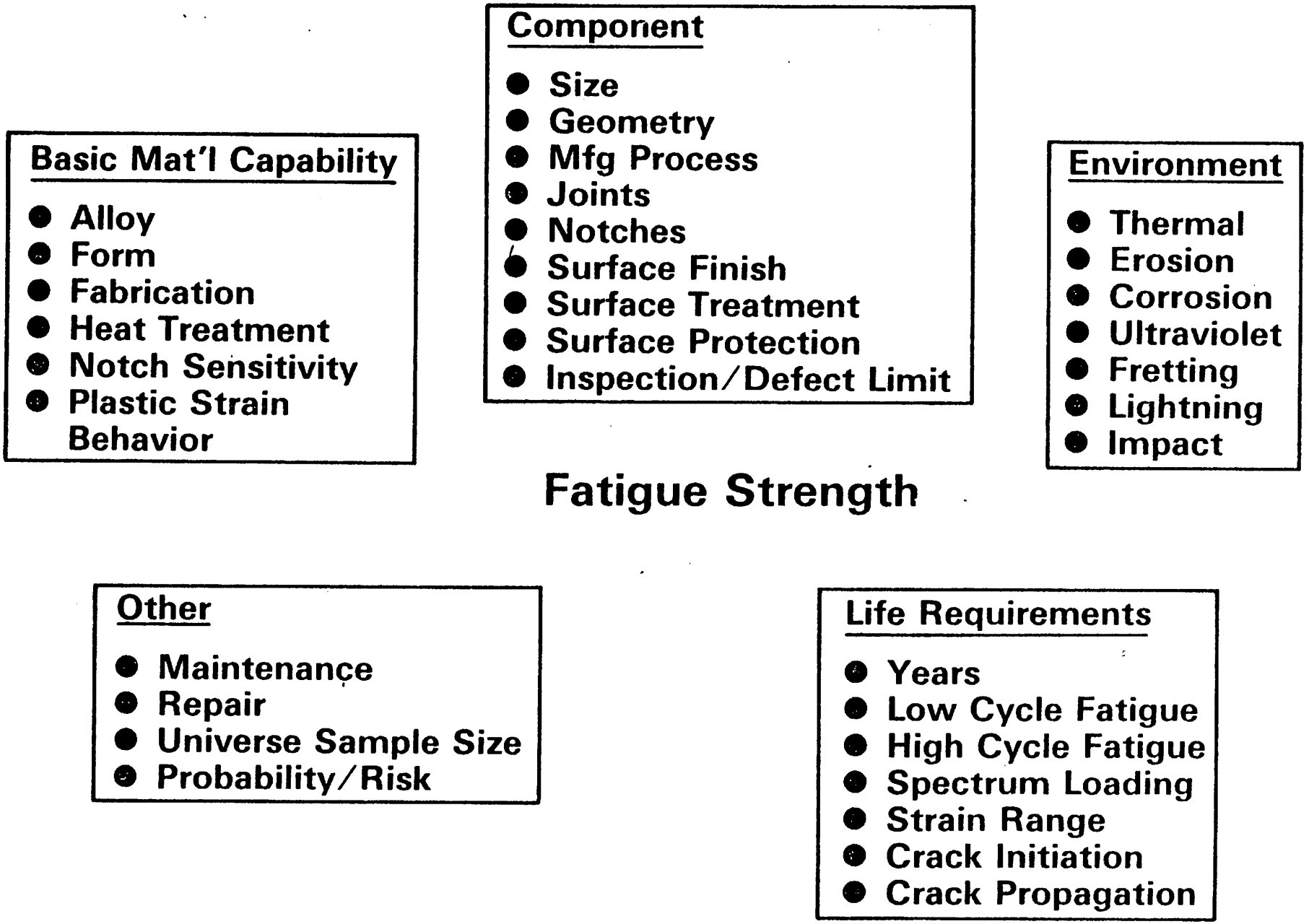
Component
Size
Geometry
Mfg Process
Joints
Notches
Surface Finish
Surface Treatment
Surface Protection
Inspection/Defect Limit
Basic Mat'l Capability
Alloy
Form
Fabrication
Heat Treatment
Notch Sensitivity
Plastic Strain Behavior
Environment
Thermal
Erosion
Corrosion
Ultraviolet
Fretting
Lightning
Impact
Fatigue Strength
Other
Maintenance
Repair
Universe Sample Size
Probability/Risk
Life Requirements
Years
Low Cycle Fatigue
High Cycle Fatigue
Spectrum Loading
Strain Range
Crack Initiation
Crack Propagation

TYPICAL S-N DIAGRAM

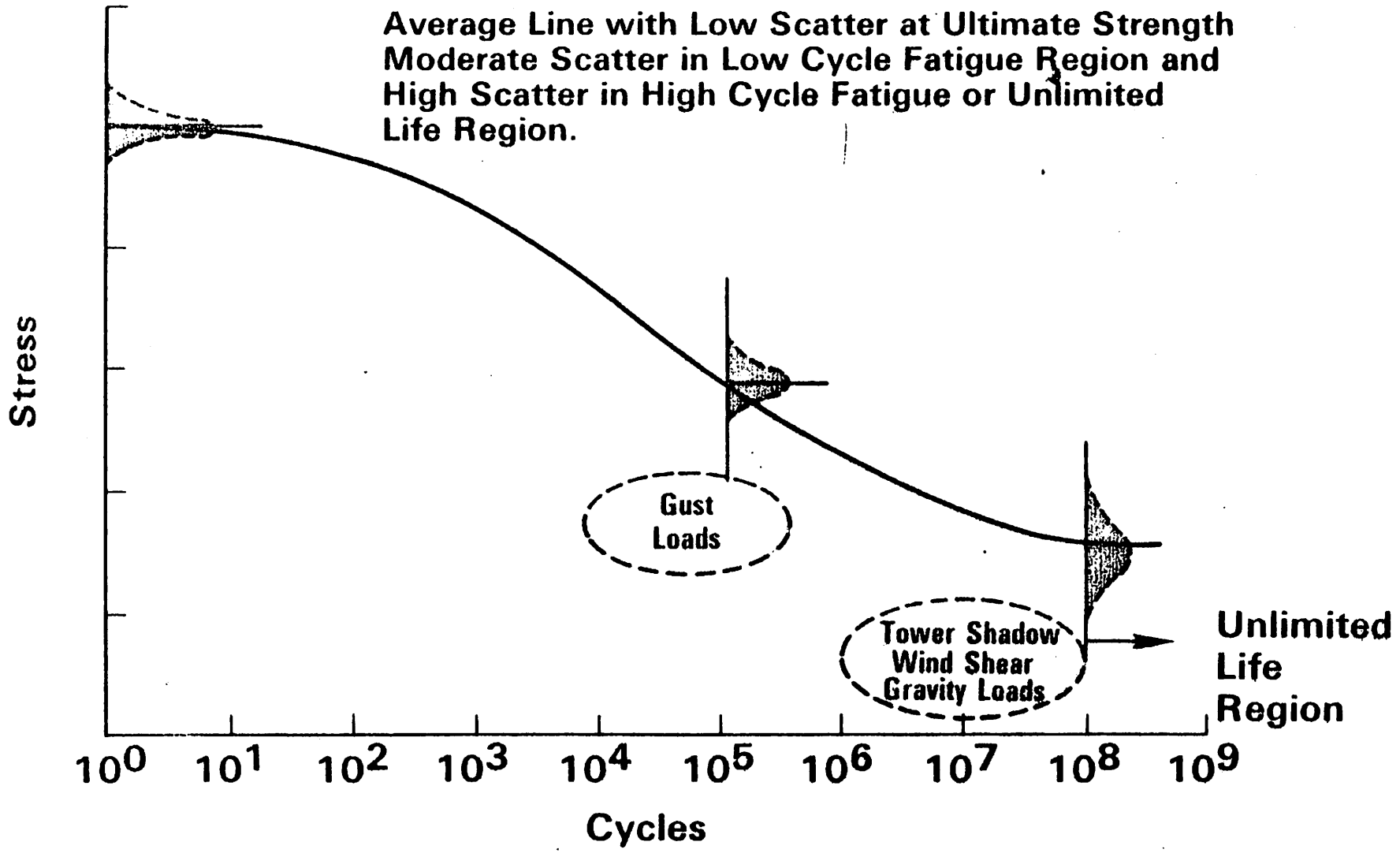

Ex. 4

TYPICAL LABORATORY.SPECIMEN

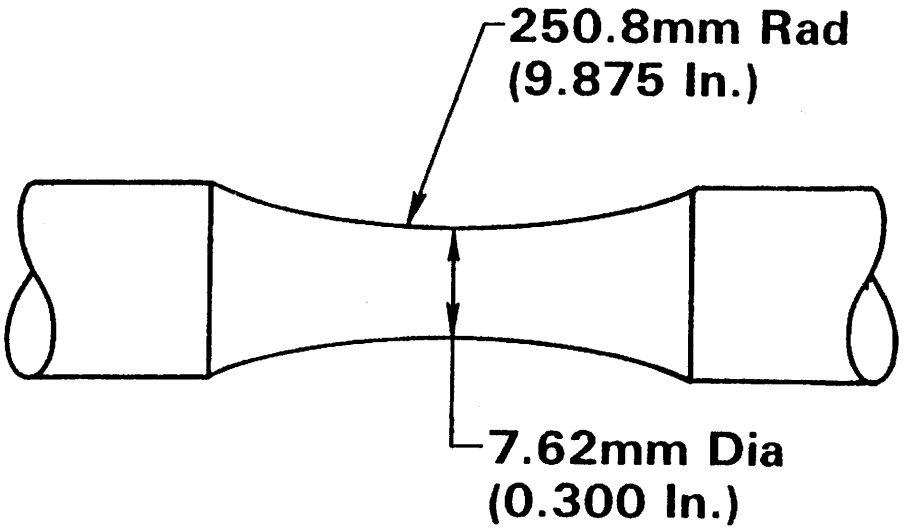

Smooth

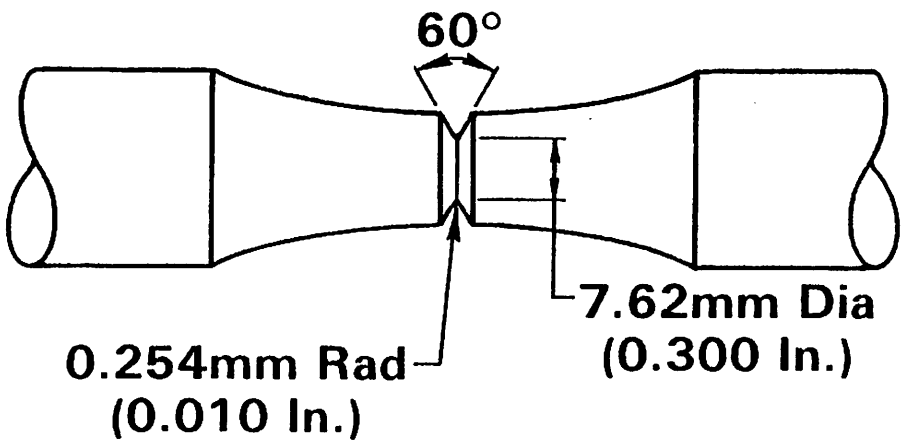

Notched

RELATIVE SIZE OF SPECIMEN vs FULL SCALE BLADE

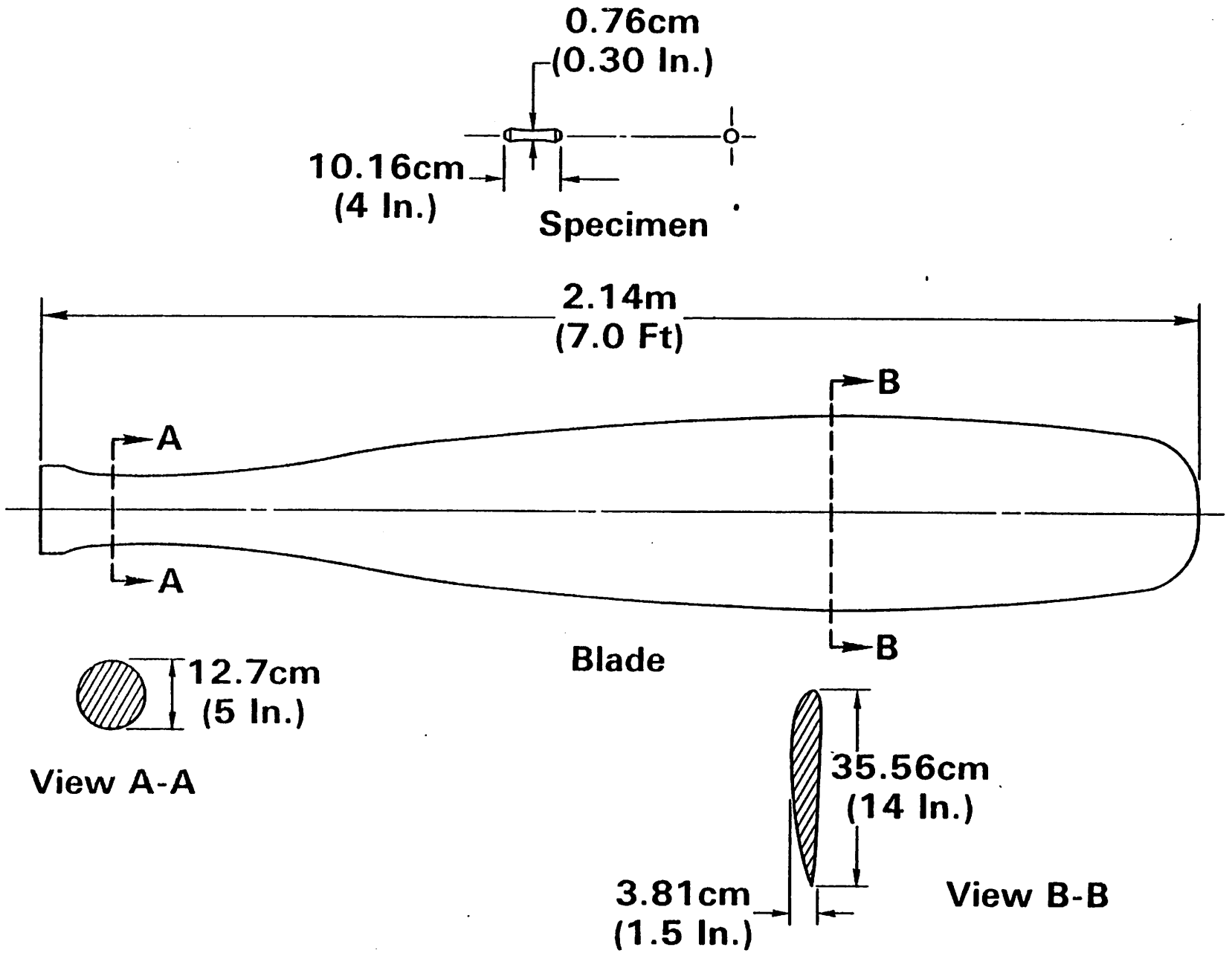

EXHIBIT 7

SERVICE INDUCED DAMAGE

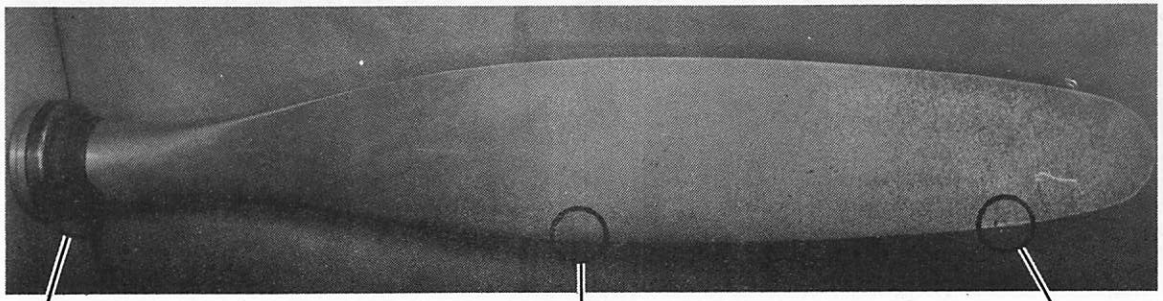

Fretting Corrosion

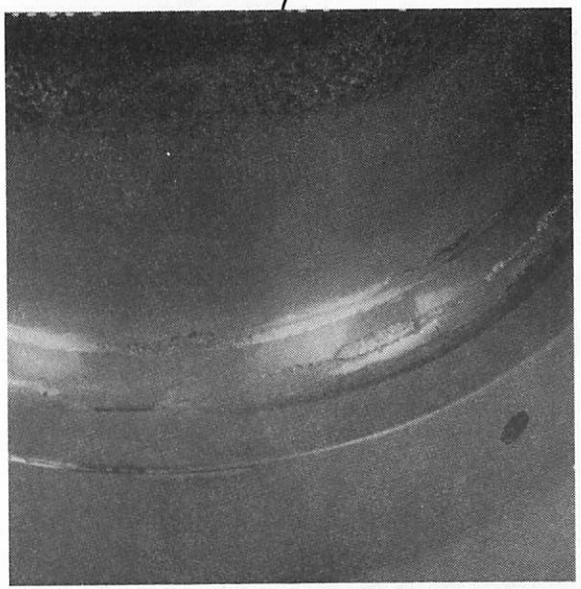

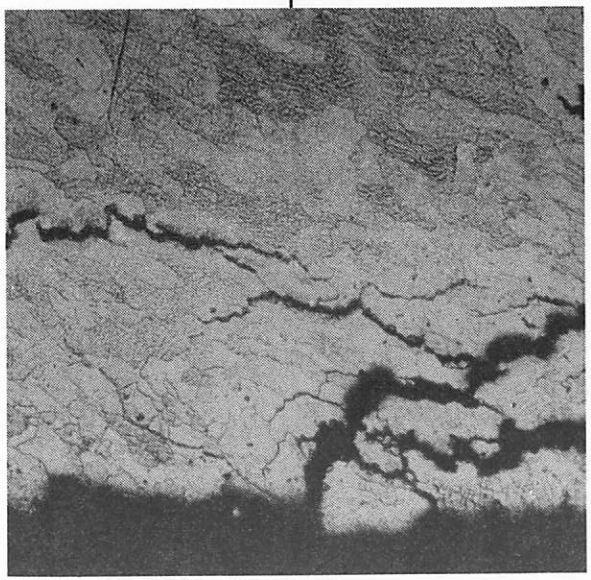

Stress Corrosion

Erosion

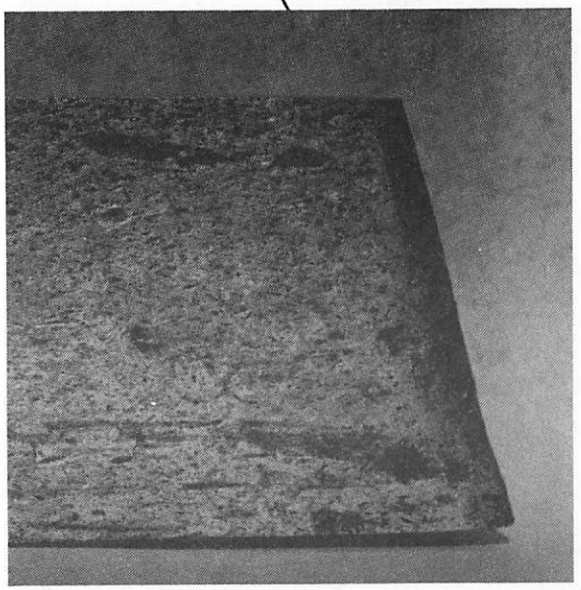

FORGED HIGH STRENGTH ALUMINUM ALLOY

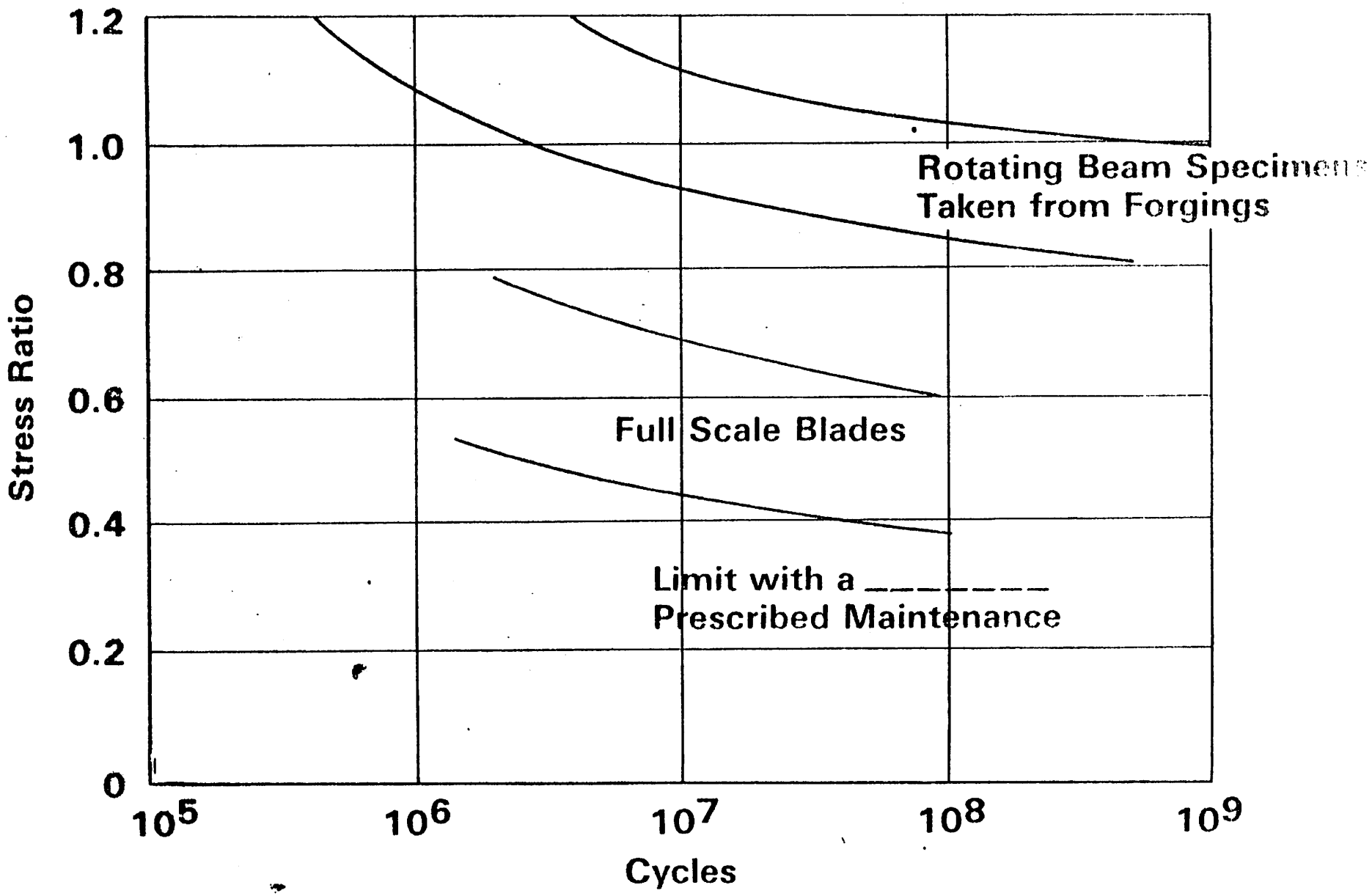

MODERATE STRENGTH STEEL ALLOY

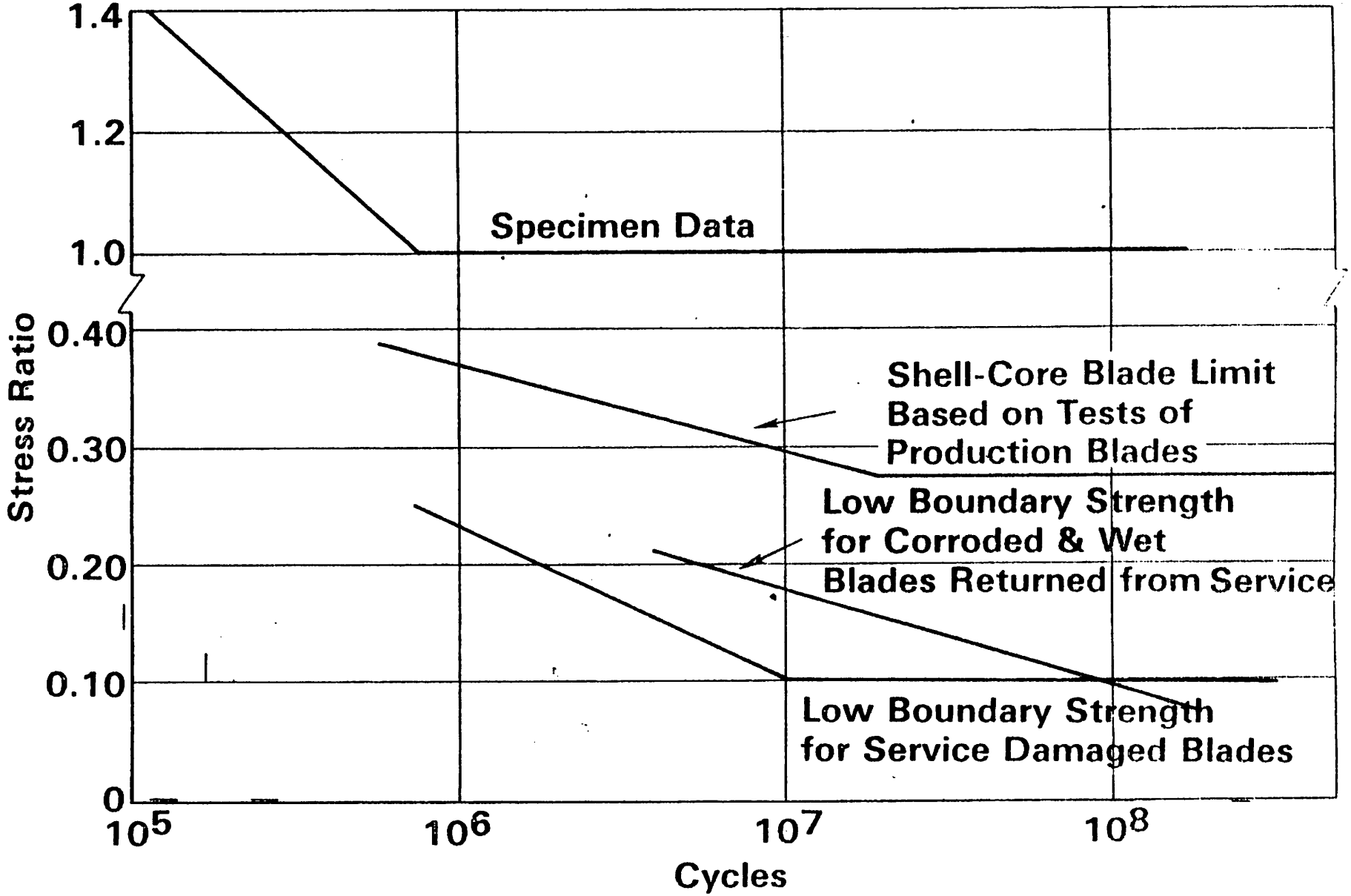

18A20 ONE-PIECE STEEL BLADE

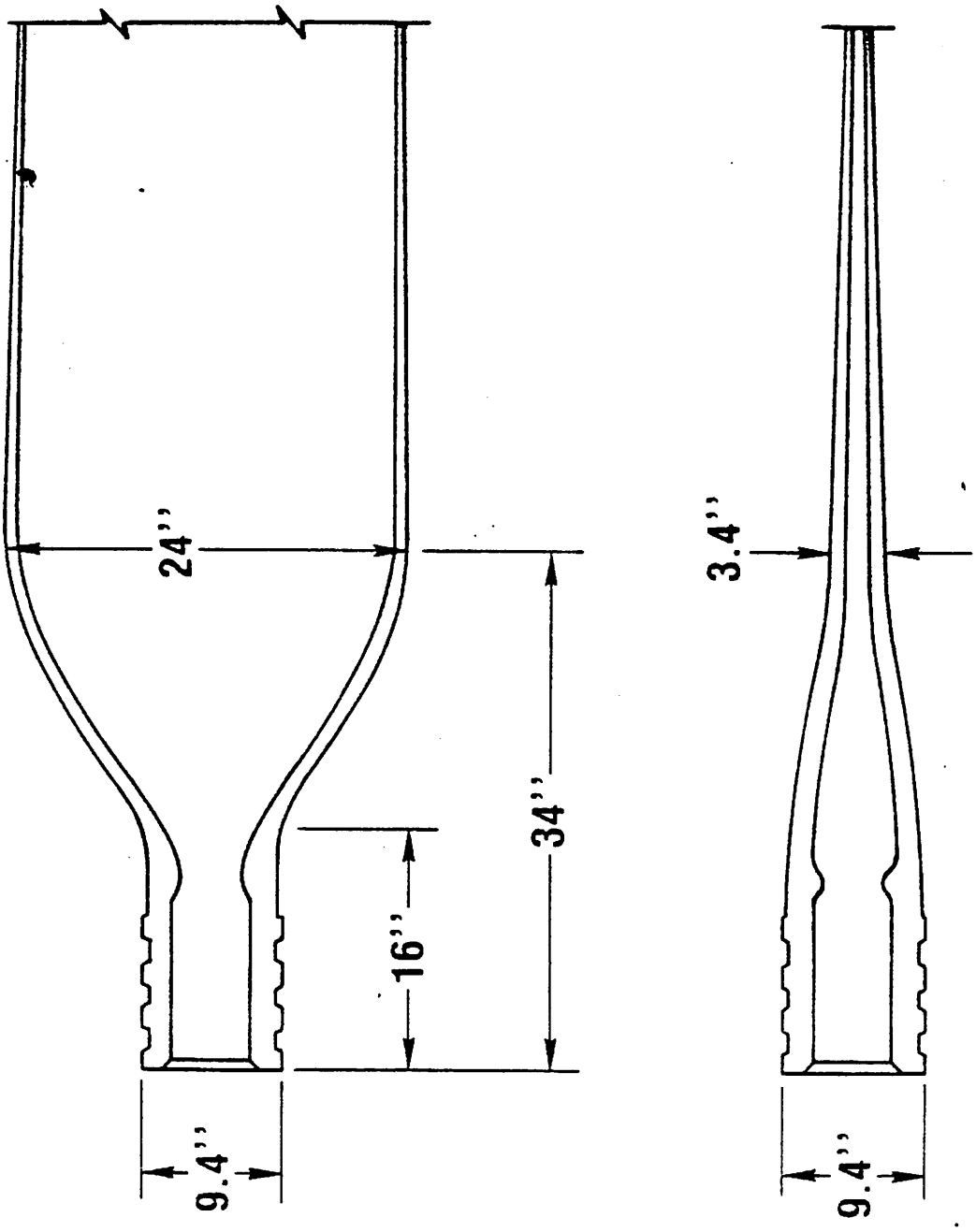

Ex. 10

EXHIBIT 11

CONTROLLED FATIGUE TESTING

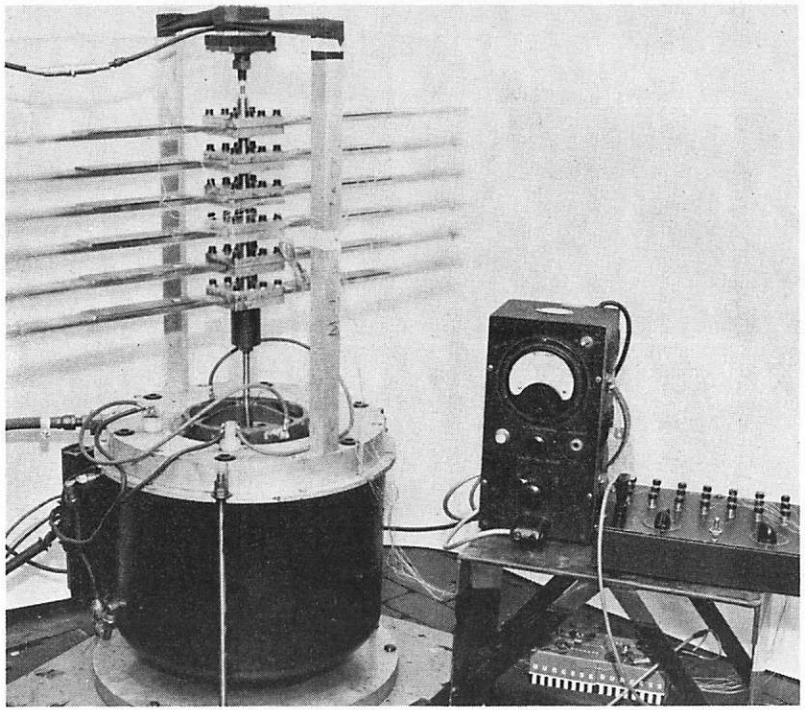

12 SPECIMENS SIMULTANEOUSLY

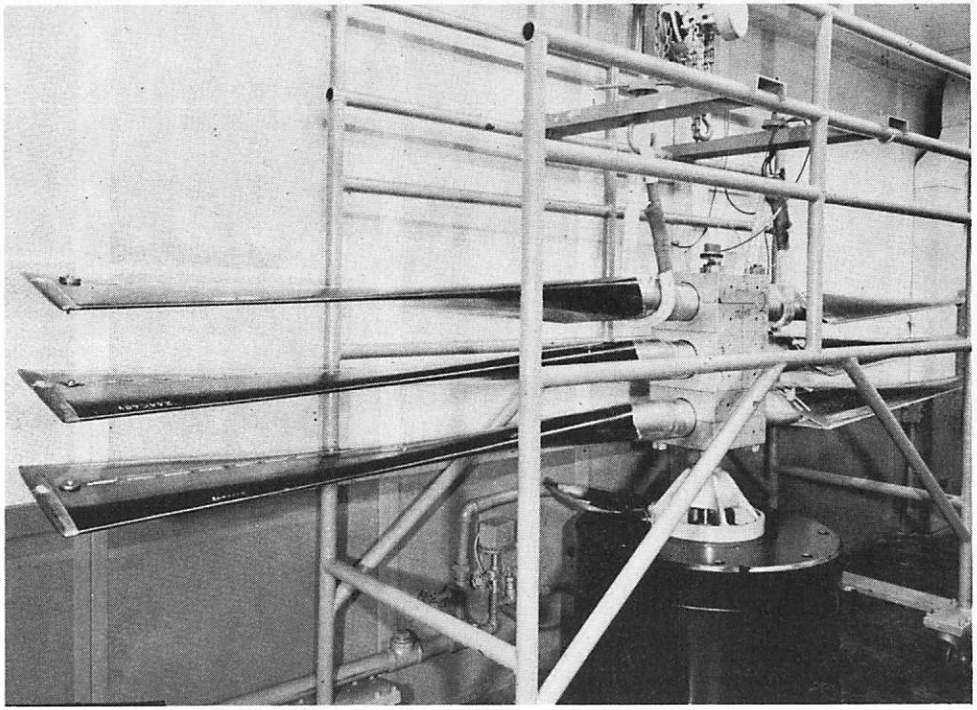

6 FULL-SCALE
BLADES SIMULTANEOUSLY

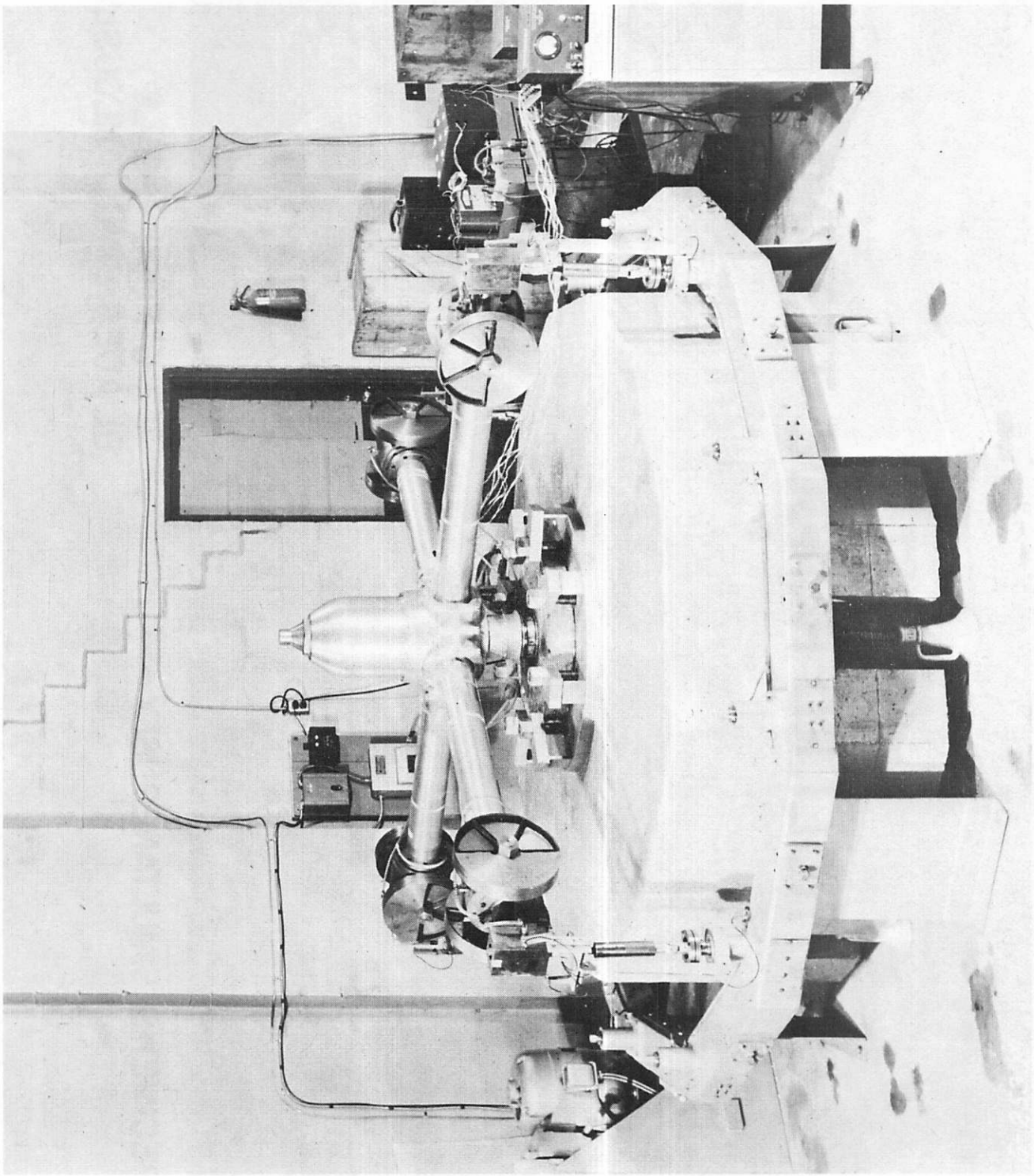

EXHIBIT 12

DESIGN LIMIT CONCEPT

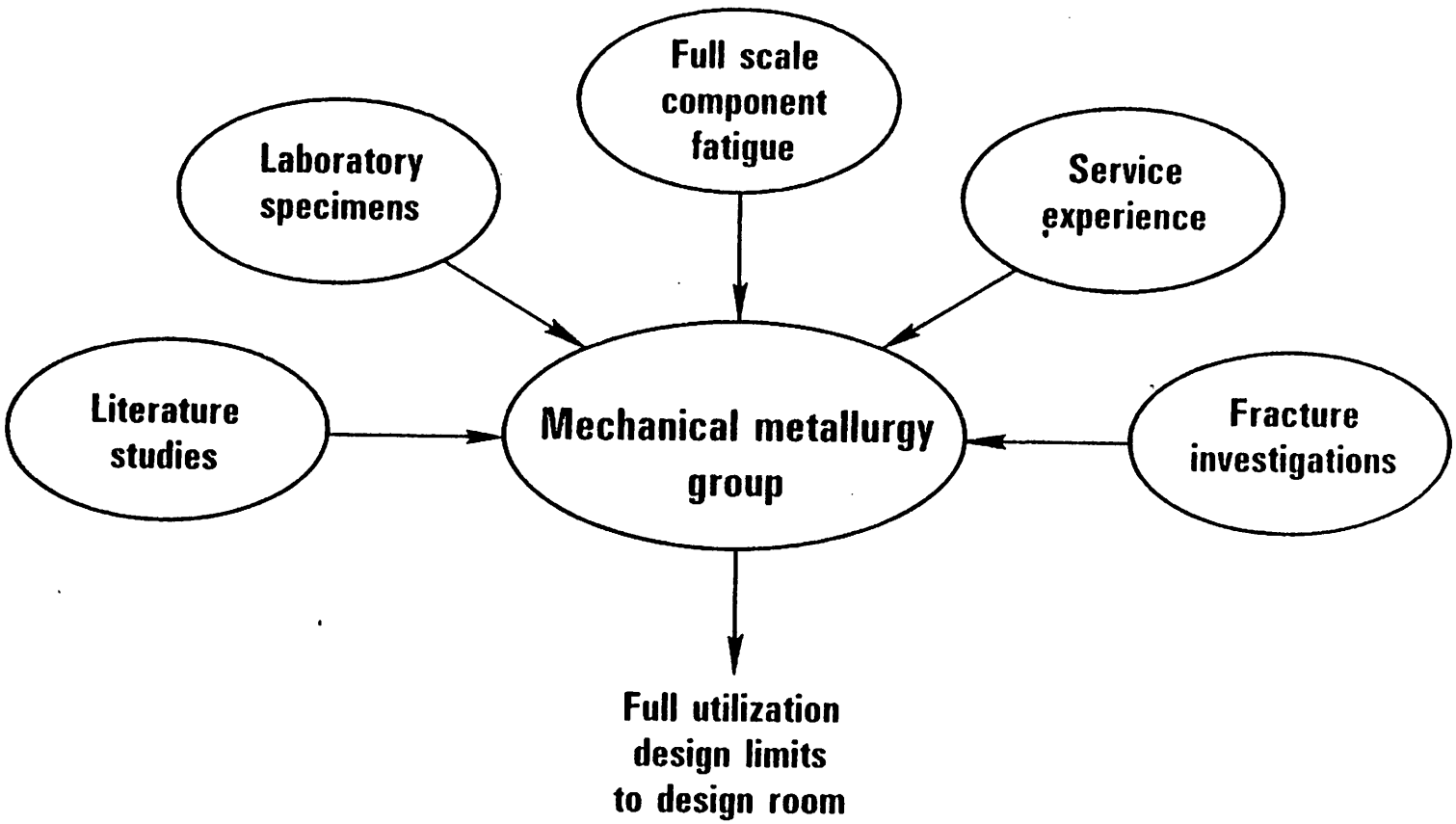

BLADE CONCEPT

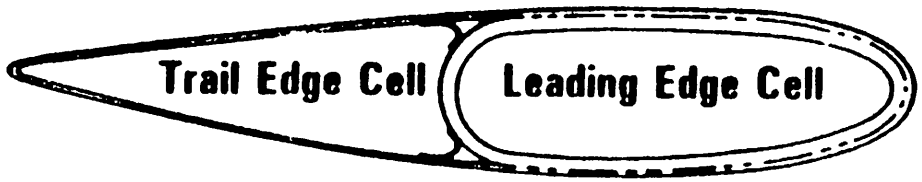

Section A-A

Blade Construction

Retention

BLADE RETENTION CONSTRUCTION

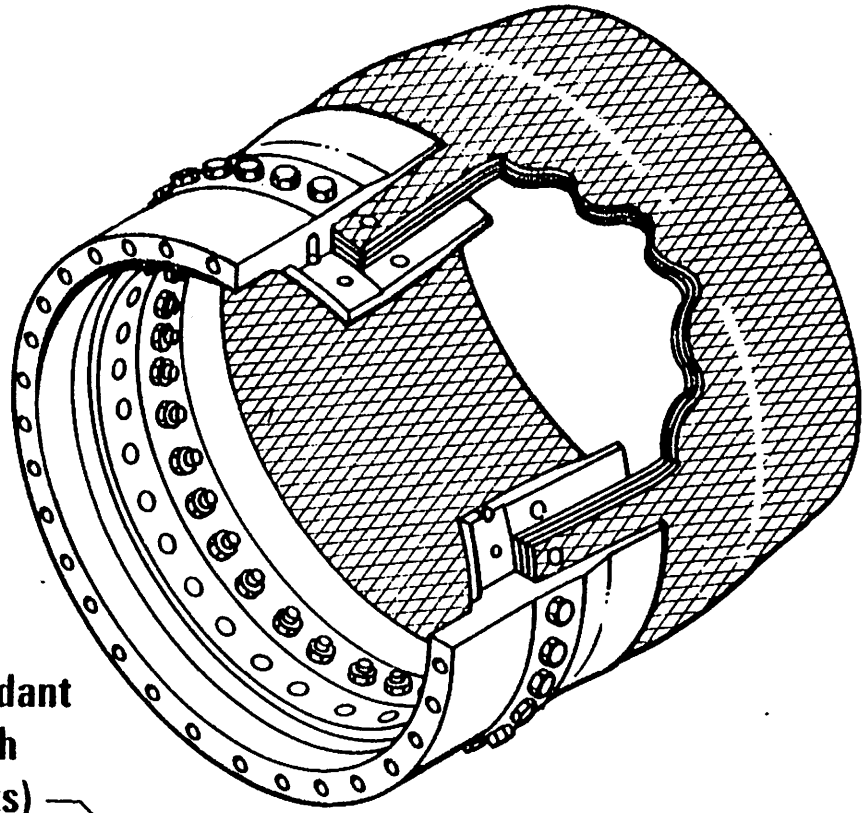

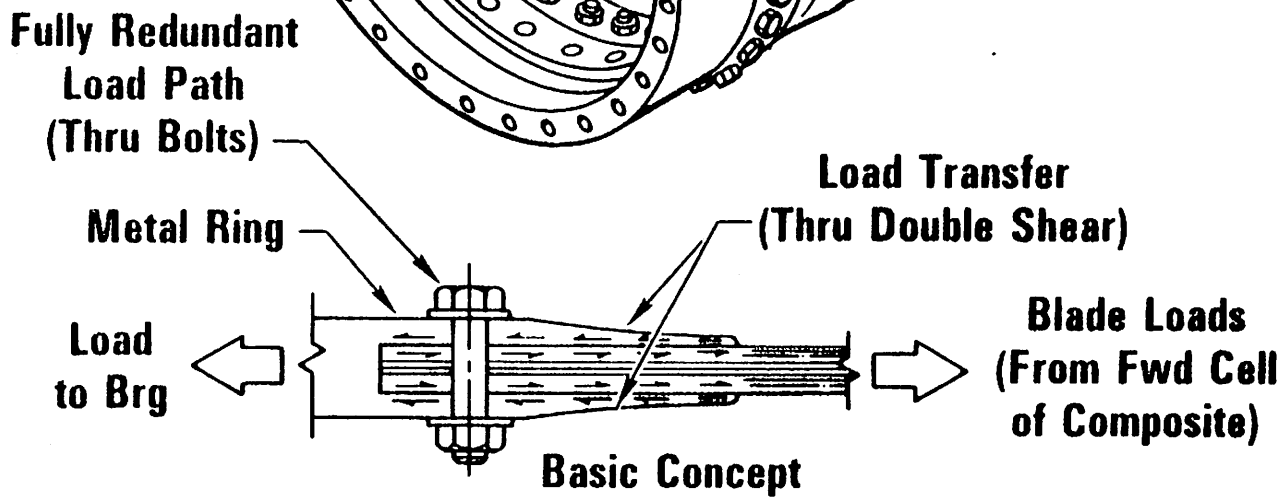

MAJOR STEPS IN DESIGN FOR FATIGUE PREVENTION

REQUIREMENTS

- BEST ASSESSMENT OF SERVICE LOADING
- EVALUATION OF ENVIRONMENT AND LIFE REQUIREMENTS
- ASSESSMENT OF APPROPRIATE MAINTENANCE

MAJOR STEPS IN DESIGN FOR FATIGUE PREVENTION

DESIGN

- SELECTION OF MATERIALS AND PROCESSES
- THEORETICAL STRESS ANALYSIS - EXPERIMENTAL SUPPORT WHERE NEEDED
- COMPONENT DESIGN LIMITS TO SATISFY LOADING, ENVIRONMENT, LIFE REQUIREMENTS, AND MAINTENANCE

MAJOR STEPS IN DESIGN FOR FATIGUE PREVENTION

VERIFICATION

- LARGE SCALE COMPONENT FATIGUE TESTING AS REQUIRED
- MEASURE LOADS IN OPERATING ENVIRONMENT
- FINAL STRESS VS. STRENGTH COMPARISON

Short note: A fracture test of the
vertical axis wind turbine VAWIAN
rotor blade (14 x 1 m)

by R. Windheim in co-operation with ERNO-Raumfahrttechnik

The Energy R+D Program of the Government of the Federal Republic of Germany includes the project "Wind energy converter system with vertical axis rotor" (3-ET 4253 A, ERNO-Raumfahrttechnik, Bremen; total costs: DM 872.000).

The objective of this project is:

Theoretical and experimental investigation in order to answer the question on the economically most favourable solution for wind energy conversion.

The work program is the following:

The WEC concept is characterized by a vertical axis, high speed rotor with straight vertical blades. The dimensions are to be referred to a power output of 20 kW and more. Wind velocity: 7 m/sec and more. A prototype will be developed and operated in order to investigate the performance and mechanical behaviour of this WEC-type by experimental results. The project is planned to be realized in three realization phases: I Development, II Fabrication and erection and III Operation and evaluation. The contract covers phase I.

A fracture test of an original rotor-blade (14 m x 1 m) designed and constructed for the vertical-axis-wind-turbine VAWIAN was accomplished by the "Institut für Leichtbau - Aachen Technical University". It was shown in this test that the safety factor (j = 1,5) against maximum loads during service will be obtained. These loads are aerodynamic and centrifugal forces (Fig. 1).

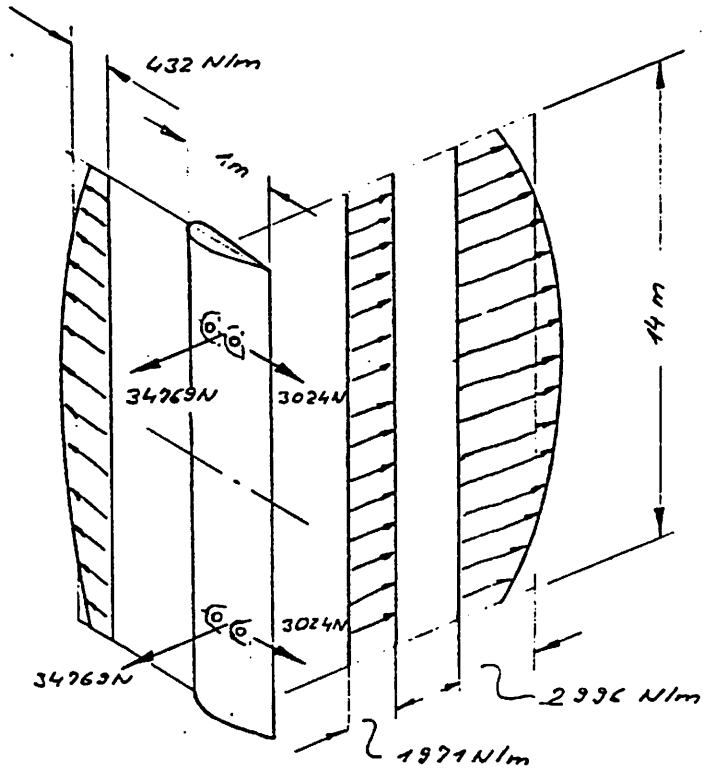

Fig. 1

Shearing forces and bending moments induced by these loads were simulated by 8 concentrated forces.
Fig. 2 shows the exactly and approximated curves of shearing forces and bending moments.

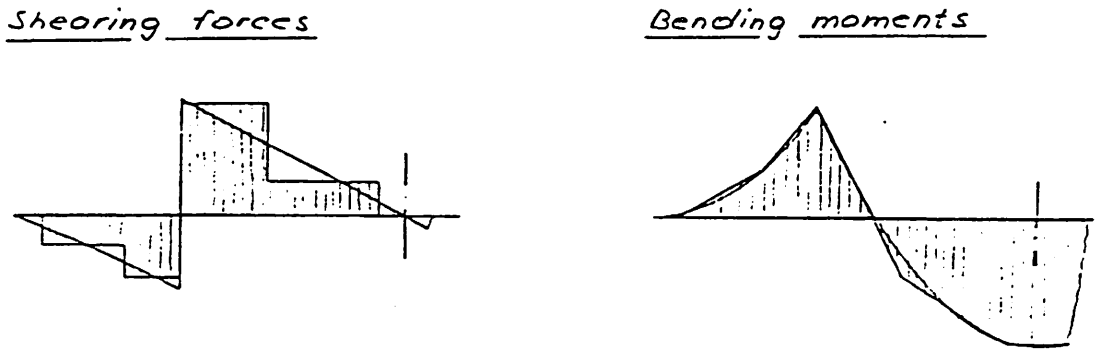

Fig. 2

Fig. 3 shows one of the symmetrical parts of the testing stand.

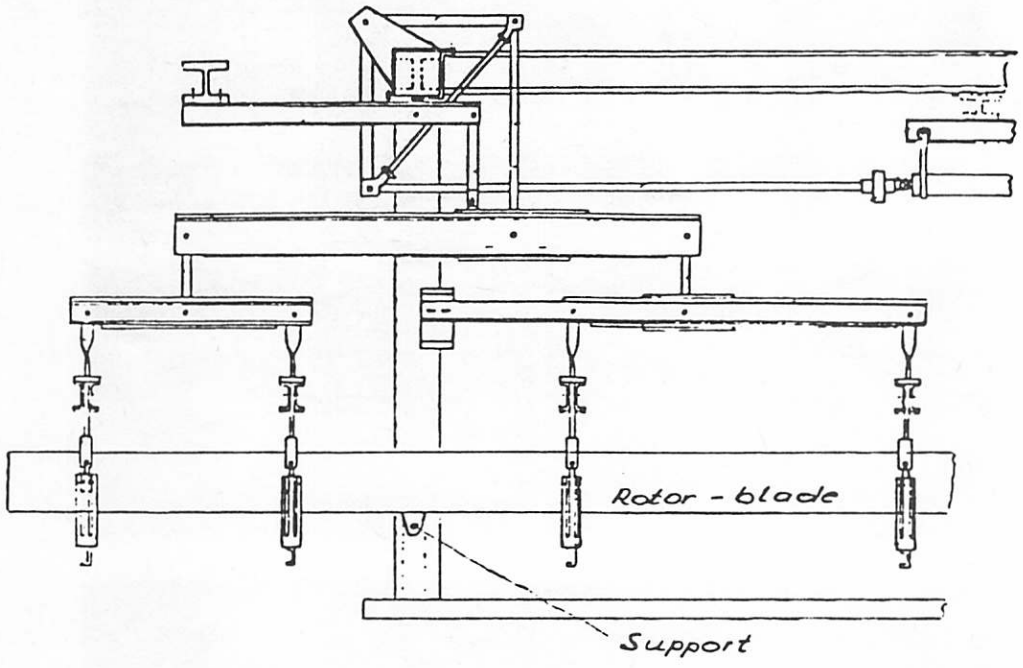

Fig. 3

A 1.5 limit load was obtained in 12 steps. After each step stresses and deformations were measured. Ten seconds after obtaining 1.5 limit load the rotor-blade was fractured near to one of the supports. This was a shear failure: no compression or tension fracture was observed.

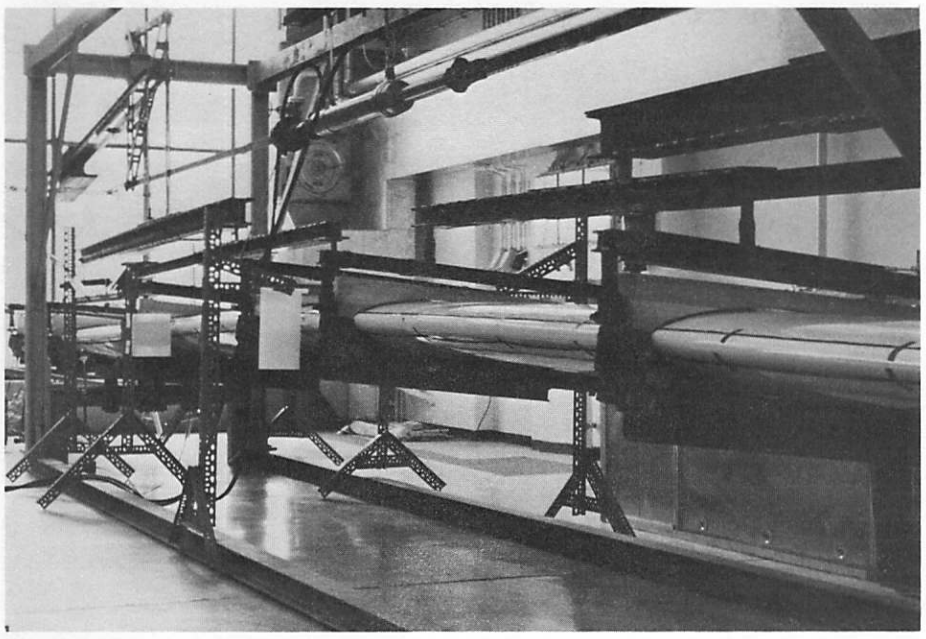

Test blade

Fracture of the blade

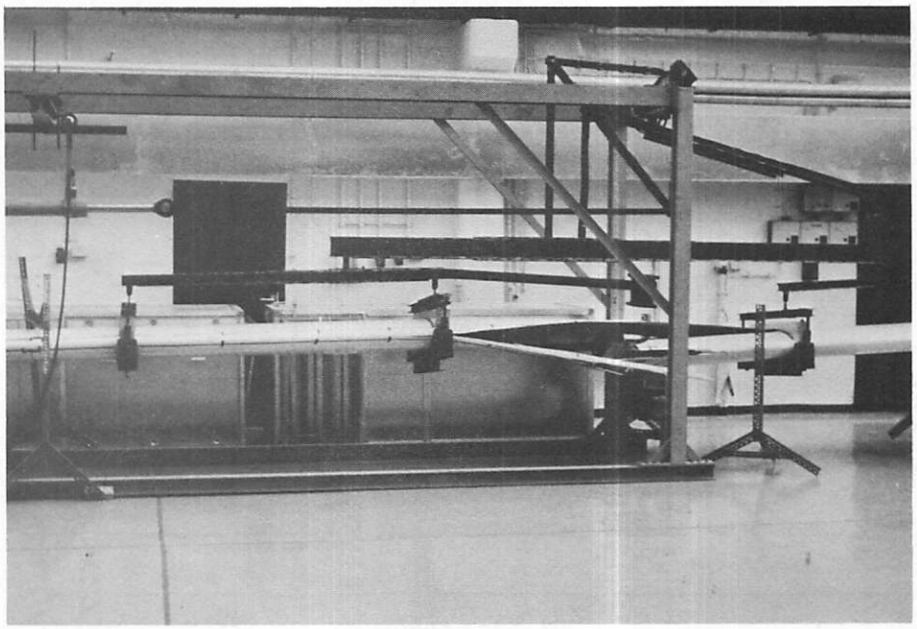

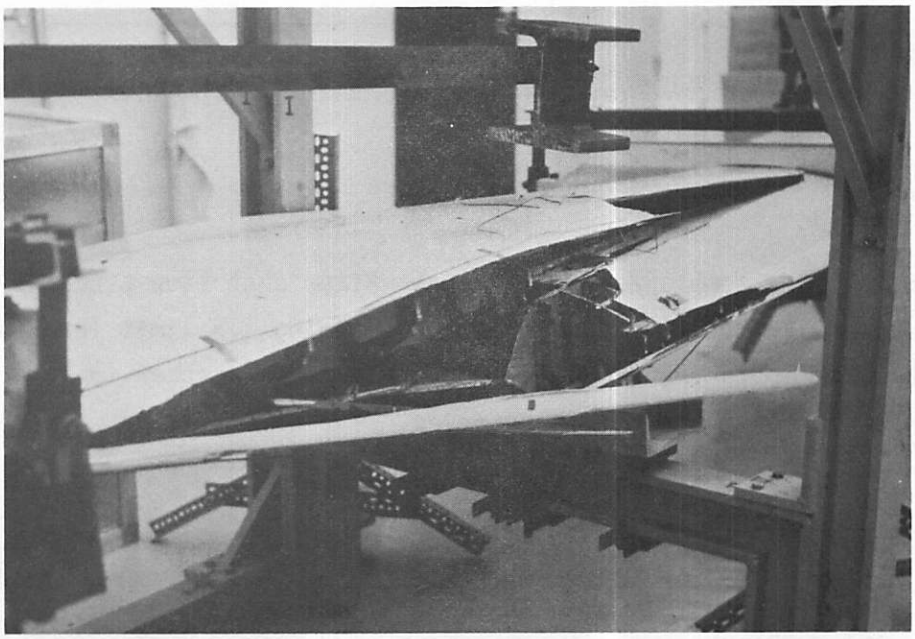

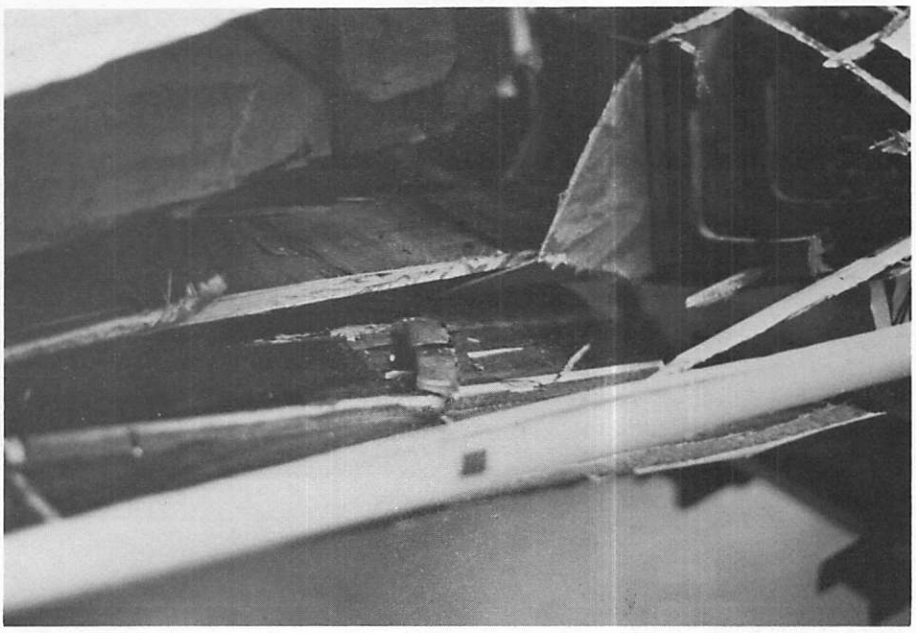

Visit to the Swedish 60 kW
research unit at Kalkugnen

The 60 W unit

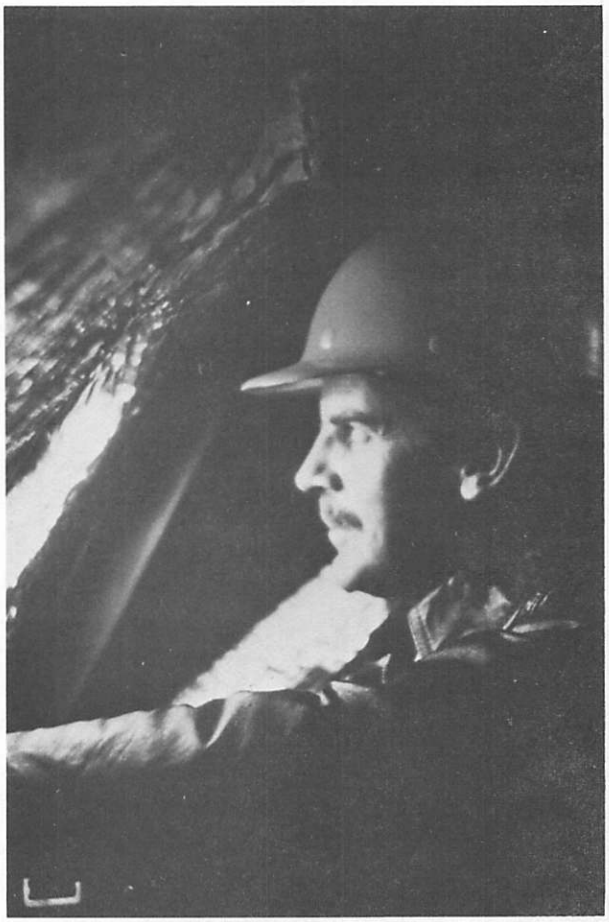

Sven Hugosson looking out of the nacelle

The 60 kW unit

Sven Hugosson (left) explains the wind power unit to the experts

LIST OF PARTICIPANTS

Sven Hugosson	NE, Sweden
Klaus Wieland	VFW, Bremen
Alfons Nowag	VFW, Bremen
André Raab	SIKOB, Sweden
Thomas Zajac	Hamilton Standard, USA
John M. Mc Saac	Hamilton Standard/KKRV Sweden
Nils Byggeth	Karlskronavarvet AB
Pär Svenkvist	KMW, Sweden
Bent Vangsy	Bølund A/S, Denmark
B. Maribo Pedersen	DTH, Lyngby, Denmark
Hans Lilholt	Risø National Lab., Denmark
Louis Divone	U.S. Dept. of Energy
Patrick Finnegan	U.S. Dept. of Energy
Göran Svensson	Swedish State Power Board
Ann-Katrin Larsson	Sydkraft AB
Rolf Windheim	KFA/PLE, Germany
Karl Pfeifer	MBB, Germany
Horst Bansemir	MBB-UD, Germany
Dieter Muser	MAN, Germany
Hans-Martin Thiele	MAN, Germany
Erich Hau	MAN, Germany